Dynamic Response and Design of Steel Structures Subjected to Pedestrian-Induced Loads

by

Houtan Tahmasebi-Orimi

Supervised by

Dr. Magdi Mohareb

Thesis submitted to the University of Ottawa
in partial fulfillment of the requirements for the degree of
DOCTOR OF PHILOSOPHY
in Civil Engineering

Department of Civil Engineering
Faculty of Engineering
University of Ottawa

Abstract

The present thesis investigates the dynamic performance of steel members under the effect of pedestrian induced dynamic forces. Towards this objective, the study adopts two main methodologies: (a) controlling the member natural frequencies to mitigate possible resonance phenomena under human-induced dynamic forces and (b) controlling acceleration levels induced in members to ensure they fall below acceptable perception levels.

While present design Canadian and American structural steel design provisions do not offer explicit natural frequency requirements, they limit member slenderness to 200 for compression members and 300 for tension members. These limits partly control the natural frequency but omit the influence of axial load level, and neither fully capture the effect to cross-sectional asymmetry, as may be the case in angle members, nor fully account for member end-connection details. Within this context, the present research presents four contributions towards advancing the state of the art related to the analysis and design of steel members under human activities.

The first contribution examines the natural vibration response of axially loaded members with wide-flange sections. A parametric study is conducted using closed-form analytical solutions and shell finite element modelling. The study characterizes the effect of axial loads on the member natural frequencies and proposes slenderness limit thresholds based on target natural frequencies that capture the axial load level. In this respect, this part of the study develops an improved serviceability criterion than simply satisfying member slenderness requirements in the present standards.

The second contribution extends the investigation to members with angle cross-sections, which are prone to torsional–flexural coupling owing to cross-sectional asymmetry, an aspect not addressed in the first contribution. A closed-form solution is developed to determine the torsional flexural natural frequency of pin-ended members with equal leg angles. The analytical model is complemented with shell finite element modelling to tackle more general cases involving unequal leg angles and members with gusset plate end connections. A subsequent parametric investigates the effect of axial force, cross-sectional geometry, member span, and boundary conditions on the natural frequency of angle members. The findings show that satisfying present slenderness criteria does not guarantee consistent natural frequencies across members with angle cross-sections and flags the need to develop more elaborate criteria to control excessive vibrations.

The third contribution formulates a general thin-walled beam finite element formulation for the natural vibration analysis of steel members. The solution captures torsional-flexural coupling induced by cross-sectional asymmetry, and the effects of axial loading, warping, and rotary inertia. The formulation is equipped with a feature that enables the seamless modelling of the boundary conditions of gusset-plate ended connections, in which the member is considered fixed about the axis normal to the gusset but nearly pinned about the gusset axis, both axes being non-principal. The findings reveal that gusset plate end connections significantly elevate the natural frequency of the member, when compared to pinned-ended members. A simplified energy-based solution is also developed to estimate the natural frequency of members with gusset-end connections, and a dimensionless design chart is provided to streamline the calculation procedure in a design environment.

While the previous three contributions centre around quantifying the natural frequency of steel members, the final contribution transitions to the full transient response evaluation under the time-

dependent loading is induced by human walking. Towards this objective, a general purpose thin-walled beam finite element formulation is developed for the fully dynamic analysis of thin-walled beams. In addition to capturing the effects of coupling induced by cross-sectional asymmetry, axial loading, warping, and rotary inertia, the formulation incorporates the effect of damping and develops the energy equivalent force vector that characterizes the temporal and spatial distributions of forces induced by human walking. The discretized equations of motion are then solved using the Newmark time integration scheme, and the predictions of the model are validated against benchmark solutions. A parametric study explores the effects of axial force magnitude, damping model, damping ratio, boundary conditions, and characteristics of the walking function on the member acceleration response. The results are benchmarked against established human comfort thresholds. The model thus provides a basis to assess the dynamic performance of steel members against established acceleration thresholds.

In summary, the present thesis advances methods of dynamic analysis of steel members. By integrating analytical solutions, energy-based approximate methods, and finite element modelling techniques, the study offers a possible framework for the analysis and design of steel members under the effect of dynamic loads induced by pedestrian-induced loads.

Acknowledgment

I would like to express my sincere gratitude and deepest appreciation to my supervisor, Professor Magdi Mohareb, for his patient guidance, invaluable advice, and unwavering encouragement throughout the course of this research. I have been extremely fortunate to have a mentor who cared deeply about my progress and responded so generously to my questions and concerns. Without his steadfast support, this work would not have been possible.

I would like to express my sincere gratitude to the members of my thesis examining committee: Professor Shaohong Cheng from the University of Windsor, Professor Abhijit Sarkar from Carleton University, and Professor Ghasan Doudak and Professor Hassan Aoude from the University of Ottawa. I am deeply thankful for their willingness to serve on my examining committee and for devoting their valuable time to my research and the defense of this thesis.

I would also like to thank Dr. Arash Sahraei for his valuable guidance and technical support throughout this research. His advice on programming and numerical modeling greatly contributed to the successful implementation of the developed models.

My profound appreciation is owed to my beloved parents, Mehdi and Nahid, whose endless sacrifices, unconditional love, and unwavering belief in me have been the foundation of all my achievements. Their support throughout these years has been a constant source of strength and inspiration. I am equally grateful to my brother, Arman, for his encouragement, kindness, and for always standing by me. This accomplishment is as much theirs as it is mine.

I am also deeply thankful to my beloved Sheida, whose patience and encouragement have accompanied me throughout this journey. Her love and support helped me to overcome the challenges of distance and sustained me through the most demanding times of my doctoral studies.

Finally, I extend my gratitude to my colleagues and friends, whose help, encouragement, and friendship have enriched this experience and made the path more enjoyable.

Table of content

List of Figures

List of Tables

Chapter 1: Introduction

1.1. General

The present thesis investigates the dynamic behavior of thin-walled steel members subjected to human-induced excitations, with particular focus on the dynamic effects generated by walking activities. This topic has gained relevance in modern structural design in buildings and facilities where human activity (such as walking, dancing, or aerobics) can lead to serviceability concerns due to excessive vibrations.

While conventional dynamic analyses of steel structures often center around seismic and wind-induced effects, the dynamic loads generated by human actions remain less investigated and often overlooked in design. However, in slender structural components such as thin-walled members, the risk of resonance and amplified transient responses becomes non-negligible, especially when such members are subjected to compressive loads. Such conditions can lead to discomfort for occupants, potential serviceability issues, and in extreme cases, structural damage.

The primary objective of this research is to establish slenderness criteria for controlling resonance and unacceptable acceleration levels caused by human activities. Towards this goal, the current chapter provides a literature-based foundation for understanding and tackling the problem. Specifically, it includes:

(a) An overview of the various types of dynamic excitations encountered in steel buildings due to human activities, including a discussion of time-dependent forcing functions proposed by previous researchers,

(b) An investigation into the influence of excitation frequencies associated with human-induced activities on the dynamic response of thin-walled members, along with the limitations and frequency separation requirements needed to prevent resonance phenomena.

(c) an examination of comfort criteria related to displacement and acceleration thresholds for human-occupied spaces, and

(d) An overview of formulations for the dynamic analysis of thin-walled structures.

1.2. Forcing functions induced by human activity

Dynamic effects in steel buildings are most associated with external actions such as earthquakes and wind. These phenomena have been extensively studied, and comprehensive design provisions are provided in structural codes and standards to address their influence, whether treated as quasi-static or dynamic loads. However, additional dynamic effects may arise from human-induced actions, which are particularly relevant in office floors, stadiums, and pedestrian bridges. As reported by Allen [1] and Smith et al. [2], human activities can produce various forms of dynamic excitation, categorized as: (1) *harmonic loads* generated by equipment or rhythmic bodily movements (e.g., dancing or aerobics); (2) *periodic loads* due to consistent actions such as walking; (3) *transient loads* resulting from sudden changes in motion, like starting or stopping during walking or running; and (4) *impulsive loads* caused by high-impact actions such as jumping or heel-drop exercises.

Bachmann and Ammann [3] reported that a walking pedestrian generates dynamic forces in three directions: (a) vertical (transverse), (b) horizontal (lateral), and (c) longitudinal, primarily due to the periodic acceleration and deceleration of body mass (e.g., Živanović et al. [4]). Among these components, the vertical force has the highest magnitude and has therefore received the most

attention in literature. Most previous studies have focused on this component, as it predominantly governs the structural response. The horizontal component, while generally smaller, has been investigated in a limited number of studies—particularly in the context of footbridges, where it may induce resonance under certain conditions. Nevertheless, its overall influence is often considered minor. The longitudinal component, having the lowest magnitude, is typically deemed negligible and is commonly excluded from detailed dynamic analysis.

1.2.1. Characterization of Human-Walking induced Forces

Human-induced excitations, particularly those resulting from walking, can be categorized based on the duration and characteristics of the applied forces. Several modelling strategies have been introduced in the literature to represent these excitations, ranging from force waveform representations to frequency-domain descriptions that capture the spectral content of walking-induced loads (e.g., Galbraith and Barton [5]; Ellis and Ji [6]). Although these approaches aim to reflect the complexity of human motion, they often face limitations in practical applications (especially in structural vibration analysis) due to the absence of closed-form solutions and the challenges of integrating variable waveforms into time-history simulations (e.g., Murray [7]).

A more precise approach involves modelling the walking-induced load as a time-dependent concentrated force, typically expressed through a Fourier series. This method, originally devised by Ellingwood and Tallin [8] and Rainer et al. [9], has gained widespread adoption. Modern design guidelines and standards, such as those presented in Murray et al. [10] and ISO-10137 [11], commonly use this framework to characterize the vertical component of dynamic forces due to walking. The horizontal component is often derived by adapting the expression used for the vertical force, as adopted in the work of Bachmann and Ammann [3] and Ingólfsson et al. [12].

The vertical and horizontal components $F(t), G(t)$ of human-walking induced forces are given as

$$F(t) = Q + Q\sum_{i=1}^{N} \alpha_i \sin(2\pi i f_s t - \phi_i)$$
$$G(t) = Q\sum_{i=1}^{N} \beta_i \sin(2\pi i f_s t - \lambda_i) \qquad 1.1(a\text{-}b)$$

where Q denotes the static weight of the individual, typically taken as 746 N based on a nominal mass of 74.6 kg, N is the total number of harmonics needed to represent the human activity. Most references recommend using four harmonics (i.e., $N = 4$) to capture the dynamic characteristics of walking-induced loads (e.g., [7], [11]), the term f_s is the human step frequency, t is the time, α_i, β_i are dynamic load factors of the vertical and horizontal components of the forcing function and are defined as the ratio of the force associated with the i^{th} harmonic to the body weight, and ϕ_i, λ_i are the phase angles of the vertical and horizontal components corresponding to the i^{th} harmonic. For instance, if the human step frequency is taken as 2.5 Hz, the fourth harmonic component results in an exciting frequency of 10 Hz. An illustration of the use of Eq. 1.1a is graphically provided in Figure 1.1.

Human activities that induce dynamic loading on structures are generally categorized into two types: (a) *footfall-dependent activities*, such as walking and running, and (b) *rhythmic activities*, including dancing, aerobic exercises, and live concerts. The corresponding dynamic load factors α_i and phase angles ϕ_i have been widely reported in the literature for both categories. Notable studies include those by Allen et al. [13], Pernica [14], Ebrahimpour and Sack [15], and Pavic and Willford [16] for walking-related activities, and Ellis and Ji [17] for rhythmic excitation.

Table 1.1 summarizes the dynamic load factors and associated phase angles provided by these researchers. Furthermore, Allen et al. [13] reported that higher harmonic components play a more significant role in rhythmic activities, with larger dynamic load factors observed at higher frequencies. In contrast, for walking and jogging, the influence of higher harmonics diminishes (particularly in group settings) due to phase dispersion among individuals. This trend is consistent with the findings of Ebrahimpour and Sack [15], who conducted experimental studies on rhythmic jumping and highlighted the increased prominence of higher-order harmonics under synchronized group motion.

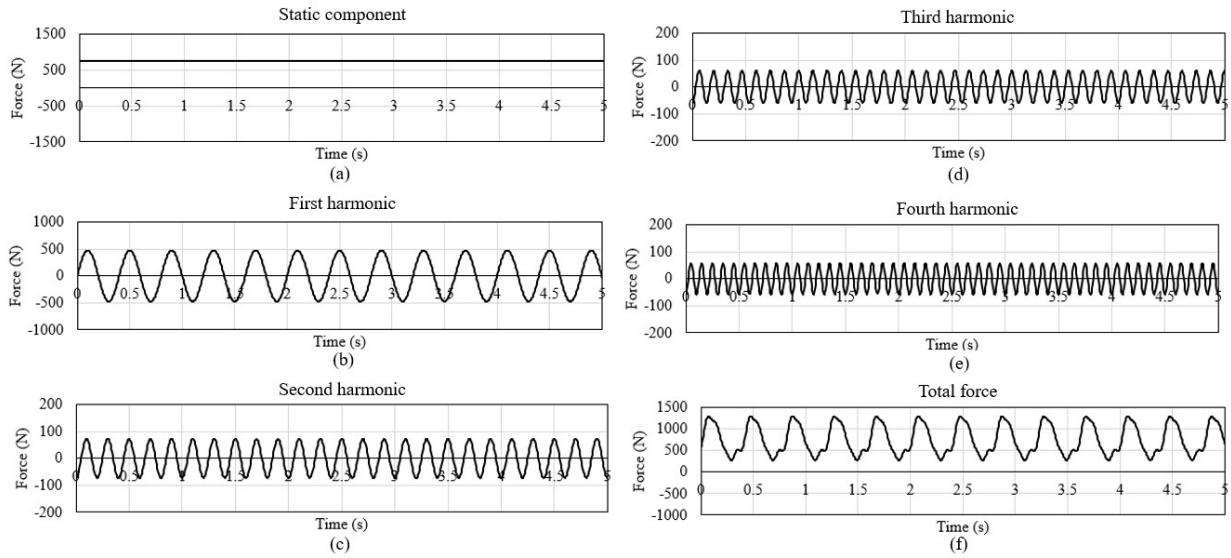

Figure 1.1 First four harmonics and the vertical component of total walking force (sum of harmonics), modelled by the Fourier series, with a walking frequency of 2.5 Hz. Person's weight = 746 N, phase angles $\phi_1 = 0;\ \phi_2 = \phi_3 = \phi_4 = \pi/2$. (a) static component, (b) first harmonic, (c) second harmonic, (d) third harmonic, (e) fourth harmonic, and (f) total force

Table 1.1 Parameters related to the vertical component of forcing function induced by human walking

Author	Dynamic load factor α_i	Phase angle ϕ_i	Comments
Bachmann [18]	$\alpha_1 = 0.4, \alpha_2 = \alpha_3 = 0.1$	$\phi_1 = 0$ $\phi_2 = \phi_3 = \pi/2$	Exciting frequency of first harmonic is 2.0- 2.4 Hz
ISO-10137 [11]	$\alpha_1 = 0.37(f_s - 1)$ $\alpha_2 = 0.1$ $\alpha_3 = \alpha_4 = 0.06$		
Young [19]	$\alpha_1 = 0.37(f_s - 0.95) \le 0.5$ $\alpha_2 = 0.0044(f_s + 12.27)$ $\alpha_3 = 0.005(f_s + 5.2)$ $\alpha_4 = 0.0051(f_s + 1.96)$		Exciting frequency of first harmonic is 2.0 Hz
Pavic and Willford [16]	$\alpha_1 = 0.41(f_s - 0.95)$ $\alpha_2 = 0.0056(f_s + 12.3)$ $\alpha_3 = 0.0064(f_s + 5.2)$ $\alpha_4 = 0.0065(f_s + 2.0)$	$\phi_1 = 0$ $\phi_2 = \phi_3 = \phi_4 = \pi/2$	Exciting frequency of first harmonic is 1.8 Hz
Smith et al. [2]	$\alpha_1 = 0.436(f_s - 0.95)$ $\alpha_2 = 0.006(f_s + 12.3)$ $\alpha_3 = 0.007(f_s + 5.2)$ $\alpha_4 = 0.007(f_s + 2.0)$	$\phi_1 = 0$ $\phi_2 = -\pi/2$ $\phi_3 = 0$ $\phi_4 = \pi/2$	$1.8 \le if_s \le 2.2$, $i = 1$ $3.6 \le if_s \le 4.4$, $i = 2$ $5.4 \le if_s \le 6.6$, $i = 3$ $7.2 \le if_s \le 8.8$, $i = 4$

Table 1.2 presents the approximate values of dynamic load factors α_i and phase angles ϕ_i proposed by Ellis and Ji [17], related to the vertical component of forcing function, which vary depending on the nature of the activity.

Table 1.2 Dynamic load factors α_i and phase angles ϕ_i for different rhythmic activities (Ellis and Ji [17])

Type of activity	Dynamic load factor and phase angle	$i=1$	$i=2$	$i=3$	$i=4$	$i=5$	$i=6$
Low impact aerobics	α_i	9/7	9/55	2/15	9/247	9/391	2/36
	ϕ_i	$-\pi/6$	$-5\pi/6$	$-\pi/6$	$-\pi/6$	$-5\pi/6$	$-\pi/2$
High impact aerobics	α_i	$\pi/2$	2/3	0	2/15	0	2/35
	ϕ_i	0	$-\pi/2$	0	$-\pi/2$	0	$-\pi/2$
Normal jumping	α_i	9/5	9/7	2/3	9/55	9/61	2/15
	ϕ_i	$\pi/6$	$-\pi/6$	$-\pi/2$	$-5\pi/6$	$-\pi/6$	$-\pi/2$

Bachmann and Ammann [3] and Ingólfsson et al. [12] proposed a specific modification to the forcing function expression to account for the horizontal component of human-induced loading (Eq. 1.1b). Table 1.3 presents a summary of dynamic load factors β_i associated with horizontal excitation, along with the corresponding step frequencies as reported by various researchers.

Table 1.3 Parameters related to the horizontal component of forcing function induced by human walking

Author	Dynamic load factor β_i	Comments
Bachmann and Ammann [3]	$\beta_1 = 0.039, \beta_2 = 0.01, \beta_3 = 0.043$ $\beta_4 = 0.012, \beta_5 = 0.015$	Step frequency of first harmonic is 2.0Hz
Bachmann [18]	$\beta_1 = \beta_3 = 0.1$	Step frequency of first harmonic is 2.0Hz
Ingólfsson et al. [12]	$\beta_1 = 0.05, \beta_2 = 0.04, \beta_3 = 0.01$	$f_s^{1st\ harmonic} = 0.5 f_s$ $f_s^{2nd\ harmonic} = 1.5 f_s$ $f_s^{3rd\ harmonic} = 2.5 f_s$

1.2.2. Alternative Forcing Functions

1.2.2.1. Zhang and Xu [20]

Zhang and Xu [20] simplified of the vertical component of forcing function defined in (Eq. 1.1a) to

$$F(t) = Q + \sum_{i=1}^{N} \alpha_i Q \sin(0.76\pi i f_s t) \tag{1.2}$$

in which the dynamic load factors corresponding to the first five Fourier coefficients were given by

$$
\begin{aligned}
\alpha_1 &= \begin{cases} -0.0698 f_s + 1.211 & 1.6Hz \le f_s \le 2.32Hz \\ -0.1784 f_s + 1.463 & 2.32Hz \le f_s \le 2.4Hz \end{cases} \\
\alpha_2 &= \begin{cases} 0.1052 f_s - 0.1284 & 1.6Hz \le f_s \le 2.32Hz \\ -0.4716 f_s + 1.210 & 2.32Hz \le f_s \le 2.4Hz \end{cases} \\
\alpha_3 &= \begin{cases} 0.3002 f_s - 0.1534 & 1.6Hz \le f_s \le 2.32Hz \\ -0.0118 f_s + 0.5703 & 2.32Hz \le f_s \le 2.4Hz \end{cases} \\
\alpha_4 &= \begin{cases} 0.0416 f_s - 0.0288 & 1.6Hz \le f_s \le 2.32Hz \\ -0.2600 f_s + 0.6711 & 2.32Hz \le f_s \le 2.4Hz \end{cases} \\
\alpha_5 &= \begin{cases} -0.0275 f_s + 0.0608 & 1.6Hz \le f_s \le 2.32Hz \\ -0.0906 f_s - 0.2132 & 2.32Hz \le f_s \le 2.4Hz \end{cases}
\end{aligned}
\tag{1.3}
$$

1.2.2.2. Gonçalves et al. [21]

An alternative group of expressions were proposed by Gonçalves et al. [21] for the vertical forcing function $F(t)$ to account for the heel impact effect associated with the third and fourth Fourier terms, i.e.,

$$
F(t) = \begin{cases} \dfrac{1}{0.04T}\left(f_{mi}F_m - Q\right)t + Q & 0 \le t < 0.04t_s \\ f_{mi}F_m\left[\dfrac{C_1}{0.02T}\left(t - 0.04T\right) + 1\right] & 0.04t_s \le t < 0.06t_s \\ F_m & 0.06t_s \le t < 0.15t_s \\ Q\left\{1 + \sum_{i=1}^{N}\alpha_i \sin\left[2\pi i f_s\left(t + 0.1T\right) + \phi_i\right]\right\} & 0.15t_s \le t < 090t_s \\ 10\left(Q - C_2\right)\left(\dfrac{t}{T} - 1\right) + Q & 0.90t_s \le t < t_s \end{cases}
\tag{1.4}
$$

where f_{mi} is the heel-impact factor (defined as the ratio of the peak magnitude of the heel-impact force and the maximum force generated by the Fourier series), T is the period of the step, t_s is the

duration of the step, and $F_m = Q\left(1+\sum_{i=1}^{i}\alpha_i\right)$ is the maximum magnitude of the force Fourier series induced by walking. In Eq. 1.4, constants C_1 and C_2 are numerical coefficients defined by

$$C_1 = Q\left(\frac{1}{f_{mi}}-1\right) \quad ; \quad C_2 = \begin{cases} Q(1-\alpha_2) & i=3 \\ Q(1-\alpha_2-\alpha_4) & i=4 \end{cases} \qquad 1.5\text{(a-b)}$$

and one recalls that parameters ϕ_i, α_i, Q, f_s have been previously defined as the phase angle, dynamic load factor, human body weight, and step frequency

1.2.2.3. Kappos [22]

Kappos [22] presented expression for the dynamic load factor α_i and the phase angle ϕ_i associated with vertical component of forcing function induced by human rhythmic activities in terms of the contact ratio γ .

$$\alpha_i = \sqrt{a_i^2 + b_i^2} \qquad \phi_i = \tan^{-1}\left(\frac{a_i}{b_i}\right) \qquad 1.6$$

in which a_i and b_i are defined by

$$a_i = \begin{cases} 0.5\left[\dfrac{\cos(2i\gamma-1)\pi-1}{2i\gamma-1} - \dfrac{\cos(2i\gamma+1)\pi-1}{2i\gamma+1}\right] & 2i\gamma \neq 1 \left(i=1,2,3...\right) \\ 0 & 2i\gamma = 1 \left(i=1,2,3...\right) \end{cases} \qquad 1.7$$

$$b_i = \begin{cases} 0.5\left[\dfrac{\sin(2i\gamma-1)\pi}{2i\gamma-1} - \dfrac{\sin(2i\gamma+1)\pi}{2i\gamma+1}\right] & 2i\gamma \neq 1 \left(i=1,2,3...\right) \\ 0 & 2i\gamma = 1 \left(i=1,2,3...\right) \end{cases} \qquad 1.8$$

Eq. 1.6-1.8 enable the application of Eq. 1.1a for rhythmic activities.

In addition, Kappos [22] proposed a specific expression for vertical component of forcing function induced by human rhythmic activities, as an alternative to Eq. 1.1a as follows

$$F(t)=\begin{cases} K_p Q \sin\left(\pi t/t_p\right) & 0 \le t \le t_p \\ 0 & t_p \le t \le T_p \end{cases} \tag{1.9}$$

where K_p is an impact factor defined by $K_p = F_{max}/Q$ in which F_{max} is the peak dynamic load, t_p is the contact duration and T_p is the period of dancing load or time between successive 'toe off'. The contact ratio defined as $\gamma = t_p/T_p$ depends on the nature of the dance and meet the condition $\gamma \le 1.0$.

Kappos [22] observed that the mean value of dynamic human induced loading to the structure is equivalent to the static weight of the individual (or individuals) involved in the activity. Accordingly, integrating Eq. 1.9 over the contact period yields:

$$\frac{1}{T_p}\int_0^{t_p} K_p Q \sin\left(\frac{\pi t}{t_p}\right) dt = Q \tag{1.10}$$

from which the impact factor can be evaluated as

$$K_p = \frac{\pi}{2\gamma} \tag{1.11}$$

The impact factor K_p corresponding to various rhythmic human activities are provided in Table 1.4. It is noted that the values of γ and K_p provided in Table 1.4 have been adopted in the UK loading code BS-6399 [23].

Table 1.4 Values of contact ratio γ and Impact factor K_p for various human rhythmic activities (Kappos [22])

Activity	Contact ratio γ	Impact factor K_p
Pedestrian movements, low impact aerobics	2/3	2.4
Rhythmic exercises, high impact aerobics	1/2	3.1
Normal jumping	1/3	4.7
High jumping	1/4	6.3

1.2.2.4. Ellis and Ji [6]

An analytical solution was developed to evaluate floor vibrations caused by dancing-type loads and was subsequently validated through comparison with experimental measurements. The findings revealed that dancing induces relatively high dynamic forces, exhibiting characteristics similar to the "toe-off" phase observed when running upstairs. This is typically followed by a brief airborne phase during which the feet lose contact with the floor, resulting in a temporary drop of the applied load to zero. The individual then returns to the floor, and the loading cycle repeats.

To quantify this behavior, Ellis and Ji [6] introduced the concept of a contact ratio γ, which represents the portion of the motion cycle during which the feet remain in contact with the floor. Table 1.5 summarizes the contact ratio values associated with various human rhythmic activities as proposed by Ellis and Ji [6].

Table 1.5 Values of contact ratio γ for various human rhythmic activities (Ellis and Ji [6])

Type of activity	Contact ratio γ
Low impact aerobics	2/3
High impact aerobics	1/2
Normal jumping	1/3

1.3. Natural Frequency Criteria

Researchers reported typical step frequency ranges associated with different human activities. For walking, step frequencies are commonly cited within the range of 1.5 to 2.5 Hz (e.g., Ebrahimpour [24]; Allen and Murray [25]; Hechler et al. [26]; Willford et al. [27]). For running, a slightly broader range of values has been observed (1.6 and 4.0 Hz) (e.g., [9]; [18]). In the case of rhythmic activities, such as dancing or live concerts, a range of 1.5 to 3.0 Hz has been suggested, while aerobic exercises tend to produce excitation frequencies between 2.0 and 4.0 Hz (e.g., Murray et al. [10]; NBC-2015 [28]; Aalami [29]).

To capture the essential dynamic characteristics of human-induced loads, most studies and design guidelines recommend considering up to four harmonics (N=4) (e.g., [7]; [11]). For example, if the fundamental step frequency is taken as 2.5 Hz, the resulting harmonic components will have exciting frequencies of 2.5 Hz, 5.0 Hz, 7.5 Hz, and 10.0 Hz. In such a case, if a structural member has a fundamental natural frequency close to one of these harmonic frequencies (especially the highest exciting frequency of 10 Hz) it may be prone to resonance with this component, potentially leading to perceptible and uncomfortable vibrations.

To minimize the risk of resonance and discomfort, the natural frequency of the structure is often recommended to be well-separated from the excitation frequencies. In particular, when the floor natural frequency is lower than the fourth harmonic induced by walking (e.g., below 10 Hz), there is a risk of resonance with that component. This concept is reflected in building code provisions: the NBC-1990 [30] originally stipulated a minimum floor natural frequency of 5 Hz to avoid resonance under rhythmic activities. However, this threshold was increased to 10 Hz in NBC-2015 [28], recognizing that human rhythmic activities (such as dancing, foot stamping, jumping, and

even walking) produce periodic forces with dominant frequencies in the 1–4 Hz range, which can induce resonance if the harmonics align with the system's natural frequencies.

1.4. Displacement and Acceleration Criteria

In the context of human-induced dynamic loading, structural displacement is typically not the governing concern when evaluating comfort or serviceability. The deflections caused by such forces are generally small and remain below perceptible levels for occupants, especially in the case of walking or rhythmic activities. As a result, displacement criteria are insufficient for assessing discomfort due to human-induced vibrations.

Instead, peak acceleration ratio (defined as the ratio of peak structural acceleration to gravitational acceleration g) is widely recognized as the most relevant measure of human perception to vibration. Human sensitivity to motion is closely tied to this ratio, with the threshold for discomfort varying based on the type of activity and the functional use of space. Various guidelines and standards have established recommended limits to ensure acceptable levels of comfort.

The NBC-1990 [30] prescribes peak acceleration ratio limits in the range of 0.4% to 0.7% for typical office and residential buildings. These limits increase to 1.5%–2.5% for indoor public spaces, and further to 4%–7% for outdoor environments where higher excitation is more acceptable. Similarly, recommendations by Allen and Murray [25] and ISO-2631-2 [31] suggest thresholds of 0.5% for office and residential settings, 1.5% for indoor public areas, and up to 5% for outdoor venues hosting rhythmic activities.

To facilitate practical assessment, Murray et al. [10] developed a comfort criterion chart (Figure 1.2), which relates the peak acceleration ratio to the excitation frequency. This graphical tool helps evaluate vibration acceptability across various usage scenarios. Notably, the most critical

frequency range for human sensitivity lies between 4 to 8 Hz, aligning with the natural resonance frequencies of internal organs. Outside this range, human tolerance increases, and higher accelerations may be considered acceptable.

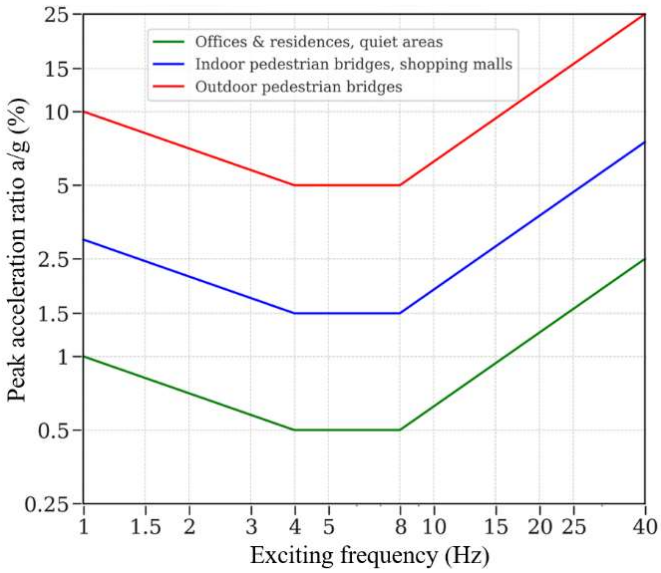

Figure 1.2 Peak acceleration a/g versus exciting frequency f_s (Adopted from [25])

1.5. Overview of Dynamic Solutions for Thin-Walled Members

Previous research on the transient dynamic analysis of thin-walled members has predominantly employed two numerical approaches: mode superposition methods and direct time integration techniques. Mode superposition, which is computationally efficient for systems with a few dominant modes, has been used in studies addressing cross-section symmetry, warping, shear deformation, and damping effects (e.g., Chen [32], Abrate [33], Bebiano et al. [34], Bebiano et al. [35], Pagani et al. [36]). Some of these studies also adopted Generalized Beam Theory (GBT) to capture advanced deformation modes (e.g., [34], [35]). Direct integration methods, particularly the Newmark method, have been widely used for analyzing asymmetric and shear-deformable thin-

walled members, capturing effects such as axial load, damping, and high-frequency dynamics (e.g., Xiang et al. [37], Carrera and Varello [38], Sahraei et al. [39], Yu et al. [40]).

An aspect common to the previous studies is the adoption of the principal directions to characterize the motion of the cross-section. While this approach simplifies the formulation, it has limitations related to the modelling of members with different boundary conditions along non-principal directions. Specifically, the ends of an angle member connected to a gusset plates can be considered as fixed about the axis normal to the gusset and nearly pinned about the axis of the gusset. Conventional solutions based on principal directions do not lend themselves to the direct modelling of such boundary conditions. In this respect, the present study develops a variational principle and finite element formulation that adopts non-principal directions to enable the seamless modelling of gusset-ended members. The analysis also captures coupling effects due to cross-sectional asymmetry, the destabilizing effect due to axial loads, warping effects, as well as rotatory effect within the framework of natural vibration and dynamic transient analyses.

Furthermore, as none of the previous studies have attempted to investigate the dynamic behavior of thin-walled steel members under pedestrian-induced moving loads, the present study adopts the models developed in the study to investigate to quantify the accelerations resulting from pedestrian induced load and assessing them against acceptable threshold accelerations.

1.6. Objectives

This research aims to develop an understanding of the dynamic response of thin-walled steel members subjected to human-induced excitations. The study addresses both the natural vibration and transient analysis for members with doubly symmetric, monosymmetric, and asymmetric angle sections under realistic boundary conditions. By employing a combination of analytical

methods and finite element formulations, the research investigates the influence of axial force magnitude, member slenderness, cross-sectional asymmetry, and connection details on the flexural and torsional vibration characteristics. The study further simulates realistic human-induced loading scenarios, including stationary and moving pedestrians, to evaluate displacement and acceleration responses against comfort thresholds. The ultimate objective is to establish reliable design criteria and vibration control strategies that can be applied to ensure the serviceability and acceptable dynamic performance of structural members in structures.

1.7. Thesis Overview

The thesis consists of six chapters

After the present introductory chapter, Chapter 2 develops criteria to control human-induced vibrations in steel members with doubly symmetric cross-sections. The study provides a description of typical time-dependent forcing functions induced by human walking as proposed by past researchers. Analytical solutions are then used to investigate the effect of axial force magnitude and type (i.e., compression or tension), member slenderness, and cross-sectional geometry on the pure flexural and pure torsional natural frequencies of the member. By postulating a natural frequency threshold aiming to avoid/control resonance phenomena under anticipated human-induced excitations, the study shows that consistent dynamic criteria depend not only on member slenderness, but also on the axial force level, and cross-sectional geometry.

Chapter 3 develops natural frequency criteria to control human-induced vibrations of axially loaded steel members with angle cross-sections. An analytical solution is developed for coupled flexural–torsional free vibration of pin-ended members with equal and unequal leg cross-sections. The natural vibration analysis is also extended to angle members with end gusset plate connections

though shell finite element modelling. The study investigates the effects of axial load in the member, load eccentricity, and cross-sectional dimensions on the natural frequency of the member. The results show the importance of considering axial load effects and end details on the natural frequency of the member.

Chapter 4 formulates a variational principle, a thin-walled beam finite element, and an energy-based approximate solution for the natural vibration analysis of thin-walled steel members with asymmetric cross-sections. A novel feature of the formulation is that it adopts non-principal directions for the displacements cross-section displacement, a feature that enables the seamless modelling angle members with end gusset plate connections. The solution is then used to conduct a systematic parametric study that investigates the effects of axial load, member slenderness ratio, cross-sectional geometry on the torsional flexural natural vibration analysis of angle members. A design-oriented dimensionless design chart is then developed to estimate the natural frequency of angle members.

While chapters 2-4 focus on the natural vibration analysis of thin-walled members, chapter 5 develops a finite element formulation for the transient dynamic analysis of thin-walled members subjected to time dependent forces. The solution incorporates the effects of axial loading, flexural-torsional coupling, warping, rotary inertia, and damping. The model is employed to characterize member accelerations generated by the vertical and horizontal components of dynamic forces induced by human walking. Parameters investigated include member span, axial load level, and walking speed. Member cross-sections investigated are doubly symmetric I-sections and Gusset-ended members with angle cross-sections. Scenarios investigated include walking on a treadmill and walking along the span at constant speed.

Chapter 6 concludes the study by presenting a summary of the main contributions, main conclusions and key findings, and recommendations for further research.

Apart from the present introductory chapter and the conclusion chapter, the thesis is written in a paper format. Where appropriate, supporting mathematical derivations and supplementary results are presented in Appendices A-N which are provided at the end of the thesis.

Figure 1.3 illustrates the methodological framework adopted in this thesis. All proposed solutions originate from the Hamiltonian principle. From this foundation, three types of approaches are developed: (a) the equations of motion and associated boundary conditions are derived through integration by parts (Chapters 4); (b) approximate solutions for characterizing natural frequencies are obtained by assuming suitable displacement functions (Chapters 4); and (c) finite element formulations are constructed for natural vibration analysis (Chapter 4) and transient vibration analysis (Chapter 5).

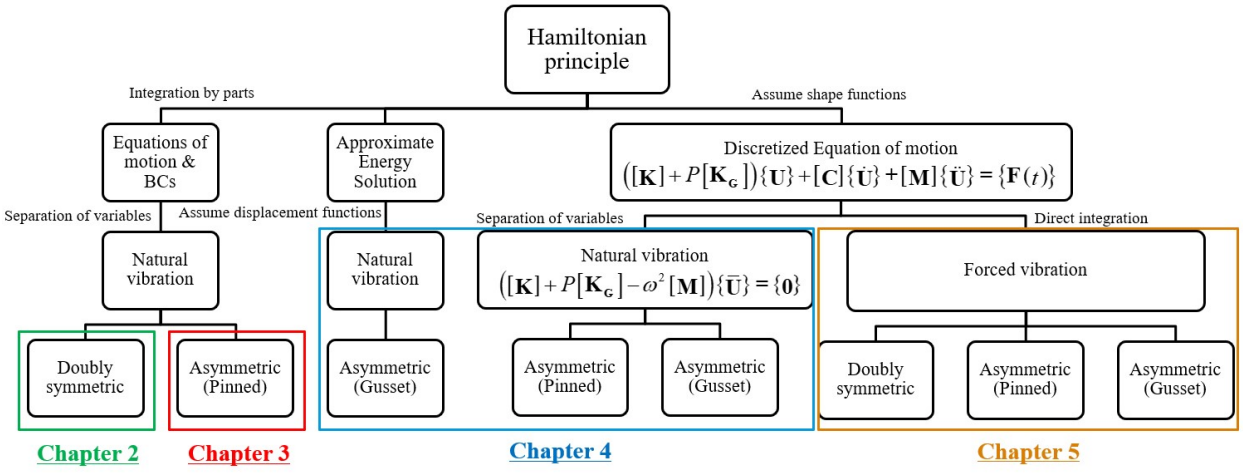

Figure 1.3 Overall methodological framework of the thesis

1.8.Notation

C_1 , C_2 : Numerical coefficients (Eq. 1.4)

f_{mi} : Heel-impact factor

f_s : Human step frequency

$F(t)$: Dynamic forcing function induced by human activity (Vertical component)

F_m : Maximum magnitude of the force Fourier series induced by walking

$G(t)$: Dynamic forcing function induced by human activity (Horizontal component)

K_p : Impact factor

N : Number of harmonics

Q : Human body weight

t : Time

t_s : Time duration of the step

T : Time period of the step

T_p : Time period of dancing load

α_i, β_i : Dynamic load factors

ϕ_i, λ_i : Phase angles

γ : Contact ratio

References

1. Allen, D., *ATC Design Guide 1: Minimizing floor vibrations (1st ed.).* . 1999, Redwood City, CA:: Applied Technology Council;.
2. Smith, A.L., S.J. Hicks, and P.J. Devine, *Design of floors for vibration: A new approach*. 2007: Steel Construction Institute Ascot, Berkshire, UK.
3. Bachmann, H. and W. Ammann, *Vibrations in structures: induced by man and machines*. Vol. 3. 1987: Iabse.
4. Živanović, S., A. Pavic, and P. Reynolds, *Vibration serviceability of footbridges under human-induced excitation: a literature review.* Journal of sound and vibration, 2005. **279**(1-2): p. 1-74.
5. Galbraith, F. and M. Barton, *Ground loading from footsteps.* The Journal of the Acoustical Society of America, 1970. **48**(5B): p. 1288-1292.
6. Ellis, B. and T. Ji, *Floor vibration induced by dance-type loads: verification.* Structural Engineer, 1994. **72**: p. 37-37.
7. Murray, T.M., Ungar, E. E., & Davis, D. B. , *Facts for Steel Buildings No. 5: Vibration.* . 2018: American Institute of Steel Construction (AISC).
8. Ellingwood, B. and A. Tallin, *Structural serviceability: floor vibrations.* Journal of Structural engineering, 1984. **110**(2): p. 401-418.
9. Rainer, J., G. Pernica, and D.E. Allen, *Dynamic loading and response of footbridges.* Canadian Journal of Civil Engineering, 1988. **15**(1): p. 66-71.
10. Murray, T.M., et al., *Vibrations of steel-framed structural systems due to human activity*. 2016: American Institute of Steel Construction.
11. ISO-10137, *International Organization for Standardization*, in *Bases for design of structures--serviceability of buildings and walkways against vibrations*. 2007, International Organization for Standardization: International Organization for Standardization.
12. Ingólfsson, E.T., C.T. Georgakis, and J. Jönsson, *Pedestrian-induced lateral vibrations of footbridges: A literature review.* Engineering Structures, 2012. **45**: p. 21-52.
13. Allen, D.E., J. Rainer, and G. Pernica, *Vibration criteria for assembly occupancies.* Canadian Journal of Civil Engineering, 1985. **12**(3): p. 617-623.

14. Pernica, G., *Dynamic load factors for pedestrian movements and rhythmic exercises.* Canadian Acoustics, 1990. **18**(2): p. 3-3.
15. Ebrahimpour, A. and R. Sack, *Design live loads for coherent crowd harmonic movements.* Journal of Structural Engineering, 1992. **118**(4): p. 1121-1136.
16. Pavic, A. and M. Willford, *Vibration serviceability of post-tensioned concrete floors.* Appendix G in post-tensioned concrete floors design handbook-technical report, 2005. **43**: p. 99-107.
17. Ellis, B. and T. Ji, *Loads generated by jumping crowds: numerical modelling.* Structural Engineer, 2004. **82**(17): p. 35-40.
18. Bachmann, H., *Vibration problems in structures: practical guidelines*. 1995: Springer Science & Business Media.
19. Young, P. *Improved floor vibration prediction methodologies*. in *ARUP vibration seminar*. 2001.
20. Zhang, S. and L. Xu, *Human-induced vibration of cold-formed steel floor systems: Parametric studies.* Advances in Structural Engineering, 2020. **23**(10): p. 2030-2043.
21. Gonçalves, M.S., A. Pavic, and R.L. Pimentel, *Vibration serviceability assessment of office floors for realistic walking and floor layout scenarios: Literature review.* Advances in Structural Engineering, 2020. **23**(6): p. 1238-1255.
22. Kappos, A.J., *Dynamic loading and design of structures.* . 2001, London, UK: : Spon Press.
23. BS-6399, *Loading for buildings.*, in *BS 6399: Part 1: Code of practice for dead and imposed loads.* 1996, British Standards Institution.
24. Ebrahimpour, A., Hamam, A., Sack, R. L., & Patten, W. N., *Measuring and modeling dynamic loads imposed by moving crowds.* Journal of Structural Engineering, 1996. **122(12)**: p. 1468-1474.
25. Allen, D. and T.M. Murray, *Design criterion for vibrations due to walking.* Engineering Journal, 1993. **30**(4): p. 117-129.
26. Hechler, O., et al. *Design guide for floor vibrations*. in *Proceedings of EuroSteel 2008 Conference*. 2008.
27. Willford, M., P. Young, and C. Field, *Predicting footfall-induced vibration: Part 1.* Proceedings of the Institution of Civil Engineers-Structures and Buildings, 2007. **160**(2): p. 65-72.

28. NBC-2015, *National Building Code of Canada 2015: Volume 2 – Commentaries (including Commentary A: Serviceability criteria for deflections and vibrations).* in *National Research Council of Canada.* 2015, Canadian Commission on Building and Fire Codes.: Ottawa, ON: .
29. Aalami, B.O., *Vibration design of concrete floors.* Redwood City: ADAPT Corporation, 2014.
30. NBC-1990, *National building code of Canada*. National Research Council Canada. Associate Committee on the National Building Code. 1990: Associate Committee on the National Building Code, National Research Council.
31. ISO-2631-2, *Evaluation of human exposure to whole-body vibration–Part 2: Human Exposure to continuous and shock-induced vibrations in buildings (1 to 80 Hz)*. 1989, International Standards Organization Geneva.
32. Chen, J., *Transient Analysis of stiffened panel structure by a finite strip-mode superposition method*, in *Advances in Steel Structures (ICASS'99)*. 1999, Elsevier. p. 839-847.
33. Abrate, S. *Transient response of beams, plates, and shells to impulsive loads*. in *ASME International Mechanical Engineering Congress and Exposition*. 2007.
34. Bebiano, R., D. Camotim, and N. Silvestre, *Dynamic analysis of thin-walled members using Generalised Beam Theory (GBT).* Thin-Walled Structures, 2013. **72**: p. 188-205.
35. Bebiano, R., et al., *Dynamic analysis of high-speed railway bridge decks using generalised beam theory.* Thin-Walled Structures, 2017. **114**: p. 22-31.
36. Pagani, A., et al., *Dynamic response of aerospace structures by means of refined beam theories.* Aerospace Science and Technology, 2015. **46**: p. 360-373.
37. Xiang, T., et al., *Dynamic analysis of thin-walled open section beam under moving vehicle by transfer matrix method.* Structural Engineering and Mechanics, 2008. **30**(5): p. 603-617.
38. Carrera, E. and A. Varello, *Dynamic response of thin-walled structures by variable kinematic one-dimensional models.* Journal of Sound and Vibration, 2012. **331**(24): p. 5268-5282.
39. Sahraei, A., et al., *Finite element formulation for the dynamic analysis of shear deformable thin-walled beams.* Thin-Walled Structures, 2022. **173**: p. 108989.

40. Yu, Y., et al., *Integrated Dynamic Analysis of Thin-Walled Beams: Coupled Bidirectional Bending, Torsion, and Axial Vibrations Under Axial Loads.* Applied Sciences, 2024. **14**(23): p. 11390.

41. Alenezi, A.M. and M. Mohareb, *Buckling solutions for compression members with end restraints defined along non-principal directions.* Journal of Constructional Steel Research, 2021. **181**: p. 106505.

Chapter 2: Natural frequency criteria for controlling human-induced vibrations in doubly symmetric Members [1]

2.1. Abstract

Present Canadian design standards for steel members prescribe a member slenderness limit of 200 for compression members and 300 for tension members to guard, in part, against excessive vibrations. The different threshold limits in both types of members reflect the fact that compressive forces tend to lower the natural frequency of members while tensile forces tend to increase it. The stepwise threshold slenderness limits presently provided in standards, while recognizing the influence of the type of axial force on the natural frequency of the member, do not reflect the effect of axial force magnitude within the member.

Within this context, the present study aims to present slenderness limits for axially loaded members associated with a more consistent serviceability criterion based on the natural vibration, which reflects the level of axial loading. Towards this goal, a parametric study is conducted on compressive and tensile members with doubly symmetric cross-sections by (a) developing a shell finite element model in ABAQUS based on stressed eigenvalue natural vibration analysis, and (b) closed-form analytical solutions.

The study examines the effect of cross-sectional geometry, axial load level, and connection details on the natural frequencies of axially loaded members and proposes slenderness limits aimed to control excessive vibrations under human activity.

[1] This chapter has been published as Tahmasebi, and H. Sahraei, A. and Mohareb, M. Slenderness limits to control vibrations in axially loaded members with doubly symmetric cross-sections. Proceedings of the Canadian Society of Civil Engineering Annual Conference CSCE, Niagara, 2024.

Keywords:

Wide flange sections, compression members, tension members, slenderness ratio, natural vibration, human activity, dynamic effects,

2.2. Introduction & literature review

Dynamic effects in steel buildings are principally induced by earthquakes and wind effects. Both effects have received significant attention in past research and correspondingly elaborate provisions have been provided in various codes and standards to tackle their effect either as quasi-static loads or as dynamic loads.

Additional dynamic effects can arise in steel buildings from human activities (e.g., Allen [1] and Smith et al. [2]) such as (1) Periodic loads induced by rhythmic human activities such as dancing and aerobics, (2) Transient loads arising from the movement of people, including walking, and running, and (3) Impulsive loads due to, for example, single jumps and heel-drop impacts. In this context, the present research explores the possibility of developing design criteria for limiting vibrations in axially loaded steel members subjected to human-induced activities, by controlling their fundamental natural frequency. The natural frequency of a member in turn depends on the cross-sectional properties of the member, its boundary conditions, and the level of axial loading in the member, in addition to the member's slenderness.

In this respect, Section E.2 of the Murray et al. [3] and Clause 10.4.2.1 for CAN/CSA-S16 [4] set a threshold effective slenderness ratio of 200 for compression members. For tension members, Section D.1 of Murray et al. [3] and Clause 10.4.2.2 CAN/CSA-S16 [4] set a recommended slenderness ratio of 300 with the permission to waive this limit under specific conditions. The slenderness limit is intended to facilitate the handling of members during construction and control

excessive vibrations under harmonic loads such as those induced in wind bracing designed for tension loads. Limiting the slenderness of a member indirectly controls its natural frequency and consequently influences its susceptibility to undergo vibrations induced by human activities.

Bachmann and Ammann [5] reported that the walking of a single pedestrian produces dynamic forces in all three directions (a) vertical (b) lateral and (c) longitudinal, induced by accelerating and decelerating of the mass of their body (e.g., Živanović et al. [6]). The vertical component of the force has the highest magnitude, and its effects have thus been investigated more than the lateral and longitudinal components.

A common approach is to express excitation due to human walking as a time-dependent concentrated force (e.g., Ellingwood and Tallin [7] and Rainer et al. [8]) in the form of a Fourier series. In this respect, design standards (e.g., Murray et al. [3] and ISO-10137 [9]) characterize the transverse force $F_w(t)$ induced by human-induced activities as

$$F_w(t) = Q + Q\sum_{i=1}^{N} \alpha_i \sin\left(2\pi i f_s t - \phi_i\right) \tag{2.1}$$

where Q is the static weight of the human, normally taken as $76Kg \times 9.81m/s^2 = 746N$, index $i = 1, 2...N$ denotes harmonic terms and N is the total number of harmonics needed to represent human activity and is normally taken as three or four (e.g., Murray et al. [3], ISO-10137 [9]), f_s is the human step frequency, t is the time, α_i is a dynamic load factor associated with the mode i and is defined as the ratio of the transverse force associated with the i^{th} harmonic to the body weight, and ϕ_i is the phase lag for the i^{th} harmonic. Thus, if, for example, the human step frequency f_s is 2.5 Hz, and the number of harmonics is taken as $N = 4$, it induces four harmonic forces with

frequencies $if_s = 2.5, 5.0, 7.5, \& 10$. Hence a floor with a fundamental natural frequency of around 10 Hz can exhibit resonance with the highest harmonic $i = 4$ of $F_w(t)$. Historically, NBC-1990 [10] stipulated that floors with fundamental natural frequencies less than 5 Hz are prone to resonance due to human rhythmic activities. This threshold was increased to 10 Hz in NBC-2015 [11] which also recognized that rhythmic activities such as dancing, foot stamping, jumping exercises, and walking induce periodic forces with exciting frequencies in the range of 1 to 4 Hz.

In addition to the vertical force component, a lateral force component is induced by human activities (Ingólfsson et al. [12]) which can take the form

$$F_v(t) = Q\sum_{i=1}^{N} \beta_i \sin(2\pi i f_s t - \phi_i) \qquad 2.2$$

where β_i is a dynamic load factor defined as the ratio of the lateral force associated with the i^{th} harmonic to the body weight. Bachmann and Ammann [5] reported the first five harmonics for the lateral forcing function induced by human walking. The authors reported that the first and third harmonics of the lateral forcing function are the dominant ones.

Table 2.1 provides the range of exciting frequencies induced by human activities including (a) footfall-dependent activities which include walking and running, and (b) rhythmic activities which include dancing, lively concerts, and aerobics. For footfall-dependent activities, most researchers recommend a step frequency f_s ranging from 1.5 to 2.5 Hz for walking, and a step frequency ranging from 1.6 to 4.0 Hz for running. For rhythmic activities, a step frequency ranging from 1.5 to 3 Hz has been recommended for dancing and lively concerts, and 2 to 4 Hz for aerobics.

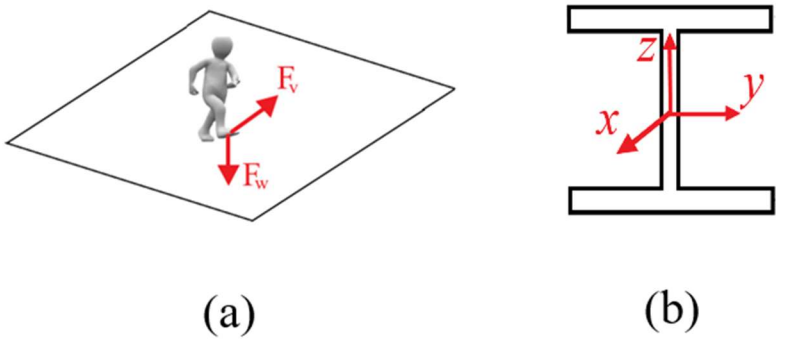

Figure 2.1 (a) Components of force induced by human walking, (b) Axes definition.

Table 2.1 Range of frequencies induced by human activities

	Activity	Source	Step frequency range (Hz)
Footfall dependent activities	Walking	Ebrahimpour [13]	1.5-2.5
		Bachmann [14]	
		Rainer et al. [8]	1.6-2.2
		Allen and Murray [15]	
		Hechler et al. [16]	1.6-2.5
		Willford et al. [17]	1.6-2.2
		Smith et al. [2]	
		Aalami [18]	1.8-2.1
	Running	Rainer et al. [8]	1.6 -4.0
		Bachmann et al. [14]	2.0-3.0
		ISO-10137 [9]	2.0-4.0
		Murray et al. [3]	1.6-4.0
		Huang et al. [19]	3.5
Rhythmic activities	Dancing	Aalami [18]	1.5-3.0
		NBC-2015 [11]	1.5-2.7
		Murray et al. [3]	
	Lively concert	Aalami [18]	1.5-3.0
		NBC-2015 [11]	1.5-2.7
		Murray et al. [3]	
	Aerobics	Aalami [18]	2.0-4.0
		NBC-2015 [11]	2.0-2.75
		Murray et al. [3]	

Table 2.2 provides a summary of dynamic load factors α_i, β_i and the corresponding phase angles ϕ_i reported by different authors. In addition, Allen et al. [20] reported that dynamic load factors for higher harmonics become substantial in the case of rhythmic activities. Conversely, the dynamic load factors induced by walking and jogging associated with higher harmonics are less significant, especially as the number of people in the crowd increases. Similar findings were reported by Ebrahimpour and Sack [21] who conducted experiments on rhythmic jumping activities.

Table 2.2 Parameters related to the vertical and lateral components of forcing function induced by human walking.

Author	Dynamic load factor α_i	Dynamic Load factor β_i	Phase angle ϕ_i	Comments
Bachmann et al. [5]		$\beta_1 = 0.039, \beta_2 = 0.010$ $\beta_3 = 0.043, \beta_4 = 0.012$ $\beta_5 = 0.015$		$if_s = 2.0Hz \ \ (i = 1)$
Bachmann et al. [14]	$\alpha_1 = 0.4,$ $\alpha_2 = \alpha_3 = 0.1$		$\phi_1 = 0$ $\phi_2 = \pi/2$ $\phi_3 = \pi/2$	$if_s = 2.0 - 2.4Hz \ \ (i = 1)$
Bachmann et al. [14]		$\beta_1 = \beta_3 = 0.1$		$if_s = 2.0Hz \ \ (i = 1)$
ISO 10137[9]	$\alpha_1 = 0.37(f_s - 1)$ $\alpha_2 = 0.1$ $\alpha_3 = \alpha_4 = 0.06$			
Young [22]	$\alpha_1 = 0.37(f_s - 0.95) \le 0.5$ $\alpha_2 = 0.0044(f_s + 12.27)$ $\alpha_3 = 0.005(f_s + 5.2)$ $\alpha_4 = 0.0051(f_s + 1.96)$			$if_s = 2.0Hz \ \ (i = 1)$
Pavic and Willford [23]	$\alpha_1 = 0.41(f_s - 0.95)$ $\alpha_2 = 0.0056(f_s + 12.3)$ $\alpha_3 = 0.0064(f_s + 5.2)$ $\alpha_4 = 0.0065(f_s + 2.0)$		$\phi_1 = 0$ $\phi_2 = \pi/2$ $\phi_3 = \pi/2$ $\phi_4 = \pi/2$	$if_s = 1.8Hz \quad (i = 1)$

Smith [2]	$\alpha_1 = 0.436\left(f_s - 0.95\right)$ $\alpha_2 = 0.006\left(f_s + 12.3\right)$ $\alpha_3 = 0.007\left(f_s + 5.2\right)$ $\alpha_4 = 0.007\left(f_s + 2.0\right)$		$\phi_1 = 0$ $\phi_2 = -\pi/2$ $\phi_3 = 0$ $\phi_4 = \pi/2$	$1.8i \le if_s \le 2.2i \left(i = 1..4\right)$
Ingólfsson et al. [12]		$\beta_1 = 0.05$ $\beta_2 = 0.04$ $\beta_3 = 0.01$		$if_s = \left(2i - 1\right) f_s \left(i = 1 \text{ to } 3\right)$

2.3. Analytical Solution

The natural vibration response of an axially loaded member with a doubly symmetric cross-section subjected to a compressive force P is governed by the differential equation of motion (e.g., Vlasov [24])

$$
\begin{aligned}
&EI_z \frac{\partial^4 w}{\partial x^4} + P\frac{\partial^2 w}{\partial x^2} + m\frac{\partial^2 w}{\partial t^2} = 0 \\
&EI_y \frac{\partial^4 v}{\partial x^4} + P\frac{\partial^2 v}{\partial x^2} + m\frac{\partial^2 v}{\partial t^2} = 0 \\
&EI_\omega \frac{\partial^4 \theta}{\partial x^4} - \left(GJ - P\frac{I_0}{A}\right)\frac{\partial^2 \theta}{\partial x^2} + \rho\left(I_0 \frac{\partial^2 \theta}{\partial t^2} - I_\omega \frac{\partial^4 \theta}{\partial x^2 \partial t^2}\right) = 0
\end{aligned}
\qquad 2.3\text{(a-c)}
$$

which E is the young modulus, G is the shear modulus, J is the Saint-Venant torsional constant, m is the mass of the member per unit length, v, w are the displacements in the plane of the cross-section, θ is the angle of twist, I_y, I_z are the moment of inertia about the weak and strong axes, I_0 is the polar moment of inertia, and I_ω is the warping constant. The equations of motion presented are based on the Vlasov thin-walled beam theory, postulating that the cross-section moves as a rigid in its own plane and that the shear strains within the mid-surface are deemed negligible. The equations omit the effect of damping. For natural vibration, the displacement field

can be assumed to take the form $v(x,t)=V(x)\sin\omega_y t, w(x,t)=W(x)\sin\omega_z t$, and $\theta(x,t)=\phi(x)\sin\omega_x t$. in which ω_z,ω_y and ω_x respectively represent the flexural natural frequencies about the weak axis, the strong axis, and the torsional natural frequency. By substituting into Eq. 2.3(a-c) one obtains

$$\begin{aligned} &EI_z\frac{d^4W}{dx^4}+P\frac{d^2W}{dx^2}-m\omega_z^2W=0\\ &EI_y\frac{d^4V}{dx^4}+P\frac{d^2V}{dx^2}-m\omega_y^2V=0\\ &EI_\omega\frac{\partial^4\phi}{\partial x^4}-\left(GJ-P\frac{I_0}{A}-\rho I_\omega\omega_x^2\right)\frac{\partial^2\phi}{\partial x^2}-\rho I_0\omega_x^2\phi=0 \end{aligned} \qquad 2.4\text{(a-c)}$$

The corresponding solution takes the form

$$\begin{aligned} W(x)&=B_1\sin(\alpha_1 x)+B_2\cos(\alpha_1 x)+B_3\sinh(\alpha_2 x)+B_4\cosh(\alpha_2 x)\\ V(x)&=A_1\sin(\beta_1 x)+A_2\cos(\beta_1 x)+A_3\sinh(\beta_2 x)+A_4\cosh(\beta_2 x)\\ \phi(x)&=C_1\sin\lambda_1 x+C_2\cos\lambda_1 x+C_3\sinh\lambda_2 x+C_4\cosh\lambda_2 x \end{aligned} \qquad 2.5\text{(a-c)}$$

in which A_1-A_4, B_1-B_4 and C_1-C_4 are integration constants to be obtained from the boundary conditions, and $\alpha_1,\alpha_2,\beta_1,\beta_2,\lambda_1,\lambda_2$ are given by

$$\begin{aligned} \alpha_1&=\sqrt{\frac{P}{2EI_z}+\sqrt{\left(\frac{P}{2EI_z}\right)^2+\frac{m\omega_z^2}{2EI_z}}} \qquad \alpha_2=\sqrt{-\frac{P}{2EI_z}+\sqrt{\left(\frac{P}{2EI_z}\right)^2+\frac{m\omega_z^2}{2EI_z}}}\\ \beta_1&=\sqrt{\frac{P}{2EI_y}+\sqrt{\left(\frac{P}{2EI_y}\right)^2+\frac{m\omega_y^2}{2EI_y}}} \qquad \beta_2=\sqrt{-\frac{P}{2EI_y}+\sqrt{\left(\frac{P}{2EI_y}\right)^2+\frac{m\omega_y^2}{2EI_y}}}\\ \lambda_1&=\sqrt{\frac{1}{2EI_\omega}\left(GJ-P\frac{I_0}{A}-\rho I_\omega\omega_x^2\right)+\frac{1}{2EI_\omega}\sqrt{\left(GJ-P\frac{I_0}{A}-\rho I_\omega\omega_x^2\right)^2+4\rho EI_\omega I_0\omega_x^2}}\\ \lambda_2&=\sqrt{-\frac{1}{2EI_\omega}\left(GJ-P\frac{I_0}{A}-\rho I_\omega\omega_x^2\right)+\frac{1}{2EI_\omega}\sqrt{\left(GJ-P\frac{I_0}{A}-\rho I_\omega\omega_x^2\right)^2+4\rho EI_\omega I_0\omega_x^2}} \end{aligned} \qquad 2.6\text{(a-f)}$$

For a simply supported member, $W, W'', V, V'', \phi, \phi''$ vanish at both ends. By substituting into Eq. 2.5, placing the resulting equations into a matrix form, and setting to zero the determinant of the matrix of coefficients, one obtains $\alpha_2, \beta_2, \lambda_2 = n\pi/l$, which leads to the solution[2]

$$\omega_z = \frac{\pi^2}{l}\sqrt{\frac{EA}{m}}\frac{\sqrt{1-\left(P/P_{E-z}\right)}}{\left(l/r_z\right)},\quad \omega_y = \frac{\pi^2}{l}\sqrt{\frac{EA}{m}}\frac{\sqrt{1-\left(P/P_{E-y}\right)}}{\left(l/r_y\right)}$$
$$\omega_x = \frac{\pi^2}{l}\sqrt{\frac{EA+\pi^2\left(GJAl^2/I_\omega\right)}{m\left(Ar_0^{\,4}/I_\omega\right)}}\sqrt{\frac{1-P/P_{E-x}}{\pi^2 I_\omega/\left(Ar_0^{\,4}\right)+\left(l/r_0\right)^2}} \qquad 2.7\ (\text{a-c})$$

in which $\left(P_{E-z}, P_{E-y}, P_{E-x}\right) = \left\{\left(\pi/l\right)^2 EI_z,\quad \left(\pi/l\right)^2 EI_y,\quad \left[EI_\omega\left(\pi/l\right)^2 + GJ\right]\Big/ r_0^2\right\}$ are the elastic buckling loads corresponding to flexure about the weak and strong axes and the torsional buckling load, respectively, r_z, r_y are the radii of gyration about weak and strong axes, $r_0 = \sqrt{r_z + r_y}$. Eq. 2.7 , shows the dependency of the natural frequency on the axial load ratio as well as the slenderness ratio. As expected, when the axial load approaches the elastic buckling load, Eq. 2.7 predicts a natural frequency of zero.

2.4. Reference Case

A 5m span axially loaded member with W200x52 cross-section ($A = 6650mm^2$, $I_y = 5.27\times10^{-5}m^4, I_z = 1.78\times10^{-5}m^4, r_y = 89mm, r_z = 51.8mm, m = 52.1kg/m$) is considered as a reference case. The maximum slenderness ratio of the member is $0 < l/r_z = 96.5 < 200$, i.e., the chosen member has an intermediate length. Steel properties are $\left(F_y = 350MPa, E = 2\times10^5\ MPa, G = 7.7\times10^4\ MPa\right)$. The member is assumed to be simply

[2] Calculations related to the analytical solution are provided in Appendix A and Appendix B

supported in all three directions. The member is assumed to be subjected to an axial force *P* which is the percentage of elastic buckling loads.

2.5. Finite Element Models

The natural frequency of the member is determined based on the closed-form solution in Eq. 2.7 , a model based on the thin-walled beam B31OS element as well as a model based on the shell finite element S4, both in the ABAQUS library.

The B31OS[3] element in ABAQUS is a two-node thin-walled beam element with seven degrees of freedom (DOFs) per node; three displacements, three rotations, and a warping deformation. The element captures global warping effects. A mesh study has shown that convergence is achieved with less than 100 elements along the span. The displacements along the lateral, transverse, and longitudinal directions were restrained at one end and along the lateral and transverse directions at the other end. The analysis involves two steps: In the first step, the element is axially loaded by a force *P.* In the second step, the stressed natural frequency of the member is computed by evoking the geometric nonlinear feature of ABAQUS.

[3] The B31OS element in ABAQUS/Standard is a two-node thin-walled beam element that captures warping effects. Hence, it is particularly suited for modeling members such as I-, channel-, and angle-sections, where cross-sectional warping plays a significant role. The element uses linear interpolation for the displacement and rotation and warping fields and predicts the axial force, bending moments, shearing forces, twisting moment, and bimoments.

The S4 element [4] is a four-node quadrilateral element with six degrees of freedom per node, three translations, and three rotations. To simulate the boundary conditions in the shell model, the displacements in the lateral, transverse, and longitudinal directions were restrained at the bottom flange-to-web junction at one end of the beam, while restraining the lateral and transverse directions displacements of the bottom flange-to-web junction along the other end. Also, the lateral displacements were restrained at the top flange-to-web junctions at both ends of the beam.

The EQUATION feature in ABAQUS was utilized to suppress cross-sectional distortion across all sections on the span and to enforce the first Vlasov assumption regarding the rigidity of the cross-section within its own plane.

Again, the analysis was done in Two steps. The axial loading is initially lumped at the four flange tips at both ends. Subsequently, the natural frequency of the member is determined through a natural vibration analysis. Nonlinear geometric effects are evoked to capture second-order effects of the axial load effect on the computed natural frequency. A mesh study was conducted for the S4 model. Two meshes were attempted for the unloaded reference member. The first one had two elements along the flange width, two elements along the web height, and 100 elements along the longitudinal axis of the member, totaling 600 elements. A finer mesh was attempted with four elements per flange, four elements along the web height, and 200 along the longitudinal axis of the member, totaling 2400 elements. The predicted fundamental natural frequency based on the

[4] The S4 element in ABAQUS/Standard is a four-node, quadrilateral, general-purpose shell element featuring finite membrane strain. The element uses a full integration, thus eliminating the possibility of spurious zero-energy modes and avoiding the need for hourglass control. To prevent shear locking, an assumed-strain approach is applied to the membrane strain field, while transverse shear strains are assumed constant through the thickness, providing accurate out-of-plane bending response. Owing to its robust formulation, the S4 element offers high accuracy in modeling both bending and membrane actions, making it particularly suitable for problems involving large deflections, finite membrane strains, and thin- to moderately thick shell structures.

first mesh was found to be 16.36 Hz while that based on the second mesh was 16.28 Hz, a difference of less than 0.5 percent. Comparatively, the fundamental natural frequency based on the closed-form solution was found to be 16.44 Hz.

2.6. Slenderness limits

Solving Eqs. 2.7 for the slenderness ratios l/r_z, l/r_y, and l/r_0 corresponding to the target frequencies ω_z, ω_y, and ω_x, yields

$$\begin{aligned}
\left(l/r_z\right) &\le \frac{\pi^2}{l}\sqrt{\frac{EA}{m}}\frac{\sqrt{1-\left(P/P_{E-z}\right)}}{\omega_z} = \left(l/r_z\right)_{P=0}\sqrt{1-\left(P/P_{E-z}\right)} \\
\left(l/r_y\right) &\le \frac{\pi^2}{l}\sqrt{\frac{EA}{m}}\frac{\sqrt{1-\left(P/P_{E-y}\right)}}{\omega_y} = \left(l/r_y\right)_{P=0}\sqrt{1-\left(P/P_{E-y}\right)} \qquad \text{2.8(a-c)} \\
\left(l/r_0\right) &\le \frac{\pi}{r_0}\sqrt{\frac{\pi^2 A\left[EI_\omega + GJ\left(l/\pi\right)^2\right]}{mI_0}\frac{\left(1-P/P_{E-x}\right)}{\omega_x^2} - I_\omega/I_0}
\end{aligned}$$

in which the slenderness ratios of the unloaded member are associated with target natural frequencies ω_z, ω_y, and ω_x are respectively $\left(l/r_z\right)_{P=0} = \left(\pi^2/l\sqrt{EA/m}\right)\Big/\omega_z$, $\left(l/r_y\right)_{P=0} = \left(\pi^2/l\sqrt{EA/m}\right)\Big/\omega_y$ and $\left(l/r_0\right)_{P=0} \le \frac{\pi}{r_0}\sqrt{\left(\pi^2 A\left[EI_\omega + GJ\left(l/\pi\right)^2\right]\right)\Big/mI_0\omega_x^2 - I_\omega/I_0}$.

2.7. Comparison with Finite Element Model

Eq. 2.7a-b can be expressed in a dimensionless form by dividing both sides by $\pi^2/l\sqrt{EA/m}$. Also, Eq. 2.7c can be expressed in a dimensionless form by dividing both sides by $\pi^2/l\sqrt{\left(EA+\pi^2 GJAl^2/I_\omega\right)\Big/\left(mAr_0^4/I_\omega\right)}$ yielding

$$\bar{\omega}_z = \frac{\sqrt{1-\left(P/P_{E-z}\right)}}{\left(l/r_z\right)} \quad , \quad \bar{\omega}_y = \frac{\sqrt{1-\left(P/P_{E-y}\right)}}{\left(l/r_y\right)} \quad , \quad \bar{\omega}_x = \sqrt{\frac{1-P/P_{E-x}}{\pi^2 I_\omega/\left(Ar_0^4\right)+\left(l/r_0\right)^2}} \qquad 2.9\text{(a-c)}$$

in which $\bar{\omega}_z, \bar{\omega}_y, \bar{\omega}_x$ are the normalized natural frequencies, and P is taken as positive when in compression.

Figure 2.2(a-c) depicts the interaction between the natural frequency and axial load magnitude for the three natural vibration modes. Close agreement is observed between the predictions of the closed-form solutions, the B31OS thin-walled beam model, and the S4 shell model. Increasing the compressive axial load is observed to reduce the natural frequency, making the member more prone to vibrate under dynamic loads. When the applied load approaches the elastic buckling load, the natural frequency is observed to tend toward zero.

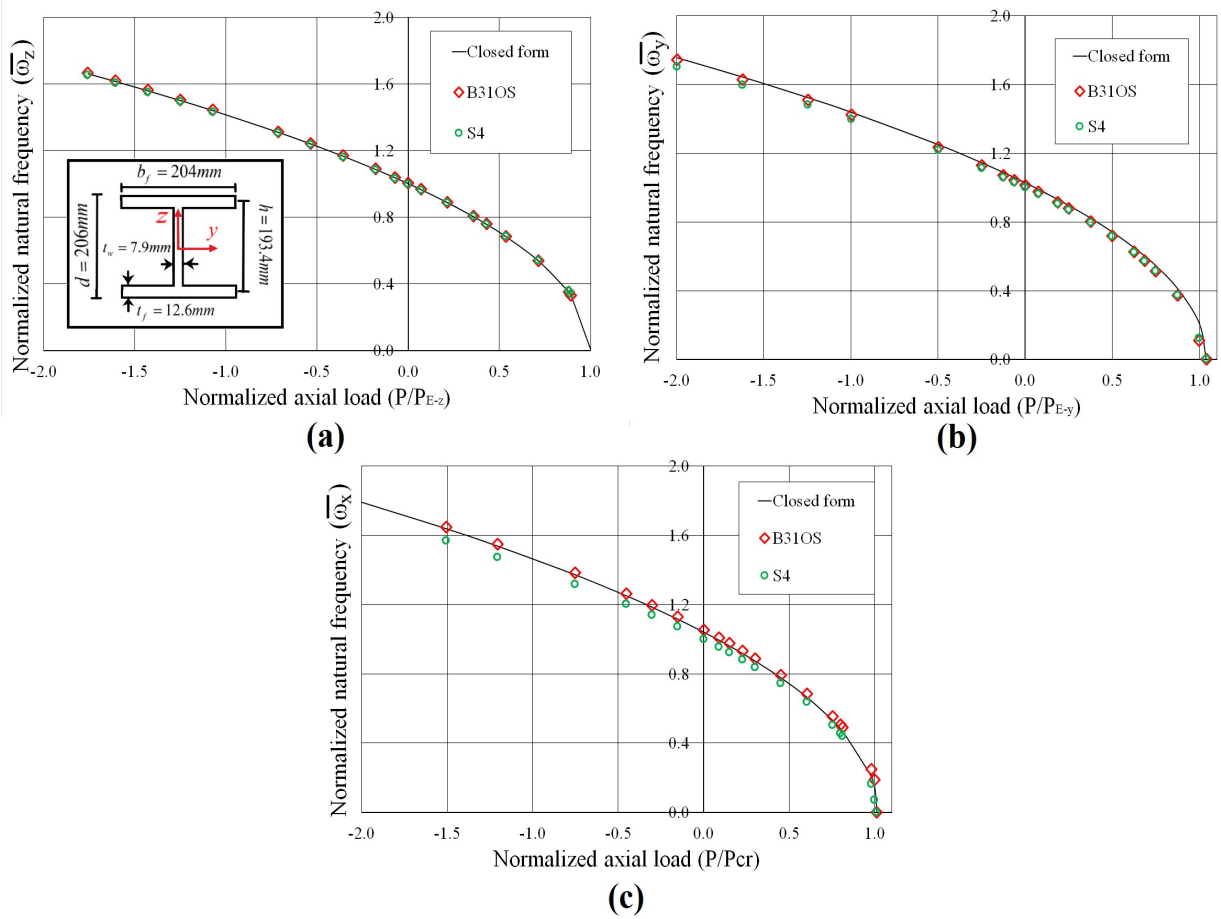

Figure 2.2 Normalized interaction diagrams for natural frequency versus axial load corresponding to (a) weak axis flexure, (b) strong axis flexure (c) torsion,

2.8. Framework for controlling the natural frequency

Present slenderness thresholds in design standards provide an indirect means to control the natural frequency of the axially loaded member. While they stipulate different slenderness threshold values that depend on the type of axial loading (tension versus compression), they do not capture the influence of the magnitude of the applied axial load.

An improved means of controlling the natural frequency of an axially loaded member would need to account for the level of axial loading acting on the member. For a tension member, the applied force cannot exceed the member's tensile resistance T_r, i.e., $-T_r \le P \le 0$ in which

$T_r = \text{Min}\left(\phi A_g F_y, \phi_u A_n F_u, \phi_u A_{ne} F_u\right)$, where ϕ is resistance factor, ϕ_u is the resistance factor for fracture, A_g is the gross area, A_n is the equivalent net area, A_{ne} is the effective net area for shear lag, F_y is the yield strength of the steel, and F_u is its tensile strength. Also, for a compression member, the applied force cannot exceed the compressive resistance C_r of the member i.e., $0 \le P \le C_r$ in which $C_r = \phi A F_y \left(1+\lambda^{2n}\right)^{-1/n}$, $\lambda = \left(KL/r\right)\sqrt{F_y/\pi^2 E}$, and $n = 1.34$.

The natural frequency computations were conducted for all sections in the W150, W200, W250, W310, W360, W410, and W460 series of the Handbook of the Steel Construction, and the natural frequencies $\omega_z, \omega_y, \omega_x$ versus the smaller radius of gyration r_z is reported in Figure 2.3 in the presence and the absence of the maximum axial loading as predicted by the relevant resistance equations. In all cases, member spans were taken to correspond to the slenderness threshold (i.e., $l/r_{\min} = 300$ for tension members and $kl/r_{\min} = l/r_{\min} = 200$ for compression members). Adopting the threshold maximum slenderness values of 200 and 300 is intended to tackle the longest

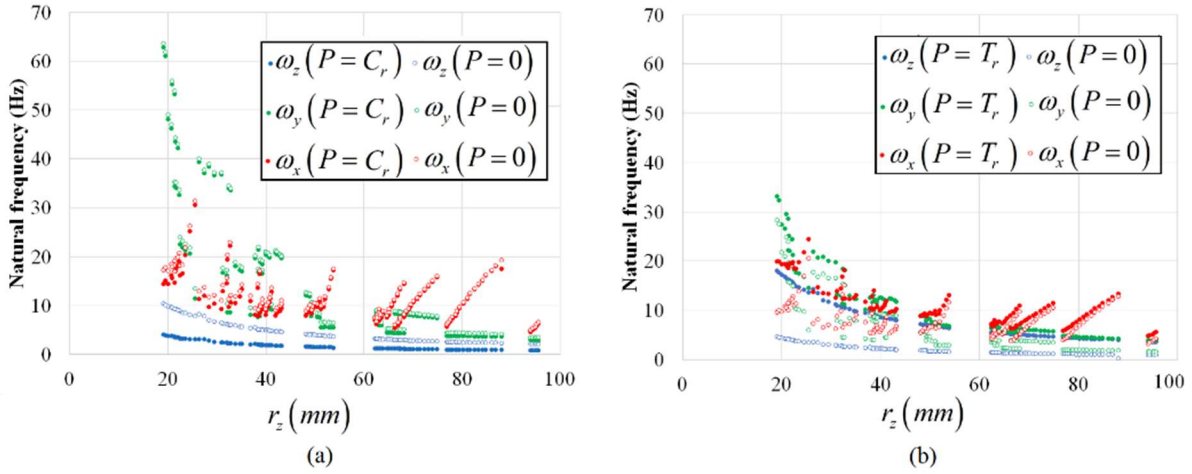

members that are the most prone to vibration.

Figure 2.3 Natural frequencies versus minimum radius of gyration for (a) compression members, and (b) tensile members.

Figure 2.3a shows that compressive forces reduce the natural frequency of the member, as expected. The reduction in the natural frequency ω_z corresponding to the flexural mode about the weak axis is considerable. For example, the most pronounced reduction in natural frequency is observed to correspond to r_z = 19.5 mm, in which case, the natural frequency ω_z drops from 10.14 Hz when the member is unloaded to 4.03 Hz when the member is subjected to an axial compressive force C_r.

Figure 2.3a shows that the weak axis flexural mode of vibration ω_z corresponds to the lowest natural frequency for all cross-sections. The magnitude of the torsional natural frequency ω_x and flexural frequency about the strong axis ω_y highly depend on the radius of gyration, with $\omega_x > \omega_y$ in some cases and $\omega_x < \omega_y$ with no discernable trend.

Figure 2.3b shows that the presence of tensile axial forces increases the natural frequency of the member. The increase in natural frequency ω_z corresponding to the weak axis flexural mode is significant. For instance, for r_z = 19.5 mm, the natural frequency ω_z increases from 4.5 Hz when the member is unloaded to 17.63 Hz when the member is subjected to the peak tension load T_r.

For the W150, W200, W250, W310, W360, W410, and W460 series, the compressive axial load is set to the member axial resistance C_r. By adopting a target natural frequency value of 12 Hz for $\omega_z, \omega_y, \omega_z$ (i.e., 1.2 x the highest exciting frequency induced by a human step of 2.5 Hz), the corresponding threshold lengths are determined from Eqs. 8(a-c), which are then normalized relative to r_z. The predicted slenderness limits l/r_z are depicted in Figure 2.4 which shows the

minimum, average, and maximum values obtained for each series. As a general trend, the threshold slenderness l/r_z is observed to decrease with member size, i.e., the W150 series corresponds to the highest l/r_z values and the W460 series corresponds to the lowest values. Similar plots are provided in Figure 2.5 for tension members with similar trends.

2.9. Summary and conclusion

The present research focused on the natural vibration analysis of axially loaded steel members with doubly symmetric sections in relation to dynamic effects associated with human activities, with a primary objective goal to develop criteria for mitigating excessive transient dynamic effects under human activities.

While present standards stipulate slenderness limits for compression members that are lower than those for tension members, and hence implicitly recognize the comparatively detrimental effect of compressive forces on the member's natural frequency, it was shown that more consistent dynamic criteria require accounting for the magnitude axial force within the member, as well as its cross-sectional properties.

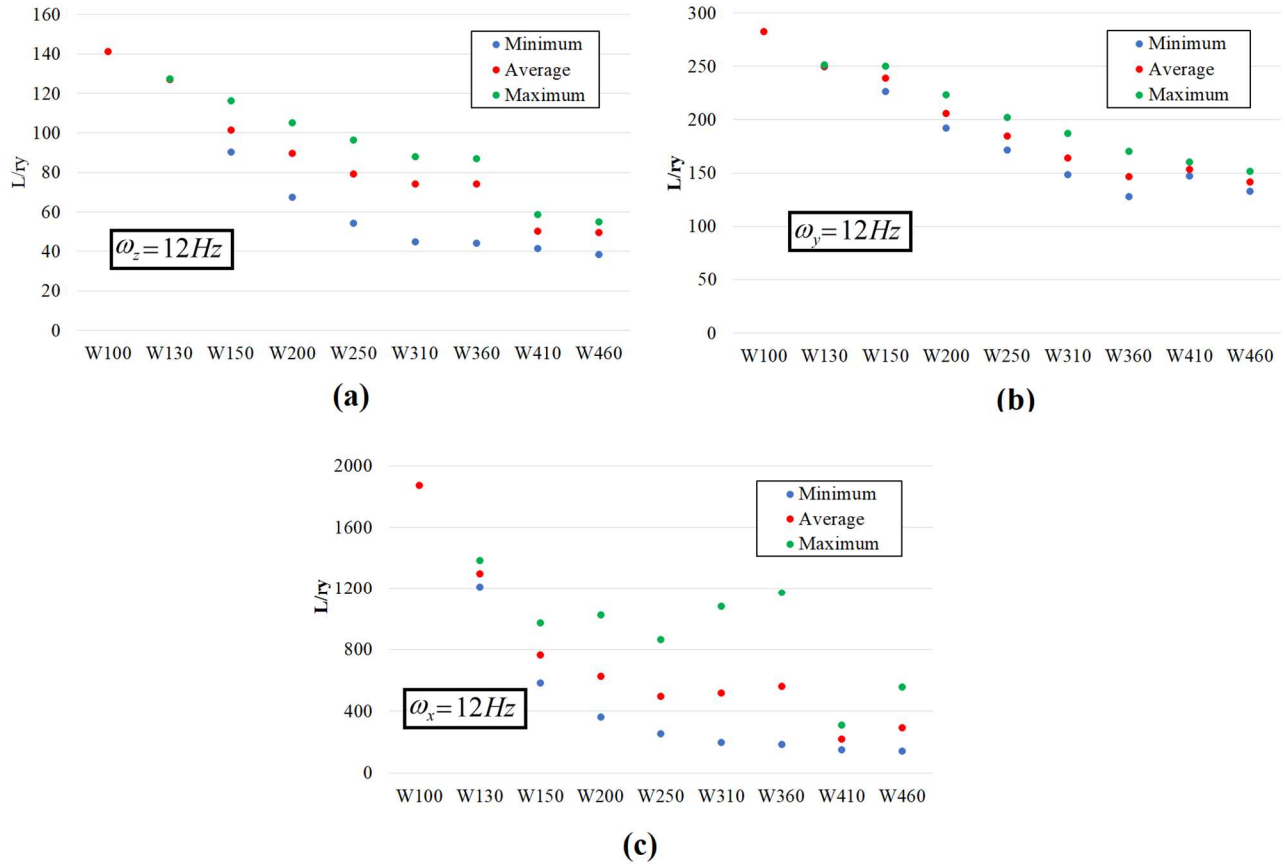

Figure 2.4 Required slenderness limits for compression members corresponding to $\omega = 12Hz$ based on (a) weak axis flexural mode, (b) strong axis flexural mode, and (c) torsional mode.

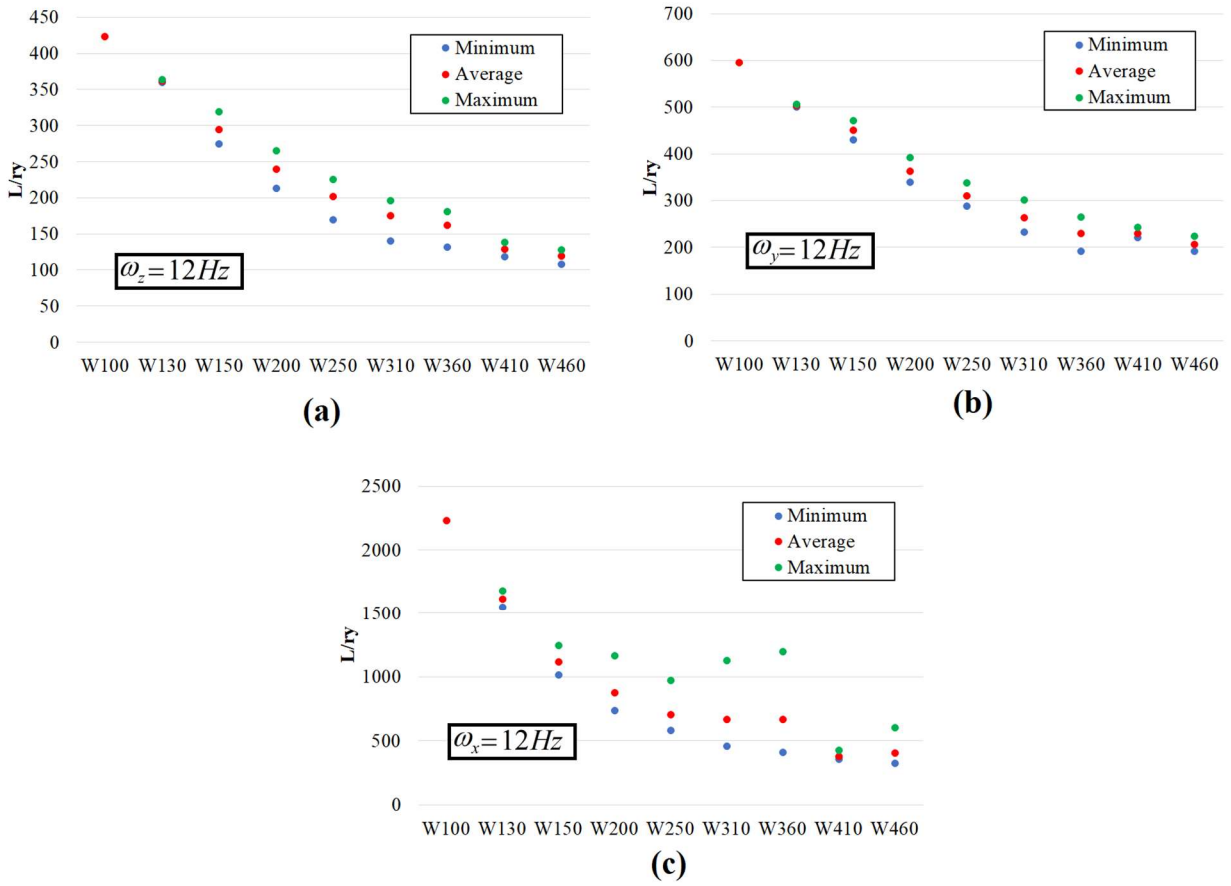

Figure 2.5 Required slenderness limits for tensile members corresponding to $\omega = 12Hz$ based on (a) weak axis flexural mode, (b) strong axis flexural mode, and (c) torsional mode.

2.10. Notation

A : Area

A_g : Gross area

A_n : Equivalent net area

A_{ne} : Effective net area for shear lag

$A_1 - A_4$, $B_1 - B_4, C_1 - C_4$: Integration constants

C_r : Compressive resistance

E : Elasticity modulus

F_y : Yield strength

$F_v(t)$: Lateral component of forcing function induced by human activities

$F_w(t)$: Transverse component of forcing function induced by human activities

F_u : Tensile strength

f_s : Human step frequency

G : Shear modulus

I_y, I_z : Moments of inertia about y and z axis

I_ω : Warping constant

I_0: Polar moment of inertia

J : Saint-Venant torsional constant

l: Length

m : Mass per unit length

N : Number of harmonics

P : Axial load

$P_{E-z}, P_{E-y}, P_{E-x}$: Elastic buckling loads corresponding to flexure about the weak and strong axes and the torsional buckling load

Q : Human body weight

r_z, r_y : Radii of gyration about weak and strong axes

t: Time

T_r : Tensile resistance

v, w, θ_x : In-plane displacements and angle of twist

α_i : Dynamic load factors for harmonic i related to transverse component of forcing function

β_i : Dynamic load factors for harmonic i related to lateral component of forcing function

ϕ_i : Phase angle for harmonic i related to transverse component of forcing function

ϕ_u : Resistance factor for fracture

$\omega_z, \omega_y, \omega_x$: Flexural natural frequencies about the weak axis, the strong axis, and the torsional natural frequency

$\bar{\omega}_z, \bar{\omega}_y, \bar{\omega}_x$: Normalized natural frequencies

2.11. References

1. Allen, D., *ATC Design Guide 1: Minimizing floor vibrations (1st ed.).* . 1999, Redwood City, CA:: Applied Technology Council;.
2. Smith, A.L., S.J. Hicks, and P.J. Devine, *Design of floors for vibration: A new approach*. 2007: Steel Construction Institute Ascot, Berkshire, UK.
3. Murray, T.M., et al., *Vibrations of steel-framed structural systems due to human activity*. 2016: American Institute of Steel Construction.
4. CAN/CSA-S16, *Design of steel structures,Canada*, in *CSA S16:19*. 2019, Canadian Standard Association: Toronto: CSA.
5. Bachmann, H. and W. Ammann, *Vibrations in structures: induced by man and machines*. Vol. 3. 1987: Iabse.
6. Živanović, S., A. Pavic, and P. Reynolds, *Vibration serviceability of footbridges under human-induced excitation: a literature review.* Journal of sound and vibration, 2005. **279**(1-2): p. 1-74.
7. Ellingwood, B. and A. Tallin, *Structural serviceability: floor vibrations.* Journal of Structural engineering, 1984. **110**(2): p. 401-418.
8. Rainer, J., G. Pernica, and D.E. Allen, *Dynamic loading and response of footbridges.* Canadian Journal of Civil Engineering, 1988. **15**(1): p. 66-71.
9. ISO-10137, *International Organization for Standardization*, in *Bases for design of structures--serviceability of buildings and walkways against vibrations*. 2007, International Organization for Standardization: International Organization for Standardization.
10. NBC-1990, *National building code of Canada*. National Research Council Canada. Associate Committee on the National Building Code. 1990: Associate Committee on the National Building Code, National Research Council.
11. NBC-2015, *National Building Code of Canada 2015: Volume 2 – Commentaries (including Commentary A: Serviceability criteria for deflections and vibrations).* in *National Research Council of Canada.* 2015, Canadian Commission on Building and Fire Codes.: Ottawa, ON: .

12. Ingólfsson, E.T., C.T. Georgakis, and J. Jönsson, *Pedestrian-induced lateral vibrations of footbridges: A literature review.* Engineering Structures, 2012. **45**: p. 21-52.
13. Ebrahimpour, A., Hamam, A., Sack, R. L., & Patten, W. N., *Measuring and modeling dynamic loads imposed by moving crowds.* Journal of Structural Engineering, 1996. **122(12)**: p. 1468-1474.
14. Bachmann, H., *Vibration problems in structures: practical guidelines*. 1995: Springer Science & Business Media.
15. Allen, D. and T.M. Murray, *Design criterion for vibrations due to walking.* Engineering Journal, 1993. **30**(4): p. 117-129.
16. Hechler, O., et al. *Design guide for floor vibrations*. in *Proceedings of EuroSteel 2008 Conference*. 2008.
17. Willford, M., P. Young, and C. Field, *Predicting footfall-induced vibration: Part 1.* Proceedings of the Institution of Civil Engineers-Structures and Buildings, 2007. **160**(2): p. 65-72.
18. Aalami, B.O., *Vibration design of concrete floors.* Redwood City: ADAPT Corporation, 2014.
19. Huang, H., Y. Gao, and W.-S. Chang, *Human-induced vibration of cross-laminated timber (CLT) floor under different boundary conditions.* Engineering Structures, 2020. **204**: p. 110016.
20. Allen, D.E., J. Rainer, and G. Pernica, *Vibration criteria for assembly occupancies.* Canadian Journal of Civil Engineering, 1985. **12**(3): p. 617-623.
21. Ebrahimpour, A. and R. Sack, *Design live loads for coherent crowd harmonic movements.* Journal of Structural Engineering, 1992. **118**(4): p. 1121-1136.
22. Young, P. *Improved floor vibration prediction methodologies*. in *ARUP vibration seminar*. 2001.
23. Pavic, A. and M. Willford, *Vibration serviceability of post-tensioned concrete floors.* Appendix G in post-tensioned concrete floors design handbook-technical report, 2005. **43**: p. 99-107.
24. Vlasov, V.Z., *Thin-walled elastic beams.* PST Catalogue, 1959. **428**.

Chapter 3: Natural frequency criteria for controlling human-induced vibrations in angle Members [5]

3.1. Abstract

The susceptibility of axially loaded steel members with angle cross-sections to vibrations depends on their fundamental natural frequency. Design steel standards guard against excessive vibrations by enforcing slenderness limits of 200 for compression members and 300 for tension members. This approach indirectly controls the member's natural vibration but does not reflect the effect of axial force level within the member, nor the type of connection at the member ends on its susceptibility to excessive vibrations.

For members with angle cross-sections, in which the shear centre is offset from the section centroid, the fundamental vibration mode involves a combination of flexure and torsional deformations. The corresponding natural frequency depends on the cross-section geometry, member span, level of axial loading with the member, end connection details, and the eccentricity of the axial relative to gusset plates at both ends of the member. Within this context, the present study presents the results of a parametric study that investigates such effects by conducting a series of natural vibration analyses based on a stressed eigen-value type of solution, for a spectrum of compressive and tensile members with angle cross-sections. The analyses are based on closed-form solutions and shell finite element models developed in ABAQUS. The study presents a step towards proposing refined slenderness limits for axially loaded members.

[5] This chapter has been published as Tahmasebi, and H. Sahraei, A. and Mohareb, M. Natural vibration analysis for axially loaded steel members with angle cross-sections. Proceedings of the Canadian Society of Civil Engineering Annual Conference CSCE, Niagara, 2024.

Keywords

Angle sections, compression members, tension members, natural vibration, dynamic effects, human activity

3.2. Introduction and literature review

Past research on the dynamic analysis of buildings has heavily focused on their dynamic response to earthquakes and wind effects. Comparatively, dynamic effects due to human activities have received less attention. Relevant studies include the work of Bachmann and Ammann [1], Allen [2], and Smith et al. [3]. In these studies, dynamic effects on structural members due to human activity such as walking, running, aerobics, etc. have been reported to manifest in three directions: transversely, laterally, and longitudinally. Živanović et al. [4] compiled the forcing functions induced by human activities as measured by previous researchers. For a given member, given that the magnitudes of the transverse components of the dynamic forces induced by human activities tend to be larger than that of the lateral and longitudinal components, the transverse response of members received the most attention from researchers. Within this context, the present study focuses on the dynamic response of axially loaded members with angle cross-sections, both transversely and laterally.

The Murray et al. [5] and CAN/CSA-S16 [6] limit the slenderness ratio for compression members to a threshold of 200 and that of tension members to a threshold of 300. Limiting member slenderness provides an indirect means of controlling their vibration, as the natural frequency of members depends, among other factors, on the member's slenderness.

Ellingwood and Tallin [7] characterized the transverse force induced by human activities as a Fourier series in the form

$$F_w(t) = Q + Q\sum_{i=1}^{N} \alpha_i \sin\left(2\pi i f_s t - \phi_i\right) \tag{3.1}$$

which Q is the static weight of a human (commonly assumed as 76 kg), i is the harmonic terms ranging from 1 to N, where N represents the total number of harmonics needed to represent human activity, typically taken as three or four, f_s denotes the frequency of human steps, t is the time, α_i is a dynamic load factor associated with the mode i, and ϕ_i is the corresponding phase lag. For instance, if the human step frequency is 3Hz and the number of harmonics taken as four, the forcing function will have four exciting frequencies of 3, 6, 9, and 12 Hz. In this case, a floor (or a member) with a fundamental natural frequency of 12 Hz may resonate with the highest harmonic. Eq. 3.1 has been adopted in standards such as Murray et al. [5] and ISO-10137 [8].

Additionally, the lateral force component induced by human activities, as given by Ingólfsson et al. [9], can be expressed as

$$F_v(t) = Q\sum_{i=1}^{N} \beta_i \sin\left(2\pi i f_s t - \lambda_i\right) \tag{3.2}$$

where β_i and λ_i are dynamic load factor and phase angle defined as the ratio of the lateral force associated with the i^{th} harmonic to the human body weight. A summary of dynamic load factors α_i, β_i and phase angle ϕ_i, λ_i for various types of human activity, as proposed by various studies provided by Tahmasebi-Orimi et al. [10]. The step frequency associated with walking ranges from 1.5 to 2.5 Hz, from 1.6 to 4.0 Hz for running, and from 1.5 to 3 and 2 to 4 Hz for aerobics.

In this study, our focus lies in investigating the natural frequency analysis of axially loaded members of angle cross-sections. Owing to the asymmetry of these cross-sections, their natural vibration response is coupled torsional-flexural. Relevant studies include the work of Friberg [11]

who investigated the natural vibration of simply supported members subjected to axial loads. Banerjee and Fisher [12] investigated the influence of axial load on the natural frequency. Using finite element, Tanaka and Bercin [13] investigated the effect of boundary conditions for members with no axial loads. Hashemi and Richard [14] expanded the study to axially loaded members and boundary conditions. Ambrosini [15] experimentally investigated the natural vibration of members with asymmetric cross-sections.

While the above solutions provide solutions for the natural frequency of axially loaded members, no attempts were made to develop design criteria for limiting the vibration of such members in the context of structural steel construction. Within this context, the present pilot study presents a step towards developing criteria for controlling the vibrations of axially loaded members of angle cross-sections by limiting their natural frequency.

Two sets of boundary conditions are examined: (a) members with ends that are pinned in all directions (Figure 3.1a) and (b) members with ends that are connected to gusset plates (Figure 3.1b).

Gusset plate connections would result in a near-pin condition of the member end about the fixation parallel to the gusset plate (Figure 3.1b) but results in a fixation of the member end about the $\hat{z}$ axis normal to the gusset plate. It is noted here that both axes $\hat{y}$, $\hat{z}$ do not align with the principal directions y , z of the member. Hence the classical equations of natural vibration for asymmetric members are not applicable in this situation.

Since Case B is representative of the end connections expected in practice and in the absence of closed-form solutions for it, designers may conservatively opt to treat the problem as pinned in all directions (Case A). The present study investigates the difference between both treatments.

As the study does not attempt to model any slip that may occur between the angle and the gusset plate, the findings are primarily applicable to welded connections or slip-critical bolted connections.

The paper first presents available analytical solutions in Sections 3 and 4, defines a typical reference case in Section 5, presents the specifics of the shell-based finite element model in Section 6, a verification of the model in Section 7, and then conducts a parametric to study the effect of axial force on the natural frequency in Section 8, and then illustrates the boundary effects for gusset plate members in Section 9.

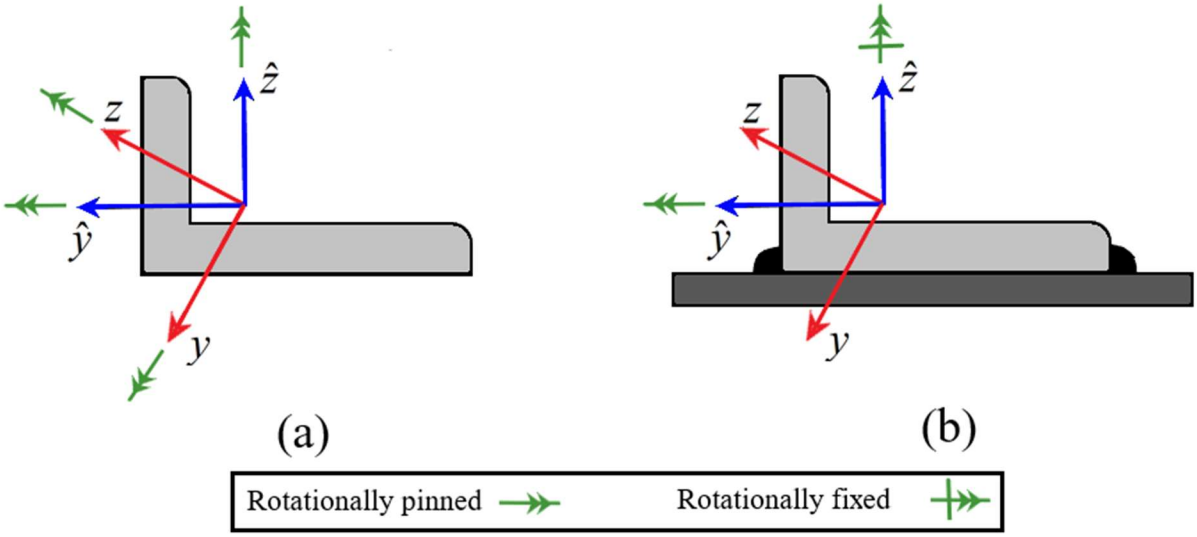

Figure 3.1 (a) Pinned-Pinned boundary conditions, (b) Typical gusset plate connection for angle member with angle cross-section.

3.3. Analytical Solution

Ghandi and Shiri [16] developed the equations of motion of governing the dynamic response of axially loaded members with asymmetric cross-sections as

$$EI_z v^{iv} + Pv'' - Pz_r\theta_x'' + m\ddot{v} - mz_r\ddot{\theta}_x = 0$$
$$EI_y w^{iv} + Pw'' + Py_r\theta_x'' + m\ddot{w} + my_r\ddot{\theta}_x = 0 \qquad 3.3\text{(a-c)}$$
$$EI_\omega \theta_x^{iv} - GJ\theta_x'' + Pr_0^2\theta_x'' - Pz_r v'' + Py_r w'' - mz_r\ddot{v} + my_r\ddot{w} + mr_0^2\ddot{\theta}_x = 0$$

in which E is the Young modulus, G is Shear modulus, J is the Saint-Venant torsional constant, m is the mass of the member per unit length, P is the axial force (taken as positive when compressive), v, w are the displacements in the plane of the cross-section, θ is the angle of twist, I_y, I_z are the moment of inertia, r_0^2 is the polar radius of gyration about the shear centre moment of inertia, I_ω is the warping constant, and (y_r, z_r) are the coordinates of the shear centre relative to the centroid. In Eq. 3.3(a-c), EI_y, EI_z represent the flexural stiffness of the member, GJ is its Saint Venant torsional rigidity, EI_ω is its warping stiffness, and all terms constraining the axial compressive force P represent the destabilizing effect, and all terms containing the mass m of the member per unit length represents the inertial terms. When the section is asymmetric, (y_r, z_r) do not vanish, and the equations of motion are coupled.

3.4. Analytical solutions for members pinned in all directions.

3.4.1. Asymmetric sections

For natural vibration, the solution can be assumed to take the form:

$$\begin{Bmatrix} v(x,t) \\ w(x,t) \\ \theta(x,t) \end{Bmatrix} = \begin{Bmatrix} V(x) \\ W(x) \\ \theta_x(x) \end{Bmatrix} \sin(\omega t) \qquad 3.4$$

From Eq. 3.4, by substituting into Eq. 3.3, one obtains

$$\begin{aligned} &EI_z V^{iv} + PV'' - Pz_r\theta_x'' - m\omega^2 V + m\omega^2 z_r\theta_x = 0 \\ &EI_y W^{iv} + PW'' + Py_r\theta_x'' - m\omega^2 W - m\omega^2 y_r\theta_x = 0 \\ &EI_\omega\theta_x^{iv} - GJ\theta_x'' + Pr_0^2\theta_x'' - Pz_r V'' + Py_r W'' + m\omega^2 z_r V - m\omega^2 y_r W - m\omega^2 r_0^2\theta_x = 0 \end{aligned} \qquad 3.5\ (a\text{-}c)$$

For a member that is simply supported relative to both displacements and the angle of twist, the displacement function can be assumed to take the form

$$\begin{Bmatrix} V(x) \\ W(x) \\ \theta_x(x) \end{Bmatrix} = \begin{Bmatrix} A_i \\ B_i \\ C_i \end{Bmatrix} \sin\left(\frac{\pi x}{l}\right) \tag{3.6}$$

From Eq. 3.6 by substituting into Eq. 3.5, one recovers the eigenvalue problem

$$\left(\mathbf{K} + P\mathbf{K}_{\mathbf{g}} - \omega^2\mathbf{M}\right)\mathbf{U} = 0 \tag{3.7}$$

in which, the following matrices have been defined

$$\begin{aligned}
\mathbf{K} &= \begin{bmatrix} EI_z(\pi/l)^4 & 0 & 0 \\ 0 & EI_y(\pi/l)^4 & 0 \\ 0 & 0 & EI_\omega(\pi/l)^4 + GJ(\pi/l)^2 \end{bmatrix} \\
\mathbf{K}_{\mathbf{g}} &= \begin{bmatrix} -(\pi/l)^2 & 0 & z_r(\pi/l)^2 \\ 0 & -(\pi/l)^2 & -y_r(\pi/l)^2 \\ z_r(\pi/l)^2 & -y_r(\pi/l)^2 & r_0^2(\pi/l)^2 \end{bmatrix} \\
\mathbf{M} &= \begin{bmatrix} m & 0 & -mz_r \\ 0 & m & my_r \\ -mz_r & my_r & mr_0^2 \end{bmatrix} \quad ; \quad \mathbf{U} = \begin{Bmatrix} A_i \\ B_i \\ C_i \end{Bmatrix}
\end{aligned} \tag{3.8}$$

For an axial load P, the natural frequency ω is obtained by setting the determinant of the matrix of coefficients to zero, i.e., $\left|\mathbf{K} + P\mathbf{K}_{\mathbf{g}} - \omega^2\mathbf{M}\right| = 0$, leading to the bi-cubic equation

$$A\omega^6 + B\omega^4 + C\omega^2 + D = 0 \tag{3.9}$$

in which

$$
\begin{aligned}
A &= -m^3 r_0^2 + m^3 {y_r}^2 + m^3 {z_r}^2 \\
B &= m^2 (\pi/l)^2 \left\{ EI_z r_0^2 (\pi/l)^2 - EI_z {y_r}^2 (\pi/l)^2 + EI_y r_0^2 (\pi/l)^2 - EI_y {z_r}^2 (\pi/l)^2 \right. \\
&\qquad \left. + EI_\omega (\pi/l)^2 + GJ + P\left(r_0^2 - 3{y_r}^2 - 3{z_r}^2\right) \right\} \\
C &= -m(\pi/l)^4 \left\{ E^2 I_y I_z r_0^2 (\pi/l)^4 + E^2 I_z I_\omega (\pi/l)^4 + E^2 I_y I_\omega (\pi/l)^4 + EI_z GJ (\pi/l)^2 \right. \\
&\quad + EI_y GJ (\pi/l)^2 + P\left(2GJ - 2EI_z {y_r}^2 (\pi/l)^2 - 2EI_y {z_r}^2 (\pi/l)^2 + 2EI_\omega (\pi/l)^2\right) \\
&\qquad \left. - P^2\left(r_0^2 + 3{y_r}^2 + 3{z_r}^2\right) \right\} \\
D &= (\pi/l)^6 \left\{ E^3 I_y I_z I_\omega (\pi/l)^6 + E^2 I_y I_z GJ (\pi/l)^4 + P(\pi/l)^2 \left(EI_y GJ + EI_z GJ \right.\right. \\
&\qquad \left. - E^2 I_y I_z r_0^2 (\pi/l)^2 + E^2 I_y I_\omega (\pi/l)^2 + E^2 I_z I_\omega (\pi/l)^2\right) + P^2 \left(EI_\omega (\pi/l)^2 \right. \\
&\qquad \left. - EI_y r_0^2 (\pi/l)^2 - EI_z r_0^2 (\pi/l)^2 - EI_y {z_r}^2 (\pi/l)^2 - EI_z {y_r}^2 (\pi/l)^2 + GJ\right) \\
&\qquad \left. - P^3\left(r_0^2 + {y_r}^2 + {z_r}^2\right) \right\}
\end{aligned}
\qquad \text{3.10(a-d)}
$$

The smallest positive root for ω as obtained from Eq. 3.9 corresponds to the fundamental natural frequency of the system.

3.4.2. Monosymmetric Sections

For a monosymmetric section the z axis is an axis of symmetry, as may be the case for an equal leg angle, one has $z_r = 0$. By substituting into Eq. 3.10, one obtains

$$
\left(\overline{A}\omega^4 + \overline{B}\omega^2 + \overline{C}\right)\left(EI_z\left(\frac{\pi}{l}\right)^4 + P\left(\frac{\pi}{l}\right)^2 - m\omega^2\right) = 0 \qquad \text{3.11}
$$

in which

$$\overline{A} = m^2 r_0^2 - m^2 y_r{}^2$$
$$\overline{B} = -mEI_y r_0^2 \left(\frac{\pi}{l}\right)^4 - mEI_\omega \left(\frac{\pi}{l}\right)^4 - mGJ\left(\frac{\pi}{l}\right)^2 - Pmr_0^2\left(\frac{\pi}{l}\right)^2 - Pmr_0^2\left(\frac{\pi}{l}\right)^2 + 2Pmy_r{}^2\left(\frac{\pi}{l}\right)^2$$
$$\overline{C} = E^2 I_y I_\omega \left(\frac{\pi}{l}\right)^8 + EI_y GJ\left(\frac{\pi}{l}\right)^6 + PEI_y r_0^2\left(\frac{\pi}{l}\right)^6 + PEI_\omega\left(\frac{\pi}{l}\right)^6 + PGJ\left(\frac{\pi}{l}\right)^4 + P^2 r_0^2\left(\frac{\pi}{l}\right)^4 - P^2 y_r{}^2\left(\frac{\pi}{l}\right)^4$$

3.12

which yields the natural frequency corresponding to pure flexure about the z axis

$$\omega = \omega_z = \sqrt{\frac{\left(EI_z\left(\pi/l\right)^4 + P\left(\pi/l\right)^2\right)}{m}} \qquad 3.13$$

and that corresponding to the torsional flexural vibration

$$\omega = \sqrt{\frac{-\overline{B} + \sqrt{\overline{B}^2 - 4\overline{A}\overline{C}}}{2\overline{A}}} \qquad 3.14$$

3.5. Reference Case

A 4m span axially loaded member with L152x102x16 is considered. Cross-sectional properties are $A = 3790mm^2, I_y = 1.005\times10^7 mm^4, I_z = 1.789\times10^6 mm^4,$ $r_y = 51.5mm,$ $r_z = 21.7mm,$ $m = 52.1kg/m$. Steel properties are $n = 1.34$, $F_y = 350MPa, F_u = 450MPa,$ $E = 2\times10^5\ MPa,$ $G = 7.7\times10^4\ MPa$. It is required to determine the natural frequency of the member for the case where both ends are pinned, both the analytical solution in Eq. 3.9 and using shell finite element modelling.

3.6. Finite Element Model

The finite element model is primarily intended to model axially loaded members with end gusset plate connections since no closed-form solutions exist for such boundary conditions.

3.6.1. Model Description

The finite element model is based on the shell finite element S4 in the ABAQUS library. The S4 element is a four-node quadrilateral shell element with six degrees of freedom per node, three translations, and three rotations. To simulate pin end conditions, the angle of twist and displacements along the y and z directions were restrained for all nodes along the member ends. Two master nodes were defined at the section centroids at both ends. The displacements of the master nodes along the y and z directions were coupled to those of the shear centre at the corner node. Longitudinal displacements of end nodes were related to the longitudinal displacement of the corresponding master node to allow the member ends to pivot about the centroidal axes of the cross-section. The longitudinal displacement of the master node at one end of the member was restrained while the master node at the other end was subjected to an axial force. A linearly elastic isotropic material characterization with $E = 200,000MPa$ and $G = 77,000MPa$ is adopted for the sought natural vibration analysis.

The analysis was conducted in two steps. Initially, the axial load was applied to the master node at the member end which is free to move longitudinally. Next, the natural frequency of the axially loaded member was determined through a natural frequency eigenvalue analysis. In this step, nonlinear geometric effects were introduced to capture second-order effects due to the axial load when computing the natural frequency. A mesh study was conducted for the S4 model.

3.6.2. Mesh Study and Verification

Two meshes were attempted for the unloaded reference member. The first one had five elements along the short leg, eight elements along the long leg, and 200 elements along the longitudinal axis of the member, totaling 2600 elements. A finer mesh was also attempted with 10 elements along the short leg, 16 elements along the long leg, and 400 along the longitudinal axis of the member, totaling 10400 elements. The predicted fundamental natural frequency based on the first mesh was found to be 10.71 Hz while that based on the second mesh was 10.67 Hz, a difference of less than 0.2 percent. Comparatively, the fundamental natural frequency based on the analytical solution was found to be 10.74 Hz.

3.7. Verification for a Member Pinned in all directions.

The reference case is used to assess the validity of the finite element model against the predictions of the closed-form solution for the case of a member pinned in all directions. Toward this goal, the natural frequency of the reference case is examined for various levels of axial force, both in tension (negative) and compression (positive). The natural frequency is normalized by dividing it by the natural frequency ω_p of the member in the absence of axial loading, while the applied axial force is normalized by dividing it by the torsional flexural elastic critical load P_{cr} of the member. Figure 3.2 presents a comparison of the predictions of the closed-form solution and that predicted by the ABAQUS model.

Close agreement is observed between the predictions of the analytical and shell model solutions. As the applied compressive load increases, the natural frequency is observed to decrease. Conversely, the natural frequency increases with the increase of the applied tensile force. As the

compressive force approaches the torsional flexural elastic critical load P_{cr} of the member, the natural frequency is found to tend to zero.

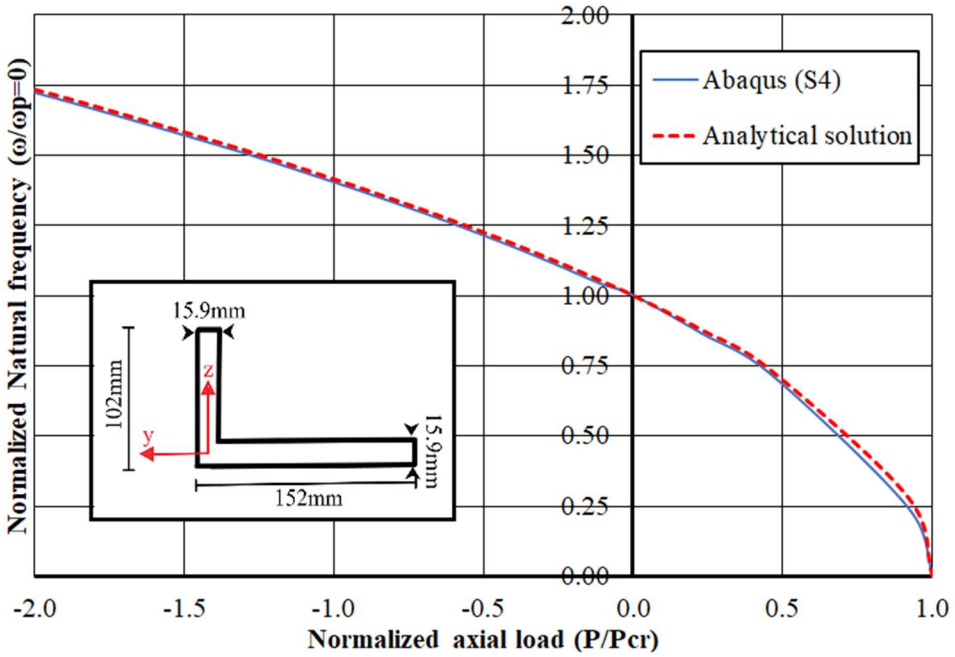

Figure 3.2 Interaction diagram of normalized natural frequency versus normalized axial load

3.8.Effect of axial force on natural frequency in slender members

The natural frequency was computed for all equal leg angles for the L76x76, L102x102, and L152x152 series in the handbook of steel construction, totaling 17 sections. The member length was taken to comply with the maximum slenderness ratio $(KL/r)_{\max} = (L/r)_{\max} = 200$ for compression members (Figure 3.3a) and $(L/r)_{\max} = 300$ for tension members. For compression members, the axial load level was taken to equal the maximum compression resistance $C_r = \phi A F_y \left(1+\lambda^{2n}\right)^{-1/n}$ as given by the Canadian Standard which, F_y is the yield strength of the steel, $\lambda = (KL/r)\sqrt{F_y/\pi^2 E}$, and $n = 1.34$. While tension members were subjected to an axial load equal to its tensile resistance as given by $T_r = \min\left(\phi A_g F_y, \phi_u A_n F_u, \phi_u A_{ne} F_u\right)$, where ϕ is resistance

factor, ϕ_u is resistance factor for fracture, A_g is the gross area, A_n is the equivalent net area, A_{ne} is the effective net area(which is taken as A_n in the absence of information about the specifics of the connection), and F_u is its tensile strength. The minimum, average, and maximum predicted natural frequencies are provided for each series (Figure 3.3(a,b)). As a general observation, the natural frequencies for compression members are significantly lower than those of tension members, indicating their proneness to vibrations. For compression members, Figure 3.3a shows that the natural frequencies vary within a narrow range for each series, but they are observed to decrease with the angle size while the range of natural frequencies is wider for tension members (Figure 3.3b).

Figure 3.4(a,b) provide the natural frequency of 79 unequal leg angles for the L51x38, L64x38, L64x51, L76x51, L76x64, L89x64, L89x76, L102x76, L102x89, L127x76, L127x89, L152x89, L152x102, L178x102, L203x102, and L203x152 series. Figure 3.4a depicts the fundamental natural frequencies for unloaded members with lengths corresponding to the slenderness requirement $\left(KL/r\right)_{\max} = \left(L/r\right)_{\max} = 200$ for compression members and for members with lengths corresponding to the maximum slenderness ratio for tension members $\left(L/r\right)_{\max} = 300$. The figure shows that present slenderness limits yield inconsistent natural frequencies owing to the difference in member spans allowed in both cases. When accounting for the axial load level in both cases i.e., compression members subject to an axial load equal to the maximum resistance C_r and tension members subject to the maximum resistance T_r, the discrepancy between the predicted natural frequency becomes more pronounced (Figure 3.4b). The results suggest that developing design criteria associated with more consistent natural frequencies (and hence more consistent vibration

levels under human activities) would be achieved by incorporating the axial load level as a parameter.

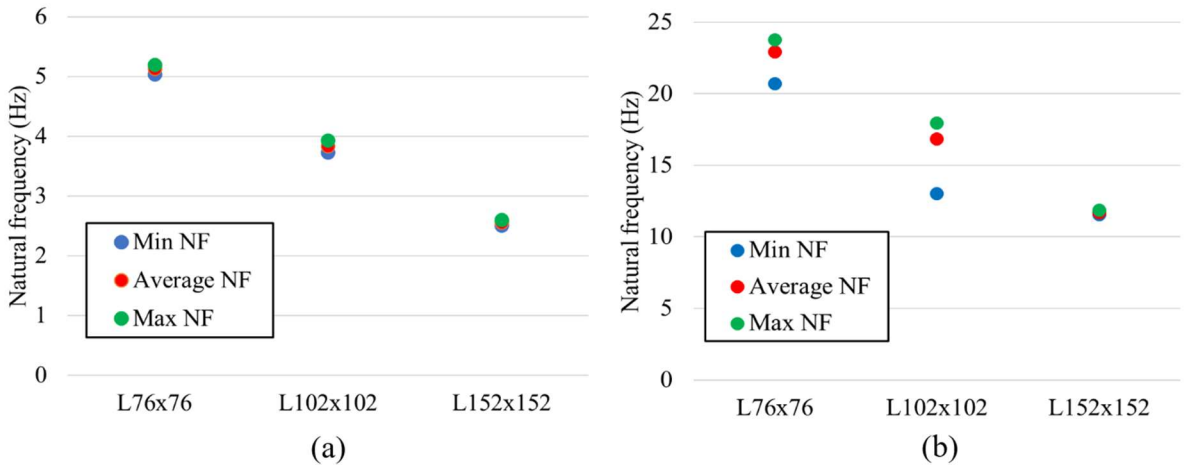

Figure 3.3 Natural Frequency (NF) of members for equal leg angles for (a) compression members, and (b) tensile members.

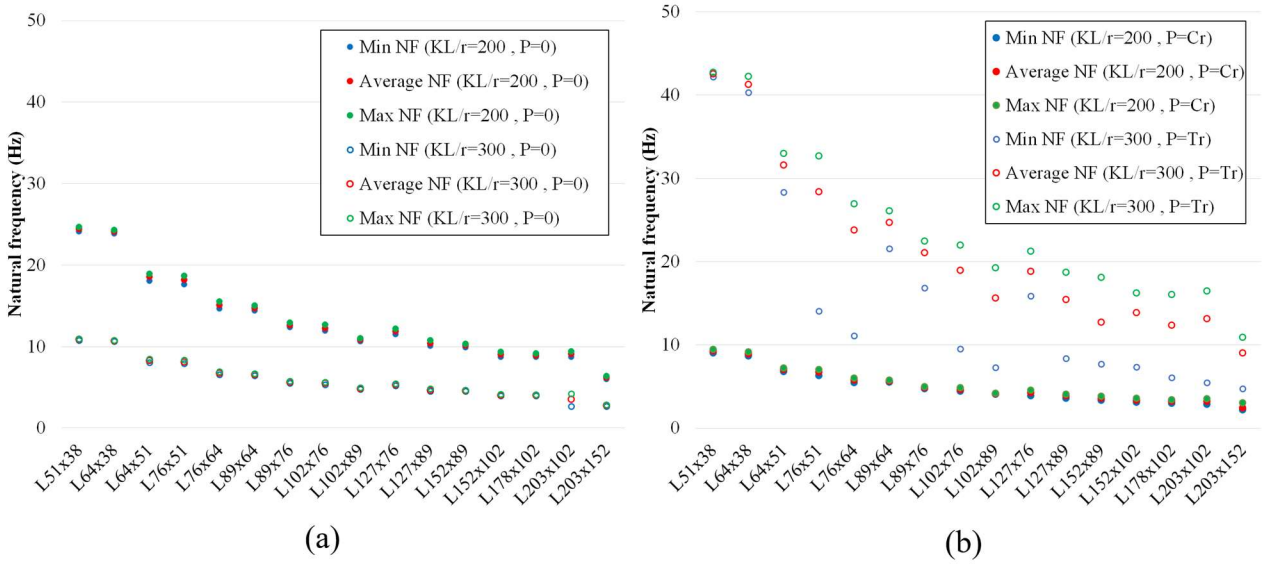

Figure 3.4 Natural frequency (NF) for unequal legs for (a) unloaded members, (b) axially loaded members with a force equal compression resistance C_r or tensile resistance T_r

3.9. Natural Frequency of Members with Gusset Plate Connections

Eq. 3.13 and Eq. 3.14 are applicable to members with pinned-end conditions about the principal axes (y and z in Figure 3.1a). Yet for end gusset connections (Figure 3.1b), the member is fixed about the $\hat{z}$ axis and pinned about the $\hat{y}$ non-principal directions. The fixity end condition about the principal directions is unknown. Thus, the natural frequency for members with end gusset connections is conducted based on the shell model in the present section. The specifics of the model are similar to those described in Section 5 while restraining the rotation of the two master nodes at both ends about the z axis.

Figure 3.5 compares the interaction diagrams for the reference member between the natural frequency of the member and the axial force for the case of pin end condition and gusset end plate connection. For the latter case, the axial load at a natural frequency of zero was found equal to the elastic buckling load for the member as reported by Alenezi and Mohareb [17].

Another aspect of the gusset plate connection is that the axial force within the gusset plate is eccentric relative to the member centroidal axis. This eccentricity induces bending moments about the y axis of the member in the member in addition to the axial force. It is of interest to investigate the effect of this eccentricity on the natural frequency of the member. Towards this goal, the additional bending moments induced by the eccentric axial force are applied to both master nodes at the end of the member and the corresponding interaction diagram is overlaid on Figure 3.5.

When the member is subjected to a high compressive force, the presence of additional bending moments is shown to have a detrimental effect on the predicted natural frequency for the member when compared to the case of concentric loading. The difference in natural frequencies in both cases tends to decrease as the magnitude of the applied compressive force reduces. The difference

between both natural frequencies in both cases tends to essentially disappear when the member is subjected to a tensile force.

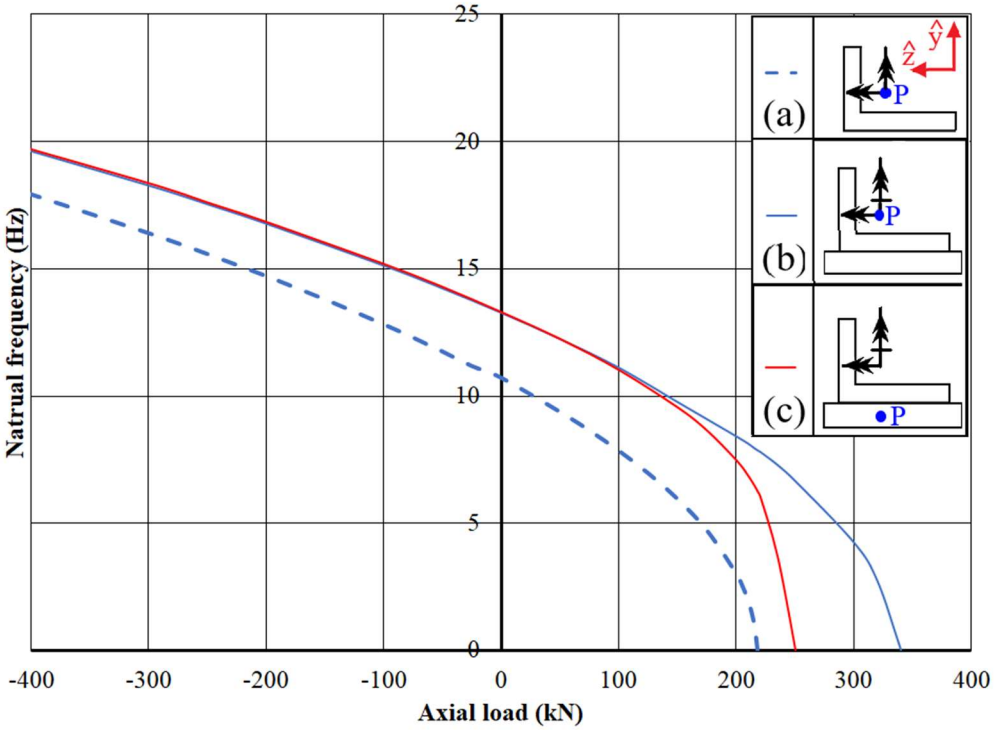

Figure 3.5 Interaction diagrams for natural frequency vs axial load for (a) pined member, (b) gusset plate connection with eccentricity neglected, and (c) gusset plate connection with eccentricity.

Figure 3.6 shows the natural frequency of three compression members with the nearly equal cross-sectional area examined, (1) L152x102x16 with the short leg parallel to the gusset plate, (2) L127x127x16 and (3) L152x102x16 with the long leg parallel to the gusset plate. Member lengths are taken as the maximum value corresponding to slenderness $\left(KL/r = L/r = 200\right)$. The corresponding member lengths are 4.35, 4.96, and 4.35m respectively. The axial load is taken equal to the compression resistance $C_r = \phi A F_y \left(1+\lambda^{2n}\right)^{-1/n}$. The corresponding axial force levels are 156.7, 159.7, and 156.7kN, respectively. Three types of connections at member ends are considered for each section; a pinned connection in all three directions, a gusset plate connection in which the load eccentricity is omitted, and a gusset plate connection in which the load

eccentricity is captured. The analysis reveals that the natural frequencies for members with pin connections are significantly lower than those of gusset plate connections. The difference is observed to increase as the outstanding leg dimension increases. The results show that adopting closed-form solutions available for members with pin-end connections to the members with end-gusset plate connections would grossly overestimate the natural frequency of the members. Also, it is shown that the effect of eccentricity on the natural frequency is pronounced for members with high compressive load levels and reduces with the compressive force magnitude and has essentially no effect on tension members.

A comparison between the gusset plate connection with and without eccentricity reveals that the detrimental effect of axial force eccentricity on the natural frequency is reduced as the length of the outstanding leg increases. This is attributed to the fact that the moment of inertia about the $\hat{y}$ axis (Figure 3.1) (which resists that the larger moment induced by the eccentricity) also increases.

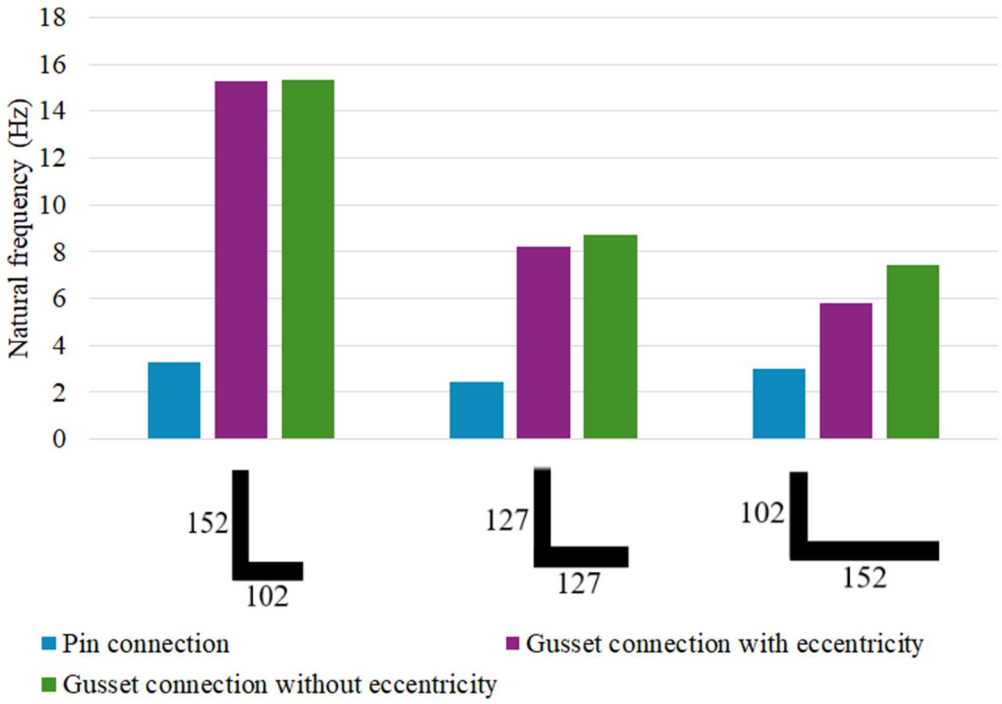

Figure 3.6 Effect of end boundary conditions, load eccentricity, and leg ratio on natural frequency.

3.10. Conclusions

Axially loaded compression members were shown to have a lower natural frequency than unloaded compression members while axially loaded tension members have a higher natural frequency than unloaded tension members. Thus, developing criteria for controlling vibrations due to human activity, must account for member slenderness, and axial force level.

The natural frequency of angle members with gusset plate connections is significantly larger than that of the hypothetical case of a pin-end connection. The adoption of available closed-form solutions for the latter case for members with end-gusset plate connections leads to overly conservative predictions for the natural frequency of the members.

In gusset plate connections, the eccentricity of the axial force provided by the gusset is detrimental to the natural frequency of compression members (in comparison to the hypothetical case of concentric loading). The effect of eccentricity is pronounced for high axial force levels and reduces as the compressive force reduces and has essentially no effect on tension members.

For angle members with unequal legs connected to gusset plates through the longer leg, the effect of compressive force eccentricity is found to be more pronounced than those connected to the shorter leg.

3.11. Notation

A : Area

A_g : Gross area

A_n : Equivalent net area

A_{ne} : Effective net area for shear lag

$A_1 - A_4$, $B_1 - B_4, C_1 - C_4$: Integration constants

C_r : Compressive resistance

E : Elasticity modulus

F_y : Yield strength

$F_v(t)$: Lateral component of forcing function induced by human activities

$F_w(t)$: Transverse component of forcing function induced by human activities

F_u : Tensile strength

f_s : Human step frequency

G : Shear modulus

I_y, I_z : Moments of inertia about y and z axis

I_ω : Warping constant

I_0 : Polar moment of inertia

J : Saint-Venant torsional constant

$\mathbf{K}$: Stiffness matrix

$\mathbf{K_g}$: Geometric matrix

l : Length

m : Mass per unit length

$\mathbf{M}$: Mass matrix

N : Number of harmonics

P : Axial load

P_{cr} : Torsional flexural elastic critical load

Q : Human body weight

r_z, r_y : Radii of gyration about weak and strong axes

r_0^2 : Polar radius of gyration

t : Time

T_r : Tensile resistance

$\mathbf{U}$: Displacement vector

v, w, θ_x : In-plane displacements and angle of twist

y_r, z_r : Coordinates of the shear centre relative to the centroid

α_i : Dynamic load factors for harmonic i related to transverse component of forcing function

β_i : Dynamic load factors for harmonic i related to lateral component of forcing function

ϕ_i : Phase angle for harmonic i related to transverse component of forcing function

λ_i : Phase angle for harmonic i related to lateral component of forcing function

ϕ_u : Resistance factor for fracture

ω : Coupled torsional flexural natural frequency

ω_p : Natural frequency in absence of axial loading

3.12. References

1. Bachmann, H. and W. Ammann, *Vibrations in structures: induced by man and machines*. Vol. 3. 1987: Iabse.
2. Allen, D., *ATC Design Guide 1: Minimizing floor vibrations (1st ed.).* . 1999, Redwood City, CA:: Applied Technology Council;.
3. Smith, A.L., S.J. Hicks, and P.J. Devine, *Design of floors for vibration: A new approach*. 2007: Steel Construction Institute Ascot, Berkshire, UK.
4. Živanović, S., A. Pavic, and P. Reynolds, *Vibration serviceability of footbridges under human-induced excitation: a literature review.* Journal of sound and vibration, 2005. **279**(1-2): p. 1-74.
5. Murray, T.M., et al., *Vibrations of steel-framed structural systems due to human activity*. 2016: American Institute of Steel Construction.
6. CAN/CSA-S16, *Design of steel structures,Canada*, in *CSA S16:19*. 2019, Canadian Standard Association: Toronto: CSA.
7. Ellingwood, B. and A. Tallin, *Structural serviceability: floor vibrations.* Journal of Structural engineering, 1984. **110**(2): p. 401-418.
8. ISO-10137, *International Organization for Standardization*, in *Bases for design of structures--serviceability of buildings and walkways against vibrations*. 2007, International Organization for Standardization: International Organization for Standardization.
9. Ingólfsson, E.T., C.T. Georgakis, and J. Jönsson, *Pedestrian-induced lateral vibrations of footbridges: A literature review.* Engineering Structures, 2012. **45**: p. 21-52.
10. Tahmasebi-Orimi, H., A. Sahraei, and M. Mohareb, *Slenderness limits to control vibrations in axially loaded members with doubly symmetric cross-sections.*, in *CSCE*, P.o.t.C.S.o.C.E.A.C. CSCE, Editor. 2024, CSCE: Niagara.
11. Friberg, P., *Coupled vibrations of beams—an exact dynamic element stiffness matrix.* International Journal for numerical methods in engineering, 1983. **19**(4): p. 479-493.
12. Banerjee, J. and S. Fisher, *Coupled bending–torsional dynamic stiffness matrix for axially loaded beam elements.* International journal for numerical methods in engineering, 1992. **33**(4): p. 739-751.

13. Tanaka, M. and A. Bercin, *Finite element modelling of the coupled bending and torsional free vibration of uniform beams with an arbitrary cross-section.* Applied Mathematical Modelling, 1997. **21**(6): p. 339-344.
14. Hashemi, S.M. and M.J. Richard, *Free vibrational analysis of axially loaded bending-torsion coupled beams: a dynamic finite element.* Computers & Structures, 2000. **77**(6): p. 711-724.
15. Ambrosini, D., *On free vibration of nonsymmetrical thin-walled beams.* Thin-Walled Structures, 2009. **47**(6-7): p. 629-636.
16. Ghandi, E. and B. Shiri, *On triply coupled vibration of eccentrically loaded thin-walled beam using dynamic stiffness matrix method.* Struct. Eng. Mech, 2017. **62**(6): p. 759-769.
17. Alenezi, A.M. and M. Mohareb, *Buckling solutions for compression members with end restraints defined along non-principal directions.* Journal of Constructional Steel Research, 2021. **181**: p. 106505.

Chapter 4 Finite element formulation for the free vibration analysis of axially loaded angle members with gusset end connections [6]

4.1. Abstract

The present study focuses on quantifying the natural frequency of axially loaded members with angle cross-sections. Such members are commonly connected to adjacent ones through gusset plates that provide a nearly pinned end condition about the axis parallel to the gusset and full fixity about the orthogonal direction. Since both axes are non-principal, classical natural frequency solutions, based on displacements along principal directions, become inapplicable. The present study thus develops a family of solutions that characterize the natural frequency of angle members with gusset plate end connections, including a finite element formulation, an energy-based approximate solution, and a dimensionless design chart. The formulation incorporates the effects of axial loading, torsional-flexural coupling induced by cross-sectional asymmetry, rotary inertia, and warping, while enabling the analyst to define different boundary conditions along non-principal directions. The validity of the solution is established through comparisons with shell finite element solutions. The findings reveal that the natural frequency of angle compression members with gusset plate end-connections is significantly higher than that of pin-ended members. A systematic parametric study documents the effects of rotary inertia, axial load ratio, leg width to thickness ratio, connected to unconnected leg ratio, and member slenderness, on the natural frequency of the member. A design example is provided to illustrate the utility of the proposed

[6] This chapter has been published as Tahmasebi-Orimi, H., A. Sahraei, and M. Mohareb, Natural vibration of axially loaded angle members with gusset plate end connections. Journal of Constructional Steel Research, 2025. 235: p. 109824.

simplified energy-based approximate solution in the design of vibration-resistant axially loaded angle members.

Keywords

Axially loaded members, angle cross-sections, end gusset plate connections, natural vibration, finite element analysis, energy based approximate solution.

4.2. Introduction and Scope

Axially loaded members in steel construction are commonly made of monosymmetric or asymmetric angle cross-sections. Such members are commonly connected to adjoining beams and/or columns through gusset plate connections (Figure 4.1a). When such members possess high slenderness, they become prone to excessive vibrations under human activity. A possible means to control the members propensity to undergo excessive vibrations is to ensure that their fundamental natural frequency exceeds the expected exciting frequencies induced by human activities by an acceptable margin.

Yet, owing to the complex nature of the boundary conditions of axially loaded angle members with gusset plate end connections, no closed-form solutions are available to estimate their fundamental natural frequency. Specifically, gusset plate connections (Figure 4.1a) would result in a near-pin end condition with respect to flexure about the y axis (parallel to the gusset plate), and a fixation with respect to flexure about the z axis (perpendicular to the gusset plate), both (y,z) axes being non-principal. Since the classical equations of motion, and resulting closed form natural frequency solutions for members with asymmetric cross-sections are formulated in terms of the displacements along the principal directions $(\hat{y},\hat{z})$ rather than the geometric axes (y,z), applying

the boundary conditions associated with gusset plate end connections presents a challenge in formulating simple closed-form solutions for the problem.

Yet, available natural frequency expressions are expressed in terms of displacements that are defined along the principal directions rather than along the geometric axes and hence do not provide a direct means to quantify the natural frequency of angle members with gusset plate end connections. Under existing solutions, the designer can idealize the angle member either (a) as pinned in both directions, thus underestimating its natural frequency, (b) as fixed in both directions leading to an unconservative estimate, or (c) fixing the member about a principal direction and pinning it about the orthogonal direction, which would be inconsistent with the directions of pin and fixity in gusset connections. Within this context, the present study develops a more general solution in which the displacements are defined along non-principal directions that enables the analyst to define a fixity condition along an axis normal to the gusset and a pin condition along the orthogonal direction to more accurately characterize the natural frequency of angle member with gusset connections. Towards this goal, the present study develops a variational principle, a finite element, and an approximate energy-based solution for the natural vibration analysis of axially loaded asymmetric members. The formulation adopts non-principal coordinates to seamlessly model the boundary conditions associated with gusset plate end connections, while capturing the effects of coupling due to cross-sectional asymmetry, axial loading, global and warping, and rotary inertia.

4.3. Literature review

The classical thin-walled beam theory developed by Vlasov [1] is widely used in the analysis of thin-walled members. The Vlasov beam is predicated on two kinematic assumptions; (1) The

cross-section remains rigid (undistorted) in its own plane throughout deformation, and (2) The transverse shear deformation within the middle surface of the cross-section is negligible. The theory of Gjelsvik [2] adopts the Vlasov kinematic assumptions while incorporating the through-thickness warping effect by adopting the Kirchhoff plate bending assumption postulating the normality of a line normal to the cross-section middle surface throughout deformation.

Natural vibration analysis solutions for thin-walled members involve several methodologies: (a) Analytical solutions (e.g., Kim et al. [3], Tanaka et al. [4], Prokić et al. [5]) , (b) Dynamic stiffness matrix solutions (e.g., Friberg [6], Banerjee et al. [7], Banerjee et al. [8], Eisenberger et al. [9], Kim et al. [10], and Li et al. [11]) , and (c) Finite element formulations (e.g., Kim et al. [12], Tanaka et al. [13], Duan [14], (Vo et al. [15],Vo et al. [16]), De Borbon et al. [17], Jrad et al. [18], and Sahraei et al. [19]).

The primary motivation of the present study is to develop a family of natural vibration solutions for members with angle cross-sections that capture the effects of warping, rotary inertia, axial loading and flexural torsional coupling owing to the cross-sectional asymmetry, with the ability to characterize boundary conditions along non-principal directions. A survey of studies related to natural vibration analysis of members with asymmetric cross-sections is summarized in Table 4.1 and the key features of these studies are discussed in the following.

Torsional flexural coupling effects due to cross-sectional asymmetry were captured in the analytical and finite element solutions of Mei [20] and the dynamic stiffness matrix solution of Friberg [6]. Global warping effects were captured in the analytical solution of Tanaka and Bercin [4], the finite element solution of Duan [14] and the closed-form solution of Prokic´ et al. [5]. Local and global warping effects include the finite element solutions of Vo et al. ([15], [16]) and the closed form and finite element solutions of Sahraei et al. [19]. Eisenberger et al. [9] formulated

a solution that captures rotary inertial effects. Also, the studies of [12], [15], [16], and [17] capture rotary inertia and shear deformation effects. Sahraei et al. [19] developed a finite element that captures rotary inertial and coupling effects arising due to shear deformation. The effect of axial loading on the natural vibration analysis was incorporated in the analytical solutions of Kim [3] and Prokic´ et al. [5], the finite element formulations of Vo et al. ([15], [16]) and De Borbon et al. [17], and the dynamic stiffness solutions of Banerjee and Fisher [7], Kim et al. [10], Li et al. [11], and Ghandi et al. [21]. In the previous studies, the displacements were defined along the principal directions. This restriction makes them inapplicable to members with angle cross-sections with end gusset plate connections, in which the end conditions along a non-principal direction (parallel to gusset) differs from that along the orthogonal direction. Such boundary conditions were tackled only recently in (Alenezi et al. [22]) in the context of buckling analysis of compression members. Yet, the authors are unaware of any treatment for this type of problem in the context of natural vibration. In order to fill this gap, the present study formulates a family of solutions for the natural vibration analysis of axially loaded asymmetric members, capturing warping and rotary inertia effects by (a) formulating the governing equations of motion and boundary conditions, (b) developing characteristic equations for members with boundary conditions defined along non-principal directions (e.g., members with end gusset plate connections), (c) formulating a finite element solution, and (d) developing an energy-based approximate solution.

Table 4.1 Features of Natural Vibration Analyses for Members with Asymmetric Cross-sections

	Solution Type			Boundary conditions*				Effects captured					
Reference	Analytical	Finite element	Dynamic stiffness	CC	CF	PP	GP	Axial load	Local warping	Global warping	Shear deformation	Rotatory inertial	Additional features
Friberg [6]			✓	✓		✓							
Banerjee and Fisher [7]			✓	✓	✓	✓		✓					
Kim et al. [12]	✓	✓				✓		✓		✓	✓	✓	Eccentric axial load
Eisenberger et al. [9]			✓	✓	✓	✓						✓	
Tanaka and Bercin [13]		✓		✓	✓	✓							
Tanaka and Bercin [4]	✓			✓	✓	✓				✓			
Kim et al. [10]			✓	✓	✓	✓		✓			✓	✓	
Li et al. [11]			✓	✓	✓	✓		✓		✓			
Duan [14]		✓		✓	✓	✓				✓			Eccentric axial load
Vo and Lee [15]	✓	✓			✓	✓		✓			✓		Composite open cross sections
Vo et al. [16]		✓		✓	✓	✓		✓	✓	✓		✓	Bending moments
De Borbon et al. [17]		✓		✓	✓	✓		✓		✓	✓	✓	
Prokić et al. [5]	✓				✓	✓		✓		✓			Cross-sectional point symmetric, CP BC
Ghandi and Shiri [21]			✓			✓		✓		✓			
Jrad et al. [18]		✓		✓	✓	✓				✓		✓	
Sahraei et al. [19]		✓			✓				✓	✓	✓	✓	
Present study		✓				✓	✓	✓	✓			✓	

*CC: Clamped-Clamped, CF: Clamped-Free, PP: Pinned-Pinned, CP: Clamped-Pinned, GP: Gusset plate connection

4.4. Assumptions and Modelling Idealizations

The finite element formulation is based on the following assumptions.

The member response follows Vlasov/Gjelsvik (e.g., Vlasov [1], Gjelsvik [2]) kinematic assumptions:

i. The member cross-section does not deform in its plane throughout deformation (i.e., it undergoes no cross-sectional distortion).

ii. Shear strains within the mid-surface of the cross-section are negligible.

iii. A line normal to the middle surface of the cross-section prior to deformation remains normal to the middle surface after deformation.

Material is homogenous linearly elastic isotropic, i.e., it obeys Hooke's law.

The member is subjected to a static axial force. i.e., variations in the axial load magnitudes which could trigger parametric excitations are outside the scope of the present analysis.

Infinitesimal longitudinal strains are assumed throughout vibration.

In addition, the following modelling idealizations were made when analyzing angle members with end gusset plate connections

a. The flexural stiffness of the gusset plate is conservatively omitted, i.e., the angle member is idealized as a pin-ended member about the axis parallel to the gusset.

b. The effect of the eccentricity of the axial load line of relative to the section centroidal axis is considered negligible.

4.5. Formulation

Figure 4.1c depicts the global Cartesian coordinate system (x, y, z) adopted and a right-handed curvilinear coordinate system (x, s, n), in which s is a tangential coordinate and $-e/2 \le n \le e/2$ is a normal coordinate. Figure 4.1d depicts a member subjected to a time-independent compressive force P. Under load P, the member deforms axially from the un-deformed Configuration 1 to Configuration 2. The corresponding longitudinal displacement is $u_p(x)$. At Configuration 2, the member is considered to be at the onset of natural vibration, about which it tends to vibrate into a coupled flexural-torsional mode in the presence of the constant axial load P. Throughout vibration (i.e., in going from Configuration 2 to 3), an arbitrary point offset from the cross-section mid-

surface undergoes displacements $u(x,s,n,,t)$, $v(x,s,n,t)$ and $w(x,s,t)$ along the (x,s,n) directions.

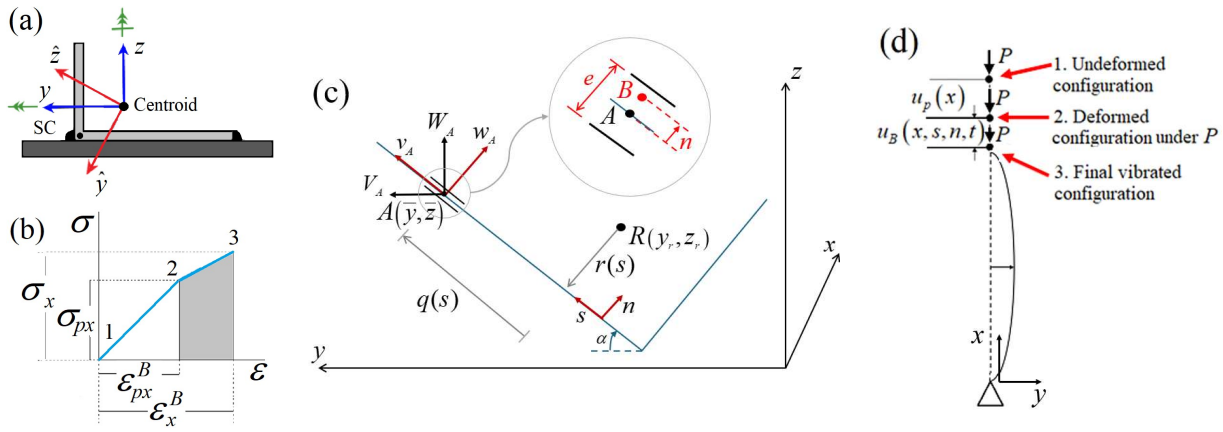

Figure 4.1(a) Gusset plate end connections for members with angle cross-section, (b) Stress-strain schematic associated with stages of deformation, (c) Coordinate system and notation for member with asymmetrical angle cross-section, (d) Stages of deformation in the $x-y$ plane

4.5.1. Overview of Kinematics of Thin-Walled Beam Theory

4.5.1.1. Displacement of a point on the middle surface

Based on the first Vlasov assumption (Vlasov [1], Gjelsvik [2]), the in-plane displacements $V_A(x,s,t), W_A(x,s,t)$ for an arbitrary point $A\left[x,\bar{y}(s),\bar{z}(s)\right]$ located on the middle surface are related to displacements $v(x,t), w(x,t)$ of the pole $R(y_r,z_r)$ through

$$\begin{aligned} V_A(x,s,t) &= v(x,t)-(\bar{y}-y_r)\theta_x(x,t) \\ W_A(x,s,t) &= w(x,t)+(\bar{z}-z_r)\theta_x(x,t) \end{aligned} \qquad 4.1(a\text{-}b)$$

in which $\theta_x(x,t)$ is the angle of twist of the cross section. The in-plane displacements $v_A(x,s,t), w_A(x,s,t)$ along the tangent and normal directions are defined by projecting the displacements in Eq. 4.1 along the tangential and normal directions, yielding

$$\begin{aligned} v_A(x,s,t) &= \cos\alpha(s)\,v(x,t) + \sin\alpha(s)\,w(x,t) - r(s)\,\theta_x(x,t) \\ w_A(x,s,t) &= -\sin\alpha(s)\,v(x,t) + \cos\alpha(s)\,w(x,t) + q(s)\,\theta_x(x,t) \end{aligned} \qquad 4.2\text{(a-b)}$$

in which $\alpha(s)$ represents the angle between the tangent to contour at the point of interest and the y axis and is taken as positive in the clockwise direction. The normal and tangential distances $r(s)$ and $q(s)$ (Figure 4.1c) from the pole to point A are given by

$$\begin{Bmatrix} q(s) \\ r(s) \end{Bmatrix} = \begin{bmatrix} \cos\alpha & \sin\alpha \\ -\sin\alpha & \cos\alpha \end{bmatrix} \begin{Bmatrix} (\bar{y} - y_r) \\ (\bar{z} - z_r) \end{Bmatrix} \qquad 4.3\text{(a-b)}$$

Owing to Assumption (1.ii) stipulating zero shear strain within the middle surface, the longitudinal displacement $u_A(x,s,t)$ for point $A\left[x, \bar{y}(s), \bar{z}(s)\right]$ is obtained (e.g, Vlasov [1])[7] by

$$u_A(x,s,t) = u_p(x) - \bar{y}(s)\,v'(x,t) - \bar{z}(s)\,w'(x,t) + \bar{\omega}(s)\,\theta_x'(x,t) \qquad 4.4$$

in which $\bar{\omega}(s) = \int_{s_0}^{s} h(s)ds$ is the global sectorial coordinate.

4.5.1.2. Displacement for a point offset from the middle surface

The displacements a point $B\left[x, y(s,n), z(s,n)\right]$ offset by a distance n from the mid-surface (Figure 4.1c), are related to displacements $v(x,t), w(x,t)$ of pole $R(y_r, z_r)$ by evoking the Kirchhoff plate assumption (1.iii) yielding

$$\begin{aligned} u_B(x,s,n,t) &= u_p(x) - y(s,n)\,v'(x,t) - z(s,n)\,w'(x,t) + \omega(s,n)\,\theta_x'(x,t) \\ v_B(x,s,n,t) &= C(s,n)\,v(x,t) + S(s,n)\,w(x,t) - \psi(s,n)\,\theta_x(x,t) \\ w_B(x,s,t) &= -\sin\alpha(s)\,v(x,t) + \cos\alpha(s)\,w(x,t) + q(s)\,\theta_x(x,t) \end{aligned} \qquad 4.5\text{ (a-c)}$$

[7] The procedure for expressing Eq.4.4 is recovered in Appendix C

in which coordinates $y(s,n)=\bar{y}(s)+\bar{\bar{y}}(s,n)$, $z(s,n)=\bar{z}(s)+\bar{\bar{z}}(s,n)$ and $\omega(s,n)=\bar{\omega}(s)+\bar{\bar{\omega}}(s,n)$, and coordinates $y(s,n), z(s,n)$ and $\omega(s,n)$ of point B are the sum of coordinates $\left[\bar{y}(s),\bar{z}(s),\bar{\omega}(s)\right]$ of the projection A of point B on the mid-surface and the coordinates $\left(\bar{\bar{y}},\bar{\bar{z}},\bar{\bar{\omega}}\right)$ of point B relative to A as given by

$$\bar{\bar{y}}=-n\sin\alpha(s),\bar{\bar{z}}=n\cos\alpha(s),\bar{\bar{\omega}}=-nq(s) \qquad 4.6\text{ (a-c)}$$

In Eq. 4.5(b), functions $C(s,n)=\cos\alpha(s)\left[1+n\,\partial\alpha(s)/\partial s\right]$, $S(s,n)=\sin\alpha(s)\left[1+n\,\partial\alpha(s)/\partial s\right]$ and $\psi(s,n)=r(s)+n\left[1-(\bar{y}-y_r)\sin\alpha(s)\partial\alpha(s)/\partial s+(\bar{z}-z_r)\cos\alpha(s)\partial\alpha(s)/\partial s\right]$ have been defined. For a section consisting of straight segments, one has $\partial\alpha(s)/\partial s=0$, yielding

$$C=\cos\alpha(s),S=\sin\alpha(s),\psi=r(s)+n \qquad 4.7\text{ (a-c)}$$

4.5.2. Strain-displacement relationships

The Green Lagrange strain-displacement relationships are given by

$$\varepsilon_{px}^{B}=\frac{\partial u_p}{\partial x}+\frac{1}{2}\left(\frac{\partial u_p}{\partial x}\right)^2 \qquad \varepsilon_{x}^{B}=\frac{\partial u_B}{\partial x}+\frac{1}{2}\left[\left(\frac{\partial u_B}{\partial x}\right)^2+\left(\frac{\partial v_B}{\partial x}\right)^2+\left(\frac{\partial w_B}{\partial x}\right)^2\right]$$
$$\gamma_{xs}^{B}=2\varepsilon_{xs}^{B}=\frac{\partial u_B}{\partial s}+\frac{\partial v_B}{\partial x}+\frac{\partial u_B}{\partial x}\frac{\partial u_B}{\partial s}+\frac{\partial v_B}{\partial x}\frac{\partial v_B}{\partial s}+\frac{\partial w_B}{\partial x}\frac{\partial w_B}{\partial s} \qquad 4.8\text{ (a-d)}$$
$$\gamma_{xn}^{B}=2\varepsilon_{xn}^{B}=\frac{\partial u_B}{\partial n}+\frac{\partial w_B}{\partial x}+\frac{\partial u_B}{\partial x}\frac{\partial u_B}{\partial n}+\frac{\partial v_B}{\partial x}\frac{\partial v_B}{\partial n}+\frac{\partial w_B}{\partial x}\frac{\partial w_B}{\partial n}$$

in which ε_{px}^{B} is the longitudinal strain due to the static axial load, and $\varepsilon_{x}^{B},\varepsilon_{xs}^{B},\varepsilon_{xn}^{B}$ are the total normal and shear strains at configuration 3. From Eqs. 4.5-4.7, substituting into Eq. 4.8(b-d) yields

$$\varepsilon_x^B = u_p' - yv'' - zw'' + \omega\theta_x'' + \frac{1}{2}\left[\left(u_p' - yv'' - zw'' + \omega\theta_x''\right)^2 + \left(Cv' + Sw' - \psi\theta_x'\right)^2 + \left(-Sv' + Cw' + q\theta_x'\right)^2\right]$$

$$\gamma_{xs}^B = \left(-y_{,s}v' - z_{,s}w' + \omega_{,s}\theta_x' + Cv' + Sw' + \psi\theta_x'\right) + \left(u_p' - yv'' - zw'' + \omega\theta_x''\right)\left(-y_{,s}v' - z_{,s}w' + \omega_{,s}\theta_x'\right)$$
$$+ \left(Cv' + Sw' - \psi\theta_x'\right)\left(C_{,s}v + S_{,s}w - \psi_{,s}\theta_x\right) + \left(-Sv' + Cw' + q\theta_x'\right)\left(-\alpha_{,s}Cv - \alpha_{,s}Sw + q_{,s}\theta_x\right)$$

$$\gamma_{xn}^B = \left(-y_{,n}v' - z_{,n}w' + \omega_{,n}\theta_x' - Sv' + Cw' + q\theta_x'\right)$$
$$+ \left(u_p' - yv'' - zw'' + \omega\theta_x''\right)\left(-y_{,n}v' - z_{,n}w' + \omega_{,n}\theta_x'\right) + \left(Cv' + Sw' - \psi\theta_x'\right)\left(C_{,n}v + S_{,n}w - \psi_{,n}\theta_x\right)$$

4.9 (a-c)

in which all $(\bullet)_{,s}$ $(\bullet)_{,n}$ denote differentiation with respect to coordinates s, n.

4.5.3. Variational principle

The variational form of Hamilton's principle (e.g., Meirovitch [23]) takes the form

$$\int_{t_1}^{t_2} \delta L_a dt = \int_{t_1}^{t_2} \left(\delta T - \delta U\right) dt = 0 \qquad 4.10$$

in which L_a is the Hamiltonian functional, T is the kinetic energy, U is the internal strain energy, δ denotes the variation of the argument functional, and all integrations are performed between arbitrary time limits $t = t_1$ and t_2. Figure 4.1b schematically depicts the longitudinal stress-strain relationship. The strain from Configuration 1 to 2 characterizes the member shortening under static axial load P and strain from Configuration 2 and 3 represents the additional time dependent strain induced by flexural-torsional vibrations. The internal strain energy U stored in the member throughout its deformation from Configuration 2 to 3 is represented by the hatched area and expressed as

$$U = \int_V \left[\sigma_{px}\left(\varepsilon_x^B - \varepsilon_{px}^B\right) + \frac{1}{2}\left(\sigma_x - \sigma_{px}\right)\left(\varepsilon_x^B - \varepsilon_{px}^B\right) + \frac{1}{2}\tau_{xs}\gamma_{xs}^B + \frac{1}{2}\tau_{xn}\gamma_{xn}^B\right] dV \qquad 4.11$$

For a linearly elastic isotropic material behavior (Assumptions 2), stresses σ_{xx}, τ_{xs} and τ_{xn} are related to the corresponding strains through $\sigma_x = E\varepsilon_x^B, \tau_{xs} = G\gamma_{xs}^B, \tau_{xn} = G\gamma_{xn}^B$ in which E is Young's modulus and G is the shear modulus. By substituting into Eq. 4.11, one obtains

$$U = \frac{1}{2}\int_V \left[\sigma_{px}\left(\varepsilon_x^B - \varepsilon_{px}^B\right) + E\varepsilon_x^B\left(\varepsilon_x^B - \varepsilon_{px}^B\right) + G\left(\gamma_{xs}^B\right)^2 + G\left(\gamma_{xn}^B\right)^2 \right] dV \tag{4.12}$$

From Eq. 4.12, by noting that $\int_V (\ )dV = \int_L \int_A (\ )dAdz$, evaluating the area integrals, adopting centroidal axes i.e., $\int_A ydA = \int_A zdA = 0$, taking the pole to coincide with the shear centre, i.e., $\int_A y\omega dA = \int_A z\omega dA = 0$, choosing a principal sectorial origin, i.e., $\int_A \omega dA = 0$ and using the identities in Eq. 4.3 and Eq. 4.9, one obtains [8]

$$\begin{aligned} U = {} & \frac{1}{2}\int_0^l EI_z v''^2 + EI_y w''^2 + EI_\omega \theta_x''^2 + GJ\theta_x'^2 + 2EI_{yz} v''w''dx \\ & -\frac{1}{2}\int_0^l P\left(v'^2 + w'^2 + \left(I_p/A\right)\theta_x'^2 + 2z_r v'\theta_x' - 2y_r w'\theta_x'\right)dz \end{aligned} \tag{4.13}$$

in which the sectional properties $\left(A, I_z, I_y, I_{yz}, I_\omega, I_p\right) = \int_A \left[1, y^2, z^2, yz, \omega^2, q^2 + \left(r+n\right)^2\right] dA$ have been defined and $I_{yz} = \int_A yzdA \neq 0$ since (y,z) are non-principal directions. The kinetic energy T is given by [9]

$$T = \frac{1}{2}\int_0^l \int_A \rho\left(\dot{u}_B{}^2 + \dot{v}_B{}^2 + \dot{w}_B{}^2\right)dAdx \tag{4.14}$$

[8] The details for developing Eq.4.13 is provided in Appendix D

[9] The expression of I_p is defined in Appendix E

in which ρ is the density and all dots denote time derivatives of the argument functions. From Eq. 4.5(a-c) and Eq. 4.7 (a-c), by substituting into Eq. 4.14 one obtains[10]

$$T = \frac{\rho}{2}\int_0^l \int_A \left[\left(u_p - y\dot{v}' - z\dot{w}' + \omega\dot{\theta}_x' \right)^2 + \left(\dot{v}C + \dot{w}S - \left(r + n \right)\dot{\theta}_x \right)^2 + \left(-\dot{v}S + \dot{w}C + q\dot{\theta}_x \right)^2 \right] dA dx \quad 4.15$$

From Eq. 4.13 and Eq. 4.15, by substituting into Eq. 4.10, one obtains

$$\begin{aligned} \int_{t_1}^{t_2} \delta L_a dt = -\int_{t_1}^{t_2} \int_0^l \Big(& EI_z v''\delta v'' + EI_y w''\delta w'' + EI_\omega \theta_x''\delta\theta_x'' + GJ\theta_x'\delta\theta_x' + \underline{EI_{yz} v''\delta w'' + EI_{yz} w''\delta v''} \Big) \\ & - P\Big[v'\delta v' + w'\delta w' + \left(I_p / A \right)\theta_x'\delta\theta_x' + \underline{\underline{z_r\theta_x'\delta v' + z_r v'\delta\theta_x' - y_r\theta_x'\delta w' - y_r w'\delta\theta_x'}} \Big] \\ & + \rho\Big[\left(-A\ddot{v} - \underline{\underline{z_r A\ddot{\theta}_x}} \right)\delta v + \left(-A\ddot{w} + \underline{\underline{y_r A\ddot{\theta}_x}} \right)\delta w + \left(\underline{\underline{-z_r A\ddot{v} + y_r A\ddot{w}}} - I_p\ddot{\theta}_x \right)\delta\theta_x \Big] \\ & - \rho\left(I_z\ddot{v}'\delta v' + I_y\ddot{w}'\delta w' + I_\omega\ddot{\theta}_x'\delta\theta_x' + \underline{I_{yz}\ddot{v}'\delta w' + I_{yz}\ddot{w}'\delta v'} \right) dx dt = 0 \end{aligned} \quad 4.16$$

in which the first integral represents the contribution of the internal strain energy, the second integral represents the destabilizing/stabilizing effect due to the axial compressive/tensile force P, the third integral represents the translational inertial effect, and the last integral represents the rotary inertial effect. The terms with a single underline represent the coupling effect arising from adopting non-principal directions, while those with a double underline represent the coupling arising from the asymmetry of the cross-section.

4.5.4. Equations of motion and boundary conditions

From Eq. 4.16, by conducting integration by parts, grouping like terms, noting that $\delta v, \delta w, \delta\theta_x$ are arbitrary functions, and that for natural vibration, one has $\left\langle v(x,t), w(x,t), \theta_x(x,t) \right\rangle = \left\langle V(x), W(x), \theta_x(x) \right\rangle \sin(\omega t)$, one recovers the equations of motion

[10] The procedure for obtaining Eq.4.15 is provided in Appendix F

$$EI_z V^{iv} - PV'' - Pz_r\theta_x'' + EI_{yz}W^{iv} + \rho\omega^2 I_z V'' + \rho\omega^2 I_{yz}W'' - \rho A\omega^2 V - \rho A\omega^2 z_r\theta_x = 0$$
$$EI_y W^{iv} - PW'' + Py_r\theta_x'' + EI_{yz}V^{iv} + \rho\omega^2 I_y W'' + \rho\omega^2 I_{yz}V'' - \rho A\omega^2 W + \rho A\omega^2 y_r\theta_x = 0$$
$$EI_\omega\theta_x^{iv} - GJ\theta_x'' - \left(I_P/A\right)P\theta_x'' - Pz_r V'' + Py_r W'' + \rho\omega^2 I_\omega\theta_x'' - \rho A\omega^2 z_r V + \rho A\omega^2 y_r W - \rho I_s\omega^2\theta_x = 0$$

4.17

and the possible boundary conditions for the problem, i.e.,

$$\left(EI_z V''(0) + EI_{yz}W''(0)\right)\delta V'(0) = 0 \qquad \left(EI_z V''(l) + EI_{yz}W''(l)\right)\delta V'(l) = 0$$
$$\left(EI_y W''(0) + EI_{yz}V''(0)\right)\delta W'(0) = 0 \qquad \left(EI_y W''(l) + EI_{yz}V''(l)\right)\delta W'(l) = 0$$
$$EI_\omega\theta_x''(0)\delta\theta_x'(0) = 0 \qquad EI_\omega\theta_x''(l)\delta\theta_x'(l) = 0$$
$$\left(PV'(0) + Pz_r\theta_x'(0) - EI_z V'''(0) - EI_{yz}W'''(0) + \rho\omega^2 I_z V'(0) + \omega^2 I_{yz}W'(0)\right)\delta V(0) = 0$$
$$\left(PV'(l) + Pz_r\theta_x'(l) - EI_z V'''(l) - EI_{yz}W'''(l) + \rho\omega^2 I_z V'(l) + \omega^2 I_{yz}W'(l)\right)\delta V(l) = 0 \qquad \text{4.18(a-l)}$$
$$\left(PW'(0) - Py_r\theta_x'(0) - EI_y W'''(0) - EI_{yz}V'''(0) + \rho\omega^2 I_y W'(0) + \omega^2 I_{yz}V'(0)\right)\delta W(0) = 0$$
$$\left(PW'(l) - Py_r\theta_x'(l) - EI_y W'''(l) - EI_{yz}V'''(l) + \rho\omega^2 I_y W'(l) + \omega^2 I_{yz}V'(l)\right)\delta W(l) = 0$$
$$\left(GJ\theta_x'(0) + \left(I_p/A\right)P\theta_x'(0) + Pz_r V'(0) - Py_r W'(0) - EI_\omega\theta_x'''(0) + \rho\omega^2 I_\omega\theta_x'(0)\right)\delta\theta_x(0) = 0$$
$$\left(GJ\theta_x'(l) + \left(I_p/A\right)P\theta_x'(l) + Pz_r V'(l) - Py_r W'(l) - EI_\omega\theta_x'''(l) + \rho\omega^2 I_\omega\theta_x'(l)\right)\delta\theta_x(0) = 0$$

4.5.5. Analytical Solution – Members Pinned in all directions

For a member pinned in all three directions, the displacement fields $\langle V(x) \quad W(x) \quad \theta_x(x)\rangle = \langle A \quad B \quad C\rangle \sin(\pi x/l)$ satisfy all the essential and natural boundary conditions of the problem. By substituting into Eq. 4.16, expressing the result in matrix form, and setting to zero the determinant of the resulting matrix of coefficients, one obtains

$$\left|\tilde{\mathbf{K}} - P\tilde{\mathbf{K}}_{\mathbf{G}} + \omega^2\tilde{\mathbf{M}}\right| = 0$$

$$\tilde{\mathbf{K}} = (\pi/l)^4 \begin{bmatrix} EI_z & EI_{yz} & 0 \\ EI_{yz} & EI_y & 0 \\ 0 & 0 & EI_\omega + GJ/(\pi/l)^2 \end{bmatrix}, \tilde{\mathbf{K}}_{\mathbf{G}} = (\pi/l)^2 \begin{bmatrix} 1 & 0 & z_r \\ 0 & 1 & -y_r \\ z_r & -y_r & I_P/A \end{bmatrix} \qquad 4.19$$

$$\tilde{\mathbf{M}} = \rho \begin{bmatrix} A + (\pi/l)^2 I_z & (\pi/l)^2 I_{yz} & Az_r \\ (\pi/l)^2 I_{yz} & A + (\pi/l)^2 I_y & -Ay_r \\ Az_r & -Ay_r & I_P + (\pi/l)^2 I_\omega \end{bmatrix}$$

When the axial load vanishes (i.e., $P = 0$), the natural frequency ω is obtained by setting the determinant of the matrix of coefficients to zero, i.e, $\left|\tilde{\mathbf{K}} - \omega^2\tilde{\mathbf{M}}\right| = 0$. For the special case where principal axes are adopted, i.e. $I_{yz} = 0$, one recovers the bi-cubic equation

$$\tilde{A}\omega^6 + \tilde{B}\omega^4 + \tilde{C}\omega^2 + \tilde{D} = 0 \qquad 4.20$$

in which

$$\begin{aligned}
\tilde{A} &= \rho^3\left(z^2{}_r A^2 I_y + y^2{}_r A^2 I_z - A^2 I_\omega - A I_y I_P\right)(\pi/l)^2 - \rho^2 I_z{}^2 I_P (\pi/l)^2 \\
&\quad + \rho^3\left(y^2{}_r A^3 + z^2{}_r A^3 - A^2 I_P\right) - \rho^3 A I_\omega\left(I_y + I_z\right)(\pi/l)^4 - \rho^3 I_y I_z I_\omega (\pi/l)^6 - \rho^3 I_y I_z I_P (\pi/l)^4 \\
\tilde{B} &= -\rho^2 A^2 E\left(z^2{}_r I_y + y^2{}_r I_z\right)(\pi/l)^4 + 3\rho^2 E I_y I_z I_\omega (\pi/l)^8 + 2\rho^2 E I_y I_z I_P (\pi/l)^6 \\
&\quad + \rho^2 A E I_\omega\left(I_y + I_z\right)(\pi/l)^6 + \rho^2 A E I_P\left(I_y + I_z\right)(\pi/l)^4 + \rho^2 A E I_\omega\left(I_y + I_z\right)(\pi/l)^6 \\
&\quad + \rho^2 A G J\left(I_y + I_z\right)(\pi/l)^4 + \rho^2 A^2 E I_\omega (\pi/l)^4 + \rho^2 A^2 G J (\pi/l)^2 + \rho^2 I_y I_z G J (\pi/l)^6 \\
\tilde{C} &= -3E^2\rho I_y I_z I_\omega (\pi/l)^{10} - E^2\rho I_P I_y I_z (\pi/l)^8 - 2\rho E I_y I_z G J (\pi/l)^8 - \rho A E^2 I_\omega\left(I_y + I_z\right)(\pi/l)^8 \\
&\quad - \rho A E G J\left(I_y + I_z\right)(\pi/l)^6 \\
\tilde{D} &= E^3 I_y I_z I_\omega (\pi/l)^{12} + E^2 I_y I_z G J (\pi/l)^{10}
\end{aligned} \qquad 4.21$$

4.5.6. Energy Solution – Member with end Gusset Plate Connections

For a member fixed about a non-principal direction and pinned about the orthogonal direction and relative to twist, the displacement fields $\langle V(x), W(x), \theta_x(x)\rangle = \langle A(1-\cos(2\pi x/l)), B\sin(\pi x/l), C\sin(\pi x/l)\rangle$ satisfy all the essential and natural boundary conditions. By substituting into Eq. 4.16, performing all integrals, expressing the result in a matrix form, and setting to zero the determinant of the matrix of coefficients, one obtains

$$
\begin{aligned}
&\left|\tilde{\mathbf{K}} - P\tilde{\mathbf{K}}_{\mathbf{G}} + \omega^2\tilde{\mathbf{M}}\right| = 0 \\
&\tilde{\mathbf{K}} = -\left(\frac{E\pi^4}{2l^3}\right)\begin{bmatrix} 16I_z & (16/3\pi)I_{yz} & 0 \\ (16/3\pi)I_{yz} & I_y & 0 \\ 0 & 0 & I_\omega + \left(GJl^2\right)/\left(\pi^2 E\right) \end{bmatrix}, \\
&\tilde{\mathbf{K}}_{\mathbf{G}} = \frac{\pi^2}{2l}\begin{bmatrix} 4 & 0 & z_r(16/3\pi) \\ 0 & 1 & -y_r \\ z_r(16/3\pi) & -y_r & \left(I_p/A\right) \end{bmatrix} \\
&\tilde{\mathbf{M}} = \frac{\rho l}{2}\begin{bmatrix} 3A + 4\pi^2\left(I_z/l^2\right) & (16\pi/3)\left(I_{yz}/l^2\right) & (16/3\pi)Az_r \\ (16\pi/3)\left(I_{yz}/l^2\right) & A + \pi^2\left(I_y/l^2\right) & -Ay_r \\ (16/3\pi)Az_r & -Ay_r & I_p + \pi^2\left(I_\omega/l^2\right) \end{bmatrix}
\end{aligned}
\qquad 4.22
$$

4.5.7. Finite Element formulation

The displacement functions are related to the nodal vectors $\mathbf{v}_\mathbf{n}^\mathbf{T} = \langle v(0) \quad v'(0) \quad v(l) \quad v'(l)\rangle$, $\mathbf{w}_\mathbf{n}^\mathbf{T} = \langle w(0) \quad w'(0) \quad w(l) \quad w'(l)\rangle$ and $\boldsymbol{\theta}_\mathbf{n}^\mathbf{T} = \langle \theta_x(0) \quad \theta_x'(0) \quad \theta_x(l) \quad \theta_x'(l)\rangle$ through

$$
v(x) = \mathbf{H}_\mathbf{v}^\mathbf{T}(x)\mathbf{v}_\mathbf{n} \quad ; \quad w(x) = \mathbf{H}_\mathbf{w}^\mathbf{T}(x)\mathbf{w}_\mathbf{n} \quad ; \quad \theta_x(x) = \mathbf{H}_\mathrm{v}^\mathrm{T}(x)\boldsymbol{\theta}_\mathbf{n} \qquad 4.23
$$

in which

$$\mathbf{H}_{\mathbf{v}}^{\mathbf{T}} = \left\langle \left(1-3\zeta^2+2\zeta^3\right) \quad L\left(\zeta-2\zeta^2+\zeta^3\right) \quad \left(3\zeta^2-2\zeta^3\right) \quad L\left(\zeta^3-\zeta^2\right) \right\rangle$$
$$\mathbf{H}_{\mathbf{w}}^{\mathbf{T}} = \left\langle \left(1-3\zeta^2+2\zeta^3\right) \quad -L\left(\zeta-2\zeta^2+\zeta^3\right) \quad \left(3\zeta^2-2\zeta^3\right) \quad -L\left(\zeta^3-\zeta^2\right) \right\rangle \qquad \zeta = x/L \quad 4.24$$

are the vectors of Hermitian polynomials. From Eq. 4.23, by substituting into Eq. 4.17, noting that t_1, t_2 are arbitrary times and $\delta\mathbf{v_n}, \delta\mathbf{w_n}, \delta\boldsymbol{\theta}_\mathbf{n}$ arbitrary functions, one obtains

$$\left(\mathbf{K}+P\mathbf{K_G}\right)\mathbf{U}_\mathbf{N}\left(t\right)+\left(\mathbf{M_1}+\mathbf{M_2}\right)\ddot{\mathbf{U}}_\mathbf{N}\left(t\right)=\mathbf{0} \qquad 4.25$$

in which $\mathbf{K}$ is the stiffness matrix, $\mathbf{K_G}$ is a geometric matrix that accounts for the effect of the axial force P, $\mathbf{M_1}$ is the mass matrix that accounts for the translational inertial effects, $\mathbf{M_2}$ is the mass matrix that accounts for the rotatory inertial effects, $\mathbf{U}_\mathbf{N}^\mathbf{T} = \left\langle \mathbf{v}_\mathbf{n}^\mathbf{T} \quad \mathbf{w}_\mathbf{n}^\mathbf{T} \quad \boldsymbol{\theta}_\mathbf{n}^\mathbf{T} \right\rangle$ and

$$\left(\mathbf{K},\mathbf{K_G},\mathbf{M_1},\mathbf{M_2}\right) =$$
$$\left(\begin{bmatrix} \mathbf{K_{vv}} & \mathbf{K_{vw}} & \mathbf{0} \\ \mathbf{K_{vw}^T} & \mathbf{K_{ww}} & \mathbf{0} \\ \mathbf{0} & \mathbf{0} & \mathbf{K_{\theta\theta}} \end{bmatrix}, \begin{bmatrix} \mathbf{G_{vv}} & \mathbf{0} & \mathbf{G_{v\theta}} \\ \mathbf{0} & \mathbf{G_{ww}} & \mathbf{G_{w\theta}} \\ \mathbf{G_{v\theta}^T} & \mathbf{G_{w\theta}^T} & \mathbf{G_{\theta\theta}} \end{bmatrix}, \begin{bmatrix} \mathbf{M_{vv}} & \mathbf{0} & \mathbf{M_{v\theta}} \\ \mathbf{0} & \mathbf{M_{ww}} & \mathbf{M_{w\theta}} \\ \mathbf{M_{v\theta}^T} & \mathbf{M_{w\theta}^T} & \mathbf{M_{\theta\theta}} \end{bmatrix}, \begin{bmatrix} \mathbf{I_{vv}} & \mathbf{I_{vw}} & \mathbf{0} \\ \mathbf{I_{vw}^T} & \mathbf{I_{ww}} & \mathbf{0} \\ \mathbf{0} & \mathbf{0} & \mathbf{I_{\theta\theta}} \end{bmatrix} \right) \qquad 4.26$$

in which the following submatrices have been defined

$$\mathbf{K}_{\mathbf{vv}} = EI_z \int_l \mathbf{H}_{\mathrm{v}}''(x)\mathbf{H}_{\mathrm{v}}^{\mathrm{T}''}(x)\,dx \quad ; \quad \mathbf{K}_{\mathbf{ww}} = EI_y \int_l \mathbf{H}_{\mathrm{w}}''(x)\mathbf{H}_{\mathrm{w}}^{\mathrm{T}''}(x)\,dx$$

$$\mathbf{K}_{\boldsymbol{\theta\theta}} = EI_\omega \int_l \mathbf{H}_{\mathrm{v}}''(x)\mathbf{H}_{\mathrm{v}}^{\mathrm{T}''}(x)\,dx + GJ\int_l \mathbf{H}_{\mathrm{v}}'(x)\mathbf{H}_{\mathrm{v}}^{\mathrm{T}'}(x)\,dx \quad ; \quad \mathbf{K}_{\mathbf{vw}} = EI_{yz}\int_l \mathbf{H}_{\mathrm{v}}''(x)\mathbf{H}_{\mathrm{w}}^{\mathrm{T}''}(x)\,dx$$

$$\mathbf{K}_{\mathbf{wv}} = \mathbf{K}_{\mathbf{vw}}^{\mathrm{T}} = EI_{yz}\int_l \mathbf{H}_{\mathrm{w}}''(x)\mathbf{H}_{\mathrm{v}}^{\mathrm{T}''}(x)\,dx$$

$$\mathbf{G}_{\mathbf{vv}} = \int_l \mathbf{H}_{\mathrm{v}}'(x)\mathbf{H}_{\mathrm{v}}^{\mathrm{T}'}(x)\,dx \quad ; \quad \mathbf{G}_{\mathbf{ww}} = \int_l \mathbf{H}_{\mathrm{w}}'(x)\mathbf{H}_{\mathrm{w}}^{\mathrm{T}'}(x)\,dx \quad ; \quad \mathbf{G}_{\boldsymbol{\theta\theta}} = \frac{I_p}{A}\int_l \mathbf{H}_{\mathrm{v}}'(x)\mathbf{H}_{\mathrm{v}}^{\mathrm{T}'}(x)\,dx$$

$$\mathbf{G}_{\mathbf{v\theta}} = \mathbf{G}_{\boldsymbol{\theta}\mathbf{v}}^{\mathbf{T}} = z_r \int_l \mathbf{H}_{\mathrm{v}}'(x)\mathbf{H}_{\mathrm{v}}^{\mathrm{T}'}(x)\,dx \quad ; \quad \mathbf{G}_{\mathbf{w\theta}} = \mathbf{G}_{\boldsymbol{\theta}\mathbf{w}}^{\mathbf{T}} = -y_r \int_l \mathbf{H}_{\mathrm{w}}'(x)\mathbf{H}_{\mathrm{v}}^{\mathrm{T}'}(x)\,dx$$

$$\mathbf{M}_{\mathbf{vv}} = \rho A\int_l \mathbf{H}_{\mathrm{v}}(x)\mathbf{H}_{\mathrm{v}}^{\mathrm{T}}(x)\,dx \quad ; \quad \mathbf{M}_{\mathbf{ww}} = \rho A\int_l \mathbf{H}_{\mathrm{w}}(x)\mathbf{H}_{\mathrm{w}}^{\mathrm{T}}(x)\,dx \quad ; \quad \mathbf{M}_{\boldsymbol{\theta\theta}} = \rho I_p \int_l \mathbf{H}_{\mathrm{v}}(x)\mathbf{H}_{\mathrm{v}}^{\mathrm{T}}(x)\,dx$$

$$\mathbf{M}_{\mathbf{v\theta}} = \mathbf{M}_{\boldsymbol{\theta}\mathbf{v}}^{\mathbf{T}} = \rho z_r A\int_l \mathbf{H}_{\mathrm{v}}(x)\mathbf{H}_{\mathrm{v}}^{\mathrm{T}}(x)\,dx \quad ; \quad \mathbf{M}_{\mathbf{w\theta}} = \mathbf{M}_{\boldsymbol{\theta}\mathbf{w}}^{\mathbf{T}} = -\rho y_r A\int_l \mathbf{H}_{\mathrm{w}}(x)\mathbf{H}_{\mathrm{v}}^{\mathrm{T}}(x)\,dx$$

$$\mathbf{I}_{\mathbf{vv}} = \rho I_z \int_l \mathbf{H}_{\mathrm{v}}'(x)\mathbf{H}_{\mathrm{v}}^{\mathrm{T}'}(x)\,dx \quad ; \quad \mathbf{I}_{\mathbf{ww}} = \rho I_y \int_l \mathbf{H}_{\mathrm{w}}'(x)\mathbf{H}_{\mathrm{w}}^{\mathrm{T}'}(x)\,dx \quad ; \quad \mathbf{I}_{\boldsymbol{\theta\theta}} = \rho I_\omega \int_l \mathbf{H}_{\mathrm{v}}'(x)\mathbf{H}_{\mathrm{v}}^{\mathrm{T}'}(x)\,dx$$

$$\mathbf{I}_{\mathbf{vw}} = \mathbf{I}_{\mathbf{wv}}^{\mathbf{T}} = \rho I_{yz}\int_l \mathbf{H}_{\mathrm{v}}'(x)\mathbf{H}_{\mathrm{w}}^{\mathrm{T}'}(x)\,dx$$

4.27

When y and z coincide with the principal directions, matrices $\mathbf{K}_{\mathbf{vw}}$ and $\mathbf{I}_{\mathbf{vw}}$ will vanish. Also, for doubly symmetric sections, the coupling matrices $\mathbf{G}_{\mathbf{v\theta}}, \mathbf{G}_{\mathbf{w\theta}}, \mathbf{M}_{\mathbf{v\theta}}, \mathbf{M}_{\mathbf{w\theta}}$ will vanish, while for monosymmetric sections either $\mathbf{G}_{\mathbf{v\theta}}, \mathbf{M}_{\mathbf{v\theta}}$ or $\mathbf{G}_{\mathbf{w\theta}}, \mathbf{M}_{\mathbf{w\theta}}$ will vanish, depending on the axis of symmetry. For free vibrations, one has $\mathbf{U}_{\mathrm{N}}(t) = \mathbf{D}_{\mathrm{N}} \sin \omega t$ and Eq. 4.25 yields

$$\left[\mathbf{K} + P\mathbf{K}_{\mathbf{G}} - \omega^2\left(\mathbf{M}_1 + \mathbf{M}_2\right)\right]\mathbf{D}_{\mathrm{N}} = \mathbf{0} \tag{4.28}$$

in which $\mathbf{D}_{\mathrm{N}}$ is the mode shape.

4.6. Verification

4.6.1. Reference Case A

4.6.1.1. Description

A 4m axially loaded member has a L152x102x16 cross-section (Figure 4.1a). Cross-sectional properties are $A = 3790mm^2, I_{\hat{y}} = 1.01\times10^7\, mm^4, I_{\hat{z}} = 1.79\times10^6\, mm^4$, $r_{\hat{y}} = 51.5mm$, $r_{\hat{z}} = 21.7mm$, $m = 52.1kg/m$. The slenderness ratio about the non-principal minor axis is $l/r_z = 138.4$, and that about the principal major and minor axes is $l/r_{\hat{y}} = 77.7$, $l/r_{\hat{z}} = 184.1$. Steel properties are $E = 2\times10^5\ MPa, G = 7.7\times10^4\ MPa$. The member is pinned at both ends relative to lateral and transverse displacements and twist, and axially restrained at its centroid at one end, and subjected to axial load $-2P_{cr} \le P \le P_{cr}$ (positive when in compression) at the other end, P_{cr} being the elastic flexural-torsional buckling load as determined from (e.g., AISC Design [24], CSA [25]) as

$$\begin{gathered}\left(P_{cr}-P_{\hat{y}}\right)\left(P_{cr}-P_{\hat{z}}\right)\left(P_{cr}-P_{\hat{x}}\right)-P_{cr}{}^2\left(P_{cr}-P_{\hat{z}}\right)\left(\hat{y}_r/r_0\right)^2-P_{cr}{}^2\left(P_{cr}-P_{\hat{y}}\right)\left(\hat{z}_r/r_0\right)^2=0 \\ P_{\hat{y}}=\left(\pi/l\right)^2 EI_{\hat{y}} \quad , \quad P_{\hat{z}}=\left(\pi/l\right)^2 EI_{\hat{z}} \quad , \quad P_{\hat{x}}=\left[\left(\pi/l\right)^2 EI_{\hat{\omega}}+GJ\right]\Big/r_0^2\end{gathered} \qquad 4.29\text{(a-d)}$$

where $I_{\hat{y}}, I_{\hat{z}}$ are the principal moments of inertia, and $r_0 = \sqrt{\hat{y}_r^2 + \hat{z}_r^2 + r_{\hat{y}}^2 + r_{\hat{z}}^2}$ is the polar radius of gyration about the shear centre. The smallest critical load as predicted by Eqs. 4.29 is found to correspond to $P_{\hat{z}}$ and equal to 221 kN.

4.6.1.2. Present model

In the present model, the displacements along the principal directions and angle of twist were restrained at both ends. The longitudinal displacement is restrained at one end and the axially

loaded at the other end. Two meshes were attempted for the case $P = 0$; consisting of eight and 16 elements. The corresponding fundamental natural frequencies predicted were 10.78 Hz and 10.77 *Hz*, respectively, a difference of 0.01 percent indicating that eight elements are enough to attain convergence. Comparatively, the analytical solution in Eq. 4.20 predicted a fundamental natural frequency of 10.74 *Hz*, in close agreement with the present model prediction.

4.6.1.3. Shell model

A finite element model is developed based on the S4 element in the ABAQUS library. The S4 element is a four-node quadrilateral shell element with six degrees of freedom per node, three translations, and three rotations. To simulate pin end conditions, the angle of twist and displacements along the y and z directions were restrained for all nodes along the member ends. Two master nodes were defined at the section centroid at both ends. The longitudinal displacement of the master nodes was restrained while at the other end was subjected to the axial force. The analysis was conducted in two steps. Initially, the axial load was applied at the longitudinally unrestrained end master node. Next, the natural frequency of the axially loaded member was determined through a natural frequency eigenvalue analysis step, in which geometric nonlinear effects were evoked to capture second-order effects due to axial loading. Two meshes were attempted for the unloaded reference member. The first one had five elements along the short leg, eight elements along the long leg, and 200 elements along the span, totaling 2600 elements. In the second mesh the number of elements were doubled in all three directions. The corresponding fundamental natural frequencies predicted were 10.71 Hz and 10.67 Hz, respectively, a difference of less than 0.2 percent indicating convergence was achieved by the coarser mesh. Both values are in close agreement with the fundamental natural frequency predicted by the present model.

4.6.2. Reference Case B

4.6.2.1. Description

Reference case B has the same geometry as Case A while assuming gusset plate connections at both ends entailing a full rotational restraint about the z axis and a near-pin condition at member ends about the y axis (Figure 4.2b), i.e., the partial rotational restraint about the y axis offered by the gusset plates to the member ends is conservatively neglected. The critical load P_{cr} based on the analytical solution of Alenezi and Mohareb [22] is 339.7 kN. This value compares closely to 338.6 kN to that predicted by a shell model based on the S4 element of ABAQUS in the same study.

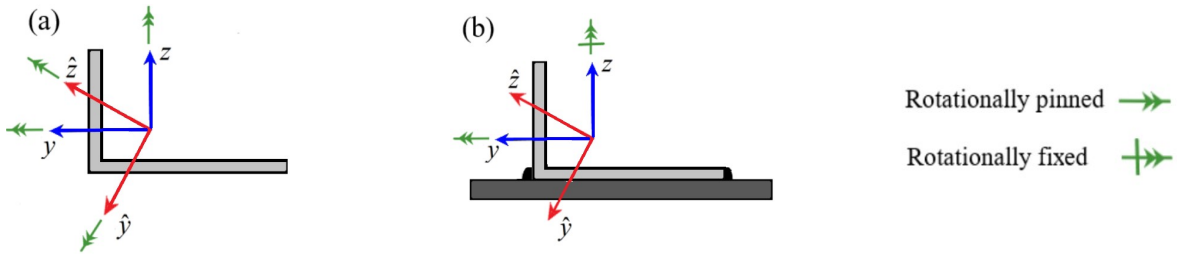

Figure 4.2(a) Pinned boundary conditions versus (b) gusset plate fixity conditions

4.6.2.2. Modelling considerations

The specifics of the present finite model are similar to those previously described for Reference Case A with two differences; (1) cross-sectional properties $\left\{I_{\hat{y}}, I_{\hat{z}}, I_{\hat{y}\hat{z}}, I_{\hat{s}}, \hat{y}_r, \hat{z}_r\right\}$ were adopted instead of $\left\{I_y, I_z, I_{yz}=0, I_p, y_r, z_r\right\}$, and (2) the rotation about z axis was restrained at both ends (as opposed to being released). Again, the specifics of the shell model are similar to those of the shell model for Reference Case A, while restraining the rotation about the z axis at both ends.

4.6.2.3. Shell Model

The specifics of the shell model are similar to those described for reference case "A". To simulate the rotational restraint provided by the gusset plate connection, and additional rotational restraint about the z-axis (Figure 4.2) was introduced at the master node. Two mesh configurations were tested for the unloaded reference member. The first mesh consisted of four elements along the short leg, five along the long leg, and 100 along the span, resulting in a total of 900 elements. In the second mesh, the resolution was increased to five elements along the short leg, eight along the long leg, and the number of elements along the span was doubled. The fundamental natural frequencies predicted by both meshes were 13.41 Hz and 13.39 Hz, respectively, differing by less than 0.2%, indicating that convergence was achieved with the coarser mesh. Both values closely match the fundamental natural frequency predicted by the present model.

4.6.3. Comparison

Figure 4.3 provides a comparison of the interaction relationships between natural frequency and axial force for the pin connected member in Case A and that of gusset plate connection in Case B. In both cases, the applied axial force is normalized relative to the elastic buckling force P_{cr}^{pin} for Case A. Also, the natural frequency is normalized relative to the natural frequency $\omega_{P=0}^{pin}$ in the absence of axial load (i.e., $P=0$) for Case A. The predictions of the analytical solutions are observed to closely match those of the ABAQUS shell model.

In general, the normalized interaction diagram for Case B is larger than that of Case A with a natural frequency ratio of 1.24 at zero axial load and a critical load ratio of 1.56 at zero natural frequency. Very close agreement is observed between the predictions of the present model (involving only 56 DOFs) and those of the shell model (involving 16,800DOFs). The larger natural

frequency for Case B is attributed to the rotational restraints at both ends about the z axis. As the compressive axial force increases, the difference in natural frequencies between cases A and B becomes more pronounced. Figure 4.4 depicts the corresponding fundamental mode shapes. In the S4 model, the angle of twist at a given cross-section was calculated by averaging the angles of twist at the shear centre and the tip points of the angles. The mode shapes were normalized with respect to the peak transverse displacement. A close agreement is observed between the mode shapes predicted by both models. For the pin ended connection, the ratio of peak lateral to transverse displacement is found to be larger than that for the gusset end connection. Conversely, the twist angle for the case of the gusset end connection is found to be larger relative to that of the pinned end connection.

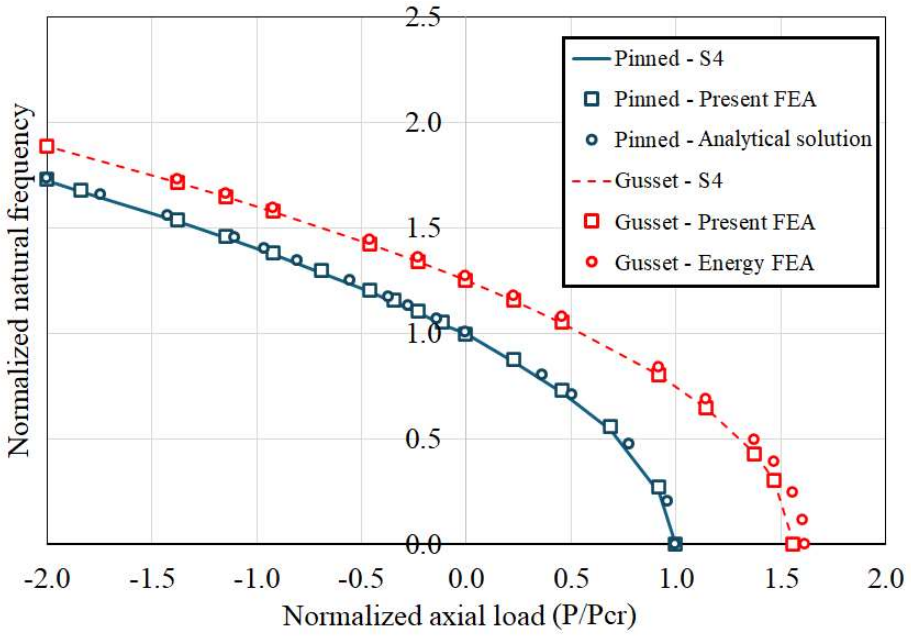

Figure 4.3 Normalized natural frequency $\omega/\omega_{P=0}^{pin}$ vs Normalized Axial Force P/P_{cr}^{pin}

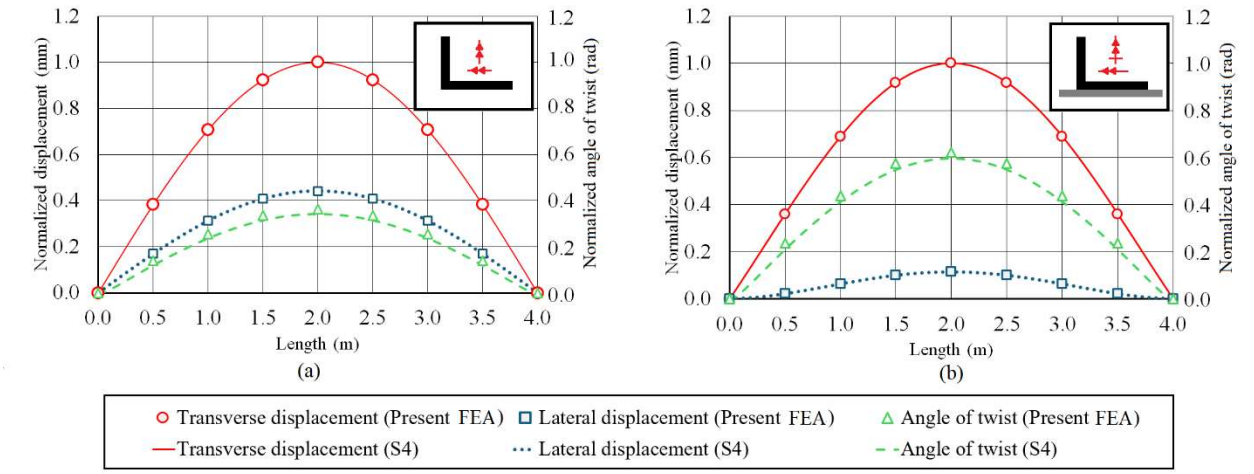

Figure 4.4 Normalized fundamental vibration mode shapes for $P/P_{cr}^{pin}=0$ (shear centre displacements and angle of twist) for members with (a) Pin end connections and (b) Gusset plate end connections

Figure 4.5 presents the normalized natural frequency versus the normalized axial load for angle cross-sections with different aspect ratios for pinned end and gusset plate end connections. Two spans were investigated: L = 4 m and 6 m. The results indicate that the member span, cross-sectional aspect ratio, and thickness do not affect the normalized interaction diagrams when the axial force is normalized relative to the classical buckling load in the case of pin end connection (or relative to the buckling load reported in Alenezi and Mohareb [22] in the case of gusset plate connection), and the natural frequency is normalized relative to the natural frequency of the member under zero load as predicted by Eq. 4.20 in the case of pin end connection, and Eq. 4.22 in the case of gusset plate connection.

Figure 4.6 depicts the normalized interaction diagram for a 4m span pin-ended member with a L203×102×16 cross-section (Figure 4.6a) and gusset plate connections (Figure 4.6b). The close agreement between the predictions of the present finite element solution and the analytical solution in Eq. 4.19 for the pin-ended member, and with the energy-based solution in Eq. 4.22 in the case of gusset plate connection suggests the validity of the present formulation and implementation.

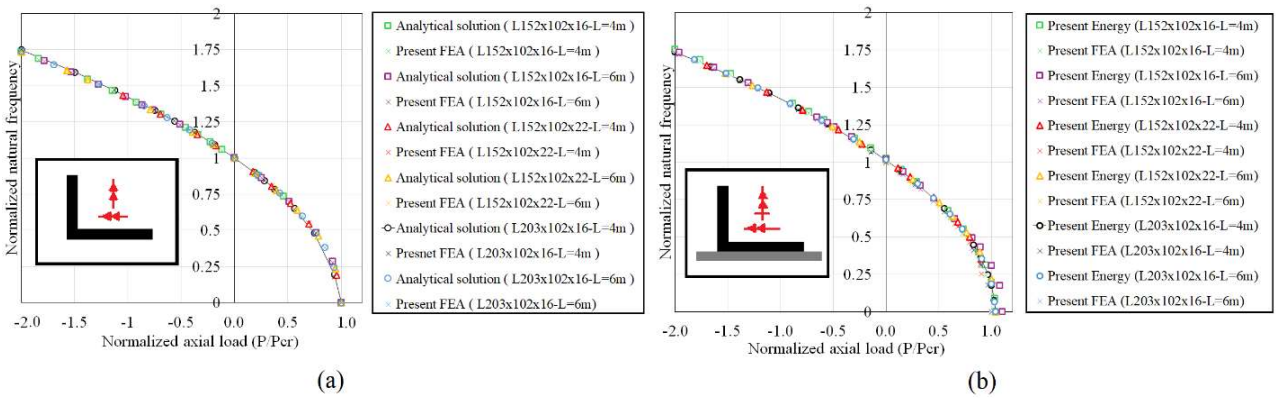

Figure 4.5 Normalized natural frequency vs Normalized Axial Force - Comparison of present FEA, analytical and energy solutions for various cross-sections and spans - (a) Pin end connections and (b) Gusset plate end connections

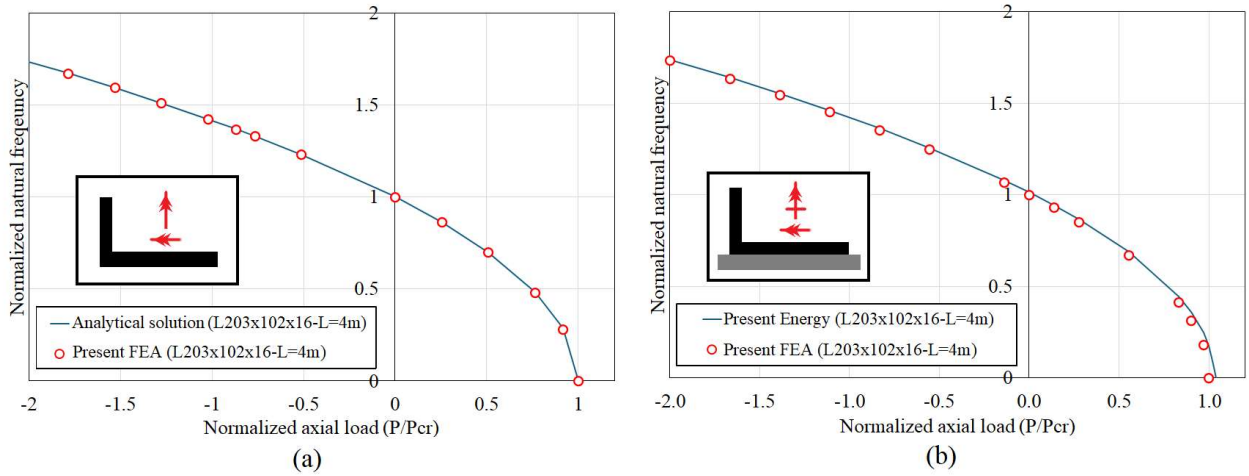

Figure 4.6 Comparison of FEA solution and analytical and present energy solution - Normalized natural frequency vs Normalized Axial Force for members with (a) Pin end connections and (b) Gusset plate end connections

4.6.4. Effect of rotary inertia

One recalls that Eqs. 4.28, which provides the basis to characterize the natural frequency, account for the rotary inertia effect. To assess the validity and implementation of the rotary inertia aspect of the formulation, the predictions of the present model are compared to those of Sahraei et al. [19] who investigated the influence of rotary inertia on the natural frequencies of cantilever members with 4m and 6m spans with a W250×58 doubly symmetric cross-section. Cross sectional dimensions are $b = 203\ mm, d = 238.5\ mm, t_w = 8.0\ mm$, and $t_f = 13.5\ mm$. The mass density

per unit volume is taken as $\rho = 7800\ kg/m^3$ and the cross-sectional properties are $A = 7389mm^2$, $I_y = 8.707\times10^7\,mm^4$, $I_z = 1.883\times10^6\,mm^4$, $I_\omega = 2.68\times10^{11}\,mm^6$. The present solution and that of Sahraei et al. [19] can predict the natural frequency in the presence or absence of rotary inertial effects (by omitting the relevant rotary inertia terms). While the present solution captures the effect of axial loading but omits shear deformation effects, the solution in Sahraei et al. [19] captures shear deformation effects but omits the effect of axial loading. Natural frequency predictions of both solutions are expected to agree, for long span members in which shear deformation effects are negligible, with no axial loading. As expected, very close natural frequencies are predicted by both models for minor and major axis flexural vibration modes and for torsional modes (Table 4.2). This is the case irrespective of whether rotary inertia effects are accounted for or omitted. The comparison reveals that the impact of rotary inertia becomes noticeable in higher modes. The differences observed between the predictions of the present study and that of Sahraei et al. [19] arise primarily due to shear deformation effects considered in Sahraei et al. [19] but neglected in the current study.

Table 4.2 Effect of rotary inertia for cantilever member with W250x58 doubly symmetric I cross-section

	Minor axis Flexural mode (Cycle/sec), L=6m							**Major axis Flexural mode (Cycle/sec), L=6m**							**Torsional mode (Cycle/sec), L=4m**						
	1	2	3	4	5	6	7*	8	9	10	11	12	13	14*	15	16	17	18	19	20	21 *
	Without Rotary inertia			With rotary inertia				Without rotary inertia			With rotary inertia				Without Rotary inertia			With rotary inertia			
Mode #	Sahraei et al. [19]	Present study	(2-1)/(2) %	Sahraei et al. [19]	Present study	(5-4)/(5) %	(2-5)/(2) %	Sahraei et al. [19]	Present study	(9-8)/(9) %	Sahraei et al. [19]	Present study	(12-11)/(12) %	(9-12)/(12) %	Sahraei et al. [19]	Present study	(16-15)/(16) %	Sahraei et al. [19]	Present study	(19-18)/(18) %	(16-19)/(16) %
1	3.97	3.97	0.1	3.97	3.97	0.1	0.0	8.48	8.54	0.8	8.47	8.54	0.8	0.1	17.2	17.3	0.5	17.2	17.3	0.3	0.3
2	24.8	24.9	0.4	24.8	24.9	0.4	0.1	50.9	53.5	4.9	50.7	53.3	4.9	0.5	69.1	69.2	0.2	68.9	69.1	0.2	0.2
3	69.1	69.7	0.9	68.9	69.5	0.9	0.3	134	150	10.6	133	148	10.3	1.2	166	169	1.8	165	168	1.8	0.6
4	134	137	1.7	134	136	1.7	0.5	243	294	17.3	240	287	16.5	2.3	307	318	3.6	304	315	3.5	1.1
5	220	226	2.7	218	224	2.6	0.8	369	471	21.7	364	464	21.6	1.6	489	518	5.7	482	509	5.3	1.8
6	325	337	3.8	321	334	3.7	1.2	506	726	30.3	498	689	27.7	5.0	707	768	7.9	694	749	7.4	2.5
7	447	481	7.0	441	469	5.8	2.6	650	1007	35.5	639	945	32.4	6.2	957	1093	12.4	934	1031	9.4	5.6
8	587	628	6.5	577	615	6.1	2.1	798	1231	35.2	785	1184	33.7	3.9	1234	1418	13.0	1200	1355	11.5	4.4
9	742	806	8.0	728	785	7.3	2.6	950	1477	35.7	934	1410	33.7	4.5	1536	1819	15.6	1487	1718	13.4	5.6
10	912	1013	10.0	891	975	8.6	3.8	1104	1746	36.8	1087	1654	34.3	5.3	1857	2280	18.5	1793	2116	15.3	7.2

Note: * Represents the effect of rotary inertia

4.6.5. Members with Z cross-section

The present finite element model is used to generate axial force-natural frequency interaction plots for two axially loaded members with Z cross-sections. Both members have a span of 4m, and a thickness $t_w = 15.9$ mm. Two sets of web height and flange width are taken: $\left(b_w, b_f\right) = \left(406, 102\right) mm$ which corresponds to $b_f / b_w =$ 0.25, and $\left(b_w, b_f\right) = \left(203, 203\right) mm$ corresponding to $b_f / b_w = 1.00$. When the web of a Z cross-sections is connected to a gusset plate it can be considered fixed about the y axis and nearly pinned about the x axis (Figure 4.7), both directions being non-principal. In Figure 4.7, the natural frequency and axial load are normalized relative to those of a member with end pin connections in all directions. The buckling loads for both members were reported in [22] and serve as a basis to assess the validity of the present solution for the limiting case where the natural frequency vanishes. In this respect, the present solution predicts normalized axial force ratios of 1.58 for $b_f / b_w =$ 0.25 and 3.22 for $b_f / b_w = 0.50$. These ratios exactly match the axial force ratios reported in [22]. For comparison, a shell finite element model was developed in ABAQUS to evaluate the natural frequency axial load ratios of 0.5, 1.0, and -1.5. As depicted in Figure 4.7, shell model predictions are in close proximity to those of the present solution, showcasing the ability of the present formulation to tackle sections with a comparatively large global warping constant.

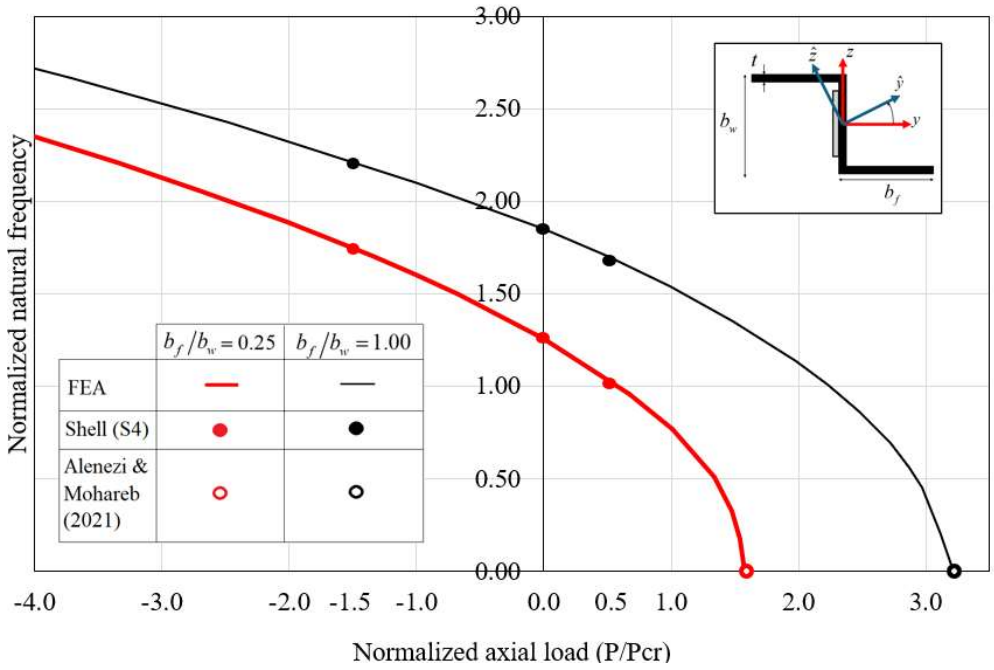

Figure 4.7 Normalized natural frequency versus axial force ratio for Z sections

4.7. Parametric Study

4.7.1. Effect of rotary inertia

The effect of rotary inertia in members is investigated for both reference cases. Span was taken as 2m ($P_{cr} = 845kN$ for pin members and $P_{cr} = 2579\ kN$ for gusset end members) and the compressive axial load level was taken as $P/P_{cr} = 0.5$ in both cases. Table 4.3 shows that the rotary inertia effect has a negligible effect on lower modes and a minor effect on higher modes. The rotary inertia effect is found to be more pronounced for the case of gusset plate end connections.

Table 4.3 Effect of rotary inertia for L152x102x16 cross-section

	Natural frequency (Cycle/sec)					
	Pinned end connection			Gusset plate end connection		
	1	2	3*	4	5	6*
Mode #	With rotary inertia	Without rotary inertia	(2-1)/(2) %	With rotary inertia	Without rotary inertia	(5-4)/(5) %
1	29.77	29.79	0.05	54.54	54.56	0.05
2	79.35	79.46	0.13	82.04	82.18	0.18
3	138.6	138.8	0.11	143.1	143.2	0.04
4	148.4	148.9	0.34	150.3	150.7	0.32
5	222.8	223.3	0.21	238.8	238.9	0.04
6	255.8	256.0	0.07	273.4	274.3	0.32
7	369.8	370.0	0.07	343.5	343.8	0.10
8	445.1	447.8	0.59	440.8	441.3	0.10
9	490.3	490.7	0.08	492.9	501.5	1.71
10	492.8	501.6	1.75	569.4	570.0	0.11
11	622.5	623.1	0.10	570.1	574.0	0.68
12	769.0	771.2	0.28	712.8	713.8	0.15
13	770.1	777.5	0.95	893.5	896.1	0.28
14	962.2	963.8	0.17	952.3	963.0	1.11
15	1062	1105	3.87	1058	1072	1.31
16	1137	1139	0.22	1070	1100	2.76
17	1190	1211	1.72	1297	1300	0.28
18	1365	1368	0.27	1418	1444	1.84
19	1637	1642	0.33	1571	1577	0.38
20	1709	1752	2.45	1811	1895	4.43

Note: *Represents the effect of rotary inertia

4.7.2. Effect of member slenderness and leg ratio

Figure 4.8a illustrates the influence of the angle aspect ratio a/b and slenderness ratio $L/r_{\min}$ on the natural frequency axial force interaction diagram for members with gusset end connections. Towards this objective three aspect ratios were investigated; (1) $a/b = 2/3$ (corresponding to an L152×102×16 with the longer leg connected to the gusset), (2) $a/b = 1$ (corresponding to

L152×152×16), and (3) $a/b = 3/2$ (corresponding to an L152×102×16 with the shorter leg connected to the gusset). For each case, three slenderness ratios; $L/r_{\min} = 100$, 150, and 200 were investigated. The natural frequencies were normalized with respect to that of an identical pin-ended member with no axial force, while the axial loads were normalized with respect to the torsional flexural buckling load of an identical pin-ended member and were varied within the range $-3 \le P/P_{cr}^{Pin} \le 1$. The normalized natural frequency is observed to increase with the aspect ratio. In the absence of axial loading, the normalized natural frequencies $\omega/\omega_{P=0}^{pin}$ are found to be 1.24, 1.47, and 1.94, respectively while member slenderness is observed to generally have a negligible effect. As the compressive force increases, the aspect ratio has a more pronounced effect on natural frequency. In the limiting case where the natural frequency is zero, the corresponding normalized critical load ratio $\overline{P} = P/P_{cr}^{pin}$ corresponds to the buckling load of the member and is found to range from 1.43 to 1.55 for $a/b = 2/3$, from 1.98 to 2.12 for $a/b = 1$, and from 3.11 to 3.40 for $a/b = 3/2$, depending on the slenderness ratio. The observed narrow bands for $\overline{P} = P/P_{cr}^{pin}$ indicate that the member slenderness plays a rather minor role.

The investigation is extended to members with pin end connections for comparison. The natural frequency-axial force interaction diagrams in Figure 4.8b shows that, within the normalized axial force range $-2 \le P/P_{cr}^{Pin} \le 1$ investigated, the normalized natural frequency $\overline{\omega} = \omega/\omega_{P=0}^{pin}$ is independent of the slenderness ratio $L/r_{\min}$ and the aspect ratio a/b .

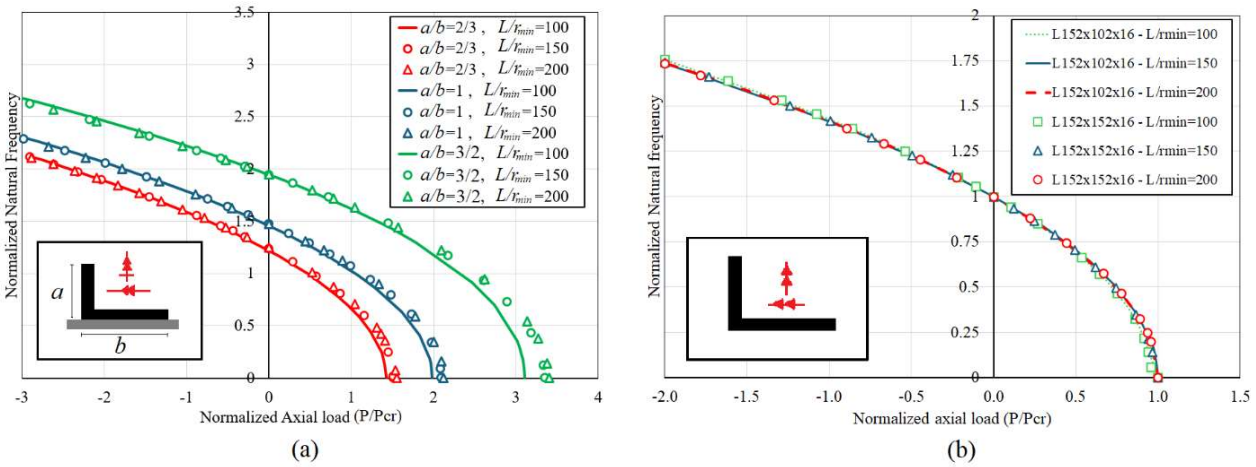

Figure 4.8 Normalized natural frequency $\bar{\omega} = \omega / \omega_{P=0}^{pin}$ versus Axial Force $\overline{P} = P / P_{cr}^{pin}$ for members with angle cross-sections $\left(a/b = 2/3\,, 1\,,\ \text{and}\ 1.5\right)$ with (a) gusset plates connections, and (b) pin-ended members

4.7.3. Effect of leg ratio

Figure 4.9 provides the natural frequency for five angle members with no axial loads. Angle thicknesses are taken as 16mm. The width for one of the legs is kept constant at 152 mm while the width of the other leg is varied to correspond to aspect ratios of $a/b = 1/2, 2/3, 1.0, 3/2, 2.0$. Member spans were varied to keep the slenderness ratio constant at $KL/r_{\min} = 184$. The smallest natural frequency is found to correspond to the equal leg angle (Case 3). This is because this case corresponds to the largest $r_{\min}$, and hence the longest span L and hence the most flexible member. This in turn corresponds to the lowest natural frequency. The natural frequency is observed to have a minimum value for angles with equal leg and increases as the leg ratio a/b deviates from unity. The results highlight the influence of both the ratio and connection type on the natural frequency.

Case number	Connection configuration	$\frac{a}{b}$	Span (m)	$\omega_{P=0}^{pin}$ (Hz)	$\omega_{P=0}^{Gusset}$ (Hz)	$\frac{\omega_{P=0}^{Gusset}}{\omega_{P=0}^{pin}}$
1		1/2	2.92	14.8	17.6	1.19
2	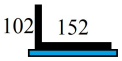	2/3	4.00	10.7	13.4	1.25
3	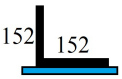	1	5.40	7.96	11.7	1.47
4	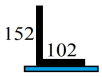	3/2	4.00	10.7	20.6	1.92
5		2	2.84	15.7	34.8	2.22

Figure 4.9 Effect of leg ratio on the natural frequency of angles of gusset plate connection

4.7.4. Effect of leg slenderness

Three 4m span members with L152×102 cross-sections are considered so as to keep the aspect ratio constant at $a/b = 2/3$. The slenderness ratio is kept constant at $KL/r_{\min} = 184$, while varying the angle thickness such that a/t. Figure 4.10 shows that the normalized natural frequency versus axial force diagrams essentially coincide in all three cases, suggesting that the leg slenderness ratio a/t has a negligible influence on the normalized natural frequency.

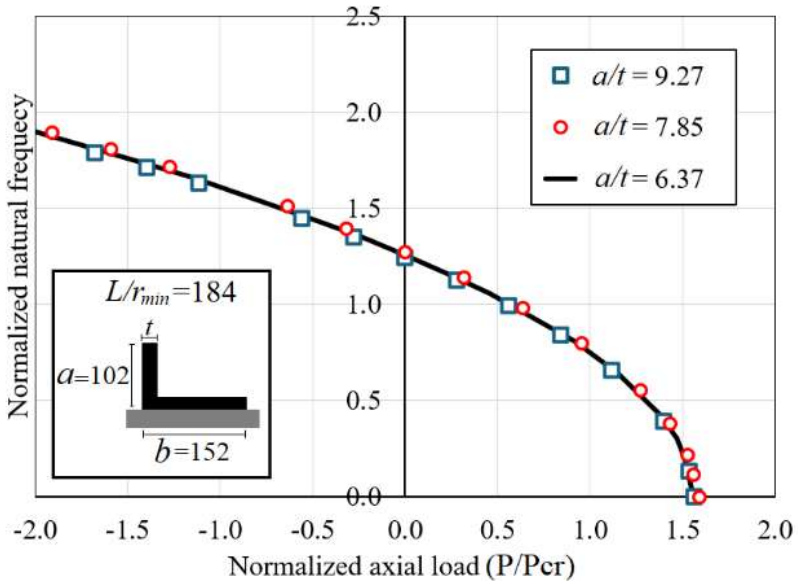

Figure 4.10 Effect of leg slenderness on natural frequency ($a/b = 2/3$, $KL/r_{\min} = 184$).

4.7.5. Comparison of Mode Shapes

Figure 4.11 depicts the fundamental vibration mode shapes for a 4m span member with L152×102×16 cross-section, connected to gusset plates at both ends, as characterized by the lateral and transverse displacements of the shear centre and the angle of twist. The mode shapes are normalized by dividing all displacements by the peak transverse displacement. For both axial loading scenarios considered $P/P_{cr} = 0$ and $P/P_{cr} = 0.5$, the mode shapes predicted by the analytical solution, shell model (S4), and present finite element analysis (FEA) are in close agreement.

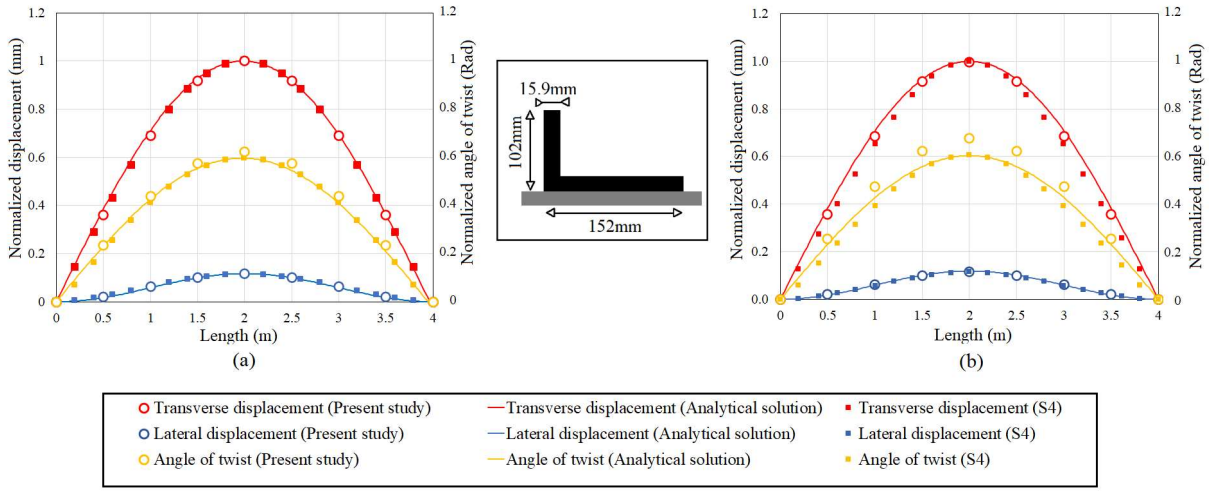

Figure 4.11 Normalized fundamental vibration mode shapes (shear centre displacements and angle of twist) for members with Gusset plate end connections for (a) $P/P_{cr}^{pin}=0$**, and (b)** $P/P_{cr}^{pin}=0.5$

4.8. Design Aid

The energy-based eigenvalue solution in Eq. 4.22 is used to generate dimensionless interaction diagrams for the normalized natural frequency $\omega/\omega_{P=0}^{pin}$ versus the normalized axial force P/P_{cr}^{pin} in which $\omega_{P=0}^{pin}=\pi^2\sqrt{EI_{\hat{z}}/mL^4}$ is the fundamental natural frequency about the minor axis for a member pinned at both ends in the absence of axial force, and $P_{cr}^{pin}=\pi^2EI_{\hat{z}}/l^2$ is the flexural buckling load about the minor axis of a member pinned at both ends. Plots have been provided for leg ratios of $a/b=(1/2),(2/3),1,(3/2),2$. A comparison against the predictions of shell-based models (Figure 4.12 a) shows that the energy solution provides accurate predictions for $a/b=(1/2),(2/3),1,(3/2)$ but over-predicts the natural frequency for $a/b=2$. This is attributed to the fact that in this case, the assumed displacement functions $\langle V(x),W(x),\theta_x(x)\rangle=\langle A(1-\cos(2\pi x/l)),B\sin(\pi x/l),C\sin(\pi x/l)\rangle$ do not accurately characterize the mode shapes of the angle. Towards developing design charts, we recall that the natural frequency ω for a

structural steel angle member $\left(E=200GPa, G=77GPa\right)$ with specified boundary conditions, solely depends on its geometric parameters and axial force level, i.e., $\omega = f\left(a,b,t,l,P\right)$. Using the Buckingham Pi theorem, the number of independent parameters is reduced from five to four, e.g., $\omega/\omega_{P=0}^{pin} = g\left[\left(a/b\right),\left(a/t\right),\left(l/a\right),\left(P/P_{cr}^{pin}\right)\right]$. In addition, the present study has numerically shown that $\omega/\omega_{P=0}^{pin}$ is practically independent on (1) the member slenderness l/a (Figure 4.8) and (2) the leg slenderness a/t (Figure 4.10), i.e., for practical purposes, one has $\omega/\omega_{P=0}^{pin} \approx g\left[\left(a/b\right),\left(P/P_{cr}^{pin}\right)\right]$. This outcome enables developing the design charts in Figure 4.12 b for axially loaded members with gusset end connections with angle members with aspect ratios $a/b=\left(1/2\right),\left(2/3\right),1,\left(3/2\right)$ The use of Figure 4.12 b in a design context will be illustrated in design example in Section 4.9.

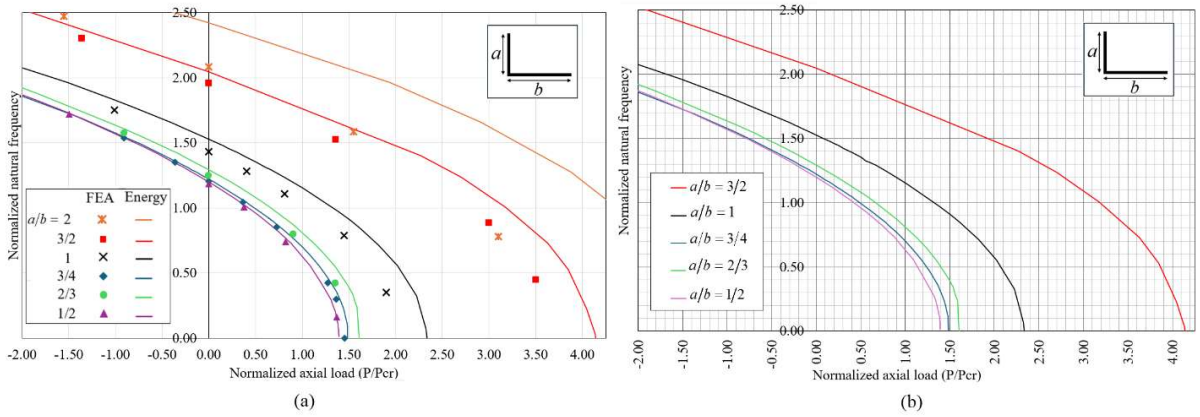

Figure 4.12 (a) Comparison of energy-based and FEA solutions for various aspect ratios a/b (b) Design-Aid: Normalized natural frequency versus Normalized axial force

4.9. Design example

A steel compression member ($F_y = 350MPa$) with an L203×102×13 cross-cross-section has a 4 m span and is connected to gusset plates at both ends through its longer leg. The elastic torsional

flexural buckling load for such a member is $P_{cr} = 289kN$ (Alenezi and Mohareb [22]). The member is subjected to a service axial load $P_s = 0.45P_{cr} = 130kN$ which corresponds to a factored load of $P_f = 1.3P_s = 169kN$. To guard against excessive vibrations induced by human walking with a step frequency ($f_{st} = 3Hz$), the designer is to target a fundamental frequency for the member exceeding $12Hz$, in accordance with NBC [26] requirements.

The chosen section satisfies sub-compactness requirements according to ANSI-AISC 360 [24] as well as the slenderness requirement (i.e., $Kl/r_{\min} = 181 < 200$). The compressive resistance of the member is found to be $\phi P_n = 0.9 \times 0.877\left[\pi^2 E/\left(Kl/r_{\min}\right)\right] A_g = 176kN > P_f = 1.3P_s = 169kN$, i.e., the member satisfies the static strength requirement. The natural frequency as predicted by Eq. 4.22 is found to be 9.50 Hz, which falls below the target value of $12Hz$, i.e., the member is found prone to excessive vibration. A second attempt is made with an L203×152×13 section $(Kl/r_{\min} = 121 < 200)$ which has a critical load $P_{cr} = 800kN$. The given service load becomes $P_s = 0.16P_{cr}$ and the corresponding factored load is $P_f = 0.21P_{cr}$. The compressive resistance of the member is found to be $\phi P_n = 0.9 \times 0.877\left[\pi^2 E/\left(Kl/r_{\min}\right)\right] A_g = 461kN > P_f$. The fundamental frequency as computed by the energy based approximate solution in Eq. 4.22 is 18.38 Hz, which exceeds the target natural frequency of $12Hz$, i.e., the chosen section meets the dynamic design criterion stipulated by NBC-2015 [26]. The natural frequency of 18.38 Hz predicted by Eq. 4.22 compares with 17.73Hz as predicted by the present finite element model, a 3.5%, difference, and 17.65 Hz as predicted by the shell finite element a 4.0% difference, showcasing that proposed energy solution closely predicts the natural frequency.

The buckling load for a member pinned at both ends is $P_{cr} = \pi^2 EI_{\hat{z}} / l^2 = 579.2kN$. For an applied load of 169 kN, the normalized axial load is $P/P_{cr} = 0.29$. Given this ratio, from the plot for $a/b = 3/4$ on Figure 4.12 b, one obtains a normalized natural frequency ratio $\omega/\omega_{p=0}^{pin} = 1.10$ in which the natural frequency of a pin ended member with no axial force is $\omega_{p=0}^{pin} = \pi^2 \sqrt{EI_{\hat{z}} / mL^4} = 16.3Hz$. The natural frequency of the chosen axially loaded member with gusset end connections is $16.3 \times 1.10 = 17.9Hz$, i.e., the design chart solution thus overestimates the natural frequency by 0.9% in this case.

It is noted that treating both ends as pinned in all directions while including the detrimental effect of the compressive axial force effect would yield a natural frequency of $13.9Hz$ which would underestimate the natural frequency by 22% compared to the shell finite element analysis.

4.10. Summary and Conclusions

The present study formulates a finite element and an energy-based solution to determine the natural frequency and mode shape of axially loaded members with asymmetric cross-sections. The formulation is intended for members with angle cross-sections connected to gusset plates in which the axis of fixity does not coincide with one of the principal directions. The solutions capture the effects of torsional flexural coupling induced by cross-sectional asymmetry, axial loading, rotary inertia, local warping, while enabling different fixity end conditions along non-principal directions. The present finite element and energy-based solutions were shown to agree well with shell-based finite element models, thus providing a suitable design-oriented equation to characterize the fundamental natural frequency of axially loaded members with angle cross-sections with end gusset connections. The main conclusions of the study are:

1. The natural frequency of members with gusset end connections is significantly higher than those with pin end connections. The differences between both cases become more pronounced as the compressive axial force in the member increases.
2. Rotary inertia has a negligible impact on the natural frequency of lower modes of members with unequal leg angles. For higher modes, rotary inertia is found to reduce the natural frequency by less than 5%.
3. As the ratio of the outstanding leg to the connected leg increases, the natural frequency of gusset-connected member is found to become significantly higher relative to that of a pin-ended member with the same geometry.
4. For angle members with gusset plate end connections, the natural frequency increases as leg ratio deviates from unity. In contrast, the member slenderness ratio has a minimal impact on the natural frequency.
5. The leg width to thickness ratio has no observable effect on the natural frequency of angle members with gusset plate end connections.

The following recommendations are made to extend the scope of the present study:

1. The present study has conservatively omitted the beneficial effect of partial rotational fixity provided by gusset plates to the member ends about the axis parallel to the gusset. It is recommended to model this effect for typical gusset plate geometries to quantify the increase in natural frequency of the member.

2. The present study has assumed that the axial force in the member remains constant throughout the vibration of the member. In some applications, the axial force may have a time dependent harmonic component, which would lead to parametric excitation. It is recommended to explore the stability of such systems by including geometric nonlinear effects in the dynamic analysis.

3. While the validity of the present formulation was assessed through comparisons with shell finite element predictions, it is recommended to further check the validity of the present solution against benchmark experimental results.

4. The present study was primarily motivated by developing design solutions for sizing axially loaded angle members by tuning them out of resonance. The present approach is suitable when the exciting frequency is known but the magnitudes of the forces are unknown at the design stage. When the magnitudes of the anticipated loads are additionally known, it becomes possible to conduct a full transient analysis. In this respect, it is recommended to extend the present work to perform a transient dynamic analysis.

4.11. Notation

A : Arbitrary point on the section contour

B : Arbitrary point offset from the section contour

E : Elasticity modulus

G : Shear modulus

I_y, I_z : Moments of inertia about y and z axis

I_p : Polar moment of inertia

I_ω : Warping constant

J : Saint-Venant torsional constant

L_a : Hamiltonian functional

m : Mass

P : Axial load

P_f : Factored axial load

P_n : Axial compression resistance

P_s : Serviceability axial load

$r(s), q(s)$: Distances from the pole along the normal and tangent axis at point A

R : Shear centre (Pole)

S_0: Sectorial origin

t: Time

T: Kinetic energy

U: Internal strain energy

V: Volume

u_A, v_A, w_A: Displacements of arbitrary point on contour in the tangential direction

u_B, v_B, w_B: Displacements of arbitrary point offset from contour in the tangential direction

u_p: Axial displacement under static compressive load

v_r, w_r: Displacements of pole R

$\overline{y}(s), \overline{z}(s)$: Local coordinates of point A on the middle surface

$\overline{\overline{y}}(s), \overline{\overline{z}}(s)$: Global coordinates

$V_A(x,s,t), W_A(x,s,t)$: Displacement of point A along y and z directions

$\alpha(s)$: Angle between the tangential direction and the y axis

$\varepsilon_{xs}^B, \varepsilon_{xn}^B$: Shear strain components of arbitrary point offset from contour in the tangential and normal directions

ε_x^B: Total longitudinal strain (Figure 4.1b)

ε_{px}^{B}: Longitudinal strain under axial load (Figure 4.1b)

$\sigma_x, \sigma_{xs}, \sigma_{xn}$: Stress tensor (Figure 4.1b)

ρ: Density

ω: Sectorial coordinate

$\bar{\omega}$: Global sectorial coordinate

$\overline{\overline{\omega}}$: Local sectorial coordinate

θ_x: Angle of twist

$C(s,n), S(s,n), \psi(s,n)$: Functions of s and n included in Eq. 4.5b

γ_A: Shear strain for point A on the middle surface

4.13. References

1. Vlasov, V.Z., *Thin-walled elastic beams.* PST Catalogue, 1959. **428**.
2. Gjelsvik, A., *The theory of thin-walled bars*. 1981, New York, NY, USA: Wiley.
3. Kim, M.Y., S.P. Chang, and S.B. Kim, *Spatial stability and free vibration of shear flexible thin-walled elastic beams. I: Analytical approach.* International Journal for Numerical Methods in Engineering, 1994. **37**(23): p. 4097-4115.
4. Tanaka, M. and A. Bercin, *Free vibration solution for uniform beams of nonsymmetrical cross section using Mathematica.* Computers & structures, 1999. **71**(1): p. 1-8.
5. Prokić, A., R. Mandić, and M. Vojnić-Purčar, *An improved analysis of free torsional vibration of axially loaded thin-walled beams with point-symmetric open cross-section.* Applied Mathematical Modelling, 2016. **40**(23-24): p. 10199-10209.
6. Friberg, P., *Coupled vibrations of beams—an exact dynamic element stiffness matrix.* International Journal for numerical methods in engineering, 1983. **19**(4): p. 479-493.
7. Banerjee, J. and S. Fisher, *Coupled bending–torsional dynamic stiffness matrix for axially loaded beam elements.* International journal for numerical methods in engineering, 1992. **33**(4): p. 739-751.
8. Banerjee, J. and F. Williams, *Coupled bending-torsional dynamic stiffness matrix of an axially loaded Timoshenko beam element.* International Journal of Solids and Structures, 1994. **31**(6): p. 749-762.
9. Eisenberger, M., H. Abramovich, and O. Shulepov, *Dynamic stiffness analysis of laminated beams using a first order shear deformation theory.* Composite Structures, 1995. **31**(4): p. 265-271.
10. Kim, M.-Y., H.-T. Yun, and N.-I. Kim, *Exact dynamic and static element stiffness matrices of nonsymmetric thin-walled beam-columns.* Computers & structures, 2003. **81**(14): p. 1425-1448.
11. Li, J., et al., *Coupled bending and torsional vibration of axially loaded thin-walled Timoshenko beams.* International Journal of Mechanical Sciences, 2004. **46**(2): p. 299-320.
12. Kim, M.Y., S.P. Chang, and S.B. Kim, *Spatial stability and free vibration of shear flexible thin-walled elastic beams. II: Numerical approach.* International journal for numerical methods in engineering, 1994. **37**(23): p. 4117-4140.

13. Tanaka, M. and A. Bercin, *Finite element modelling of the coupled bending and torsional free vibration of uniform beams with an arbitrary cross-section.* Applied Mathematical Modelling, 1997. **21**(6): p. 339-344.
14. Duan, H., *Nonlinear free vibration analysis of asymmetric thin-walled circularly curved beams with open cross section.* Thin-Walled Structures, 2008. **46**(10): p. 1107-1112.
15. Vo, T.P. and J. Lee, *Flexural–torsional coupled vibration and buckling of thin-walled open section composite beams using shear-deformable beam theory.* International Journal of Mechanical Sciences, 2009. **51**(9-10): p. 631-641.
16. Vo, T.P., et al., *Vibration analysis of thin-walled composite beams with I-shaped cross-sections.* Composite Structures, 2011. **93**(2): p. 812-820.
17. De Borbon, F., A. Mirasso, and D. Ambrosini, *A beam element for coupled torsional-flexural vibration of doubly unsymmetrical thin walled beams axially loaded.* Computers & structures, 2011. **89**(13-14): p. 1406-1416.
18. Jrad, W., et al., *Analytical and finite element solutions of free and forced vibration of unrestrained and braced thin-walled beams.* Journal of Vibration and Control, 2020. **26**(5-6): p. 255-276.
19. Sahraei, A., et al., *Finite element formulation for the dynamic analysis of shear deformable thin-walled beams.* Thin-Walled Structures, 2022. **173**: p. 108989.
20. Mei, C., *Coupled vibrations of thin-walled beams of open section using the finite element method.* International Journal of Mechanical Sciences, 1970. **12**(10): p. 883-891.
21. Ghandi, E. and B. Shiri, *On triply coupled vibration of eccentrically loaded thin-walled beam using dynamic stiffness matrix method.* Struct. Eng. Mech, 2017. **62**(6): p. 759-769.
22. Alenezi, A.M. and M. Mohareb, *Buckling solutions for compression members with end restraints defined along non-principal directions.* Journal of Constructional Steel Research, 2021. **181**: p. 106505.
23. Meirovitch, L., *Elements of vibration analysis.* (No Title), 1975.
24. Design, R.F., *Specification for structural steel buildings.* American Institute of Steel Construction, Chicago (IL, USA), 2022.
25. *CSA (Canadian Standards Association).* , D.o.s. structures., Editor. 2019, CSA S16: 19.: Toronto: CSA.

26. Code, N.R.C.C.A.C.o.t.N.B. and N.R.C.o.C.A.C.o.t.N.B. Code, *National building code of Canada*. 2015: Associate Committee on the National Building Code, National Research Council.

Chapter 5 Dynamic Response of Steel Members due to Walking-Induced Forces

5.1. Abstract

The present study investigates the acceleration response of structural steel members subjected to dynamic loads induced by walking. Towards this goal, a finite element formulation is developed for the analysis of thin-walled members under time-dependent loads. The solution captures the destabilizing effect induced by axial forces, torsional-flexural coupling due to cross-sectional asymmetry, rotary inertia, and warping effects. In contrast to conventional solutions, the formulation employs non-principal coordinates to enable the seamless modelling of non-conventional boundary conditions, as may be the case in angle members with gusset-end connections. The discretized equations of motion are solved using the Newmark time integration scheme. The validity of the solution is verified against published benchmark problems, and the formulation is subsequently applied to characterize the response of I-shaped and angle-shaped steel members subject to forces induced by walking. The study quantifies the effects of axial force level, cross-section asymmetry, and boundary conditions on the acceleration response of members. Comparative analyses are conducted against established acceleration thresholds based on human perception in various occupancy scenarios.

Keywords: Pedestrian-induced vibration, acceleration, thin-walled members, finite element.

5.2. Introduction and Literature review

5.2.1. Forces induced by Human Activity

Human activity–induced vibrations result from periodic loads induced by rhythmic human activities such as dancing and aerobics (e.g., [1], [2]), and transient loads arising from the movement of people (e.g., walking, running, jumping, impulsive loads induced by heel-drop impacts). While such vibrations rarely threaten structural safety, they can seriously affect human comfort, functionality and serviceability of the structure. Walking pedestrians generate dynamic forces in vertical, horizontal, and longitudinal directions [3] due to body mass acceleration and deceleration. The vertical force is the strongest and most studied. Several approaches have been proposed to characterize the forcing functions induced by human activities. Human-induced forces are characterized using force waveform diagrams and frequency spectra to capture loading patterns (e.g., [5], [6]). Although this method reflects human activity complexity, it is often impractical for structural vibration analysis due to the lack of closed-form solutions and owing to challenges in modeling waveform variations in time-history simulations (e.g., [7]). A more widely accepted and practical approach is to express forcing functions induced by human walking as a time-dependent force using a Fourier series representation [8]-[10]. Under this approach the vertical and horizontal components $F(t)$, $G(t)$ of the forcing function induced by human walking (e.g., [3], [11]), are

$$F(t) = Q + Q\sum_{i=1}^{N} \alpha_i \sin\left(2\pi i f_s t - \phi_i\right)$$
$$G(t) = Q\sum_{i=1}^{N} \beta_i \sin\left(2\pi i f_s t - \lambda_i\right) \qquad 5.1\text{(a-b)}$$

where Q is the static human weight, $i = 1, 2...N$ represents each harmonic term, N being the total number of harmonics required to model the human activity and is normally taken as three or four (e.g., [9], [10]), f_s is the human step frequency, t is the time, α_i and β_i are dynamic load amplification factors for the vertical and horizontal force components defined as the ratio of the

force associated with the i^{th} harmonic to the static human body-weight, and ϕ_i , λ_i are phase angles.

Human activities are generally classified into: (a) *Footfall-dependent activities* (e.g., walking, running), and (b) *Rhythmic activities* (e.g., dancing, aerobic exercises, live concerts). The values of the dynamic load factor α_i and the phase angle ϕ_i have been reported in the literature for walking activities ([12]-[15]), and rhythmic activities (e.g., [16]). A step frequency f_s ranging from 1.5 to 2.5 Hz has been recommended for walking, ([17]-[20]), while values between 1.6 and 4.0 Hz have been proposed for running, ([8], [21]). Step frequencies ranging from 1.5 to 3 Hz have been recommended for dancing and lively concerts, and 2.0 to 4.0 Hz for aerobics ([9], [22], [23]). Variations of Eq. 5.1 have been proposed the vertical force ([24] and [25]) and special equations were proposed for rhythmic activities ([3], [8], [26], [27]) while reference [11] proposed an expression to characterize the horizontal component of human-induced loading.

The peak acceleration ratio a/g, in which a is the peak acceleration and g is the gravitational acceleration, is widely used to quantify human perception to vibration. The perception threshold ratio is dependent upon the type of occupancy. The NBC-1990 [28] stipulates a threshold peak acceleration ratio between 0.4 - 0.7% for office and residential environments, which increases to 1.5 - 2.5% for indoor public spaces, and 4-7% for outdoor places. ISO-2631-2 [29] and Allen et al. [18] specify thresholds of 0.5% for residential and office environments, 1.5% for indoor public areas, and up to 5% for outdoor areas with rhythmic activities. Human comfort also depends on the exciting frequency (e.g., [9]) the a/g threshold is relatively low for excitation frequencies within the 4-8 Hz range, as they align with resonant frequencies of human internal organs. Outside this, accelerations are more tolerable and the corresponding a/g are higher.

5.2.2. Dynamic analysis of thin-walled members

Transient dynamic solutions for thin-walled members are based either on mode superposition techniques or direct time integration methods. Mode superposition proves especially effective in scenarios where only a few dominant modes govern the system's behavior, offering significant computational efficiency. In contrast, time integration techniques are more adept at capturing intricate, time-dependent dynamics—particularly in systems characterized by high-frequency components or localized phenomena. A survey of the features of related studies is provided in Table 5.1 and their various features are discussed in the following sections.

Thin-walled beam transient analyses employing mode superposition include the work of Chen [30] Abrate [31], Bebiano et al. [32], Bebiano et al. [33], Ding et al. [34], and Pagani et al. [35]. The above studies captured the effect of cross-section symmetry ([31],[35]), warping effects ([30], [32], [35]), shear deformation effects ([30],[31],[35]), rotational inertia effects ([30], [31], [32]), and damping effects ([32], [34], [35]). Mode superposition has also been used within the Generalized Beam Theory (GBT) context ([32], [33]) which captured damping and warping effects.

Direct integration techniques involve explicit and implicit methods. Explicit techniques, like the central finite difference method, necessitate extremely short time steps and have been adopted in analyzing wave propagation and impact phenomena in thin-walled structural elements. [36]. In contrast, implicit methods involve solving the system of equilibrium equations at each time step, enabling the use of larger time steps, and offering better solution stability. Within implicit methods, the Newmark method has been the most commonly used [36]-[45]. Some of these studies captured the effects of cross-section asymmetry [41], [43], warping [38], [39], [42], shear deformation [41], [43], rotational inertia [37], [38], damping [37], [42], and axial forces [39], [45].

Past studies focused on the member responses under dynamic uniformly distributed loads [30], [32], harmonic forces [41], [43], impulsive loads [31], [42], transient point loads [36], [34], and moving loads induced by vehicles [33], [38], [44]. None of the previously reviewed studies have addressed the dynamic response of thin-walled members subjected to moving loads induced by pedestrian walking, an aspect that the present study aims to explore.

Another common feature of the above solutions is their definition of shear centre displacements along the principal directions, which in turn facilitates the specification of boundary conditions along these directions. While this approach allows for modeling conventional boundary conditions, such as simply supported, cantilevered, or fixed configurations aligned with principal directions, it becomes unsuitable in cases where restraints are applied along non-principal directions. For example, this limitation arises when a member end is clamped about a non-principal axis and pinned along the normal direction, as is the case when an angle section is connected to a gusset plate. Such boundary conditions have been treated in buckling analysis [46] and natural vibration analysis [47] but not in the context of transient analysis. Thus, the present formulation departs from the principal axis convention by defining shear centre displacements along non-principal axes, allowing for seamless modeling of gusset plate end connections.

Table 5.1 Summary of literature review for Transient Analysis of Thin-Walled Members

	Type of analysis *	Cross-section **	Type of Load	Effects Captured					Additional features
				Warping	Rotary inertia	Shear deformation	Damping effect	Non-linear geometry	
Yuen et al. [37]	N	D					✓		Macro spline interpolation finite element technique
Xiang et al. [38]	N	A	Moving Load	✓	✓		✓		Combined of Newmark-β and the Transfer Matrix Method
Hsiao et al. [39]	N	D	UDL dynamic load	✓	✓			✓	Include Axial force effect
Tiso [40]	N	D	Point Step load and harmonic load					✓	
Carrera et al. [41]	N	D, M, A	Harmonic load	✓	✓	✓			
Zhang et al. [36]	CFD, N	D	Point load & UDL		✓	✓		✓	
Bourihane et al. [42]	N	D, M	Impulse & harmonic load	✓			✓	✓	
Sahraei et al. [43]	N	D, M, A	Harmonic load	✓		✓	✓		
Yang et al. [44]	N	M	Moving Harmonic load	✓					
Yu et al. [45]	N	A		✓	✓	✓	✓		Include Axial force effect
Chen [30]	MS	D	UDL		✓	✓	✓		
Abrate [31]	MS	A	Impulse load		✓	✓	✓		
Bebiano et al. [32]	MS	M	Periodic UDL and impulsive UDL loads	✓	✓		✓		GBT
Ding et al. [34]	MS	D	Transient point load				✓		
Pagani et al. [35]	MS	D, A	Impulsive UDL load	✓		✓	✓		
Bebiano et al. [33]	MS	M	Moving load	✓			✓		Combines GBT mode with member vibration modes

***** N = Newmark method, CFD = Central finite difference method, MS = Mode superposition method
******D =Doubly symmetric, M = Mono symmetric, A = Asymmetric

5.3. Statement of the problem

A finite element formulation is developed for the analysis of asymmetric thin-walled members subjected to a constant axial force and time dependent vertical and horizontal forces.

5.4. Assumptions

The formulation adopts the kinematic assumptions of the Gjelsvik theory [48], i.e., (a) the cross-section is considered to behave as a rigid disk in its own plane, (b) the shear strain along the mid-

surface is assumed to vanish, and (c) a generator normal to the mid-surface is assumed to remain normal to the mid-surface throughout deformation. Material is assumed to be linearly elastic isotropic. The member is considered to be subjected to a time-independent axial force in addition dynamic vertical and horizontal loads, and possibly, twisting moments to model human activity. Under the dynamic loads, the member is assumed to undergo small strains. The formulation adopts centroidal coordinates (y,z) such that $\int_A ydA = \int_A zdA = 0$. A principal sectorial origin is adopted so that the warping function ω satisfies the condition $\int_A \omega dA = 0$. The displacements in the plane of the cross-section are defined at the shear centre so as to satisfy the orthogonality conditions $\int_A \omega ydA = \int_A \omega zdA = 0$. In contrast to other formulations, the formulation adopts non-principal axes, i.e., cross-product of inertia $I_{xy} = \int_A yzdA \neq 0$ does not vanish.

5.5. Formulation

The variational form of the extended Hamilton principle for a damped system takes the form

$$\int_{t_1}^{t_2} (\delta L_a)\, dt = \int_{t_1}^{t_2} (-\delta U + \delta T + \delta W_{nc} - \delta V)\, dt = 0 \qquad 5.2$$

in which L_a is the Hamiltonian functional, U is the internal strain energy, T denotes the kinetic energy, W_{nc} is the energy dissipated by damping, and V is the potential energy due to external loads, all integrations are performed between arbitrary time limits $t = t_1$ and t_2 , and δ denotes the variation of the argument functional. Under assumptions of Section 0, the variation of internal strain energy δU [47] for a member of span l takes the form

$$\begin{aligned}\int_{t_1}^{t_2}\delta U dt = &\int_{t_1}^{t_2}\int_0^l \left(EI_z v''\delta v'' + EI_y w''\delta w'' + EI_\omega \theta_x''\delta\theta_x'' + GJ\theta_x'\delta\theta_x' + EI_{yz}v''\delta w'' + EI_{yz}w''\delta v'' \right) dxdt \\ &+ P\int_{t_1}^{t_2}\int_0^l \left[v'\delta v' + w'\delta w' + \left(I_p/A\right)\theta_x'\delta\theta_x' + z_r\theta_x'\delta v' + z_r v'\delta\theta_x' - y_r\theta_x'\delta w' - y_r w'\delta\theta_x' \right] dxdt\end{aligned} \quad 5.3$$

in Eq. 5.3 , E is Young's modulus, G is the shear modulus, P is axial load, and the sectional properties $\left(A, I_z, I_y, I_{yz}, I_\omega, I_p\right) = \int_A \left[1, y^2, z^2, yz, \omega^2, \left(y^2+z^2+{y_r}^2+{z_r}^2\right)\right] dA$ have been defined. Coordinates $\left(y_r, z_r\right)$ are those of shear centre R relative to the centroid (Figure 5.1), $v(x), w(x)$ are the displacements of the shear centre along the y, z axes, and $\theta_x(x)$ is angle of twist. Also, the variation of kinetic energy is

$$\begin{aligned}\int_{t_1}^{t_2}\delta T dt = &-\rho\int_{t_1}^{t_2}\int_0^l \left[\left(-A\ddot{v} - z_r A\ddot{\theta}_x\right)\delta v + \left(-A\ddot{w} + y_r A\ddot{\theta}_x\right)\delta w + \left(-z_r A\ddot{v} + y_r A\ddot{w} - I_p\ddot{\theta}_x\right)\delta\theta_x \right] dxdt \\ &+ \rho\int_{t_1}^{t_2}\int_0^l \left[I_z\ddot{v}'\delta v' + I_y\ddot{w}'\delta w' + I_\omega\ddot{\theta}_x'\delta\theta_x' + I_{yz}\ddot{v}'\delta w' + I_{yz}\ddot{w}'\delta v' \right] dxdt\end{aligned} \quad 5.4$$

in which all dots represent time derivatives of the argument functions, and ρ is the beam density. The variation of energy δW_{nc} dissipated by damping is given by

$$\int_{t_1}^{t_2}\delta W_{nc} dt = \int_{t_1}^{t_2}\delta \left\langle v \quad w \quad \theta_x \quad v' \quad w' \quad \theta_x' \right\rangle_{1\times 6} \left\{F_D\right\}_{6\times 1} dt \quad 5.5$$

in which F_D is the vector of damping forces. For body forces P_x, P_y, P_z acting along the (x, y, z) directions on a generic point $B\left[x, y(s,n), z(s,n), \omega(s,n)\right]$ within the member, the variation of the load potential energy term takes the form

$$\delta V = \int_{t_1}^{t_2}\int_0^l\int_n\int_s \delta\left[P_z w_B(s,n,x,t) + P_y v_B(s,n,x,t) + P_x u_B(s,n,x,t) \right] dsdndxdt \quad 5.6$$

in which, u_B, v_B, w_B are the displacements of point B. For a thin-walled cross-section consisting of straight segments, displacements u_B, v_B, w_B are expressed in terms of the displacement $u_p(x), v(x,t), w(x,t), \theta_x(x,t)$

$$\begin{aligned} u_B(x,s,n,t) &= u_p(x) - y(s,n)v'(x,t) - z(s,n)w'(x,t) + \omega(s,n)\theta_x'(x,t) \\ v_B(x,s,n,t) &= \cos\alpha(s)v(x,t) + \sin\alpha(s)w(x,t) - (r(s)+n)\theta_x(x,t) \\ w_B(x,s,t) &= -\sin\alpha(s)v(x,t) + \cos\alpha(s)w(x,t) + q(s)\theta_x(x,t) \end{aligned} \qquad 5.7$$

in which $\alpha(s)$ represents the angle between the tangent to contour at the projection B' of the point B on the middle surface, the y axis and is taken as positive in the clockwise direction and $r(s)$ and $q(s)$ are the normal and tangential distances from the shear centre to point B' on the middle surface (

5.1). From Eq. 5.7, by substituting into Eq. 5.6 , preforming the area integrals, integrating by parts, and grouping like terms , one obtains [11]

$$\int_{t_1}^{t_2} \delta V dt = -\int_{t_1}^{t_2}\int_0^l \left[q_x u_p(x) + q_y \delta v(x,t) + q_z \delta w(x,t) + m\delta\theta_x(x,t) \right] dx dt \qquad 5.8$$

in which the following line loads have been defined

[11] The steps in recovering the line loads from the body forces are provided in Appendix G.

$$q_x(x,t)=\int_n\int_s P_x(s,n,x)\,dsdn$$

$$q_y(x,t)=\int_n\int_s\left[-\frac{\partial}{\partial x}\left(P_x(s,n,x)\,y(s,n)\right)+P_y(s,n,x,t)\cos\alpha(s)-P_z(s,n,x,t)\sin\alpha(s)\right]dsdn$$

$$q_z(x,t)=\int_n\int_s\left[-\frac{\partial}{\partial x}\left(P_x(s,n,x)\,z(s,n)\right)+P_y(s,n,x,t)\sin\alpha(s)+P_z(s,n,x,t)\cos\alpha(s)\right]dsdn$$

$$m(x,t)=\int_n\int_s\left[-\frac{\partial}{\partial x}\left(P_x(s,n,x)\,\omega(s,n)\right)-P_y(s,n,x,t)\left(r(s)+n\right)+P_z(s,n,x,t)\,q(s)\right]dsdn$$

5.9(a-d)

From Eq. 5.3, 5.4, 5.5, and 5.8, by substituting into Eq. 5.2, one recovers the variational principle

$$\int_{t_1}^{t_2}\delta L_a\,dt=\int_{t_1}^{t_2}\left(-\delta U+\delta T+\delta W_{nc}-\delta V\right)dt=$$

$$-\int_{t_1}^{t_2}\int_0^l\left(EI_z v''\delta v''+EI_y w''\delta w''+EI_\omega\theta_x''\delta\theta_x''+GJ\theta_x'\delta\theta_x'+EI_{yz}v''\delta w''+EI_{yz}w''\delta v''\right)dxdt$$

$$-P\int_{t_1}^{t_2}\int_0^l\left[v'\delta v'+w'\delta w'+\left(I_p/A\right)\theta_x'\delta\theta_x'+z_r\theta_x'\delta v'+z_r v'\delta\theta_x'-y_r\theta_x'\delta w'-y_r w'\delta\theta_x'\right]dxdt$$

$$+\rho\int_{t_1}^{t_2}\int_0^l\left[\left(-A\ddot{v}-z_rA\ddot{\theta}_x\right)\delta v+\left(-A\ddot{w}+y_rA\ddot{\theta}_x\right)\delta w+\left(-z_rA\ddot{v}+y_rA\ddot{w}-I_p\ddot{\theta}_x\right)\delta\theta_x\right]dxdt$$

$$-\rho\int_{t_1}^{t_2}\int_0^l\left(I_z\ddot{v}'\delta v'+I_y\ddot{w}'\delta w'+I_\omega\ddot{\theta}_x'\delta\theta_x'+I_{yz}\ddot{v}'\delta w'+I_{yz}\ddot{w}'\delta v'\right)dxdt$$

$$-\int_{t_1}^{t_2}\int_0^l\left[q_x u_p(x)+q_y\delta v+q_z\delta w+m\delta\theta_x\right]dxdt=0$$

5.10

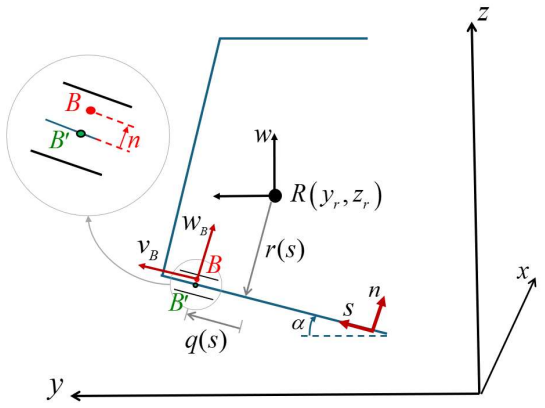

Figure 5.1 Coordinate system and displacements for asymmetrical cross-section

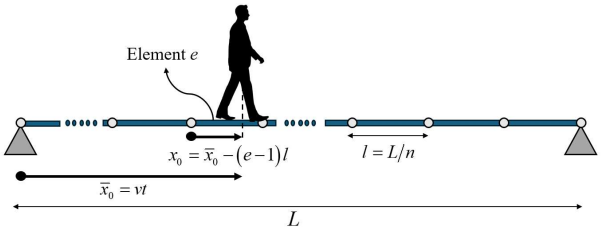

Figure 5.2 Human position during walking relative to finite elements

5.5.1. Human-induced dynamic load

When a walking individual moves along a span with a constant velocity v starting at $(x,t)=(0,0)$, the horizontal and vertical components $q_{y,m}(x,t)$, $q_{z,m}(x,t)$ of the force induced by walking is

$$\begin{aligned} q_{z,m}(x,t) &= F(t)\delta^*\left(x-\bar{x}_0(t)\right) \\ q_{y,m}(x,t) &= G(t)\delta^*\left(x-\bar{x}_0(t)\right) \end{aligned} \qquad t\in[0,L/v], \qquad \bar{x}_0(t)=vt \qquad 5.11\text{(a-b)}$$

in which δ^* is Dirac delta function, $\bar{x}_0(t)$ is the position of the human at time t measured from the end $x=0$, and $t\in[0,L/v]$ in which L/v is the duration of the human to reach the end $x=L$.

5.5.2. Finite element formulation

A two-node thin-walled beam element is developed. The element sought has seven degrees of freedom (DOFs) per node; three translational DOFs, three rotational DOFs, and warping DOF. The displacement functions are related to the nodal displacement vectors, i.e.,

$$v(x)=\mathbf{H}_{\mathrm{v}}^{\mathrm{T}}(x)\mathbf{v}_{\mathbf{n}} \quad ; \quad w(x)=\mathbf{H}_{\mathbf{w}}^{\mathrm{T}}(x)\mathbf{w}_{\mathbf{n}} \quad ; \quad \theta(x)=\mathbf{H}_{\mathrm{v}}^{\mathrm{T}}(x)\boldsymbol{\theta}_{\mathbf{n}} \qquad 5.12\text{(a-c)}$$

in which $\mathbf{H}_{\mathrm{v}},\mathbf{H}_{\mathbf{w}}$ are the vectors of the Hermitian polynomials defined by

$$\begin{aligned} \mathbf{H}_{\mathrm{v}}^{\mathrm{T}} &= \left\langle \left(1-3\zeta^2+2\zeta^3\right) \quad L\left(\zeta-2\zeta^2+\zeta^3\right) \quad \left(3\zeta^2-2\zeta^3\right) \quad L\left(\zeta^3-\zeta^2\right) \right\rangle \\ \mathbf{H}_{\mathbf{w}}^{\mathrm{T}} &= \left\langle \left(1-3\zeta^2+2\zeta^3\right) \quad -L\left(\zeta-2\zeta^2+\zeta^3\right) \quad \left(3\zeta^2-2\zeta^3\right) \quad -L\left(\zeta^3-\zeta^2\right) \right\rangle \end{aligned} \qquad \zeta=x/L$$

5.13(a-b)

and the nodal displacement vectors $\mathbf{v}_{\mathbf{n}}^{\mathrm{T}}=\langle v(0) \quad v'(0) \quad v(l) \quad v'(l)\rangle$, $\mathbf{w}_{\mathbf{n}}^{\mathrm{T}}=\langle w(0) \quad w'(0) \quad w(l) \quad w'(l)\rangle$ and $\boldsymbol{\theta}_{\mathbf{n}}^{\mathrm{T}}=\langle \theta(0) \quad \theta'(0) \quad \theta(l) \quad \theta'(l)\rangle$ have been defined.

From Eq. 4.23, by substituting into Eq. 5.10 and noting that t_1, t_2 are arbitrary times and $\delta\mathbf{v_n}, \delta\mathbf{w_n}, \delta\boldsymbol{\theta}_\mathbf{n}$ arbitrary functions, one obtains

$$\left(\mathbf{K} + P\mathbf{K_G}\right)\mathbf{U_N} + \mathbf{C}\dot{\mathbf{U}}_\mathbf{N} + \left(\mathbf{M_1} + \mathbf{M_2}\right)\ddot{\mathbf{U}}_\mathbf{N} = \mathbf{F}(t) \tag{5.14}$$

in which $\mathbf{K}$ is the stiffness matrix, $\mathbf{K_G}$ is a geometric matrix accounting for the effect of the axial force P, $\mathbf{C}$ is the Rayleigh damping matrix, $\mathbf{M_1}$ and $\mathbf{M_2}$ is the mass matrices accounting for the translational and rotatory inertial effects, inertial effects, **F(t)** is exciting force, $\mathbf{U}_\mathbf{N}^T = \left\{\mathbf{v_n} \quad \mathbf{w_n} \quad \boldsymbol{\theta}_\mathbf{n}\right\}_{12\times 1}$, and

$$\mathbf{K} = \left[\begin{array}{c|c|c} \mathbf{K_{vv}} & \mathbf{K_{vw}} & \mathbf{0} \\ \hline \mathbf{K_{vw}^T} & \mathbf{K_{ww}} & \mathbf{0} \\ \hline \mathbf{0} & \mathbf{0} & \mathbf{K_{\theta\theta}} \end{array}\right] = \int_l \left[\begin{array}{c|c|c} EI_z\mathbf{H_v''H_v^{T\prime\prime}} & EI_{yz}\mathbf{H_v''H_w^{T\prime\prime}} & 0 \\ \hline EI_{yz}\mathbf{H_w''H_v^{T\prime\prime}} & EI_y\mathbf{H_w''H_w^{T\prime\prime}} & 0 \\ \hline 0 & 0 & EI_\omega\mathbf{H_v''H_v^{T\prime\prime}} + GJ\mathbf{H_v'H_v^{T\prime}} \end{array}\right] dx$$

$$\mathbf{K_G} = \left[\begin{array}{c|c|c} \mathbf{G_{vv}} & \mathbf{0} & \mathbf{G_{v\theta}} \\ \hline \mathbf{0} & \mathbf{G_{ww}} & \mathbf{G_{w\theta}} \\ \hline \mathbf{G_{v\theta}^T} & \mathbf{G_{w\theta}^T} & \mathbf{G_{\theta\theta}} \end{array}\right] = \int_l \left[\begin{array}{c|c|c} \mathbf{H_v'H_v^{T\prime}} & 0 & z_r\mathbf{H_v'H_v^{T\prime}} \\ \hline 0 & \mathbf{H_w'H_w^{T\prime}} & -y_r\mathbf{H_w'H_v^{T\prime}} \\ \hline z_r\mathbf{H_v'H_v^{T\prime}} & -y_r\mathbf{H_v'H_w^{T\prime}} & \left(I_p/A\right)\mathbf{H_v'H_v^{T\prime}} \end{array}\right] dx$$

$$\mathbf{M_1} = \left[\begin{array}{c|c|c} \mathbf{M_{vv}} & \mathbf{0} & \mathbf{M_{v\theta}} \\ \hline \mathbf{0} & \mathbf{M_{ww}} & \mathbf{M_{w\theta}} \\ \hline \mathbf{M_{v\theta}^T} & \mathbf{M_{w\theta}^T} & \mathbf{M_{\theta\theta}} \end{array}\right] = \int_l \rho \left[\begin{array}{c|c|c} A\mathbf{H_v}\mathbf{H_v^T} & 0 & z_rA\mathbf{H_v}\mathbf{H_v^T} \\ \hline 0 & A\mathbf{H_w}\mathbf{H_w^T} & -y_rA\mathbf{H_w}\mathbf{H_v^T} \\ \hline z_rA\mathbf{H_v}\mathbf{H_v^T} & -y_rA\mathbf{H_v}\mathbf{H_w^T} & I_p\mathbf{H_v}\mathbf{H_v^T} \end{array}\right] dx$$

$$\mathbf{M_2} = \left[\begin{array}{c|c|c} \mathbf{I_{vv}} & \mathbf{I_{vw}} & \mathbf{0} \\ \hline \mathbf{I_{vw}^T} & \mathbf{I_{ww}} & \mathbf{0} \\ \hline \mathbf{0} & \mathbf{0} & \mathbf{I_{\theta\theta}} \end{array}\right] = \int_l \rho \left[\begin{array}{c|c|c} I_z\mathbf{H_v'H_v^{T\prime}} & I_{yz}\mathbf{H_v'H_w^{T\prime}} & 0 \\ \hline I_{yz}\mathbf{H_w'H_v^{T\prime}} & I_y\mathbf{H_w'H_w^{T\prime}} & 0 \\ \hline 0 & 0 & I_\omega\mathbf{H_v'H_v^{T\prime}} \end{array}\right] dx \tag{5.15(a-d)}$$

The Raleigh damping matrix $[\mathbf{C}]$ is given by

$$[\mathbf{C}] = c_0[\mathbf{M_s}] + c_1[\mathbf{K_s}] \tag{5.16}$$

as a linear combination of the mass matrix $[\mathbf{M_s}]=[\mathbf{M_1}]+[\mathbf{M_2}]$, and the stiffness matrix $[\mathbf{K_s}]=[\mathbf{K}]+P[\mathbf{K_G}]$. Constants c_0, c_1 are given by

$$c_0 = \zeta \frac{2\omega_1\omega_2}{\omega_1+\omega_2} \quad , \quad c_1 = \zeta \frac{2}{\omega_1+\omega_2} \tag{5.17(a-b)}$$

in which ζ is the damping ratio, ω_1 and ω_2 are the first and second natural frequencies. For a given set of line loads $q_y(x,t), q_z(x,t), m(x,t)$ acting on an element, one obtains the energy equivalent force vector from Eq. 5.12, by substituting into Eq. 5.8, yielding[12]

$$\int_{t_1}^{t_2} \delta V dt = -\int_{t_1}^{t_2} \delta \left\langle \mathbf{v_n}(t) \quad \mathbf{w_n}(t) \quad \boldsymbol{\theta}_\mathbf{n}(t) \right\rangle_{1\times 12} \left\{ \mathbf{F}(t) \right\}_{12\times 1} dt \tag{5.18}$$

in which the energy equivalent force vector

$$\mathbf{F}_e^{\mathbf{T}}(t)_{12\times 1} = \int_0^l \left\langle q_y(x,t)\mathbf{H}_\mathbf{v}^{\mathbf{T}}(x) \;\vdots\; q_z(x,t)\mathbf{H}_\mathbf{w}^{\mathbf{T}}(x) \;\vdots\; m(x,t)\mathbf{H}_\mathbf{v}^{\mathbf{T}}(x) \right\rangle dx \tag{5.19}$$

When a beam span is discretized into n equal elements of lengths $l = L/n$ subjected to a pedestrian walking along the span at constant velocity v (Figure 5.2) starting at $(x, t = 0, 0)$, the time-dependent horizontal and vertical force components of elements $e = 1, 2...n$ are given by

[12] The steps for obtaining Eq. 5.19 are provided in Appendix H

$$q_{ym,e}(x,t)=\begin{cases}\left[Q\sum_{i=1}^{N}\beta_i\sin\left(2\pi if_s t-\lambda_i\right)\right]\delta^*\left[x-\left(vt-(e-1)l\right)\right] & t\in\left[(e-1)l/v,\,el/v\right]\\ 0 & \text{otherwise}\end{cases}$$

$$q_{zm,e}(x,t)=\begin{cases}\left[Q+Q\sum_{i=1}^{N}\alpha_i\sin\left(2\pi if_s t-\phi_i\right)\right]\delta^*\left[x-\left(vt-(e-1)l\right)\right] & t\in\left[(e-1)l/v,\,el/v\right]\\ 0 & \text{otherwise}\end{cases}$$

5.20(a-b)

in which the time interval $\left[(e-1)l/v,\,el/v\right]$ denotes the duration during which the individual is positioned over element e, From Eq. 5.20, by substituting for $\left(q_y,q_z,m\right)=\left(q_{y.me},q_{z.me},0\right)$ into Eq. 5.19, and performing integrals, one obtains

$$\mathbf{F}_e(t)=\begin{cases}\begin{cases}\left[Q\sum_{i=1}^{N}\beta_i\sin\left(2\pi if_s t-\lambda_i\right)\right]\mathbf{H}_{\mathbf{v}}\left[x_0(t)\right]\\ \left[Q+Q\sum_{i=1}^{N}\alpha_i\sin\left(2\pi if_s t-\phi_i\right)\right]\mathbf{H}_{\mathbf{w}}\left[x_0(t)\right]\\ \mathbf{0}_{4\times1}\end{cases} & t\in\left[(e-1)l/v,\,el/v\right]\\ \mathbf{0}_{12\times1} & \text{otherwise}\end{cases} \qquad 5.21$$

in which $x_0(t)=vt-(e-1)l$ is the instantaneous location of the moving load measured from the end $x=0$ of element e(Figure 5.2).

5.6. Time Integration

Direct time integration was performed based on the Newmark integration scheme (e.g., [49]) as described in the following:

I. Initialization

1. Compute matrices $\mathbf{K}$, $\mathbf{M}$, and $\mathbf{C}$.

2. Initialize vectors $\mathbf{U}(t=0), \dot{\mathbf{U}}(t=0), \ddot{\mathbf{U}}(t=0)$.

3. Set a time step Δt and parameters δ and α such that $\delta \geq 0.5$ and $\alpha \geq 0.25(0.5+\delta)^2$. In the present implementation, the values $\delta = 1/2$ and $\alpha = 1/4$ are chosen, which are based on the unconditionally stable constant average acceleration method.

4. Form the effective stiffness matrix $\hat{\mathbf{K}} = \mathbf{K} + a_0\mathbf{M} + a_1\mathbf{C}$ in which $a_0 = 1/(\alpha\Delta t^2)$ and $a_1 = \delta/(\alpha\Delta t)$.

5. Conduct the matrix decomposition $\hat{\mathbf{K}} = \mathbf{L}\mathbf{D}\mathbf{L}^{\mathrm{T}}$.

II. For each time step:

1. Compute the effective load vector $\hat{\mathbf{R}}$ at time $t+\Delta t$

$$\hat{\mathbf{R}}(t+\Delta t) = \mathbf{R}(t+\Delta t) + \mathbf{M}\left[a_0\mathbf{U}(t) + a_2\dot{\mathbf{U}}(t) + a_3\ddot{\mathbf{U}}(t)\right] + \mathbf{C}\left[a_1\mathbf{U}(t) + a_4\dot{\mathbf{U}}(t) + a_5\ddot{\mathbf{U}}(t)\right],$$

$\mathbf{R}(t+\Delta t)$ being the applied force vector at $t+\Delta t$, $a_2 = 1/(\alpha\Delta t)$, $a_3 = (1/2\alpha) - 1$, $a_4 = (\delta/\alpha) - 1$, $a_5 = (\Delta t/2)(\delta/\alpha - 2)$.

2. Given $\hat{\mathbf{R}}(t+\Delta t)$, solve the system $\mathbf{L}\mathbf{D}\mathbf{L}^{\mathrm{T}}\mathbf{U}(t+\Delta t) = \hat{\mathbf{R}}(t+\Delta t)$ for the displacement vector $\mathbf{U}(t+\Delta t)$

3. Compute the acceleration and velocity vectors $\ddot{\mathbf{U}}(t+\Delta t)$, $\dot{\mathbf{U}}(t+\Delta t)$:

$$\ddot{\mathbf{U}}(t+\Delta t) = a_0\left[\mathbf{U}(t+\Delta t) - \mathbf{U}(t)\right] - a_2\dot{\mathbf{U}}(t) - a_3\ddot{\mathbf{U}}(t)$$
$$\dot{\mathbf{U}}(t+\Delta t) = \dot{\mathbf{U}}(t) + a_6\ddot{\mathbf{U}}(t) + a_7\ddot{\mathbf{U}}(t+\Delta t)$$

in which $a_6 = \Delta t(1-\delta)$ and $a_7 = \delta\Delta t$.

5.7. Reference Case A and Mesh Study

Reference case A consists of a 5*m* span simply supported beam has a W250x45 cross-section. Cross-sectional properties are $A = 5700mm^2, \left(I_y, I_z, J\right) = \left(7.11\times10^7, 7.03\times10^6, 2.61\times10^5\right)mm^4$, $I_\omega = 1.13\times10^{11}mm^6$, and $m = 45\,kg/m$. Steel properties in the present and following examples are $\left(E, G\right) = \left(2\times10^5, 7.7\times10^4\right)MPa$. The beam is subjected to a mid-span vertical force induced by a human walking at a speed of 1.5m/s. The forcing function caused by walking is characterized by (Eq. 5.1(a)) with $Q = 746N$, f_s = 2.5 Hz (i.e., $T_1 = 0.4\text{s}$). The force is applied for 10 cycles for a total duration of $10\times0.4 = 4\,\text{s}$. The response is evaluated from $t_1 = 0$ to $t_e = 4\text{s}$ in time increments of $\Delta t = T_1/100 = 0.004\text{s}$. The dynamic load factors are $\alpha_1 = 0.41\left(f_s - 0.95\right)$, $\alpha_2 = 0.0056\left(f_s + 12.3\right)$, $\alpha_3 = 0.0064\left(f_s + 5.2\right)$, $\alpha_4 = 0.0065\left(f_s + 2.0\right)$ and the phase angles are $\phi_1 = 0, \phi_2 = \phi_3 = \phi_4 = \pi/2$ [15]. The damping ratio ζ is taken as 0.05. The Euler buckling loads about minor and major axes are $P_{cr,z}$ is $555kN$ and $P_{cr,y}$ is $5614kN$. The first natural frequency of the member was computed as 11.17 Hz and corresponds to vibration about the minor axis, while the third natural frequency, computed as 35.45 Hz, corresponds to vibration about the major axis. The beam is analyzed using two meshes consisting of 8 and 50 elements. Figure 5.3(c,d) shows that the displacements and accelerations predicted by both meshes are in close agreement. Thus, an eight-element mesh is used in the remainder of this study.[13]

[13] Appendix J provides the specifics of simulating the forcing function along with a verification against past solutions.

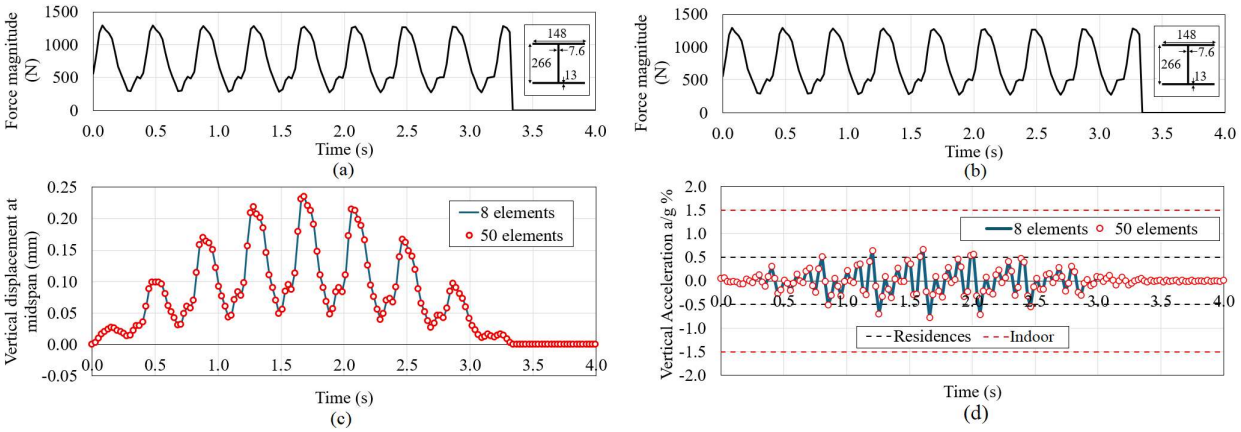

Figure 5.3 History response for Reference Case A based 8 and 50 finite elements: (a) applied force, (b) midspan vertical displacement, and (c) normalized vertical acceleration.

5.8. Asymmetric Member under Harmonic Force

5.8.1. Verification

The validity of the predictions of the present formulation is assessed for a benchmark problem and solution in [43]: A 6m span cantilever has an asymmetric C shaped cross-section (Figure 5.5b-c) with non-principal directions (y,z) and principal directions $(\hat{y},\hat{z})$. Cross-sectional properties about non-principal directions are $(A,I_\omega)=\left(2000mm^2,8.61\times10^8 mm^6\right),\left(I_y,I_z,I_{yz},J\right)=\left(3.47\times10^6,1.12\times10^6,-8.00\times10^5,5.71\times10^4\right)mm^4$ and $m=15.7\,kg/m$. All DOFs are restrained at the cantilever root and free at the tip. The damping ratio is taken as 3%. The member tip is subjected to a sinusoidal force $F(t)=F\sin(\omega_f t)=100\sin(9.33t)N$ (Figure 5a), where the exciting $\omega_f=9.33rad/s$ is taken as 90% of the fundamental natural frequency $\omega_1=10.37rad/s$ [47] . Time increments are taken as $\Delta T=0.0303s$. The free end horizontal displacement of point A at the tip of the bottom leg (Figure 5c) is sought as the primary output. Figure 5d shows close

agreement between the predictions of the present solution and that reported in [43], suggesting the validity of the present solution.[14]

5.8.2. Spatiotemporal Distribution of vertical Accelerations induced by walking

Figure 5.4 depicts the distribution along the span $x \in [0, l = 5m]$ of the normalized vertical acceleration a/g for Reference Case A under the action of a pedestrian walking, as characterized by the forcing functions in Eqs. 5.1 and 5.11a. The walking speed is taken as $v = 1.5\, m/s$ .and the acceleration response is traced in the domain $t \in [0, l/v = 3.33s]$,

The contour plots (Figure 5.4a-b) show that the accelerations alternate in time between positive and negative peaks. For a walking frequency of 2.5Hz, the frequency of the fourth harmonic is 10Hz, which corresponds $0.1s$. This value nearly matches the period between two consecutive acceleration peaks, i.e., the acceleration oscillation periods correlate heavily with the period of the fourth harmonic characterizing pedestrian walking. Also, irrespective of the location of the pedestrian along the span, the peak accelerations at a given time t are observed to occur in the neighbourhood of the mid-span. For example, at $t = 0.75s$, the pedestrian is located at $x = 1.12m$. Yet, the maximum vertical acceleration is found to be at $x/l = 0.45$. As such, in subsequent sections, accelerations under human walking will be monitored at midspan.

[14] Additional verification for is provided in Appendix J for a doubly symmetric member.

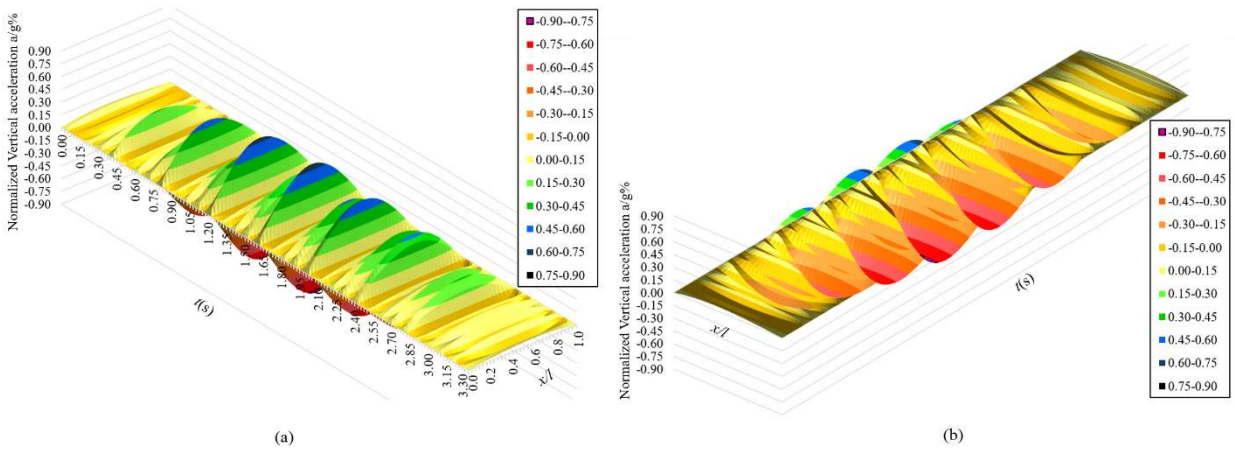

Figure 5.4 Spatiotemporal distribution of normalized vertical acceleration of Reference Case A under pedestrian walking: (a) View from above showing positive accelerations (b) View from below showing negative accelerations

5.8.3. Effect of Axial Load

An axial load is added to the problem defined in Section 5.8.1 (Figure 5.5e) and five scenarios of axial load magnitudes are investigated; $P/P_{cr} \in \{-0.2, -0.1, 0, +0.1, +0.2\}$, in which a positive P/P_{cr} denotes compression, and P_{cr} is the torsional flexural critical load for the member. The corresponding fundamental natural frequencies are 2.13, 1.91, 1.64, 1.31, and 0.82 *Hz*, respectively. Compared to the zero axial load baseline case $P/P_{cr} = 0$, compressive axial forces are observed to amplify the displacement response, as observed for $P/P_{cr} = 0.1$ and 0.2. Conversely, tensile forces reduce the displacement response, as shown for $P/P_{cr} = -0.1$ and -0.2 . The acceleration amplification in the presence of compressive loads is attributed to submatrices $\mathbf{G_{vv}}, \mathbf{G_{ww}}, \mathbf{G_{\theta\theta}}$ on the diagonal of the geometric stiffness matrix, which reduce the flexural and torsional stiffnesses of the member and amplify the displacement and acceleration responses.[15]

[15] The effect of various damping representations is investigated in Appendix K

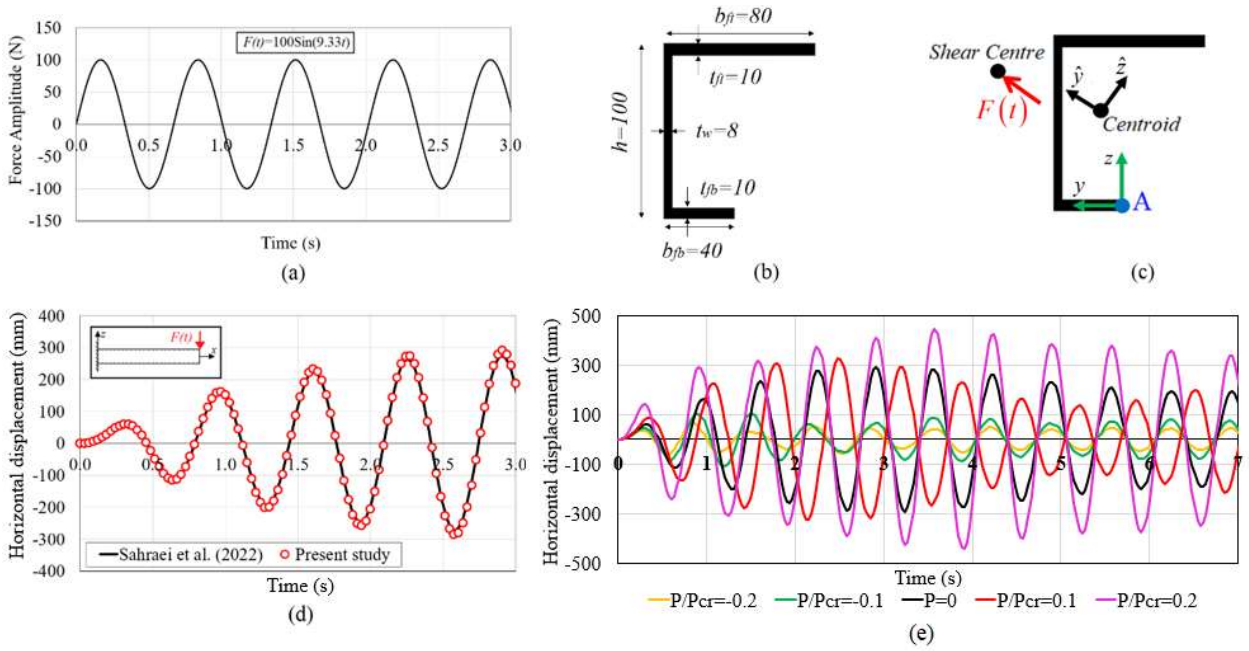

Figure 5.5 (a) Exciting force, (b) Cross-section dimensions (mm), (c) Principal directions and applied loads, (d) Major-axis displacement response at point A (along y direction). (e) Effect of axial load P (positive when compressive) on major axis displacement

5.9. Response to Walking on a Treadmill

5.9.1. Member with I Cross-Section [16]

The beam defined under Reference Case A is re-considered, while taking the damping ratio ζ as 0.03. The member is subjected to a mid-span vertical force induced by a human walking on a treadmill located at the member midspan (Figure 5.6a). The dynamic load factors α_i and phase angles ϕ_i are characterized by the forcing function described in Section 5.7.

Figure 5.6b shows that the peaks of the vertical midspan displacement are nearly synchronized with the peaks of the forcing function (Figure 5.6a). Also, Figure 5.6c suggests that the initial peak is caused by the abrupt application of the static human body weight. Overlaid on Figure 5.6c for comparison are the threshold accelerations for various occupancy usages as provided in [18]. The

[16] The dynamic response for members with angle cross-section due to walking on a treadmill is investigated in Appendix M.

acceleration response is observed to exceed the comfort threshold for residential use but lies within comfort limits for indoor and outdoor spaces. The initially high vertical acceleration amplitudes gradually stabilize over time owing to damping, as the member response transitions towards a steady state. Thus, while initial transients may exceed comfort limits for residential use, the long-term response is more controlled and tolerable, in this case.

5.9.1.1. Effect of Axial Force

The effect of axial load on the dynamic response is shown in Figure 5.6c. Three axial loading levels are considered: no force, a compressive force $0.1P_{cr,y}$, and a tensile force $-0.1P_{cr,y}$. The natural frequencies corresponding to flexure about the major axis are 33.8, 35.5, and 37.0 Hz, respectively. Again, the presence of a compression is found to amplify the vertical displacement response. In contrast to the acceleration which was shown to exceed acceptable thresholds for residential occupancy (Figure 5.6d), Figure 5.6c shows that the magnitudes of the displacements are in all three cases are well below typical span to deflection ratios of $L/360$. Across all three axial loading conditions considered, the member exhibits a sustained periodic response that is synchronized with the dynamic forces induced by walking.

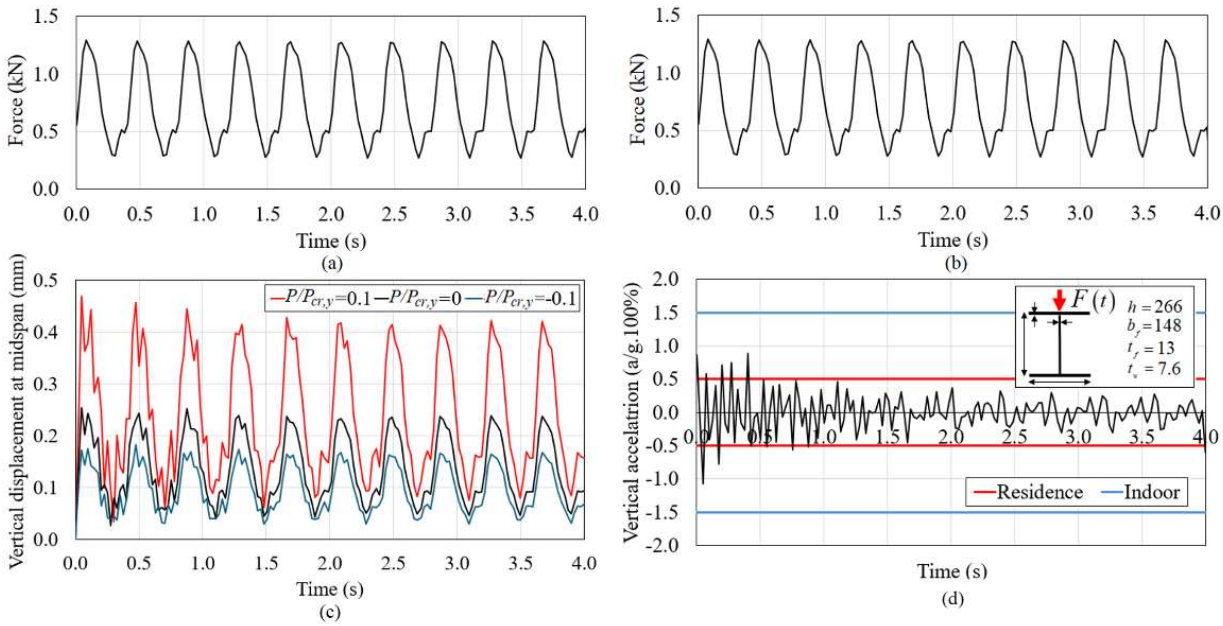

Figure 5.6 (a) and (b) Dynamic force induced by human walking on a treadmill, and (c) Midspan vertical displacement for various axial force levels ($P_{cr,y}$ is the major axis buckling load) (d) vertical acceleration ratio (a/g)

5.9.1.2. Effect of Span

Beam spans of $L = 3, 5,$ and $6.5m$ were taken for comparison. The major axis flexural natural frequencies corresponded to the third natural frequency and to take the values 98.0, 35.5, and 21.0 Hz respectively. Figure 5.7(b-e) shows that the amplitudes of mid-span displacements grow significantly as the span increases. The increased amplitudes are partly due to the greater static deflection observed in longer spans under identical human static loads. Specifically, the static deflections for spans $L = 3m, 5m,$ and $6.5m$ as determined from the expression $\delta_{st} = Pl^3/48EI_y$ are 0.029, 0.14, and $0.30mm$, respectively, and are depicted by the horizontal lines on Figure 5.7b for comparison. The static displacements are observed to be close to the average displacements determined by the dynamic analysis. Another reason for the increase in displacements is dynamic amplification. The dynamic amplification factor is defined as the ratio of the dynamic response to the deflection under a static vertical force equal to the human weight Q and is depicted in Figure

5.7(c-e) for the sudden load application term (termed as H0) in the figures and for the combined effect of impulsive plus the four harmonic terms (denoted as H0-4). The number preceding both designations denotes the span. For example, 3.0H0 denotes the amplification of the sudden load application term for the 3*m* span, 3.0H0-3 refers to a 3*m* span member under sudden application of human body weight plus the first three harmonics, and 5.0STD is the static deflection for 5*m* span member. Owing to the fact that major axis flexural natural frequencies of all three members of 98.0, 35.5, and 21.0 Hz are significantly higher than the highest exciting frequency due to human walking of 10 Hz, dynamic amplifications due to the harmonic components are relatively controlled, while that related to the sudden load application component becomes more pronounced as the span increases.

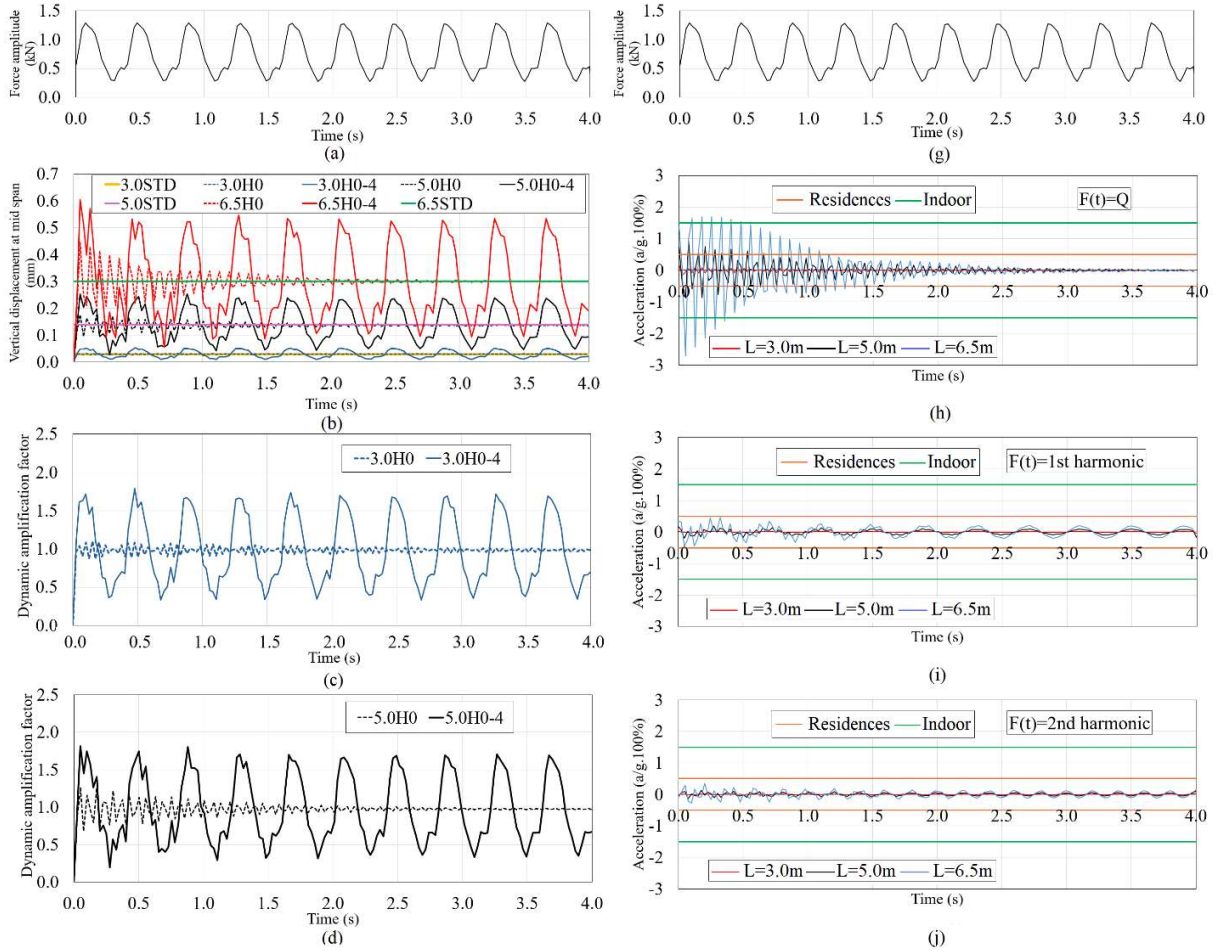

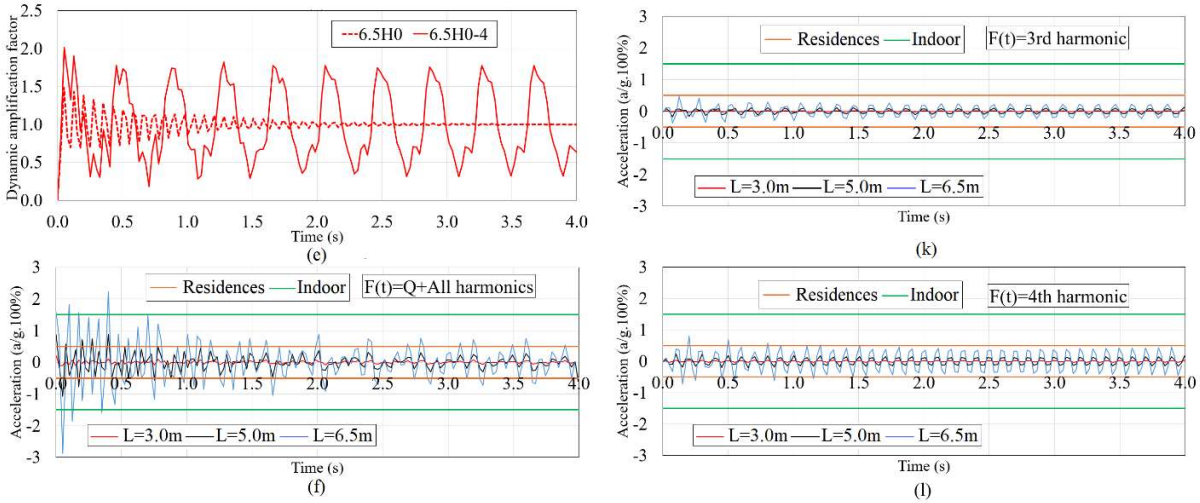

Figure 5.7 Dynamic forcing function induced by stationary walking, (b) Vertical displacements at midspan due to stationary walking at midspan; Dynamic amplification factors for member (c) L= 3m, (d) L=5m, (e) L=6.5m (f) Corresponding acceleration (g) Forcing function (c-g) Separate acceleration response for each of the five components of the forcing function (Human bodyweight and harmonics 1 to 4)

5.9.1.3. Individual Contributions of Harmonics

Figure 5.7(f-l) show the acceleration response for each of the contributions of the human walking force for the three spans considered. Initial acceleration peaks are primarily induced by the sudden application of human body weight, while the fourth harmonic plays the most significant role in maintaining sustained dynamic acceleration levels. For $L = 3m$, the response to the body weight Q and the first harmonic components remain well below all residential occupancy thresholds, shopping malls, and footbridges/outdoor structures. In contrast, the accelerations of the longest span $L = 6.5m$, approach or exceed the thresholds for residential structures and indoor spaces, owing primarily to the sudden application of the body weight Q and the first harmonic components. The second harmonic is observed to contribute to acceleration levels that may exceed acceptable thresholds for footbridges or outdoor structures for a longer span, though its effect is less pronounced relative to the first harmonic. The second and third harmonics generally have negligible contributions, with acceleration values staying well within acceptable limits for all

occupancy types. When all forcing function components are superimposed, the total acceleration response increases significantly, exceeding acceleration thresholds for all structure occupancies.[17]

5.10. Response to Walking at constant speed

5.10.1. Member with I Cross-Section

The acceleration response of the member in Reference Case A is analyzed under the vertical component of the forcing function (Eq. 5.11a) by a human walking at a speed v from the end $\bar{x}_0 = 0$ at $t = 0$ to the end $\bar{x}_0 = L$. The walking speed $v = L_s f_s$ is the product of step length L_s and the step frequency f_s. The step frequency f_s is held constant at 2.5 Hz while varying the walking speed v to $1.0, 1.5$ and $2.0\,m/s$ which correspond to step lengths of $L_s = 0.4, 0.6$ and $0.8m$, respectively. Figure 5.8b shows that, for a given step frequency, the step length does not significantly alter the peak amplitude of the acceleration. In this case, an increased walking speed is associated with a shorter duration of the excitation as the load traverses the span more rapidly, leading to an earlier decay of the acceleration response.

In a second scenario, the step length is maintained constant at $L_s = 0.6m$, while varying the walking speed to $1.0, 1.5$ and $2.0\,m/s$ by altering the step frequencies respectively to $f_s = 1.67, 2.50,$ and 3.33Hz. Figure 5.8(c-d) illustrates the corresponding vertical displacement and acceleration responses. An increase in the step frequency induces an increase in the dynamic displacement response and a more noticeable increase in the acceleration response.

[17] Results for the cumulative effect of all harmonics for the 5m span are provided in Appendix L

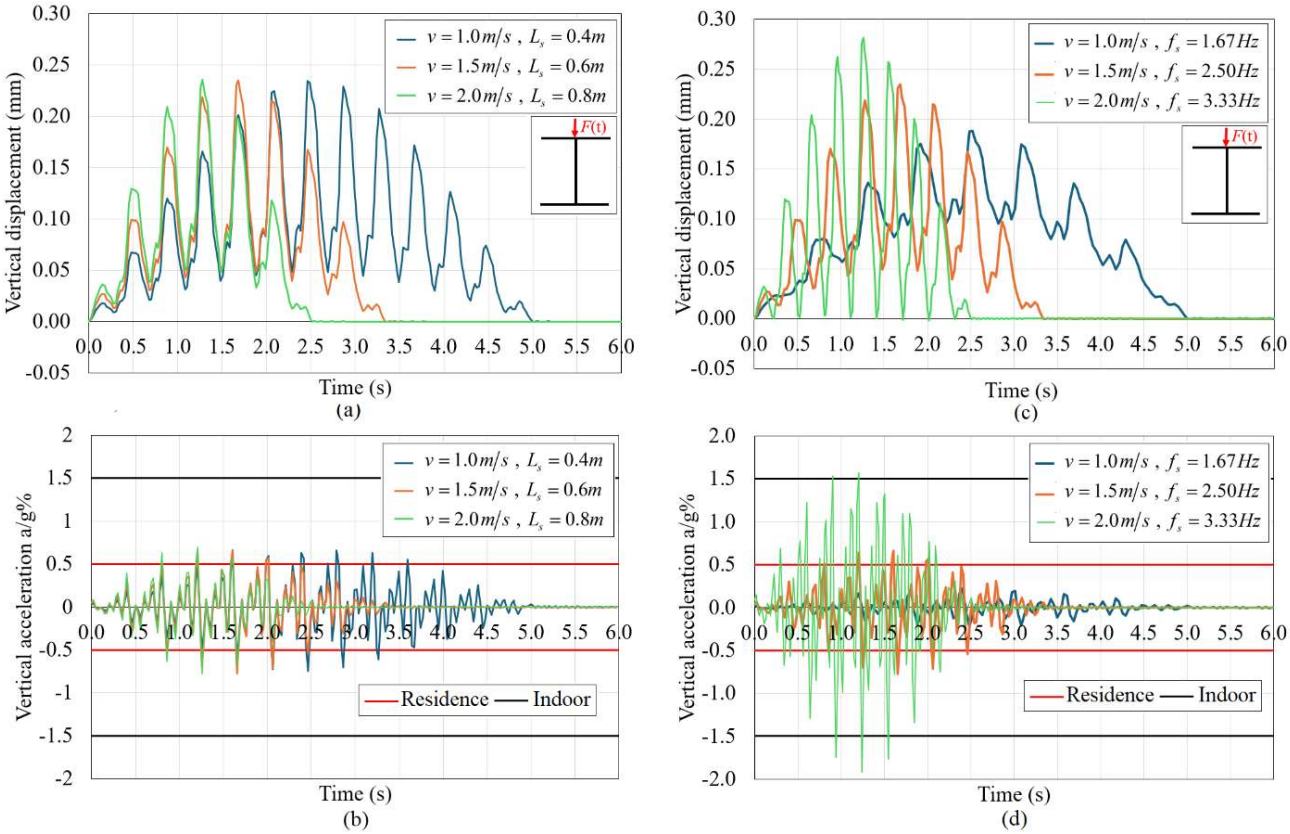

Figure 5.8 Dynamic response of the member with I section under vertical human-induced moving loads for two velocity variation scenarios: (a, b) step frequency $f_s = 2.5Hz$ with varying step length L_s; (c, d) fixed step length $L_s = 0.6m$ and varying step frequencies f_s.

5.10.1.1. Effect of span

In addition to 5m span of the beam in reference case A, a longer span of 7m is considered. The corresponding flexural natural frequencies about strong axis are 35.5 and 18.1 Hz, respectively. Both members are subjected to the vertical component of the force induced by human walking as characterized in Section 5.5.1. Figure 5.9b shows that the longer member exhibits substantially greater vertical accelerations at midspan, that that exceed the comfort thresholds for residential and indoor usage. In contrast, the shorter member exhibits more controlled accelerations that lie within acceptable limits throughout the loading period.

5.10.1.2. Effect of axial force

The influence of axial load on the vertical acceleration response of the member in reference case A is examined in Figure 5.9c. Three axial load levels are considered, a compressive force $P/P_{cr,y} = 0.25$, no axial force $P/P_{cr,y} = 0$, and a tensile force $P/P_{cr,y} = -0.25$, which correspond to major axis flexural natural frequencies of 27.4, 35.5, and 39.6 Hz, respectively. Again, the presence of a compressive axial load results in accelerations increase compared to the unloaded member. Conversely, axial tension causes a slight reduction in the accelerations.

The beam in reference case A is re-analyzed under the effect of the horizontal component the of human walking force at a constant speed $v = 1.5\,m/s$ from the end $\bar{x}_0 = 0$ at $t = 0$ to the end $\bar{x}_0 = L$. The beam is assumed to be laterally and torsionally unbraced between both ends. Both the vertical and horizontal components of human-induced walking forces as characterized by Eqs. 5.1 are assumed to act at the top flange (Point A on Figure 5.9e). In this case, the horizontal force acting at the top flange induces a twisting moment. Figure 5.9e shows that the peak horizontal acceleration at Point A on the top flange is nearly three times larger than that of Point B on the bottom flange, in a manner consistent with the low torsional stiffness of members with open sections. In this case, the horizontal accelerations exceed all acceptable thresholds.

Figure 5.9f depicts the effect of axial load on the horizontal acceleration of the member at Point A under three axial loads; a compressive force $P/P_{cr,z} = 0.5$, no axial force $P/P_{cr,z} = 0$, and a tensile force $P/P_{cr,z} = -0.5$. The fundamental natural frequencies corresponding to weak axis flexure are 7.89, 11.2, and 13.7*Hz*, respectively. Given the proximity of these values to those of the exciting frequencies in the 2.5-10 Hz range, the horizontal accelerations in this case are considerably larger under compression when compared to those of the vertical acceleration in

Figure 5.9c in the absence of axial force. Also, the amplified accelerations under the compressive force are observed to be more pronounced than in the case of tensile force.

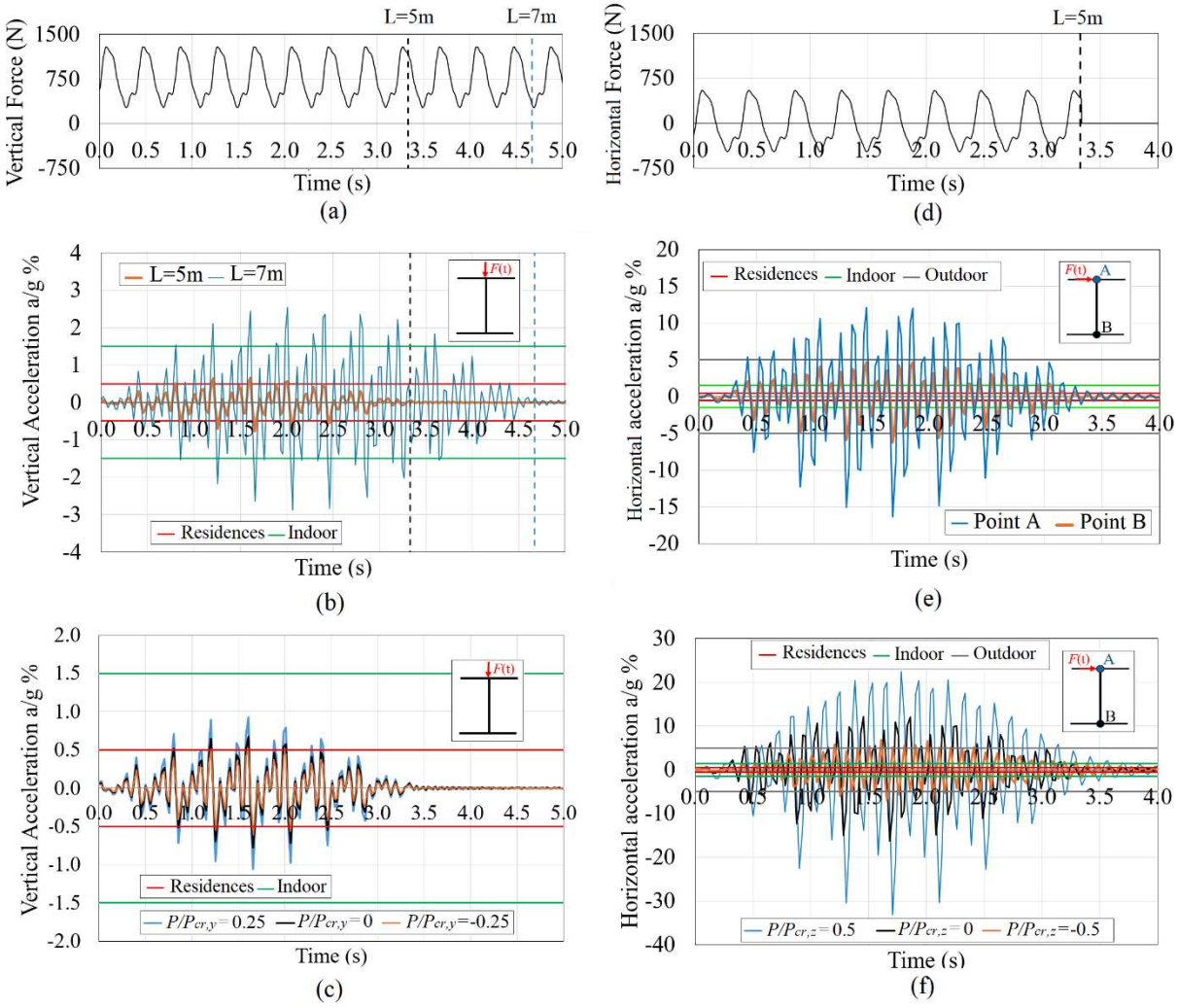

Figure 5.9 (a) Vertical component of force (b) Effect of span on vertical acceleration (c) Effect of axial load levels on vertical acceleration (d) Horizontal component of force, (e) Effect of span on horizontal acceleration of both flanges (span=5*m*), and (f) effect of axial load on top flange horizontal acceleration (span=5*m*). ($P/P_{cr,y}$ is buckling load about the major axis and $P/P_{cr,z}$ is the buckling load about minor axis)

5.10.1. Effect of lag time between pedestrians

Consider two pedestrians walking in tandem along the span of the beam of Reference Case A at a walking frequency of 2.5 Hz and the walking speed is 1.5 *m/s*. The time lag is assumed to vary from 0.75 to 0.80*s*. As discussed in Section 5.9.1.3, while the displacement response is dominated

by the first harmonic of the walking forcing function, the acceleration response is dominated by fourth harmonic. For a step frequency of 2.5Hz, the first harmonic corresponds to a period of 0.4s, which aligns with the time observed between consecutive displacement peaks in Figure 5.10(a). Also, the fourth harmonic corresponds to 10 *Hz*, which corresponds to a period of 0.1s. As such, Figure 5.10b, depicts a period of 0.1 seconds between acceleration peaks. The acceleration peaks are synchronized when the time-lag between both pedestrians is a multiple of 0.1s. This is reflected by the highest peak accelerations observed when the lag time is 0.80s. Conversely, the acceleration peaks tend to be least synchronized when the lag time is a multiple of 0.1s plus 0.5. This is reflected by the lowest acceleration peaks observed for a lag time of 0.75s. In between these two extreme cases, the magnitude of acceleration peaks are observed to increase gradually from a time lag of 0.75s up to 0.80s. Figure 5.11a shows the number of acceleration crossings of the bounds (both positive and negative) of the comfort domain while Figure 5.11b presents the proportion of the total walking duration during which acceleration exceeded the specified thresholds while both individuals were simultaneously on the beam. The results in Figure 5.11(a-b) are provided based on acceleration thresholds of a/g=0.5% and a/g=1.0% as a function of the time lag. Both metrics show peak correlation of human-induced accelerations at time lags of 0.70 s and 0.80 s a minimal correlation at 0.75s.

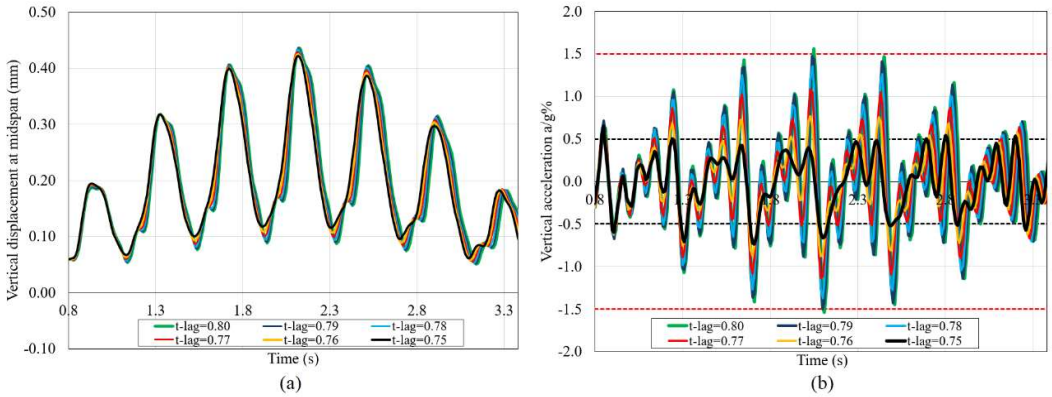

Figure 5.10 Vertical response at mid-span under two pedestrians with lag times (a) displacement and (b) acceleration

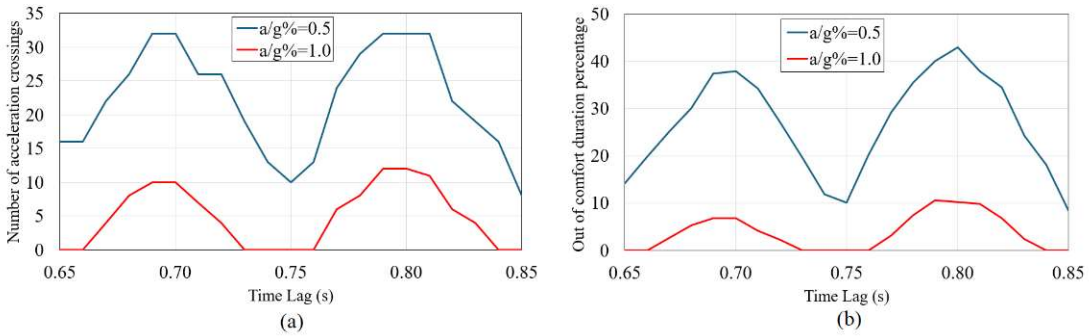

Figure 5.11 Metrics of acceleration versus time lag (a) Number of crossings, and (b) Out of comfort duration percentage

5.10.2. Member with Angle Cross-Section

5.10.2.1. Reference Case B

A member spanning 3m has an L152×102×16 cross-section as a reference case. Cross-sectional properties are $A = 3784mm^2$, $I_y = 3.14\times10^6 mm^4$, $I_z = 8.67\times10^6 mm^4$, $I_\omega = 4.55\times10^6 mm^6$, $J = 2.92\times10^5 mm^4$, and $m = 29.6\,kg/m$. The damping ratio is taken as 0.05. The member is subjected to dynamic loading due to walking is applied as defined under Section 5.7. Two types of boundary conditions are considered at the member ends: pin-end connections and gusset-end connections. For the pinned-end case, the slenderness ratio is 138, the buckling load is $P_{cr}^P = 386kN$ and the fundamental natural frequency is 19.0Hz**.** For the gusset-ended member, the buckling load is $P_{cr}^G = 592kN$ [46] and the natural frequency is 23.5Hz.

5.10.2.2. Effect of Boundary Conditions and Force Direction

As shown in Figure 5.12a, the vertical component of the applied force results in higher vertical than horizontal accelerations for the pin-ended member (Figure 5.12b). In comparison, the gusset-ended member (Figure 5.12c) exhibits lower accelerations in both directions, reflecting the increased flexural stiffness imparted by the end fixity about the axis perpendicular to the gusset. In this case, the horizontal accelerations are markedly lower than those observed for the pin-ended

member. The reduced accelerations observed in Figure 5.12c, are consistent with the higher natural frequency of the gusset-ended member (23.5Hz) relative to that of the pin-ended member (19.0Hz).

Under the horizontal force component (Figure 5.12d,e), the pin-ended member exhibits lower horizontal and vertical accelerations compared to those induced by the vertical force. Yet, the magnitudes of the horizontal and vertical accelerations are comparable. In Figure 5.12f, the lower acceleration response of the gusset-ended member compared to the pin-ended case is attributed to the additional flexural stiffness induced by rotational fixity about the axis normal to the gusset.

The horizontal component of the forcing function is observed to induce horizontal accelerations in the angle that are generally smaller than the vertical accelerations (Figure 5.12(b, e)).This behavior contrasts with that of the laterally and torsionally unbraced I-section member shown in Figure 5.9e, which exhibited greater horizontal than vertical accelerations.[18]

[18] The effect of span on the on dynamic response of angle members is investigated in Appendix N

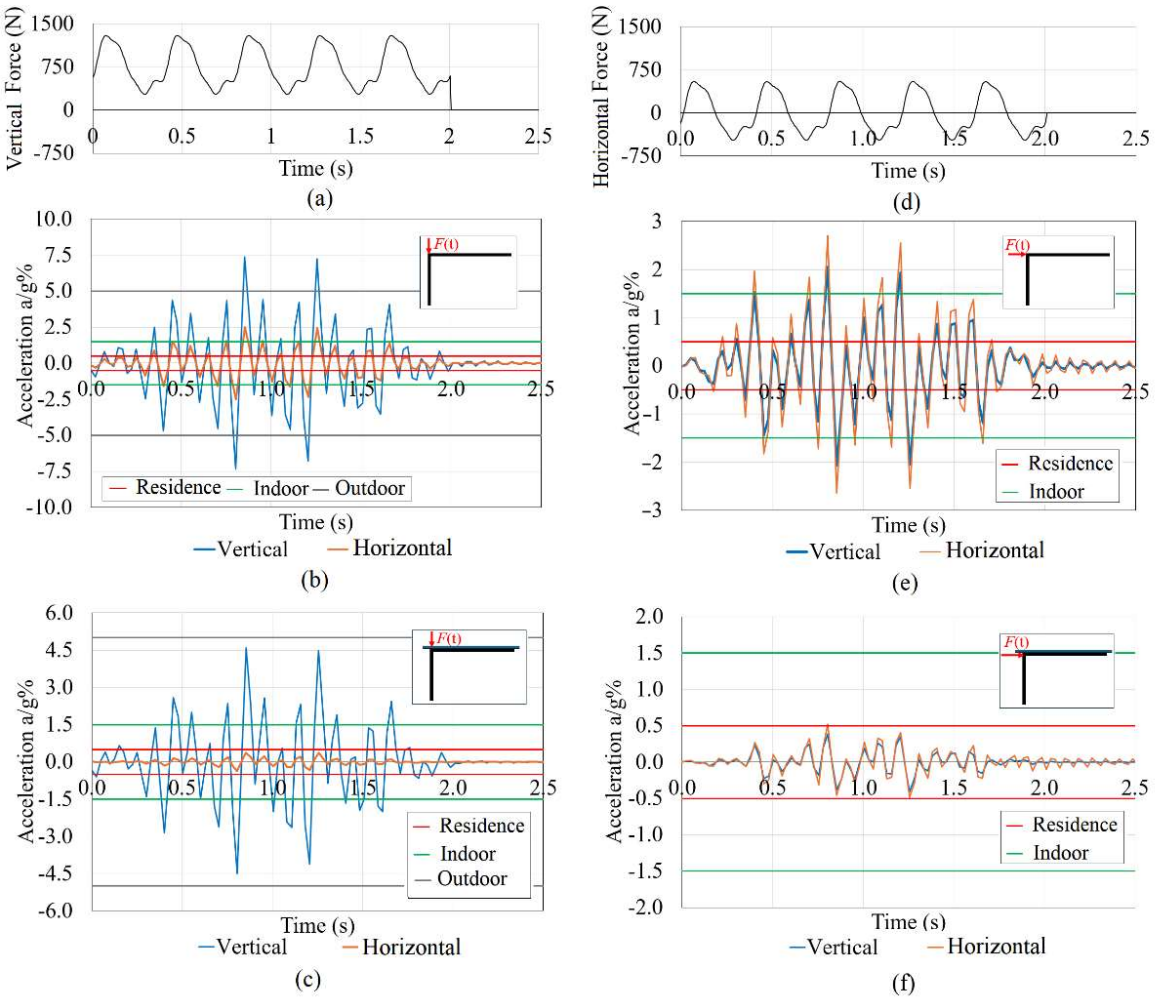

Figure 5.12 (a) Vertical component of force and corresponding accelerations for (b) pin-ended member (c) gusset-ended member. (d) Horizontal component of force and corresponding accelerations for (e) pin-ended member and (f) and gusset-ended member

5.10.3. Effect of Axial load on Pin-ended member

The member in Reference Case B is subjected to three axial load levels; $P/P_{cr}^{P} = 0.0, 0.20, 0.75$, which respectively correspond to fundamental natural frequencies of 19.0, 16.9, and 9.17 Hz. Figure 5.13(a, c, e) depict the vertical accelerations under the effect of the vertical component of the force at three points; Point 1 at the tip of the connected leg, Point 2 at the heel of the angle, and Point 3 at the tip of the outstanding leg, while Figure 5.13(b, d, f) depict the horizontal accelerations. As the axial load increases, the associated reduction in natural frequency leads to a

pronounced increase in accelerations. This is observed in Figure 5.13(a, c, e), in which the peak vertical accelerations for $P/P_{cr}^{P}=0.75$ far exceed those of $P/P_{cr}^{P}=0.20$ or $P/P_{cr}^{P}=0.0$. A similar observation is made for the horizontal acceleration in Figure 5.13(b, d, f). In Figure 5.13(a, c, e), while the vertical accelerations at $P/P_{cr}^{P}=0.0$ are nearly equal at all three points , as the load increases, the vertical accelerations of Point 1 become higher than those of Points 2 and 3, owing to twist. The behavior is attributed to the fact that, for the asymmetric angle cross-section, the off-diagonal sub-matrices $\mathbf{M}_{v\theta},\mathbf{M}_{w\theta}$ of the inertia matrix $\mathbf{M}_1$ in Eq. 5.15(b-c) induce coupling between the translational displacements and the angle of twist. Also, the off-diagonal sub-matrices $\mathbf{G}_{v\theta},\mathbf{G}_{w\theta}$ of the geometric stiffness matrix $\mathbf{K}_G$ induce similar coupling. In the absence of axial loading, the inertial coupling induced in the present problem is minimal as depicted by the nearly equal acceleration at all three points, indicating nearly no twist. The degree of additional coupling induced by sub-matrices $\mathbf{G}_{v\theta},\mathbf{G}_{w\theta}$ is proportional to the magnitude of the applied axial force. Thus, as the applied axial force increases, the translational-twist coupling effect increases, inducing a more pronounced twist, as manifested by the uneven accelerations of points 1-3.

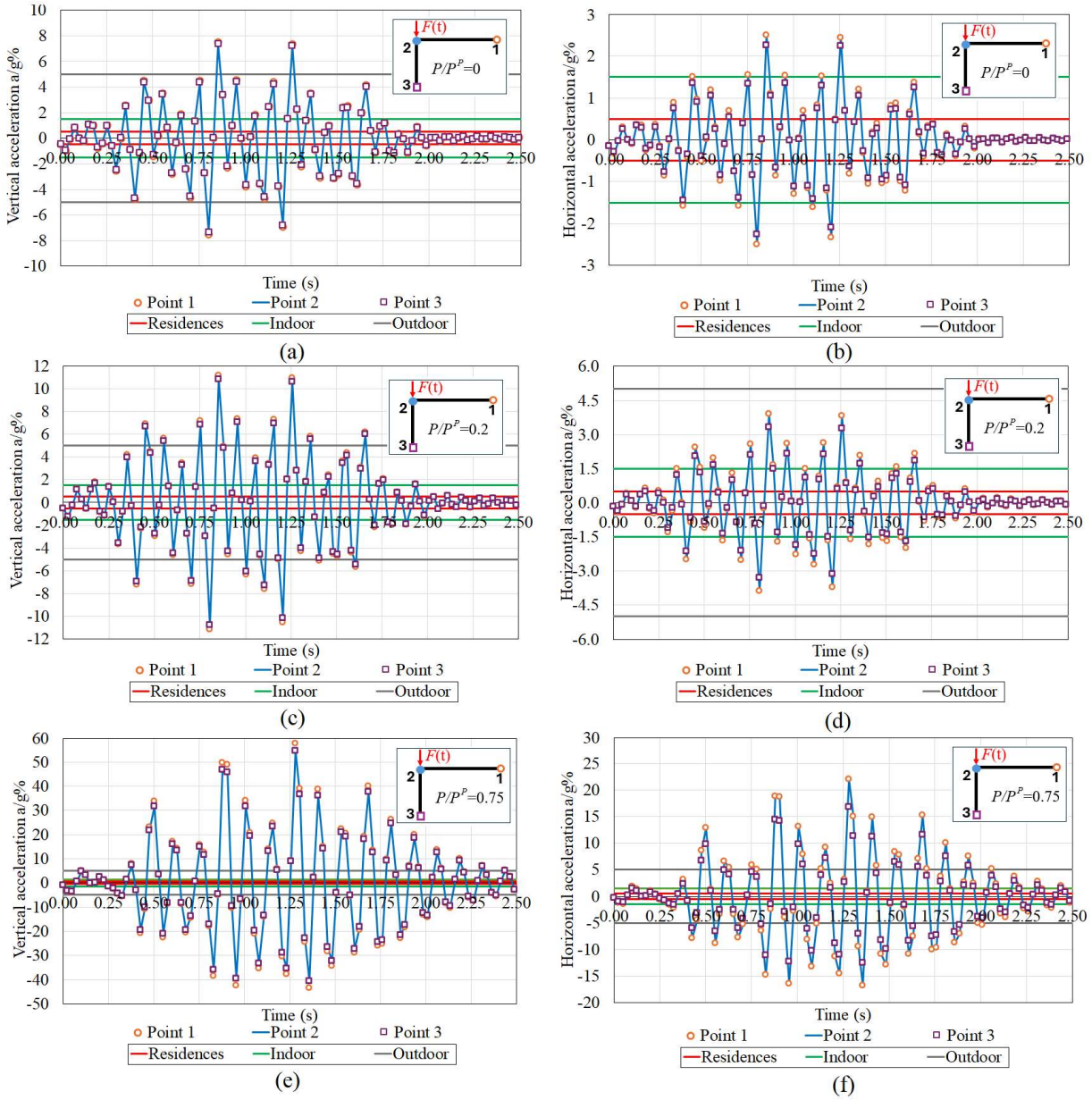

Figure 5.13 Vertical accelerations of pin-ended member for (a) $P/P_{cr}^{P}=0$**, (b)** $P/P_{cr}^{P}=0.2$**, (c)** $P/P_{cr}^{P}=0.75$**. Horizontal accelerations for (d)** $P/P_{cr}^{P}=0$**, (e)** $P/P_{cr}^{P}=0.2$**, (f)** $P/P_{cr}^{P}=0.75$**.**

5.10.3.1. Effect of Axial load on Gusset-end member

The member in Reference Case B is subjected to three axial load levels; $P/P_{cr}^{G}=0.0,\ 0.13,\ 0.65$, which respectively correspond to fundamental natural frequencies of 23.5, 21.9, and 16.6 *Hz*. Due to the higher natural frequencies relative to the pin-ended members, all acceleration responses in

Figure 5.14 are lower than those observed for the pin-ended configuration. As the axial load increases, the resulting decrease in natural frequency leads to pronounced increases in acceleration This trend is evident in Figure 5.14(a, c, e), where the peak vertical accelerations for $P/P_{cr}^{G} = 0.65$ far exceed those of $P/P_{cr}^{G} = 0.13$ and $P/P_{cr}^{G} = 0.0$. A similar observation is made for horizontal acceleration in Figure 5.14(b, d, f).

Figure 5.14(a, c, e) show that while vertical accelerations are equal at all three points when $P/P_{cr}^{G} = 0.0$, increasing the axial load leads to higher accelerations at Point 1 relative to those of Points 2 and 3. This behavior is attributed to coupling between the vertical displacement and twist, which becomes more pronounced with increasing axial force. Similarly, Figure 5.14(b, d, f) show that the horizontal accelerations at all three points increase noticeably with the increase in axial force. Again, the variation of horizontal accelerations among the three points is attributed to the torsional flexural coupling induced by axial load.

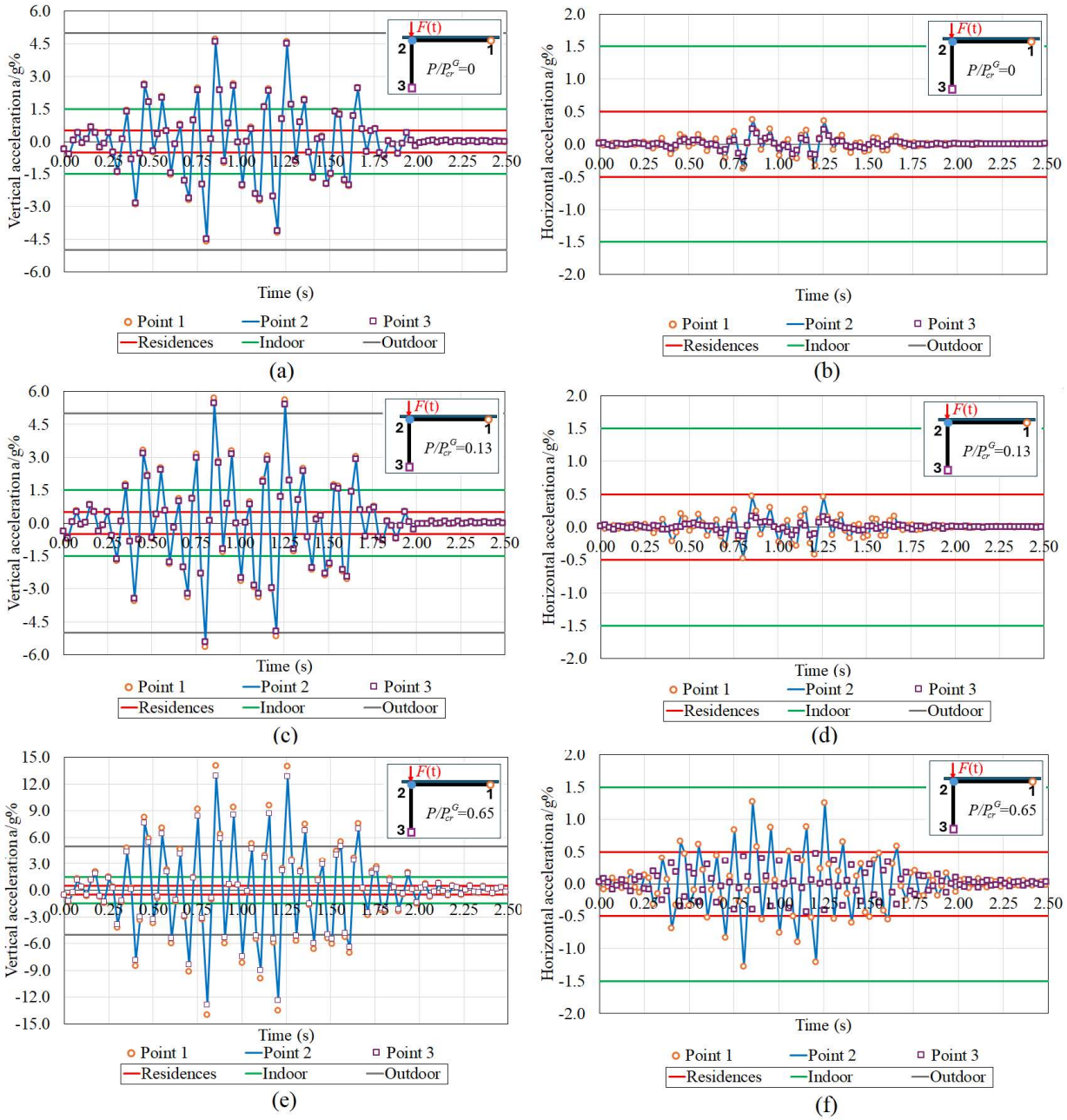

Figure 5.14 Vertical accelerations of Gusset-ended Member connection for (a) $P/P_{cr}^{G}=0$**, (b)** $P/P_{cr}^{G}=0.13$**, (c)** $P/P_{cr}^{G}=0.65$**. Horizontal accelerations for (d)** $P/P_{cr}^{G}=0$**, (e)** $P/P_{cr}^{G}=0.13$**, (f)** $P/P_{cr}^{G}=0.65$**.**

5.11. Conclusions

The following conclusions can be drawn from the present study:

1. Among the five force components induced by pedestrian walking, the sudden footfall impact and the fourth harmonic component were identified as the most influential in determining the level of induced accelerations.

2. While pedestrian-induced displacements remained within acceptable thresholds across all cases, the resulting acceleration levels exceeded perceptibility limits in several instances.

3. Increasing step frequency while maintaining step length significantly amplifies the induced acceleration levels, whereas increasing step length at a constant frequency has negligible impact.

4. Pinned-end angle members consistently exhibit larger displacements and accelerations than gusset-ended members, particularly during the initial stages of response and under compressive axial loads.

5. Pinned-end angle members consistently exhibit greater displacements and accelerations than gusset-ended members, particularly during the initial response phase and under compressive axial loading.

6. Angle-section members exhibit torsional–flexural coupling driven by both inertial and axial force effects. In the absence of axial load, inertial-induced twisting is negligible. However, axial compression significantly amplifies the coupling response, particularly at higher load levels.

7. In laterally and torsionally unbraced I-section members, the horizontal component of pedestrian-induced force generates horizontal accelerations that exceed vertical accelerations. Conversely, angle-section members exhibit lower horizontal accelerations relative to their vertical response.

8. Horizontally and torsionally unbraced I-section members subjected to pedestrian-induced horizontal forces exhibit excessive lateral and torsional deformations, leading to elevated accelerations at the top flange. It is of interest to investigate the effectiveness of horizontal bracing systems as a mitigation strategy for controlling excessive lateral and torsional responses in unbraced members subjected to pedestrian-induced excitation.

5.12. Notation

A : Arbitrary point on the section contour

B : Arbitrary point offset from the section contour

B' : Picture of point B on middle surface

C : Rayleigh damping matrix

c_0, c_1 : Damping matrix constants

E : Elasticity modulus

F_D : Damping forces vector

F(t) : Exciting force

f_s : Human step frequency

G : Shear modulus

$\mathbf{H_v}, \mathbf{H_w}$: Hermitian polynomials vectors

I_y, I_z : Moments of inertia about y and z axis

I_{yz} : Product of inertia

I_p : Polar moment of inertia about the shear centre

I_ω : Warping constant

J : Saint-Venant torsional constant

$\mathbf{K}$: Stiffness matrix

$\mathbf{K_G}$: Geometric matrix

l : Span

L_s : Human step's length

L_a : Hamiltonian functional

$\mathbf{M_1}$: Mass Matrix that accounts for the translational effects

$\mathbf{M_2}$: Mass matrix which accounts for the rotatory effects

N : Number of harmonics

n : Number of elements

P : Axial load

P_x, P_y, P_z : Body forces

$P_{cr,y}$: Euler buckling load about strong axis

$P_{cr,z}$: Euler buckling load about weak axis

P_{cr}^{G} : Buckling load of angle member with gusset end connection

P_{cr}^{P} : Buckling load of angle member with pinned end connection

q_x, q_y, q_z, m : Distributed axial load

$q_{y,m}(x,t)$, $q_{z,m}(x,t)$: Dynamic horizontal and vertical components of force induced by walking

Q : Human body weight

$r(s), q(s)$: Distances from the shear centre along the normal and tangent axis at point B'

R : Shear centre

t : Time

T : Kinetic energy

T_f : Fundamental natural period

U : Internal strain energy

$\mathbf{U_N}$: Nodal Displacement vector

V : Potential energy loss due to external loads

v : Velocity of human walking

W_{nc} : Energy dissipated by damping

$\mathbf{v_n}, \mathbf{w_n}, \boldsymbol{\theta}_\mathbf{n}$: Nodal displacement vectors associated with deformation along the y and z axes and twist DOFs.

$v(x), w(x)$: Displacements of the shear centre along the y, z . axes.

u_B, v_B, w_B : Displacements of arbitrary point offset from contour in the tangential direction

u_p : Axial displacement under static compressive load

$\overline{x}_0(t)$: The position of the human at time t measured from the end $x = 0$

y_r, z_r : Coordinates of shear centre relative to the section centroid

$\alpha(s)$: Angle between the tangent to the contour and the y axis

α_i : Dynamic amplification load factor for harmonic i

ρ : Density

δ : Variation function

δ^* : Dirac delta function

ζ : Damping ratio

ω_1, ω_2 : First and second natural frequencies

ω : Sectorial coordinate

ω_f : Exciting angular frequency

θ_x : Angle of twist

ϕ_i : Phase angle for harmonic i

5.13. References

1. Allen, D., *ATC Design Guide 1: Minimizing floor vibrations (1st ed.).* . 1999, Redwood City, CA:: Applied Technology Council;.
2. Smith, A.L., S.J. Hicks, and P.J. Devine, *Design of floors for vibration: A new approach*. 2007: Steel Construction Institute Ascot, Berkshire, UK.
3. Bachmann, H. and W. Ammann, *Vibrations in structures: induced by man and machines*. Vol. 3. 1987: Iabse.
4. Živanović, S., A. Pavic, and P. Reynolds, *Vibration serviceability of footbridges under human-induced excitation: a literature review.* Journal of sound and vibration, 2005. **279**(1-2): p. 1-74.
5. Galbraith, F. and M. Barton, *Ground loading from footsteps.* The Journal of the Acoustical Society of America, 1970. **48**(5B): p. 1288-1292.
6. Ellis, B. and T. Ji, *Floor vibration induced by dance-type loads: verification.* Structural Engineer, 1994. **72**: p. 37-37.
7. Murray, T.M., Ungar, E. E., & Davis, D. B. , *Facts for Steel Buildings No. 5: Vibration.* . 2018: American Institute of Steel Construction (AISC).
8. Rainer, J., G. Pernica, and D.E. Allen, *Dynamic loading and response of footbridges.* Canadian Journal of Civil Engineering, 1988. **15**(1): p. 66-71.
9. Murray, T.M., et al., *Vibrations of steel-framed structural systems due to human activity*. 2016: American Institute of Steel Construction.
10. ISO-10137, *International Organization for Standardization*, in *Bases for design of structures--serviceability of buildings and walkways against vibrations*. 2007, International Organization for Standardization: International Organization for Standardization.
11. Ingólfsson, E.T., C.T. Georgakis, and J. Jönsson, *Pedestrian-induced lateral vibrations of footbridges: A literature review.* Engineering Structures, 2012. **45**: p. 21-52.
12. Allen, D.E., J. Rainer, and G. Pernica, *Vibration criteria for assembly occupancies.* Canadian Journal of Civil Engineering, 1985. **12**(3): p. 617-623.
13. Pernica, G., *Dynamic load factors for pedestrian movements and rhythmic exercises.* Canadian Acoustics, 1990. **18**(2): p. 3-3.

14. Ebrahimpour, A. and R. Sack, *Design live loads for coherent crowd harmonic movements.* Journal of Structural Engineering, 1992. **118**(4): p. 1121-1136.
15. Pavic, A. and M. Willford, *Vibration serviceability of post-tensioned concrete floors.* Appendix G in post-tensioned concrete floors design handbook-technical report, 2005. **43**: p. 99-107.
16. Ellis, B. and T. Ji, *Loads generated by jumping crowds: numerical modelling.* Structural Engineer, 2004. **82**(17): p. 35-40.
17. Ebrahimpour, A., Hamam, A., Sack, R. L., & Patten, W. N., *Measuring and modeling dynamic loads imposed by moving crowds.* Journal of Structural Engineering, 1996. **122(12)**: p. 1468-1474.
18. Allen, D. and T.M. Murray, *Design criterion for vibrations due to walking.* Engineering Journal, 1993. **30**(4): p. 117-129.
19. Hechler, O., et al. *Design guide for floor vibrations*. in *Proceedings of EuroSteel 2008 Conference*. 2008.
20. Willford, M., P. Young, and C. Field, *Predicting footfall-induced vibration: Part 1.* Proceedings of the Institution of Civil Engineers-Structures and Buildings, 2007. **160**(2): p. 65-72.
21. Bachmann, H., *Vibration problems in structures: practical guidelines*. 1995: Springer Science & Business Media.
22. NBC-2015, *National Building Code of Canada 2015: Volume 2 – Commentaries (including Commentary A: Serviceability criteria for deflections and vibrations).* in *National Research Council of Canada.* 2015, Canadian Commission on Building and Fire Codes.: Ottawa, ON: .
23. Aalami, B.O., *Vibration design of concrete floors.* Redwood City: ADAPT Corporation, 2014.
24. Zhang, S. and L. Xu, *Human-induced vibration of cold-formed steel floor systems: Parametric studies.* Advances in Structural Engineering, 2020. **23**(10): p. 2030-2043.
25. Gonçalves, M.S., A. Pavic, and R.L. Pimentel, *Vibration serviceability assessment of office floors for realistic walking and floor layout scenarios: Literature review.* Advances in Structural Engineering, 2020. **23**(6): p. 1238-1255.
26. Kappos, A.J., *Dynamic loading and design of structures.* . 2001, London, UK: : Spon Press.

27. BS-6399, *Loading for buildings.*, in *BS 6399: Part 1: Code of practice for dead and imposed loads.* 1996, British Standards Institution.
28. NBC-1990, *National building code of Canada*. National Research Council Canada. Associate Committee on the National Building Code. 1990: Associate Committee on the National Building Code, National Research Council.
29. ISO-2631-2, *Evaluation of human exposure to whole-body vibration–Part 2: Human Exposure to continuous and shock-induced vibrations in buildings (1 to 80 Hz)*. 1989, International Standards Organization Geneva.
30. Chen, J., *Transient Analysis of stiffened panel structure by a finite strip-mode superposition method*, in *Advances in Steel Structures (ICASS'99)*. 1999, Elsevier. p. 839-847.
31. Abrate, S. *Transient response of beams, plates, and shells to impulsive loads*. in *ASME International Mechanical Engineering Congress and Exposition*. 2007.
32. Bebiano, R., D. Camotim, and N. Silvestre, *Dynamic analysis of thin-walled members using Generalised Beam Theory (GBT).* Thin-Walled Structures, 2013. **72**: p. 188-205.
33. Bebiano, R., et al., *Dynamic analysis of high-speed railway bridge decks using generalised beam theory.* Thin-Walled Structures, 2017. **114**: p. 22-31.
34. Ding, X., et al., *Time-domain solution for transient dynamic response of a large-diameter thin-walled pipe pile.* Earthquake Engineering and Engineering Vibration, 2015. **14**(2): p. 239-251.
35. Pagani, A., et al., *Dynamic response of aerospace structures by means of refined beam theories.* Aerospace Science and Technology, 2015. **46**: p. 360-373.
36. Zhang, S. and R. Schmidt, *Large rotation FE transient analysis of piezolaminated thin-walled smart structures.* Smart materials and structures, 2013. **22**(10): p. 105025.
37. Yuen, S. and G. Van Erp, *Transient analysis of thin-walled structures using macro spline finite elements.* Engineering structures, 1999. **21**(3): p. 255-266.
38. Xiang, T., et al., *Dynamic analysis of thin-walled open section beam under moving vehicle by transfer matrix method.* Structural Engineering and Mechanics, 2008. **30**(5): p. 603-617.
39. Hsiao, K.M., W.Y. Lin, and R.H. Chen. *Geometrically non-linear dynamic analysis of thin-walled beams*. in *Proc. World Congress Engrg., II*. 2009.

40. Tiso, P. *Optimal second order reduction basis selection for nonlinear transient analysis*. in *Modal Analysis Topics, Volume 3: Proceedings of the 29th IMAC, A Conference on Structural Dynamics, 2011*. 2011. Springer.
41. Carrera, E. and A. Varello, *Dynamic response of thin-walled structures by variable kinematic one-dimensional models.* Journal of Sound and Vibration, 2012. **331**(24): p. 5268-5282.
42. Bourihane, O., et al., *Dynamic analysis of a thin-walled beam with open cross section subjected to dynamic loads using a high-order implicit algorithm.* Engineering Structures, 2016. **120**: p. 133-146.
43. Sahraei, A., et al., *Finite element formulation for the dynamic analysis of shear deformable thin-walled beams.* Thin-Walled Structures, 2022. **173**: p. 108989.
44. Yang, Y., et al., *Internal instability of thin-walled beams under harmonic moving loads.* Thin-Walled Structures, 2022. **174**: p. 109123.
45. Yu, Y., et al., *Integrated Dynamic Analysis of Thin-Walled Beams: Coupled Bidirectional Bending, Torsion, and Axial Vibrations Under Axial Loads.* Applied Sciences, 2024. **14**(23): p. 11390.
46. Alenezi, A.M. and M. Mohareb, *Buckling solutions for compression members with end restraints defined along non-principal directions.* Journal of Constructional Steel Research, 2021. **181**: p. 106505.
47. Tahmasebi-Orimi, H., A. Sahraei, and M. Mohareb, *Natural vibration of axially loaded angle members with gusset plate end connections.* Journal of Constructional Steel Research, 2025. **235**: p. 109824.
48. Gjelsvik, A. and D. Hodges, *The theory of thin-walled bars.* Journal of Applied Mechanics, 1982. **49**(2): p. 468.
49. Bathe, K.J., *Finite element procedures*. 1996, Prentice Hall New Jersey.

Chapter 6: Summary, Conclusions, and Recommendations

6.1. Summary

Human walking induces time dependent forcing functions in the vertical and horizontal components. Such forces are represented as a combination of an impulse component due to sudden application of human weight of the structure and a series of harmonic forces with frequencies related to human walking step frequency. The present study presented an investigation of the dynamic response of thin-walled steel members subjected to human-induced forcing functions. The study focused firstly on natural frequency analysis, and subsequently on the transient dynamic response as applied to members with doubly symmetric I-sections and asymmetric angle sections. A variety of methodologies were employed; analytical solutions, energy-based approximate approaches, thin-walled beam finite element formulations, and shell-based modelling to characterize the natural frequency and acceleration responses.

The effect of span length, axial load level, and cross-sectional geometry on the natural frequencies of member with I-sections and angle cross-sections. Beyond these effects, the transient analysis also examined the effect of stationary and moving pedestrian load scenarios, highlighting the role of load position, step frequency, cross-sectional asymmetry, and the effect of higher harmonics on structural acceleration response.

A novel aspect of the research lies in its treatment of boundary conditions for asymmetric members. By formulating gusset end connections along non-principal axes, the study captured the additional fixity effects that differentiate these connections from classical pin-ended assumptions. This approach enabled a more realistic representation of the coupling between torsional and flexural modes in angle members. In the transient analysis, acceleration responses were quantified and

assessed against established human comfort thresholds. Collectively, these contributions advance the current understanding of pedestrian-induced vibrations in thin-walled members and provide design-oriented insights for establishing vibration control strategies to safeguard serviceability in thin-walled structures.

6.2. Conclusions

The main conclusions of the present study are:

1. Compressive loads reduce the natural frequency of members, underscoring the need for vibration control criteria in doubly symmetric I-sections to explicitly incorporate both member slenderness and axial force magnitude. While current standards impose more strict slenderness limits for compression members than for those in tension (implicitly recognizing the adverse effect of compressive forces) the findings of this study demonstrate that a more consistent dynamic criterion should explicitly account for both the magnitude of axial load and the cross-sectional properties of the member.
2. The natural frequency of angle members with gusset plate connections is considerably higher than that of the idealized pin-ended case. Consequently, treating gusset plate connections as pin-ended leads to overly conservative predictions of the natural frequency. The differences between both cases become more pronounced as the compressive axial force in the member increases.
3. In gusset plate connections, the eccentricity of the axial force introduced by the gusset reduces the natural frequency of compression members compared with the idealized case of concentric loading. This effect becomes more significant at higher axial force levels, diminishes as the compressive force decreases, and is negligible in tension members. For

angle members with unequal legs connected through the longer leg, the influence of axial force eccentricity is more pronounced than in members connected through the shorter leg.

4. Rotary inertia has a negligible effect on the lower natural frequencies of the member but becomes more noticeable in higher natural frequencies
5. The natural frequency for angle members with gusset plate connections are observed to be significantly higher than identical pin-ended members. Their natural frequency was shown to increase as leg ratio deviates from. In contrast, the effect of member slenderness on the natural frequency is minimal, and variations in the leg width-to-thickness ratio show no observable influence.
6. From the transient dynamic analysis of the members, it was observed that while pedestrian-induced forces produce displacements within typical serviceability thresholds, the corresponding accelerations exceeded perceptible comfort limits in several cases.
7. Among the five force components induced by pedestrian walking, the sudden footfall impact and the fourth harmonic component have the greatest influence on the induced acceleration levels.
8. Consistent with the natural frequency analysis, transient analysis shows that angle members with pinned-end connections exhibit larger displacements and accelerations than those with gusset-ended connections, owing to the greater flexibility of the pinned support condition. This effect is particularly evident in members under compressive forces and becomes more pronounced in members with longer spans.
9. In angle members, the vertical component of forces induced by human walking induce accelerations not only in the vertical direction but also in the horizontal direction due to coupling between the non-principal axes. This torsional–flexural coupling arises from both

inertial and axial force effects. While the inertial contribution is minor and produces negligible twist in members without axial load, the coupling effect associated with compressive axial forces becomes more pronounced, particularly at higher load levels.

10. The horizontal component of pedestrian-induced forces generates horizontal accelerations that exceed the vertical response in horizontally and torsionally unbraced I-section members. In contrast, angle members exhibit smaller horizontal accelerations relative to their vertical counterparts.
11. An increase in step frequency, while keeping the step length constant, leads to a significant rise in the induced acceleration levels. In contrast, variations in step length at a constant step frequency have negligible influence on the acceleration response.

6.3. Recommendation for Future work

1. The present study has conservatively omitted the beneficial effect of partial rotational fixity provided by gusset plates to the member ends about the axis parallel to the gusset. It is recommended to model this effect for typical gusset plate geometries to quantify the increase in natural frequency of gusset-ended members.
2. The present study has assumed that the axial force in the member remains constant throughout the vibration of the member. In some applications, the axial force may have a time dependent harmonic component, which would lead to parametric excitation. It is recommended to explore the stability of such systems by including geometric nonlinear effects in the dynamic analysis.
3. The effect of eccentric axial loads on the transient response of members with angle cross-sections deserves further consideration. Due to the inherent asymmetry and torsional–flexural coupling of these members, eccentric loading may amplify the dynamic response

4. and modify acceleration patterns beyond those predicted under concentric loading. Examining these effects would enhance the understanding of vibration behavior and support the development of more refined design guidelines.
5. The structural response can be further examined under the presence of multiple individuals, considering both synchronized activities and unsynchronized pedestrian walking on pathways and bridges. Such scenarios would provide a clearer understanding of group-induced vibrations and their impact on serviceability.
6. Beyond walking-induced forces, the structural response can also be assessed under other dynamic activities, such as rhythmic activities, dancing etc., which can impose higher forcing functions on structural members.
7. While the validity of the present formulation was assessed through comparisons with shell finite element predictions, it is recommended to conduct benchmark experimental studies to further assess the validity of the present solution.

Chapter 7: Appendices

Appendix A Analytical Solution for Flexural Natural Frequency of Axially loaded members with doubly symmetric cross-sections

The characteristic equation governing flexural vibration as presented in Eq. 2.4(b) is $EI_y\beta^4 + P\beta^2 - m\omega_y{}^2 = 0$. The four roots of this equation are given by

$$\beta^2 = \frac{-P \pm \sqrt{P^2 + 4EI_y m\omega_y^2}}{2EI_y}$$

$$\beta = \pm i\beta_1, \beta_2 \qquad \text{A.1}$$

$$\beta_1 = \sqrt{\frac{P}{2EI_y} + \sqrt{\left(\frac{P}{2EI_y}\right)^2 + \frac{m\omega_y^2}{2EI_y}}} \qquad \beta_2 = \sqrt{-\frac{P}{2EI_y} + \sqrt{\left(\frac{P}{2EI_y}\right)^2 + \frac{m\omega_y^2}{2EI_y}}}$$

and the corresponding solution of the equation of motion takes the form

$$V(x) = C_1 \sin(\beta_1 x) + C_2 \cos(\beta_1 x) + C_3 \sinh(\beta_2 x) + C_4 \cosh(\beta_2 x) \qquad \text{A.2}$$

where $C_1 - C_4$ are integration constants to be obtained from the boundary conditions.

$$V''(x) = -\beta_1{}^2 C_1 \sin(\beta_1 x) - \beta_1{}^2 C_2 \cos(\beta_1 x) + C_3\beta_2{}^2 \sinh(\beta_2 x) + C_4\beta_2{}^2 \cosh(\beta_2 x) \qquad \text{A.3}$$

By enforcing the boundary conditions $V(0) = V''(0) = 0$ at $x = 0$, one obtains

$$V(0) = C_2 + C_4 = 0$$
$$V''(0) = -\beta_1{}^2 C_2 + C_4\beta_2{}^2 = 0 \qquad \text{A.4(a-b)}$$

enforcing boundary conditions at $x = 0$ yields $C_2 = C_4 = 0$. Subsequently, by substituting the boundary conditions $V(l) = V''(l) = 0$ into Eq. A.3 leads to the matrix form, one obtains

$$\begin{bmatrix} \sin(\beta_1 l) & \sinh(\beta_2 l) \\ -\beta_1^2 \sin(\beta_1 l) & \beta_2^2 \sinh(\beta_2 l) \end{bmatrix} \begin{bmatrix} C_1 \\ C_3 \end{bmatrix} = 0 \quad \text{A.5}$$

By setting to zero the determinant of the matrix of coefficient in Eq. A.5, one obtains

$$\left(\beta_2^2 + \beta_1^2\right) \sin(\beta_1 l) \sinh(\beta_2 l) = 0 \quad \text{A.6}$$

The non-trivial solution is obtained from the condition $\sin(\beta_1 l) = 0$ yielding

$$\beta_1 = \frac{n\pi}{l} \quad \text{A.7}$$

By expanding the first partition of Eq. A.5 one obtains $C_3 \sinh(\beta_1 l) = 0$ i.e., $C_3 = 0$ and the corresponding mode shape is

$$V(x) = C_1 \sin(\beta_1 x) = C_1 \sin\left(\frac{n\pi x}{l}\right) \quad \text{A.8}$$

From Eq. A.7, by substituting into Eq. 2.6(c) and considering the first mode ($n = 1$), the expression for the flexural natural frequency about strong axis under axial load is given by

$$\omega_y = \sqrt{\frac{EI_y}{m}\left(\frac{n\pi}{l}\right)^4 - \frac{P}{m}\left(\frac{n\pi}{l}\right)^2} \quad \text{A.9}$$

By regrouping Eq. A.9 and defining the Euler buckling load about strong axis as $P_{E-y} = \pi^2 E A r_y^2 / l^2$, the natural frequency can be rearranged in normalized form as

$$\omega_y = \frac{\pi^2}{l}\sqrt{\frac{EA}{m}}\frac{\sqrt{\left(1 - P/P_{E-y}\right)}}{\left(l/r_y\right)^2} \quad \text{A.10}$$

By considering Euler buckling load about weak axis as $P_{E-z} = \pi^2 E A r_z^2 / l^2$ and expressing same procedure, the natural frequency about weak axis can be expressed as

$$\omega_z = \frac{\pi^2}{l}\sqrt{\frac{EA}{m}}\frac{\sqrt{\left(1 - P/P_{E-z}\right)}}{\left(l/r_z\right)^2} \qquad \text{A.11}$$

Appendix B Analytical Solution for Torsional Natural Frequency of Axially loaded members with doubly symmetric cross-sections

The characteristic equation for torsional vibration is given by

$$EI_\omega \lambda^4 - \left(GJ - P\frac{I_0}{A} - \rho I_\omega \omega_x^2 \right) \lambda^2 - \rho I_0 \omega_x^2 = 0 \qquad \text{B.1}$$

The four roots of the equation are given by

$$\begin{aligned}
\lambda^2 &= \frac{1}{2EI_\omega}\left(GJ - P\frac{I_0}{A} - \rho I_\omega \omega_x^2 \right) \pm \frac{1}{2EI_\omega}\sqrt{\left(GJ - P\frac{I_0}{A} - \rho I_\omega \omega_x^2 \right)^2 + 4\rho EI_\omega I_0 \omega_x^2} \\
\lambda &= \pm i\lambda_1, \lambda_2 \\
\lambda_1 &= \sqrt{\frac{1}{2EI_\omega}\left(GJ - P\frac{I_0}{A} - \rho I_\omega \omega_x^2 \right) + \frac{1}{2EI_\omega}\sqrt{\left(GJ - P\frac{I_0}{A} - \rho I_\omega \omega_x^2 \right)^2 + 4\rho EI_\omega I_0 \omega_x^2}} \\
\lambda_2 &= \sqrt{-\frac{1}{2EI_\omega}\left(GJ - P\frac{I_0}{A} - \rho I_\omega \omega_x^2 \right) + \frac{1}{2EI_\omega}\sqrt{\left(GJ - P\frac{I_0}{A} - \rho I_\omega \omega_x^2 \right)^2 + 4\rho EI_\omega I_0 \omega_x^2}}
\end{aligned} \qquad \text{B.2}$$

and the corresponding solution of the equation of motion takes the form

$$\phi(x) = B_1 \sin\lambda_1 x + B_2 \cos\lambda_1 x + B_3 \sinh\lambda_2 x + B_4 \cosh\lambda_2 x \qquad \text{B.3}$$

where $B_1 - B_4$ are integration constants to be obtained from the boundary conditions.

$$\phi''(x) = -B_1\lambda_1^2 \sin(\lambda_1 x) - B_2\lambda_1^2 \cos(\lambda_1 x) + B_3\lambda_2^2 \sinh(\lambda_2 x) + B_4\lambda_2^2 \cosh(\lambda_2 x) \qquad \text{B.4}$$

By enforcing the boundary conditions $\phi(0) = \phi''(0) = 0$ at $x = 0$, one obtains

$$\begin{aligned}
\phi(0) &= B_2 + B_4 = 0 \\
\phi''(0) &= -B_2\lambda_1^2 + B_4\lambda_2^2 = 0
\end{aligned} \qquad \text{B.5(a-b)}$$

enforcing boundary conditions at $x = 0$ yields $B_2 = B_4 = 0$. Subsequently, by substituting the boundary conditions $\phi(l) = \phi''(l) = 0$ into Eq. B.5 leads to the matrix form, one obtains

$$\begin{bmatrix} \sin(\lambda_1 l) & \sinh(\lambda_2 l) \\ -\lambda_1^2 \sin(\lambda_1 l) & \lambda_2^2 \sinh(\lambda_2 l) \end{bmatrix} \begin{bmatrix} B_1 \\ B_3 \end{bmatrix} = 0 \tag{B.6}$$

By setting to zero the determinant of the matrix of coefficient in Eq. B.6, one obtains

$$\left(\lambda_2^2 + \lambda_1^2\right) \sin(\lambda_1 l) \sinh(\lambda_2 l) = 0 \tag{B.7}$$

The non-trivial solution is obtained from $\sin(\lambda_1 l) = 0$ one obtains

$$\lambda_1 = \frac{n\pi}{l} \tag{B.8}$$

By expanding the first partition of Eq. B.6 one obtains $B_3 \sinh(\lambda_1 l) = 0$ i.e., $B_3 = 0$ and the corresponding mode shape is

$$\phi(x) = B_1 \sin(\lambda_1 x) = B_1 \sin\left(\frac{n\pi x}{l}\right) \tag{B.9}$$

From Eq. B.9, by substituting into Eq. 2.6(e) and considering the first mode ($n = 1$), the expression for the torsional natural frequency under axial load is given by

$$\omega_x = \sqrt{\frac{EI_\omega \left(\frac{n\pi}{l}\right)^2 + \left(GJ - P\frac{I_0}{A}\right)}{\rho\left(I_\omega + I_0\left(\frac{l}{n\pi}\right)^2\right)}} \tag{B.10}$$

By regrouping Eq. B.10 and defining the torsional Euler buckling load as $P_{E-x} = \left[EI_{\omega} \left(n\pi / l \right)^2 + GJ \right] \Big/ r_0^2$, the torsional natural frequency can be rearranged in normalized form as

$$\omega_x = \frac{\pi^2}{l} \sqrt{\frac{EA + \pi^2 \left(GJAl^2 / I_{\omega} \right)}{m\left(Ar_0^{\,4} / I_{\omega} \right)}} \sqrt{\frac{1 - P/P_{E-x}}{\pi^2 I_{\omega} / \left(Ar_0^{\,4} \right) + \left(l/r_0 \right)^2}} \qquad \text{B.11}$$

Appendix C Recovering longitudinal displacement expression based on the Vlasov kinematic Assumption

Under the Gjelsvik theory, the longitudinal displacement $u_A(x,s,t)$ for point $A[x,\bar{y}(s),\bar{z}(s)]$ located on contour is obtained from the zero-shear strain assumption at the mid-surface (Assumption (1.ii))

$$\gamma_A = \frac{\partial v_A}{\partial x} + \frac{\partial u_A}{\partial s} = 0 \tag{C.1}$$

By rearranging Eq. C.1, substituting for v_A from Eq. 4.2(a), and integrating both sides of the equation from an arbitrarily selected origin s_0 on the contour to the point of interest one obtains

$$\begin{aligned}
\int_{s_0}^{s} \frac{\partial u_A}{\partial s} ds &= -\int_{s_0}^{s} \frac{\partial}{\partial x}\left[\cos\alpha(s)\,v(x,t) + \sin\alpha(s)\,w(x,t) - r(s)\,\theta_x(x,t)\right] ds \\
&= -\int_{s_0}^{s} \left[\cos\alpha(s)\,v'(x,t) + \sin\alpha(s)\,w'(x,t) - r(s)\,\theta_x'(x,t)\right] ds \\
&= -\int_{y_0}^{\bar{y}} v'(x,t)\,dy - \int_{z_0}^{\bar{z}} w'(x,t)\,dz + \int_{\omega_0}^{\bar{\omega}} \theta_x'(x,t)\,d\omega \\
&= -v'(x,t)\int_{y_0}^{\bar{y}} dy - w'(x,t)\int_{z_0}^{\bar{z}} dz + \theta_x'(x,t)\int_{\omega_0}^{\bar{\omega}} d\omega
\end{aligned} \tag{C.2}$$

which yields

$$u_A(x,s,t) = u_p(x) - \bar{y}(s)\,v'(x,t) - \bar{z}(s)\,w'(x,t) + \bar{\omega}(s)\,\theta_x'(x,t) \tag{C.3}$$

in which $u_p(x,t) = v'(x,t)\,y_0 + w'(x,t)\,z_0 - \theta_x'(x,t)\,\omega_0$

Appendix D Expressing Internal Strain Energy in terms of displacements

Starting with the internal strain energy expression in Eq. 4.12, this appendix details the steps to express it in terms of the displacement fields. The internal strain energy U can be expressed as

$$U = U_1 - U_2 + U_3 - U_4 + U_5 + U_6$$
$$\left(U_1, U_2, U_3, U_4, U_5, U_6\right) = \frac{1}{2}\int_V \left[\sigma_{px}\varepsilon_x^B, -\sigma_{px}\varepsilon_{px}^B, \frac{1}{2}E\left(\varepsilon_x^B\right)^2, -E\varepsilon_x^B\varepsilon_{px}^B, G\left(\gamma_{xs}^B\right)^2, G\left(\gamma_{xn}^B\right)^2\right] dV \quad \text{D.1}$$

From Eq. 4.9(a), and recalling the definitions $C = \cos\alpha, S = \sin\alpha$ and $\psi = r + n$, one obtains can express the contribution U_1 as

$$U_1 = \frac{1}{2}\int_L\int_A \sigma_{px}\varepsilon_x^B \, dAdx = \frac{1}{2}\int_L\int_A \sigma_{px}\left\{u_p' - yv'' - zw'' + \omega\theta_x''\right.$$
$$\left. + \frac{1}{2}\left[\left(u_p' - yv'' - zw'' + \omega\theta_x''\right)^2 + \left(v'\cos\alpha + w'\sin\alpha - \left(r+n\right)\theta_x'\right)^2 + \left(-v'\sin\alpha + w'\cos\alpha + q\theta_x'\right)^2\right]\right\} dAdx \quad \text{D.2}$$

By expanding the bracketed terms and recalling Eqs. 4.3(a-b), one obtains

$$U_1 = \frac{1}{2}\int_L\int_A \sigma_{px}\left\{\left(u_p' - yv'' - zw'' + \omega\theta_x''\right) + \frac{1}{2}\left[u_p'^2 - 2yu_p'v'' - 2zu_p'w'' + 2\omega u_p'\theta_x'' + y^2v''^2\right.\right.$$
$$\left. + 2yzv''w'' - 2y\omega v''\theta_x'' + z^2w''^2 - 2z\omega w''\theta_x'' + \omega^2\theta_x''^2\right] + v'^2 + w'^2$$
$$\left. -2\left(\bar{z} + n\cos\alpha - z_r\right)v'\theta_x' + 2\left(\bar{y} - n\sin\alpha - y_r\right)w'\theta_x' + \left[q^2 + \left(r+n\right)^2\right]\theta_x'^2\right]\right\} dAdx \quad \text{D.3}$$

and substituting into Eq. D.3 yields

$$U_1 = \frac{1}{2}\int_L \int_A \sigma_{px} \left\{ u'_p - yv'' - zw'' + \omega\theta''_x + \frac{1}{2}\left[u'^2_p - 2yu'_p v'' - 2zu'_p w'' + 2\omega u'_p \theta''_x \right.\right.$$
$$+ y^2 v''^2 + 2yzv''w'' - 2y\omega v''\theta''_x + z^2 w''^2 - 2z\omega w''\theta''_x + \omega^2 \theta''^2_x$$
$$\left.\left. + v'^2 + w'^2 - 2(z - z_r)v'\theta'_x + 2(y - y_r)w'\theta'_x + \left[q^2 + (r+n)^2 \right]\theta'^2_x \right]\right\} dAdx$$

D.4

For small strains $\left(1 + 1/2\, u'_p\right) \approx 1$, performing the area integrals in Eq. D.4, and using the orthogonality conditions $\int_A ydA = \int_A zdA = \int_A \omega dA = \int_A y\omega dA = \int_A z\omega dA = 0$, and the relations $\left(\bar{y} - y_r\right) = q\cos\alpha - r\sin\alpha$ and $\left(\bar{z} - z_r\right) = q\sin\alpha + r\cos\alpha$ in , one obtains

$$U_1 = \frac{1}{2}\int_L \left[Pu'_p + \frac{1}{2}\left(\sigma_{px} I_z v''^2 + 2I_{yz} v''w'' + I_y w''^2 + I_\omega \theta''^2_x + Av'^2 \right.\right.$$
$$\left.\left. + Aw'^2 + 2z_r Av'\theta'_x - 2y_r Aw'\theta'_x + I_p \theta'^2_x \right)\right] dx \qquad \text{D.5}$$

in which the sectional properties $\left(A, I_z, I_y, I_{yz}, I_\omega, I_p\right) = \int_A \left[1, y^2, z^2, yz, \omega^2, q^2 + (r+n)^2\right] dA$ have been defined. From Eq. 4.8(a), and evoking again the small strain approximation $\left(1 + 1/2\, u'_p\right) \approx 1$, the second term in Eq. D.1 yields

$$U_2 = \frac{1}{2}\int_V \sigma_{px}\varepsilon^B_{px} dV = \frac{1}{2}\int_L \int_A \sigma_{px}\left(u'_p + \frac{1}{2}u'^2_p \right) dAdx = \frac{1}{2}\int_L \int_A \sigma_p u'_p dAdx = \frac{1}{2}P\int_L u'_p dx \qquad \text{D.6}$$

From Eq. 4.9, by substituting into the third term of Eq. D.1, one obtains

$$U_3 = \frac{E}{2}\int_l \int_A \left\{ \left(u'_p - yv'' - zw'' + \omega\theta'' \right) + \frac{1}{2}\left[\left(u'_p - yv'' - zw'' + \omega\theta''_x \right)^2 + \left(Cv' + Sw' - \psi\theta'_x \right)^2 \right.\right.$$
$$\left.\left. + \left(-v'\sin\alpha + w'\cos\alpha + q\theta'_x \right)^2 \right]\right\} dAdx \qquad \text{D.7}$$

By expanding brackets and considering cross-sections consisting of with straight segments, i.e., $C = \cos\alpha, S = \sin\alpha$ and $\psi = r + n$, one obtains

$$U_3 = \frac{1}{2}\int_l\int_A E\left\{u_p' - yv'' - zw'' + \omega\theta_x'' + \frac{1}{2}\left[u_p'^2 - 2yu_p'v'' - 2zu_p'w'' + 2\omega u_p'\theta_x'' + y^2v''^2 \right.\right.$$
$$+ 2yzv''w'' - 2y\omega v''\theta_x'' + z^2w''^2 - 2z\omega w''\theta_x'' + \omega^2\theta_x''^2 + v'^2 + w_x'^2$$
$$\left.\left. - 2\left[q\sin\alpha + (r+n)\cos\alpha\right]v'\theta' + 2\left[q\cos\alpha - (r+n)\sin\alpha\right]w'\theta_x' + \left[q^2 + (r+n)^2\right]\theta_x'^2\right]\right\}^2 dAdx$$

D.8

From Eq. 4.3, recalling that $(\bar{y} - y_r) = q\cos\alpha - r\sin\alpha$ and $(\bar{z} - z_r) = q\sin\alpha + r\cos\alpha$, and substituting into Eq. D.8 one obtains

$$U_3 = \frac{1}{2}\int_l\int_A E\left\{u_p' - yv'' - zw'' + \omega\theta_x'' + \frac{1}{2}\left[u_p'^2 - 2yu_p'v'' - 2zu_p'w'' + 2\omega u_p'\theta_x'' + y^2v_x''^2 \right.\right.$$
$$+ 2yzv''w'' - 2y\omega v''\theta'' + z^2w''^2 - 2z\omega w''\theta_x'' + \omega^2\theta_x''^2 + v'^2 + w'^2$$
$$\left.\left. -2(\bar{z} + n\cos\alpha - z_r)v'\theta_x' + 2(\bar{y} - n\sin\alpha - y_r)w'\theta_x' + \left[q^2 + (r+n)^2\right]\theta_x'^2\right]\right\}^2 dAdx$$

D.9

Recalling the identities $y = \bar{y} - n\sin\alpha$, $z = \bar{z} + n\cos\alpha$, and substituting into Eq. D.9, yields

$$U_3 = \frac{1}{2}\int_l\int_A E\left\{u_p' - yv'' - zw'' + \omega\theta_x'' + \frac{1}{2}\left[u_p'^2 - 2yu_p'v'' - 2zu_p'w'' + 2\omega u_p'\theta_x'' + y^2v''^2 \right.\right.$$
$$+ 2yzv''w'' - 2y\omega v''\theta_x'' + z^2w''^2 - 2z\omega w''\theta_x'' + \omega^2\theta_x''^2 + v'^2 + w'^2 \qquad \text{D.10}$$
$$\left.\left. -2(z - z_r)v'\theta_x' + 2(y - y_r)w'\theta_x' + \left[q^2 + (r+n)^2\right]\theta_x'^2\right]\right\}^2 dAdx$$

By expanding, retaining only second order terms, considering the longitudinal strain (u_p') to be small, performing the area integrals, and employing the orthogonality conditions, Eq. D.10 yields

$$U_3 = \frac{1}{2}\int_l\int_A E\left\{\left(3u_p'+1\right)y^2v''^2+\left(3u_p'+1\right)z^2w''^2+\left(3u_p'+1\right)\omega^2\theta_x''^2+u_p'v'^2+u_p'w'^2+2\left(3u_p'+1\right)yzv''w''\right.$$
$$\left.+2\left(u_p'z_r\right)v'\theta_x'-2u_p'y_rw'\theta_x'+u_p'\left(q^2+\left(r+n\right)^2\right)\theta_x'^2\right\}dAdx$$
$$\approx \frac{1}{2}\int_l\left[EI_zv''^2+EI_yw''^2+EI_\omega\theta_x''^2+2EI_{yz}v''w''+P\left(v'^2+w'^2+2z_rv'\theta_x'-2y_rw'\theta_x'+\frac{I_p}{A}\theta_x'^2\right)\right]dx$$

D.11

From Eq. 4.8(a) and Eq. 4.9, by substituting into the fourth term of Eq. D.1, one obtains

$$U_4 = \frac{1}{2}\int_l\int_A E\left\{\left(u_p'-yv''-zw''+\omega\theta_x''\right)+\frac{1}{2}\left[\left(u_p'-yv''-zw''+\omega\theta_x''\right)^2+\left(Cv'+Sw'-\psi\theta_x'\right)^2\right.\right.$$
$$\left.\left.+\left(-v'\sin\alpha+w'\cos\alpha+q\theta_x'\right)^2\right]\right\}\left(u_p'+\frac{1}{2}u_p'^2\right)dAdx \qquad \text{D.12}$$

Expanding brackets in Eq. D.12, considering the section to consist of straight segments, i.e., $C=\cos\alpha, S=\sin\alpha$ and $\psi = r+n$, and adopting the small strain approximation $u_p'+u_p'^2/2 \approx u_p'$ yields

$$U_4 = \frac{1}{2}\int_l\int_A E\left\{u_p'-yv''-zw''+\omega\theta_x''+\frac{1}{2}\left[u_p'^2-2yu_p'v''-2zu_p'w''+2\omega u_p'\theta_x''+y^2v''^2+z^2w''^2\right.\right.$$
$$+2yzv''w''-2y\omega v''\theta_x''-2z\omega w''\theta_x''+\omega^2\theta_x''^2+v'^2+w'^2-2\left[q\sin\alpha+(r+n)\cos\alpha\right]v'\theta_x'$$
$$\left.\left.+2\left[q\cos\alpha-\left(r+n\right)\sin\alpha\right]w'\theta_x'+\left[q^2+\left(r+n\right)^2\right]\theta_x'^2\right]\right\}u_p'dAdx$$

D.13

From Eq. 4.3, recalling that $\left(\bar{y}-y_r\right)=q\cos\alpha-r\sin\alpha$ and $\left(\bar{z}-z_r\right)=q\sin\alpha+r\cos\alpha$, and substituting into Eq. D.13, one obtains

$$U_4 = \frac{1}{2}\int_l\int_A E\Big\{u_p' - yv'' - zw'' + \omega\theta_x'' + \frac{1}{2}\Big[u_p'^2 - 2yu_p'v'' - 2zu_p'w'' + 2\omega u_p'\theta_x'' + y^2v''^2 + 2yzv''w'' - 2y\omega v''\theta_x'' + z^2w''^2 - 2z\omega w''\theta_x'' + \omega^2\theta_x''^2 + v'^2 + w'^2 - 2\big[\bar{z} + n\cos\alpha - z_r\big]v'\theta_x' + 2\big[\bar{y} - n\sin\alpha - y_r\big]w'\theta_x' + \Big[q^2 + (r+n)^2\Big]\theta_x'^2\Big\}u_p'dAdx$$

D.14

From $y(s,n) = \bar{y}(s) + \bar{\bar{y}}(s,n)$, $z(s,n) = \bar{z}(s) + \bar{\bar{z}}(s,n)$, and recalling that $y = \bar{y} - n\sin\alpha$ and $z = \bar{z} + n\cos\alpha$, and substituting into Eq. D.14 yields

$$U_4 = \frac{1}{2}\int_l\int_A E\Big\{u_p' - yv'' - zw'' + \omega\theta_x'' + \frac{1}{2}\Big[u_p'^2 - 2yu_p'v'' - 2zu_p'w'' + 2\omega u_p'\theta_x'' + y^2v''^2 + 2yzv''w'' - 2y\omega v''\theta_x'' + z^2w''^2 - 2z\omega w''\theta_x'' + \omega^2\theta_x''^2 + v'^2 + w'^2 - 2(z - z_r)v'\theta_x' + 2(y - y_r)w'\theta_x' + \Big[q^2 + (r+n)^2\Big]\theta_x'^2\Big]\Big\}\Big\{u_p' + \frac{1}{2}u_p'^2\Big\}dAdx \quad \text{D.15}$$

By performing the area integrals in Eq. D.15, and employing the orthogonality conditions, one obtains

$$\begin{aligned} U_4 &= \frac{1}{2}\int_l\int_A E\frac{1}{2}\Big\{u_p'y^2v''^2 + 2u_p'yzv''w'' + u_pz^2w_x''^2 + u_p'\omega^2\theta_x''^2 + u_p'v'^2 + u_p'w'^2 \\ &\qquad + 2u_p'z_rv'\theta_x' - 2u_p'y_rw'\theta_x' + u_p'\left(q^2 + (r+n)^2\right)\theta_x'^2\Big\}dAdx \qquad \text{D.16} \\ &= \frac{1}{4}\int_l P\left\{\frac{I_z}{A}v''^2 + 2\frac{I_{yz}}{A}v''w'' + \frac{I_y}{A}w_x''^2 + \frac{I_\omega}{A}\theta_x''^2 + v'^2 + w'^2 + 2z_rv'\theta_x' - 2y_rw'\theta_x' + \frac{I_p}{A}\theta_x'^2\right\}dx \end{aligned}$$

in which $I_p = \int_A\Big[q^2 + (r+n)^2\Big]dA$ is the polar moment of inertia about the shear centre. From Eq. 4.9, by substituting into the fifth term of Eq. D.1 one obtains

$$U_5 = \frac{1}{2}\int_l\int_A G\left(\gamma_{xs}^B\right)^2 dAdx = \frac{1}{2}\int_l\int_A G\left[\left(-\frac{\partial y}{\partial s}v' - \frac{\partial z}{\partial s}w' + \frac{\partial \omega}{\partial s}\theta_x' + Cv' + Sw' - \psi\theta_x'\right)\right.$$
$$+\left(u_p' - yv'' - zw'' + \omega\theta_x''\right)\left(-\frac{\partial y}{\partial s}v' - \frac{\partial z}{\partial s}w' + \frac{\partial \omega}{\partial s}\theta_x'\right) + \left(Cv' + Sw' - \psi\theta_x'\right)\left(\frac{\partial C}{\partial s}v + \frac{\partial S}{\partial s}w - \frac{\partial \psi}{\partial s}\theta_x\right)$$
$$\left.+\left(-v'\sin\alpha + w'\cos\alpha + q\theta_x'\right)\left(-\frac{\partial \alpha}{\partial s}v\cos\alpha - \frac{\partial \alpha}{\partial s}w\sin\alpha + \frac{\partial q}{\partial s}\theta_x\right)\right]dAdx$$

D.17

From $y(s,n) = \bar{y}(s) + \bar{\bar{y}}(s,n)$, $z(s,n) = \bar{z}(s) + \bar{\bar{z}}(s,n)$, and recalling that $y = \bar{y} - n\sin\alpha$ and $z = \bar{z} + n\cos\alpha$, and the identities $C = \cos\alpha, S = \sin\alpha$, $\psi = r + n$, $\partial\bar{y}/\partial s = \cos\alpha$, $\partial\bar{z}/\partial s = \sin\alpha$, by substituting into Eq. D.17, one obtains

$$U_5 = \frac{G}{2}\int_l\int_A\left\{\left[-\left(1 - n\frac{\partial \alpha}{\partial s}\right)v'\cos\alpha - \left(1 - n\frac{\partial \alpha}{\partial s}\right)w'\sin\alpha + \left(r - n\left(1 - \frac{\partial \alpha}{\partial s}(\bar{y} - y_r)\sin\alpha\right.\right.\right.\right.$$
$$\left.\left.\left.\left.+\left(\frac{\partial \alpha}{\partial s}(\bar{z} - z_r)\cos\alpha\right)\right)\theta_x' + v'\cos\alpha + w'\sin\alpha - (r+n)\theta_x'\right]\right.$$
$$+\left[\left(u_p' - yv'' - zw'' + \omega\theta_x''\right)\left(-\left(1 - n\frac{\partial \alpha}{\partial s}\right)v'\cos\alpha - \left(1 - n\frac{\partial \alpha}{\partial s}\right)w'\sin\alpha\right.\right.$$
$$\left.\left.+\left(r - n\left(1 - \frac{\partial \alpha}{\partial s}(\bar{y} - y_r)\sin\alpha + \frac{\partial \alpha}{\partial s}(\bar{z} - z_r)\cos\alpha\right)\right)\theta_x'\right)\right]$$
$$+\left[\left(v'\cos\alpha + w'\sin\alpha - (r+n)\theta_x'\right)\left(-\frac{\partial \alpha}{\partial s}v\sin\alpha + \frac{\partial \alpha}{\partial s}w\cos\alpha\right.\right.$$
$$\left.\left.-\left(-\frac{\partial \alpha}{\partial s}(\bar{y} - y_r)\cos\alpha - \frac{\partial \alpha}{\partial s}(\bar{z} - z_r)\sin\alpha\right)\theta_x\right)\right]$$
$$+\left[\left(-v'\sin\alpha + w'\cos\alpha + \left((\bar{y} - y_r)\cos\alpha + (\bar{z} - z_r)\sin\alpha\right)\theta_x'\right)\right.$$
$$\left.\left.\left(-\frac{\partial \alpha}{\partial s}v\cos\alpha - \frac{\partial \alpha}{\partial s}w\sin\alpha + \left(1 - \frac{\partial \alpha}{\partial s}(\bar{y} - y_r)\sin\alpha + \frac{\partial \alpha}{\partial s}(\bar{z} - z_r)\cos\alpha\right)\theta_x\right)\right]\right\}^2 dAdx$$

D.18

For a section consisting of straight segments, one has $\partial\alpha/\partial s = 0$ and Eq. D.18 simplifies to

$$U_5 = \frac{1}{2}\int_l\int_A G\Big\{\big(-v'\cos\alpha - w'\sin\alpha + (r-n)\theta_x' + v'\cos\alpha + w'\sin\alpha - (r+n)\theta_x'\big)$$
$$+\big(u_p' - yv'' - zw'' + \omega\theta_x''\big)\big(-v'\cos\alpha - w'\sin\alpha + (r-n)\theta_x'\big)$$
$$+\big(-v'\sin\alpha + w'\cos\alpha + \big((\overline{y}-y_r)\cos\alpha + (\overline{z}-z_r)\sin\alpha\big)\theta_x'\big)(\theta_x)\Big\}^2\, dAdx$$
$$= \frac{1}{2}G\int_l\int_A\Big\{-2n\theta_x' - u_p'v'\cos\alpha - u_p'w'\sin\alpha + u_p'(r-n)\theta_x' + yv'v''\cos\alpha + yv''w'\sin\alpha$$
$$-y(r-n)v''\theta_x' + zv'w''\cos\alpha + zw'w''\sin\alpha - z(r-n)w''\theta_x' - \omega v'\theta_x''\cos\alpha - \omega w'\theta_x''\sin\alpha$$
$$+\omega(r-n)\theta_x'\theta_x'' - v'\theta_x\sin\alpha + w'\theta_x\cos\alpha + \big((\overline{y}-y_r)\cos\alpha + (\overline{z}-z_r)\sin\alpha\big)\theta_x\theta_x'\Big\}^2\, dAdx$$

D.19

By retaining only second order terms and considering recalling the small strain assumption $(u_p' + 1/2u_p'^2 \approx u_p')$ performing the area integrals. and evoking the orthogonality conditions, Eq. D.19 yields

$$U_5 = \frac{G}{2}\int_l\int_A\Big[-2n\theta_x' - u_p'\cos(\alpha)v' - u_p'\sin(\alpha)w' + u_p'(r-n)\theta_x'\Big]^2 dAdx$$
$$= \frac{G}{2}\int_l\int_A\Big[4n^2\theta_x'^2 + 2nu_p'\cos(\alpha)v'\theta_x' + 2nu_p'\sin(\alpha)w'\theta_x' - 2nu_p'(r-n)\theta_x'^2 + 2nu_p'\cos(\alpha)v'\theta_x'$$
$$+u_p'^2\cos^2(\alpha)v'^2 + u_p'^2\cos(\alpha)\sin(\alpha)v'w' - u_p'^2(r-n)\cos(\alpha)v'\theta_x' + 2nu_p'\sin(\alpha)w'\theta_x'$$
$$+u_p'^2\cos(\alpha)\sin(\alpha)v'w' + u_p'^2\sin^2(\alpha)w'^2 - u_p'^2(r-n)\sin(\alpha)w'\theta_x' - 2nu_p'(r-n)\theta_x'^2$$
$$-u_p'^2(r-n)\cos(\alpha)v'\theta_x' - u_p'^2(r-n)\sin(\alpha)w'\theta_x' + u_p'^2(r-n)^2\theta_x'^2\Big]dAdx$$

D.20

By omitting terms involving $u_p'^2$ are omitted under the assumption of infinitesimal pre-buckling longitudinal strains, one obtains

$$
\begin{aligned}
U_5 &= \frac{G}{2}\int_l\int_A \left\{4n^2\theta_x'^2 + 4nu_p'\cos(\alpha)v'\theta_x' + 4nu_p'\sin(\alpha)w'\theta_x' - 4nu_p'(r-n)\theta_x'^2\right\}dAdx \\
&= \frac{G}{2}\int_l\int_A 4\left\{\left(n^2 - u_p'rn + u_p'n^2\right)\theta_x'^2 + n\cos\alpha u_p'v'\theta_x' + n\sin\alpha u_p'w'\theta_x'\right\}dAdx \\
&\approx \frac{G}{2}\int_l\int_A 4\left\{n^2\theta_x'^2 - u_p'rn\theta_x'^2 + n\cos\alpha u_p'v'\theta_x' + n\sin\alpha u_p'w'\theta_x'\right\}dAdx \qquad \text{D.21} \\
&\approx \frac{G}{2}\int_l\int_A 4n^2\theta_x'^2 dAdx + 2G\int_l u_p'\int_A -rn\theta_x'^2 + n\cos\alpha v'\theta_x' + n\sin\alpha w'\theta' dAdx \\
&\approx \frac{G}{2}\int_l \theta_x'^2 dx\int_s ds\int_n 4n^2 dn = 4G\frac{sn^3}{3}\int_l \theta_x'^2 dx = \frac{1}{2}GJ\int_l \theta_x'^2 dx
\end{aligned}
$$

From Eq. 4.9(c), by substituting into the sixth term of Eq. D.1, one obtains

$$
\begin{aligned}
U_6 = \frac{G}{2}\int_l\int_A \Bigg[&\left(-\frac{\partial y}{\partial n}v' - \frac{\partial z}{\partial n}w' + \frac{\partial \omega}{\partial n}\theta_x' - v'\sin\alpha + w'\cos\alpha + q\theta_x'\right) \\
&+ \left(u_p' - yv'' - zw'' + \omega\theta_x''\right)\left(-\frac{\partial y}{\partial n}v' - \frac{\partial z}{\partial n}w' + \frac{\partial \omega}{\partial n}\theta_x'\right) \qquad \text{D.22} \\
&+ \left(Cv' + Sw' - \psi\theta_x'\right)\left(\frac{\partial C}{\partial n}v + \frac{\partial S}{\partial n}w - \frac{\partial \psi}{\partial n}\theta_x\right)\Bigg] dAdx
\end{aligned}
$$

From $y(s,n) = \bar{y}(s) + \bar{\bar{y}}(s,n)$, $z(s,n) = \bar{z}(s) + \bar{\bar{z}}(s,n)$, and recalling that $y = \bar{y} - n\sin\alpha$ and $z = \bar{z} + n\cos\alpha$, and the identities $C = \cos\alpha, S = \sin\alpha$, $\psi = r + n$, $\partial\bar{y}/\partial s = \cos\alpha$, $\partial\bar{z}/\partial s = \sin\alpha$, by substituting into Eq. D.22, one obtains

$$
\begin{aligned}
U_6 = \frac{G}{2}\int_l\int_A \Big[&\left(v'\sin\alpha - w'\cos\alpha - q\theta_x' - v'\sin\alpha + \cos\alpha w' + q\theta_x'\right) \\
&+ \left(u_p' - yv'' - zw'' + \omega\theta_x''\right)\left(v'\sin\alpha - w'\cos\alpha - q\theta_x'\right) \qquad \text{D.23} \\
&+ \left(v'\cos\alpha + w'\sin\alpha - (r+n)\theta_x'\right)\left(-\theta_x\right)\Big]^2 dAdx
\end{aligned}
$$

By grouping like terms, Eq. D.23 yields

$$U_6 = \frac{1}{2} G \int_l \int_A \Big[u_p' v' \sin\alpha - u_p' w' \cos\alpha - u_p' q \theta_x' - y v' v'' \sin\alpha + y v'' w' \cos\alpha + y q v'' \theta_x' - z v' w'' \sin\alpha + z w' w'' \cos\alpha + z q w'' \theta' + \omega v' \theta_x'' \sin\alpha - \omega w' \theta_x'' \cos\alpha - \omega q \theta_x' \theta_x'' - v' \theta_x \cos\alpha - w' \theta_x \sin\alpha + (r+n) \theta_x \theta_x' \Big]^2 dA dx \quad \text{D.24}$$

Retaining only second order terms yields and considering that the longitudinal strain due to axial load is small, one obtains

$$U_6 = \frac{G}{2} \int_l \int_A u_p'^2 \left(v' \cos\alpha + w' \sin\alpha + q \theta_x' \right)^2 dA dx \approx 0 \quad \text{D.25}$$

In summary, the total internal strain energy is obtained by substituting Eq. D.5, D.6, D.11, D.16, and Eq. D.21 into Eq. D.1 yielding

$$U = \frac{1}{2} \int_l EI_z v''^2 + EI_y w''^2 + EI_\omega \theta_x''^2 + GJ \theta_x'^2 + 2EI_{yz} v'' w'' + P \left(v'^2 + w'^2 + \frac{I_p}{A} GJ \theta_x'^2 + 2 z_r v' \theta' - 2 y_r w' \theta_x' \right) dx \quad \text{D.26}$$

By taking the variation of the internal strain as given in Eq. D.26, one obtains

$$\int_{t_1}^{t_2} \delta U dt = \int_{t_1}^{t_2} \int_l \Big[EI_z v'' \delta v'' + EI_y w'' \delta w'' + EI_\omega \theta_x'' \delta \theta_x'' + GJ \theta_x' \delta \theta_x' + EI_{yz} v'' \delta w'' + EI_{yz} w'' \delta v'' + P \left(v' \delta v' + w' \delta w' + \frac{I_p}{A} \theta_x' \delta \theta_x' + z_r \theta_x' \delta v' + z_r v' \delta \theta_x' - y_r \theta_x' \delta w' - y_r w' \delta \theta_x' \right) \Big] dx dt \quad \text{D.27}$$

Appendix E Physical Significance of the Sectional Property I_p

This appendix shows that the sectional property $I_p = \int_A \left[q^2 + \left(r + n \right)^2 \right] dA$ arising in Eq. 4.13 is the polar moment of inertia about the shear centre. The polar moment of inertia I_p^* about the shear centre is given by

$$\begin{aligned} I_p^* &= I_z + I_y + A y_r^2 + A z_r^2 \\ &= \int_A \left(y^2 + z^2 + y_r^2 + z_r^2 \right) dA \\ &= \int_A \left(y^2 + z^2 + y_r^2 + z_r^2 \right) dA \\ &= \int_A \left\{ \left[\overline{y}(s) + \overline{\overline{y}}(s,n) \right]^2 + \left[\overline{z}(s) + \overline{\overline{z}}(s,n) \right]^2 + y_r^2 + z_r^2 \right\} dA \\ &= \int_A \left\{ \left[\overline{y}(s) - n \sin\alpha(s) \right]^2 + \left[\overline{z}(s) + n \cos\alpha(s) \right]^2 + y_r^2 + z_r^2 \right\} dA \\ &= \int_A \left[\left(\overline{y}^2 + n^2 \sin^2\alpha \right) + \left(\overline{z}^2 + n^2 \cos^2\alpha \right) + y_r^2 + z_r^2 \right] dA \\ &= \int_A \left(\overline{y}^2 + \overline{z}^2 + y_r^2 + z_r^2 + n^2 \right) dA \end{aligned} \qquad \text{E.1}$$

Now, consider the sectional property

$$I_p = \int_A \left[q^2 + \left(r + n \right)^2 \right] dA \qquad \text{E.2}$$

From Eq. 4.3, by substituting into Eq. E.2, one obtains

$$I_p = \int_A \left(\left[\left(\overline{y} - y_r \right) \cos\alpha + \left(\overline{z} - z_r \right) \sin\alpha \right]^2 + \left[-\left(\overline{y} - y_r \right) \sin\alpha + \left(\overline{z} - z_r \right) \cos\alpha \right]^2 + 2nr + n^2 \right) dnds \qquad \text{E.3}$$

By expanding brackets and grouping like terms, one obtains

$$I_p = \int_A \left[\left(\overline{y} - y_r \right)^2 + \left(\overline{z} - z_r \right)^2 + \underline{2nr} + n^2 \right] dnds \qquad \text{E.4}$$

The area integral of the underlined term vanishes, i.e.,

$$I_p = \int_A \left[\left(\bar{y} - y_r \right)^2 + \left(\bar{z} - z_r \right)^2 + n^2 \right] dnds \qquad \text{E.5}$$

By expanding the brackets, one obtains

$$I_p = \int_A \left(\bar{y}^2 - \underline{2 y_r \bar{y}} + {y_r}^2 + \bar{z}^2 - \underline{2 z_r \bar{z}} + {z_r}^2 + n^2 \right) dnds \qquad \text{E.6}$$

Again, the area integrals of the underlined term vanish, and one recovers the right-hand side of Eq. E.1

$$I_p = \int_A \left(\bar{y}^2 + {y_r}^2 + \bar{z}^2 + {z_r}^2 + n^2 \right) dnds = I_p^* \qquad \text{E.7}$$

Appendix F Expressing Kinetic Energy in terms of Displacements

One recalls that the kinetic energy is given by

$$T = \sum_{i=1}^{3} T_i$$
$$\left(T_1, T_2, T_3\right) = \frac{1}{2}\rho\int_0^l\int_A\left[\left(\partial u_B/\partial t\right)^2, \left(\partial v_B/\partial t\right)^2, \left(\partial w_B/\partial t\right)^2\right]dAdx \qquad \text{F.1(a-d)}$$

From Eq. 4.5(a-c), by substituting into Eqs. F.1(b-d) and expanding, one obtains

$$T_1 = \frac{1}{2}\rho\int_0^l\int_A\left(y^2\dot{v}'^2 + 2yz\dot{v}'\dot{w}' + z^2\dot{w}'^2 + \omega^2\dot{\theta}_x'^2\right)dAdx$$
$$T_2 = \frac{1}{2}\rho\int_0^l\int_A\left[\dot{v}^2\cos^2\alpha + 2\dot{v}\dot{w}\cos\alpha\sin\alpha - 2\left(r+n\right)\dot{v}\dot{\theta}_x\cos\alpha + \dot{w}^2\sin^2\alpha\right.$$
$$\left. -2\left(r+n\right)\dot{w}\dot{\theta}_x\sin\alpha + \left(r+n\right)^2\dot{\theta}_x^{\,2}\right]dAdx$$
$$T_3 = \frac{1}{2}\rho\int_0^l\int_A\left(\dot{v}^2\sin^2\alpha - 2\dot{v}\dot{w}\sin\alpha\cos\alpha - 2q\dot{v}\dot{\theta}_x\sin\alpha + \dot{w}^2\cos^2\alpha + 2q\dot{w}\dot{\theta}_x\cos\alpha + q^2\dot{\theta}_x^{\,2}\right)dAdx$$

F.2(a-c)

By performing the area integrals in Eq. F.2(a), and using the orthogonality conditions $\int_A ydA = \int_A zdA = \int_A \omega dA = \int_A z\omega dA = \int_A y\omega dA = 0$, one obtains

$$T_1 = \frac{1}{2}\rho\int_0^l\left(I_z\dot{v}_x'^2 + I_y\dot{w}'^2 + I_\omega\dot{\theta}_x'^2 + 2I_{yz}\dot{v}'\dot{w}'\right)dx \qquad \text{F.3}$$

$$\int_{t_1}^{t_2}\delta T_1 dt = \int_{t_1}^{t_2}\int_0^l\rho\left(I_z\dot{v}'\delta\dot{v}' + I_y\dot{w}'\delta\dot{w}' + I_\omega\dot{\theta}_x'\delta\dot{\theta}_x' + I_{yz}\dot{v}'\delta\dot{w}' + I_{yz}\dot{w}'\delta\dot{v}'\right)dxdt \qquad \text{F.4}$$

By performing integration by parts with respect to time, and noting that t_1 and t_2 are arbitrary, one obtains

$$\begin{aligned}\int_{t_1}^{t_2}\delta T_1 dt &= \left[\int_0^l \rho\left(I_z\dot{v}'\delta v' + I_y\dot{w}'\delta w' + I_\omega\dot{\theta}_x'\delta\theta_x' + I_{yz}\dot{v}'\delta w' + I_{yz}\dot{w}'\delta v'\right)dx\right]_{t_1}^{t_2} \\ &\quad -\int_{t_1}^{t_2}\int_0^l \rho\left(I_z\ddot{v}'\delta v' + I_y\ddot{w}'\delta w' + I_\omega\ddot{\theta}_x'\delta\theta_x' + I_{yz}\ddot{v}'\delta w' + I_{yz}\ddot{w}'\delta v'\right)dxdt \\ &= -\int_{t_1}^{t_2}\int_0^l \rho\left(I_z\ddot{v}'\delta v' + I_y\ddot{w}'\delta w' + I_\omega\ddot{\theta}_x'\delta\theta_x' + I_{yz}\ddot{v}'\delta w' + I_{yz}\ddot{w}'\delta v'\right)dxdt\end{aligned} \quad \text{F.5}$$

By performing integration by parts with respect to $\int_{t_1}^{t_2}\delta T_1 dt = \int_{t_1}^{t_2}\int_0^l \rho\left(I_z\dot{v}'\delta v' + I_y\dot{w}'\delta w' + I_\omega\dot{\theta}_x'\delta\theta_x' + I_{yz}\dot{v}'\delta w' + I_{yz}\dot{w}'\delta v'\right)dxdt$, grouping like-terms, one obtains

$$\begin{aligned}\int_{t_1}^{t_2}\delta T_1 dt &= -\left[\int_{t_1}^{t_2}\rho\left(I_z\ddot{v}'\delta v + I_y\ddot{w}'\delta w + I_\omega\ddot{\theta}_x'\delta\theta_x + I_{yz}\ddot{v}'\delta w + I_{yz}\ddot{w}'\delta v\right)dt\right]_0^l \\ &\quad +\int_{t_1}^{t_2}\int_0^l \rho\left(I_z\ddot{v}''\delta v + I_y\ddot{w}''\delta w + I_\omega\ddot{\theta}_x''\delta\theta_x + I_{yz}\ddot{v}''\delta w + I_{yz}\ddot{w}''\delta v\right)dxdt\end{aligned} \quad \text{F.6}$$

By taking the variation of Eq. F.2(b), with respect to the argument functions, one obtains

$$\begin{aligned}\int_{t_1}^{t_2}\delta T_2 dt = \rho\int_{t_1}^{t_2}\int_0^l\int_A \Big\{&\dot{v}\delta\dot{v}\cos^2\alpha + \dot{w}\delta\dot{v}\cos\alpha\sin\alpha + \dot{v}\delta\dot{w}\cos\alpha\sin\alpha - (r+n)\dot{\theta}_x\delta\dot{v}\cos\alpha \\ &-(r+n)\dot{v}\delta\dot{\theta}_x\cos\alpha + \dot{w}\delta\dot{w}\sin^2\alpha - (r+n)\dot{\theta}_x\delta\dot{w}\sin\alpha \\ &-(r+n)\dot{w}\delta\dot{\theta}_x\sin\alpha + (r+n)^2\dot{\theta}_x\delta\dot{\theta}_x\Big\}dAdxdt\end{aligned} \quad \text{F.7}$$

By performing integration by parts with respect to time and grouping like-terms, one obtains

$$\begin{aligned}\int_{t_1}^{t_2}\delta T_2 dt = \rho\int_{t_1}^{t_2}\int_0^l\int_A \Big\{&\left(-\ddot{v}\cos^2\alpha - \ddot{w}\cos\alpha\sin\alpha + (r+n)\ddot{\theta}_x\cos\alpha\right)\delta v \\ &+\left(-\ddot{v}\cos\alpha\sin\alpha - \ddot{w}\sin^2\alpha + (r+n)\ddot{\theta}_x\sin\alpha\right)\delta w \\ &+\left((r+n)\ddot{v}\cos\alpha + (r+n)\ddot{w}\sin\alpha - (r+n)^2\ddot{\theta}_x\right)\delta\theta_x\Big\}dAdxdt\end{aligned} \quad \text{F.8}$$

By taking the first variation of Eq. F.2(d) with respect to the argument functions, one obtains

$$\int_{t_1}^{t_2}\delta T_3 dt=\rho\int_{t_1}^{t_2}\int_0^l\int_A\left\{\dot{v}\delta\dot{v}\sin^2\alpha-\dot{w}\delta\dot{v}\sin\alpha\cos\alpha-\dot{v}\delta\dot{w}\sin\alpha\cos\alpha-q\dot{\theta}_x\delta\dot{v}\sin\alpha-q\dot{v}\delta\dot{\theta}_x\sin\alpha\right.$$
$$\left.+\dot{w}\delta\dot{w}\cos^2\alpha+q\dot{\theta}_x\delta\dot{w}\cos\alpha+q\dot{w}\delta\dot{\theta}_x\cos\alpha+q^2\dot{\theta}_x\delta\dot{\theta}_x\right\}dAdxdt$$

F.9

Performing integration by parts with respect to time yields

$$\int_{t_1}^{t_2}\delta T_3 dt=\rho\int_{t_1}^{t_2}\int_0^l\int_A\left\{\left(-\ddot{v}\sin^2\alpha+\ddot{w}\sin\alpha\cos\alpha+q\ddot{\theta}_x\sin\alpha\right)\delta v\right.$$
$$\left.+\left(\ddot{v}\sin\alpha\cos\alpha-\ddot{w}\cos^2\alpha-q\ddot{\theta}_x\cos\alpha\right)\delta w+\left(q\ddot{v}\sin\alpha-q\ddot{w}\cos\alpha-q^2\ddot{\theta}_x\right)\delta\theta_x\right\}dAdxdt$$

F.10

From Eq. F.6 , F.8 and F.10, by substituting into Eq. F.1(a) and grouping like-terms one obtains

$$\int_{t_1}^{t_2}\int_0^l\delta T dxdt=-\rho\int_{t_1}^{t_2}\int_0^l\left(I_z\ddot{v}'\delta v'+I_y\ddot{w}'\delta w'+I_\omega\ddot{\theta}_x'\delta\theta_x'+I_{yz}\ddot{v}'\delta w'+I_{yz}\ddot{w}'\delta v'\right)dxdt$$
$$+\rho\int_{t_1}^{t_2}\int_0^l\int_A\left\{\left[-\ddot{v}+\left((r+n)\cos\alpha+q\sin\alpha\right)\ddot{\theta}_x\right]\delta v+\left[-\ddot{w}+\left((r+n)\sin\alpha-q\cos\alpha\right)\ddot{\theta}_x\right]\delta w\right.$$
$$\left.+\left[\left((r+n)\cos\alpha+q\sin\alpha\right)\ddot{v}+\left((r+n)\sin\alpha-q\cos\alpha\right)\ddot{w}-\left((r+n)^2+q^2\right)\ddot{\theta}_x\right]\delta\theta_x\right\}dAdxdt$$

F.11

From the relations $\left(\overline{y}-y_r\right)=q\cos\alpha-r\sin\alpha$, $\left(\overline{z}-z_r\right)=q\sin\alpha+r\cos\alpha$, by substituting into Eq. F.11 one obtains

$$\int_{t_1}^{t_2}\int_0^l\delta T dxdt=-\rho\int_{t_1}^{t_2}\int_0^l\left(I_z\ddot{v}'\delta v'+I_y\ddot{w}'\delta w'+I_\omega\ddot{\theta}_x'\delta\theta_x'+I_{yz}\ddot{v}'\delta w'+I_{yz}\ddot{w}'\delta v'\right)dxdt$$
$$+\rho\int_{t_1}^{t_2}\int_0^l\int_A\left\{\left[-\ddot{v}+\left(\left(\overline{z}-z_r\right)+n\cos\alpha\right)\ddot{\theta}_x\right]\delta v+\left[-\ddot{w}+\left(-\left(\overline{y}-y_r\right)+n\sin\alpha\right)\ddot{\theta}_x\right]\delta w\right.$$
$$\left.+\left[\left(\left(\overline{z}-z_r\right)+n\cos\alpha\right)\ddot{v}+\left(-\left(\overline{y}-y_r\right)+n\sin\alpha\right)\ddot{w}-\left((r+n)^2+q^2\right)\ddot{\theta}_x\right]\delta\theta_x\right\}dAdxdt$$

F.12

From the relations, $y=\overline{y}-n\sin\alpha$, $z=\overline{z}+n\cos\alpha$, by substituting into Eq. F.12, one obtains

$$\begin{aligned}\int_{t_1}^{t_2}\delta T dt = &-\int_{t_1}^{t_2}\int_0^l \rho\left(I_z\ddot{v}'\delta v' + I_y\ddot{w}'\delta w' + I_\omega\ddot{\theta}_x'\delta\theta_x' + I_{yz}\ddot{v}'\delta w' + I_{yz}\ddot{w}'\delta v'\right)dxdt \\ &+\rho\int_{t_1}^{t_2}\int_0^l\int_A\left\{\left[-\ddot{v}+\left(z-z_r\right)\ddot{\theta}_x\right]\delta v+\left[-\ddot{w}-\left(y-y_r\right)\ddot{\theta}_x\right]\delta w\right. \\ &\left.+\left[\left(z-z_r\right)\ddot{v}-\left(y-y_r\right)\ddot{w}-\left(\left(r+n\right)^2+q^2\right)\ddot{\theta}_x\right]\delta\theta_x\right\}dAdxdt\end{aligned} \quad \text{F.13}$$

From Eq. F.13, by performing the area integrals and using the orthogonality conditions $\int_A ydA = \int_A zdA = 0$ one obtains

$$\begin{aligned}\int_{t_1}^{t_2}\delta T dt = &-\int_{t_1}^{t_2}\int_0^l \rho\left(I_z\ddot{v}'\delta v' + I_y\ddot{w}'\delta w' + I_\omega\ddot{\theta}_x'\delta\theta_x' + I_{yz}\ddot{v}'\delta w' + I_{yz}\ddot{w}'\delta v'\right)dxdt \\ &+\rho\int_{t_1}^{t_2}\int_0^l\left[\left(-A\ddot{v}-z_rA\ddot{\theta}_x\right)\delta v+\left(-A\ddot{w}+y_rA\ddot{\theta}_x\right)\delta w+\left(-z_rA\ddot{v}+y_rA\ddot{w}-I_p\ddot{\theta}_x\right)\delta\theta_x\right]dxdt\end{aligned} \quad \text{F.14}$$

in which, $I_p = \int\left[q^2+\left(r+n\right)^2\right]dA$ is the polar moment of inertia about the shear centre. By performing integration by parts of the first term with respect to the argument functions and grouping like-terms, one obtains

$$\begin{aligned}\int_{t_1}^{t_2}\int_0^l\delta T dxdt = \rho\int_{t_1}^{t_2}\int_0^l\left[\left(I_z\ddot{v}''+I_{yz}\ddot{w}''-A\ddot{v}-z_r\ddot{\theta}_x\right)\delta v+\left(I_y\ddot{w}''+I_{yz}\ddot{v}''-A\ddot{w}+y_r\ddot{\theta}_x\right)\delta w\right. \\ \left.+\left(I_\omega\ddot{\theta}_x''-z_r\ddot{v}+y_r\ddot{w}-I_p\ddot{\theta}_x\right)\delta\theta_x\right]dxdt\end{aligned} \quad \text{F.15}$$

Appendix G Recovering Line Load Expressions from Body Forces

This appendix expressing the line loads terms due to body forces which are provided in the Eq. 5.9. From Eq. 5.7, by substituting into Eq. 5.6, one obtains

$$\begin{aligned}\int_{t_1}^{t_2}\delta V dt = \int_{t_1}^{t_2}\delta\Big[-\int_0^l\int_n\int_s\Big[P_x(s,n,x)u_p(x) - \underline{P_x(s,n,x)y(s,n)v'(x,t)} \\ \underline{-P_x(s,n,x)z(s,n)w'(x,t)} + \underline{P_x(s,n,x)\omega(s,n)\theta_x'(x,t)}\Big]dsdndx \\ -\int_0^l\int_n\int_s P_y(s,n,x,t)\Big[\cos\alpha(s)v(x,t)+\sin\alpha(s)w(x,t)-\big(r(s)+n\big)\theta_x(x,t)\Big]dsdndx \\ -\int_0^l\int_n\int_s P_z(s,n,x,t)\Big[-\sin\alpha(s)v(x,t)+\cos\alpha(s)w(x,t)+q(s)\theta_x(x,t)\Big]dsdndx\Big]dt\end{aligned} \quad \text{F.16}$$

By taking integration by parts with respect to x from underlined terms in Eq. F.16, one obtains

$$\begin{aligned}\int_{t_1}^{t_2}\delta V dt = \int_{t_1}^{t_2}\delta\Big[-\int_0^l\int_n\int_s\Big[P_x(s,n,x)u_p(x) - \frac{\partial}{\partial x}\big(P_x(s,n,x)y(s,n)\big)v(x,t) \\ -\frac{\partial}{\partial x}\big(P_x(s,n,x)z(s,n)\big)w(x,t)+\frac{\partial}{\partial x}\big(P_x(s,n,x)\omega(s,n)\big)\theta_x(x,t)\Big]dsdndx \\ -\int_0^l\int_n\int_s P_y(s,n,x,t)\Big[\cos\alpha(s)v(x,t)+\sin\alpha(s)w(x,t)-\big(r(s)+n\big)\theta_x(x,t)\Big]dsdndx \\ -\int_0^l\int_n\int_s P_z(s,n,x,t)\Big[-\sin\alpha(s)v(x,t)+\cos\alpha(s)w(x,t)+q(s)\theta_x(x,t)\Big]dsdndx \\ +\Big[\int_n\int_s\Big[-P_x(s,n,x)y(s,n)v(x,t)-P_x(s,n,x)z(s,n)w(x,t) \\ +P_x(s,n,x)\omega(s,n)\theta_x(x,t)\Big]dsdn\Big]_{x=0}^{x=l}\Big]dt\end{aligned} \quad \text{F.17}$$

From Eq. F.17, by regrouping like terms one obtains (Eq. 5.8)

$$\int_{t_1}^{t_2}\delta V dt = -\int_{t_1}^{t_2}\int_0^l\Big[q_x u_p(x)+q_y\delta v(x,t)+q_z\delta w(x,t)+m\delta\theta_x(x,t)\Big]dxdt \quad \text{F.18}$$

in which line loads are defined as

$$q_x(x,t) = \int_n \int_s P_x(s,n,x)\,dsdn$$

$$q_y(x,t) = \int_n \int_s \left[-\frac{\partial}{\partial x}\left(P_x(s,n,x)\,y(s,n)\right) + P_y(s,n,x,t)\cos\alpha(s) - P_z(s,n,x,t)\sin\alpha(s) \right] dsdn$$

$$q_z(x,t) = \int_n \int_s \left[-\frac{\partial}{\partial x}\left(P_x(s,n,x)\,z(s,n)\right) + P_y(s,n,x,t)\sin\alpha(s) + P_z(s,n,x,t)\cos\alpha(s) \right] dsdn$$

$$m(x,t) = \int_n \int_s \left[-\frac{\partial}{\partial x}\left(P_x(s,n,x)\,\omega(s,n)\right) - P_y(s,n,x,t)\left(r(s)+n\right) + P_z(s,n,x,t)\,q(s) \right] dsdn$$

The above equation forms the basis of Eq. 5.9.

Appendix H Derivation of Nodal Force Vector

To reach the formulation for nodal force vector due to walking provided in Eq. 5.19 the below steps are taken. From Eq. 5.12, by substituting into Eq. 5.8 one obtains

$$\int_{t_1}^{t_2}\delta V dt=-\int_{t_1}^{t_2}\delta\int_0^l\Big[\left\langle\mathbf{v_n}(t)\right\rangle_{1\times4}^{\mathbf{T}}q_y(x,t)\mathbf{H_v}(x)+\left\langle\mathbf{w_n}(t)\right\rangle_{1\times4}^{\mathbf{T}}q_z(x,t)\delta\mathbf{H_w}(x)+\left\langle\boldsymbol{\theta}_\mathbf{n}(t)\right\rangle_{1\times4}^{\mathbf{T}}m(x,t)\delta\mathbf{H_v}(x)\Big]dxdt \tag{H.1}$$

From Eq. H.1, by separating terms and regrouping them one obtains

$$\int_{t_1}^{t_2}\delta V dt=-\int_{t_1}^{t_2}\left\langle\delta\mathbf{v_n}(t)\right\rangle_{1\times4}^{\mathbf{T}}\int_0^l\Big[q_y(x,t)\mathbf{H_v}(x)\Big]dx+\left\langle\delta\mathbf{w_n}(t)\right\rangle_{1\times4}^{\mathbf{T}}\int_0^l\Big[q_z(x,t)\mathbf{H_w}(x)\Big]dx+\left\langle\delta\boldsymbol{\theta}_\mathbf{n}(t)\right\rangle_{1\times4}^{\mathbf{T}}\int_0^l\Big[m(x,t)\mathbf{H_v}(x)\Big]dxdt \tag{H.2}$$

From Eq. H.2, by expanding in a vector format one obtains

$$\int_{t_1}^{t_2}\delta V dt=-\int_{t_1}^{t_2}\delta\left\langle\mathbf{v_n}(t)\quad\mathbf{w_n}(t)\quad\boldsymbol{\theta}_\mathbf{n}(t)\right\rangle\int_0^l\begin{Bmatrix}\Big[q_y(x,t)\mathbf{H_v}(x)\Big]\\\Big[q_z(x,t)\mathbf{H_w}(x)\Big]\\\Big[m(x,t)\mathbf{H_v}(x)\Big]\end{Bmatrix}dxdt \tag{H.3}$$

From Eq. H.3, the nodal force vector is the same as Eq. 5.19

$$\mathbf{F}_e^{\mathbf{T}}(t)_{12\times1}=\int_0^l\left\langle q_y(x,t)\mathbf{H_v^T}(x)\;\middle|\;q_z(x,t)\mathbf{H_w^T}(x)\;\middle|\;m(x,t)\mathbf{H_v^T}(x)\right\rangle dx \tag{H.4}$$

Appendix I Comparison of Forcing Function due to Walking against Nodal Forces

This appendix aims to verify the accuracy of the implemented loading function representing a human walking at a constant speed over a beam (Figure I.2). As shown in Figure I.1, the applied forcing function is constructed by superimposing the equivalent nodal forces corresponding to each time step and spatial location along the beam, reflecting the dynamic effect of the moving pedestrian load. The plots for F_1 - F_9 represent the equivalent nodal force time histories at nodes 1 to 9, while the solid black curve is summation of equivalent nodal forces for all elements and is expected to represent the temporal and spatial distribution of the force.

As an illustrative example, consider the green dashed curve F_2 which corresponds to the nodal force at node 2. Since node 2 is shared between element 1 and element 2, it receives force contributions during the period when the walking load is located on either of these elements. Consequently, the equivalent nodal force F_2 is active from approximately 0 to 0.84 seconds (considering the human's velocity, it takes 0.42 seconds to pass one element), after which the walking load progresses beyond element 2, and node 2 no longer contributes to the applied force.

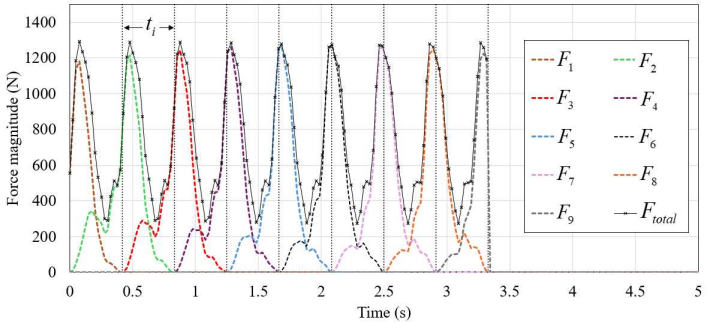

* F_i is the nodal force at node i induced by human when he is at element e and $e+1$

*Black curve is total forcing function induced by human walking calculated by summation of each member force

* t_i is the time for passing element e

Figure I.1 Magnitude of equivalent nodal vertical forces vs time

To validate the total forcing function derived from the finite element formulation, a comparison is performed between the computed forcing function (obtained through the summation of equivalent nodal forces) and the reference formulation recommended by design standards for human-induced dynamic loading (e.g., Murray et al. [9]). Figure I.2 presents this comparison, illustrating excellent agreement between the finite element-based result and the loading function prescribed by Murray et al. [9], thereby confirming the accuracy of the proposed numerical implementation.

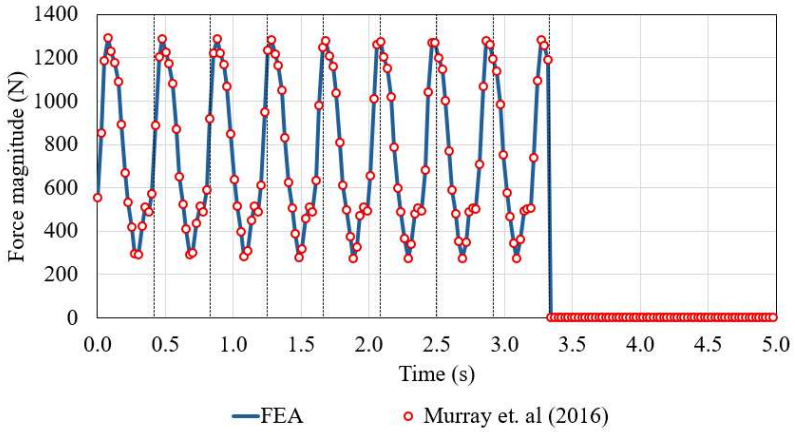

Figure I.2 Verification of modelling forcing function in FE solution with proposed equation in Murray et al. [9]

Appendix J Additional Verification for Transient Analysis

To validate the results of the present time-history response analysis, two benchmark examples from the study by Sahraei et al. [43] were reproduced. The selected example consists of a cantilever beam with a 6 m span and a W250×58 cross-section, subjected to a horizontal force $F(t)$ applied at the tip. The damping ratio ζ was taken as 0.03. Two loading scenarios were considered:

Sinusoidal Force: A harmonic force with an amplitude of 1000 N and an exciting frequency equal to half the fundamental natural frequency associated with the weak-axis flexural mode. The loading was applied for 5 cycles. The corresponding forcing function is given by $F(t) = 1000\sin(12.47t)N$. The fundamental natural frequency of the member ω_1 is 24.95 rad/s. The time step used in the analysis was taken $\Delta t = T_1/20$, where T_1 is the fundamental period of vibration.

Impulse Load: A triangular pulse that ramps up linearly from 0 to 10 kN over $T_1/4$ seconds, then descends back to 0 over the next $T_1/4$ seconds.

Figure J.1(a,b) present the forcing function and the corresponding horizontal displacement response for the sinusoidal load case, while Figure J.1(c,d) illustrate the same for the triangular load case. As observed, an excellent agreement was achieved between the results of the current study and those reported in [43], thus validating the numerical model.

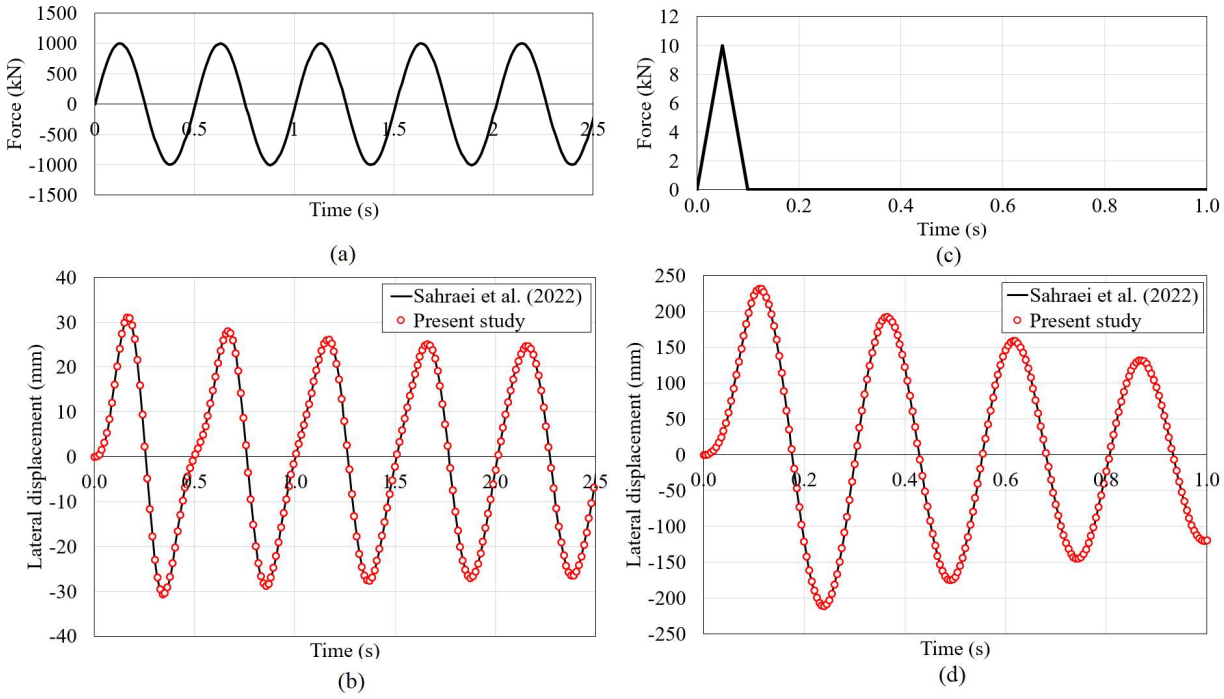

Figure J.1 Horizontal force inputs and displacement responses for sinusoidal and impulse loading scenarios Sahraei et al. [43].

Appendix K Effect of Damping

A 6 m span cantilever beam has a W250×58 cross-section. The member is subjected to a sinusoidal horizontal excitation force $F(t)=1.0\sin(12.47t)kN$ applied at web mid-height at the cantilever tip (Figure K.1a). A compressive axial load $P=0.9P_{cr}\approx 230kN$ is applied at the shear centre of the free end in which $P_{cr}=\pi^2 EI_z/4L^2=258.1kN$ is the minor axis critical load. Three damping ratios are considered: $\zeta=$ 0.03, 0.05, and 0.08. Three definitions of the damping matrix are explored: (a) mass proportional damping, i.e., $[\mathbf{C}]=c_0[\mathbf{M_s}]$, (b) Raleigh damping, i.e., $[\mathbf{C}]=c_0[\mathbf{M_s}]+c_1[\mathbf{K_s}]$ and (c) Rayleigh damping including the destabilizing effect of the axial force P $[\mathbf{C}]=c_0[\mathbf{M_s}]+c_1\left([\mathbf{K_s}]+P\left[\mathbf{K}_g\right]\right)$. The first two natural frequencies of the member are $\omega_1=8.55\ rad/s$, and $\omega_2=48.54\ rad/s$. By substituting into Eq. 5.18, one obtains the proportionality constants c_0, c_1 characterizing the damping matrix (Table K.1). Figure K.1(a-d) shows that the amplitudes of the horizontal displacement, reduce as the damping ratio increases. All three damping definitions are found to yield nearly identical responses. This is attributed to the fact that, in the present example, the damping matrix is heavily dependent on the mass matrix contribution and nearly independent of the stiffness contribution. Figure K.1d depicts only minor differences between the responses corresponding to the three damping definitions examined for a 0.08 damping ratio. In subsequent analysis, the Raleigh damping representation, and a damping ratio of 0.03 will be adopted in the remaining part of the study, unless noted otherwise.

Table K.1 Rayleigh damping coefficients for various damping ratios

ζ	$c_0(1/s)$	$c_1(s)$
0.03	0.436	0.00106
0.05	0.727	0.00175
0.08	1.16	0.00280

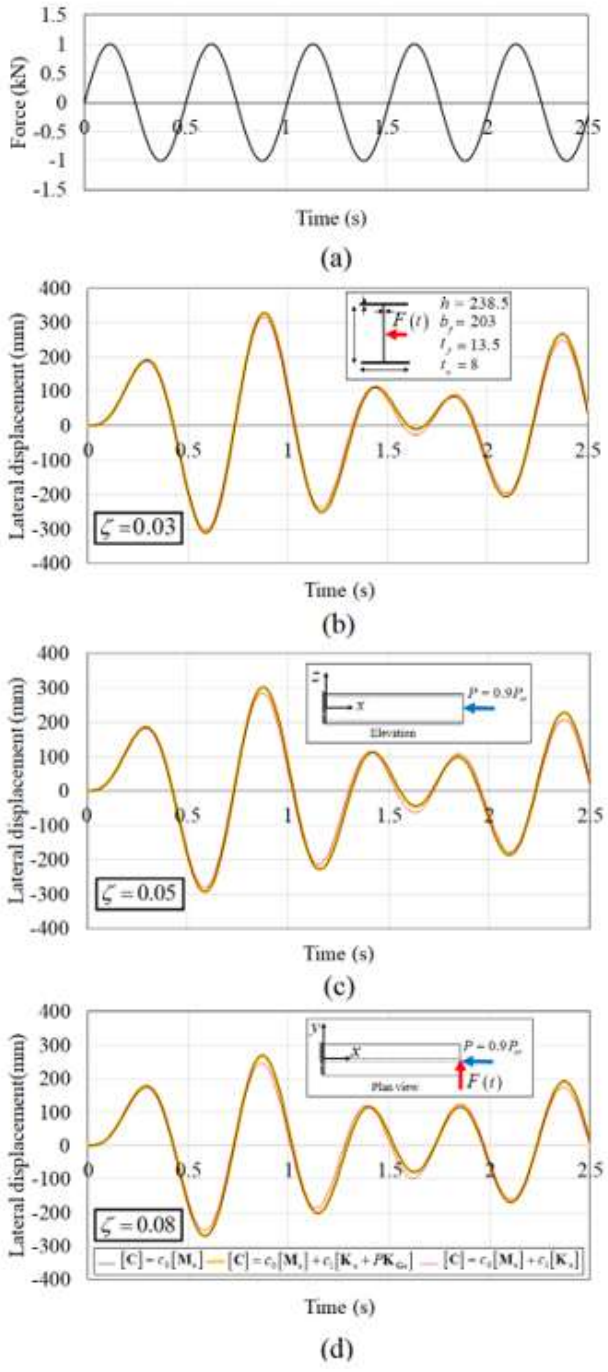

Figure K.1 (a) Harmonic force and corresponding horizontal displacement histories for damping ratios of (b) 0.03, (c) 0.05, and (d) 0.08.

Appendix L Contribution of Individual Harmonics to Acceleration

Figure L.1 shows the mid-span vertical displacement response of the referenced doubly symmetric member in Section 5.9.1. Figure L.1b depicts the vertical displacement response for a sudden application of human body weight plus the first 0, 1, 2, 3, and 4 harmonics characterizing the human induced forcing function characterizing acceleration response. From a displacement perspective, the human bodyweight Q plus the first harmonic contribution are observed to have the largest contribution to the displacement response. The inclusion of higher harmonics is observed not to alter the displacement response appreciably. Thus, for displacement-based serviceability assessments, considering only the first harmonic in combination with static body weight leads to sufficiently accurate assessment.

In contrast, the acceleration response Figure L.1(c–g) is significantly more sensitive to the inclusion of higher harmonics. While the human body weight accounts for the dominant part of the acceleration response, the addition of first to fourth harmonics increases the peak accelerations and alters the overall waveform, particularly after 1.5 seconds. This cumulative effect becomes clear when comparing the responses in Figure L.1c (no harmonics) with Figure L.1g (all harmonics), highlighting the necessity of including all harmonics when evaluating vibration comfort based on acceleration criteria. Also notable is that the influence of higher-order harmonics becomes more prominent in the later stage of the time history (after approximately 1.5 seconds). The effect of higher harmonics becomes more relevant in sustained dynamic events such as rhythmic activities.

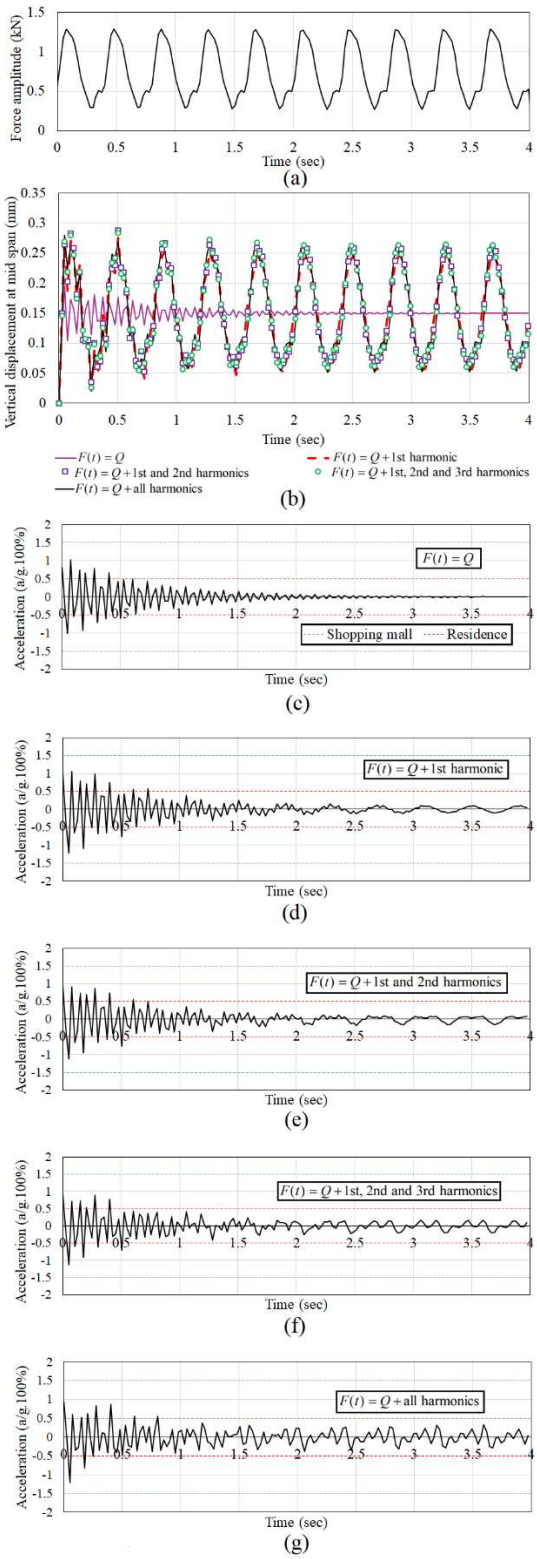

Figure L.1 (a) Human induced dynamic force, (b) Impact of number of harmonics on midspan displacement. Impact of number of harmonics on acceleration (c) Weight + no harmonics, (d) Weight + first harmonic, (e) Weight +first two harmonics, (f) Weight + first three harmonics, (g) Weight + all four harmonics

Appendix M Response of Member with Angle Cross-Section to Forces induced by Walking on a Treadmill

A 4*m* span member has an L203×152×13 angle cross-section considered as a reference case. Two types of boundary conditions are investigated at member ends: gusset plate-ended connections and pinned-ended connections. In both cases, the member is subjected to a compressive axial load of 169 kN which corresponds to $P/P_{cr}^{G} = 0.21$ for the gusset end-plate connection, $P_{cr}^{G} = 800kN$ being the critical load of the gusset ended member as determined in [46]. For the pinned-ended connection, the same compressive load corresponds to $P/P_{cr}^{P} = 0.31$, $P_{cr}^{P} = 550kN$ being the critical load for the pin-ended member. The corresponding fundamental natural frequencies are 17.7 Hz and13.20 Hz, respectively. The Damping ratio ζ is taken as 0.03. A human on a treadmill is located at midspan inducing the forcing function characterized under Section 5.7.

Figure M.1b depicts the midspan vertical, horizontal, and resultant displacements at the shear centre. Given that the applied vertical load is oriented along a non-principal direction, the angle exhibits horizontal and vertical displacements, albeit the horizontal components of the displacements are significantly smaller than the vertical ones. The pin-ended member exhibits a more flexible behavior compared to the gusset-ended member as reflected by the higher displacements observed in the former case. Yet, in both cases, the overall displacement levels are controlled and well below typical deflection serviceability limits. After the dynamic force ceases to act (i.e., after four seconds), the displacement response gradually diminishes due to damping. Figure M.1(c,d) depicts the vertical and horizontal acceleration response. While the gusset-ended member exhibits lower accelerations than pinned-ended members, it still exceeds the acceleration

thresholds for shopping malls and residential spaces, particularly throughout the initial part of the excitation.

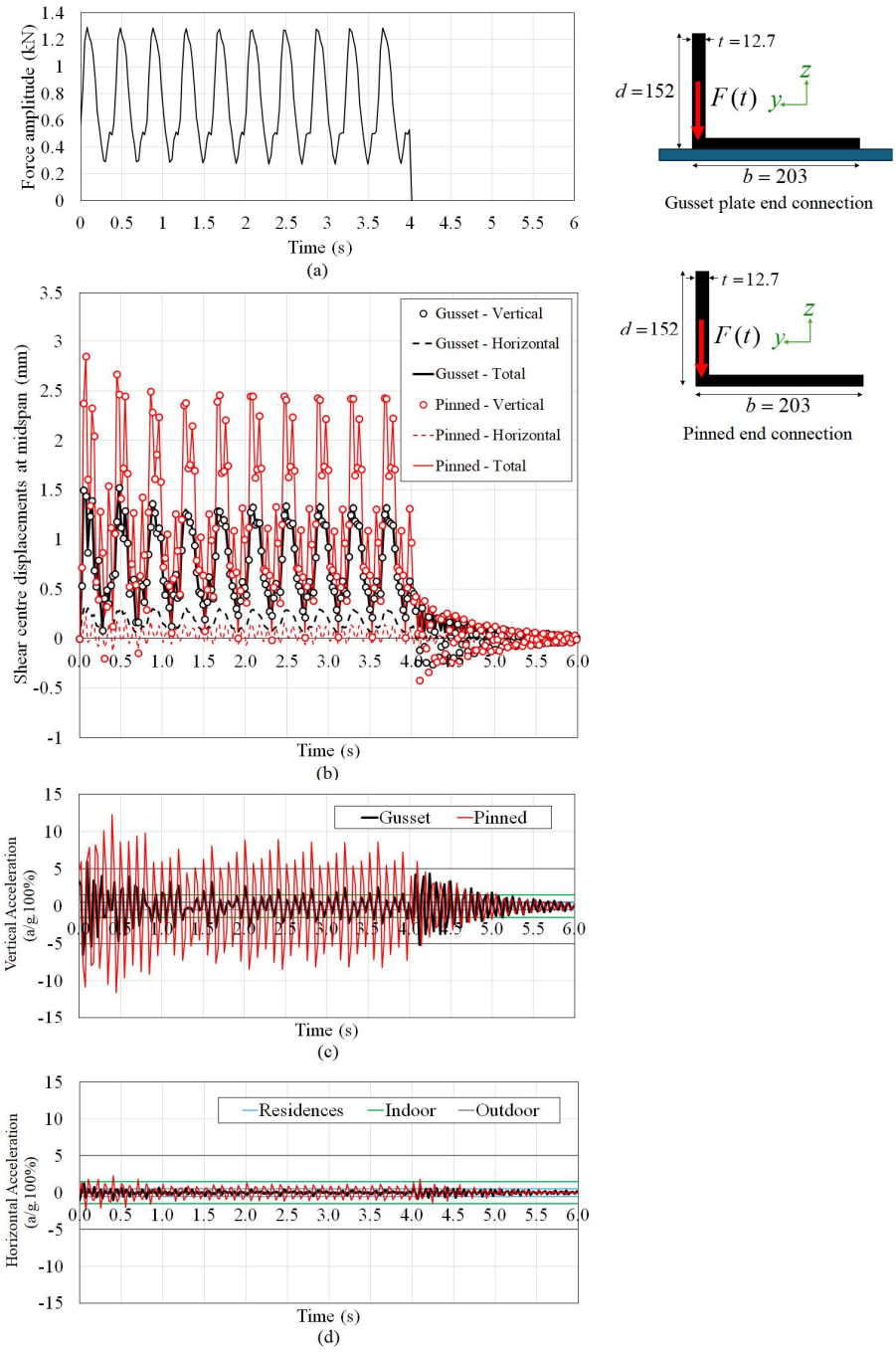

Figure M.1 (a) Force history induced by walking, (b) Displacement history response, (c) Horizontal acceleration response (a/g), and (d) Vertical acceleration response

Effect of axial load

The effect of axial force level on response of above reference case is investigated for members with gusset end-connections and pinned end-connections. Three levels of axial loads are investigated; $P = 200$, 0 , $-200kN$, which correspond to $P/P_{cr}^{G} = 0.25$ (i.e., compressive), 0, and –0.25 (tensile), in which we recall that $P_{cr}^{G} = 800kN$ denotes the elastic buckling load for the gusset-ended member. The corresponding natural frequencies are 13.5, 19.2, and 23.5 Hz, respectively. For the pin-ended member, one has $P_{cr}^{P} = 550kN$ and the axial load ratios are $P/P_{cr}^{P} = 0.36$, 0 , -0.36 which correspond to fundamental natural frequencies of 8.28, 15.9, and 20.9 Hz, respectively. As discussed in previous examples, the presence of a compressive axial load results in a significant amplification of the acceleration responses while the presence of a tensile force of the same magnitude corresponds in a reduction of the acceleration magnitude.

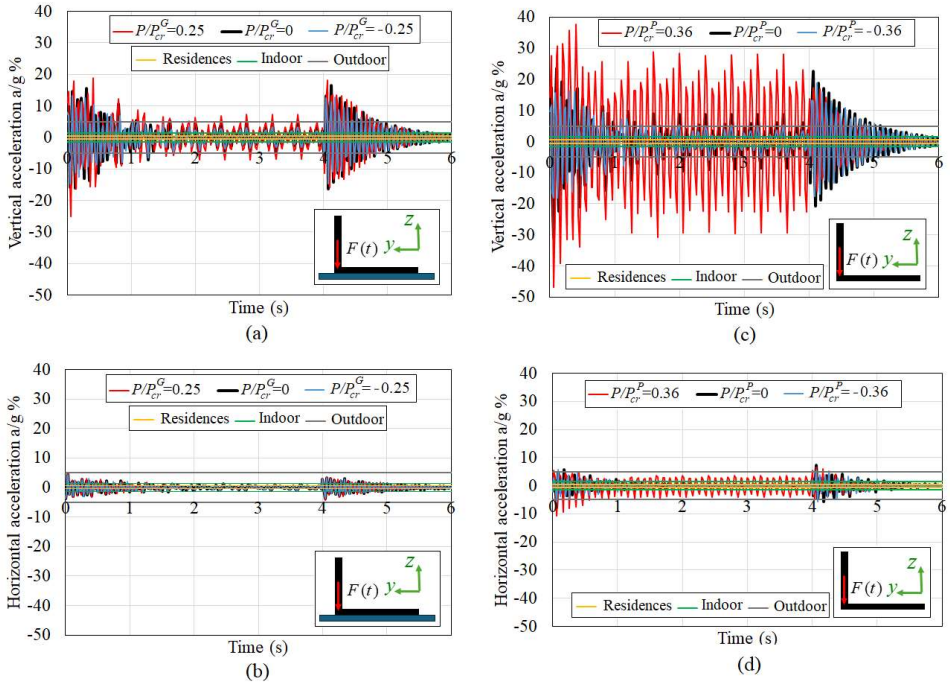

Figure M.2 Effect of axial load on Vertical displacement history of (a) gusset end member and (b) pinned end member, Horizontal displacement history of (c) gusset end member and (d) pinned end member.

Appendix N Effect of span on angle member response

Figure N.1 presents the vertical acceleration response under the vertical component of the force induced by human walking acting at the shear centre. In addition to the reference span L = 3m, two additional spans are considered: 4 and 5 m. The corresponding maximum slenderness ratios are 138, 184, and 230, respectively. The fundamental natural frequencies for the pin-ended members are 19.0, 10.71, and 6.87 Hz, respectively, and those of the gusset-ended members are 23.5,13.4, and 8.60 Hz. Figure N.1(a–d) show that as the span increases, the vertical acceleration levels for pin-ended members increase in a manner consistent with the reduction in their fundamental natural frequencies. Figure N.1(e–h) shows a similar trend for gusset-ended members. Again, the acceleration levels for gusset-ended members are lower than pin-ended members.

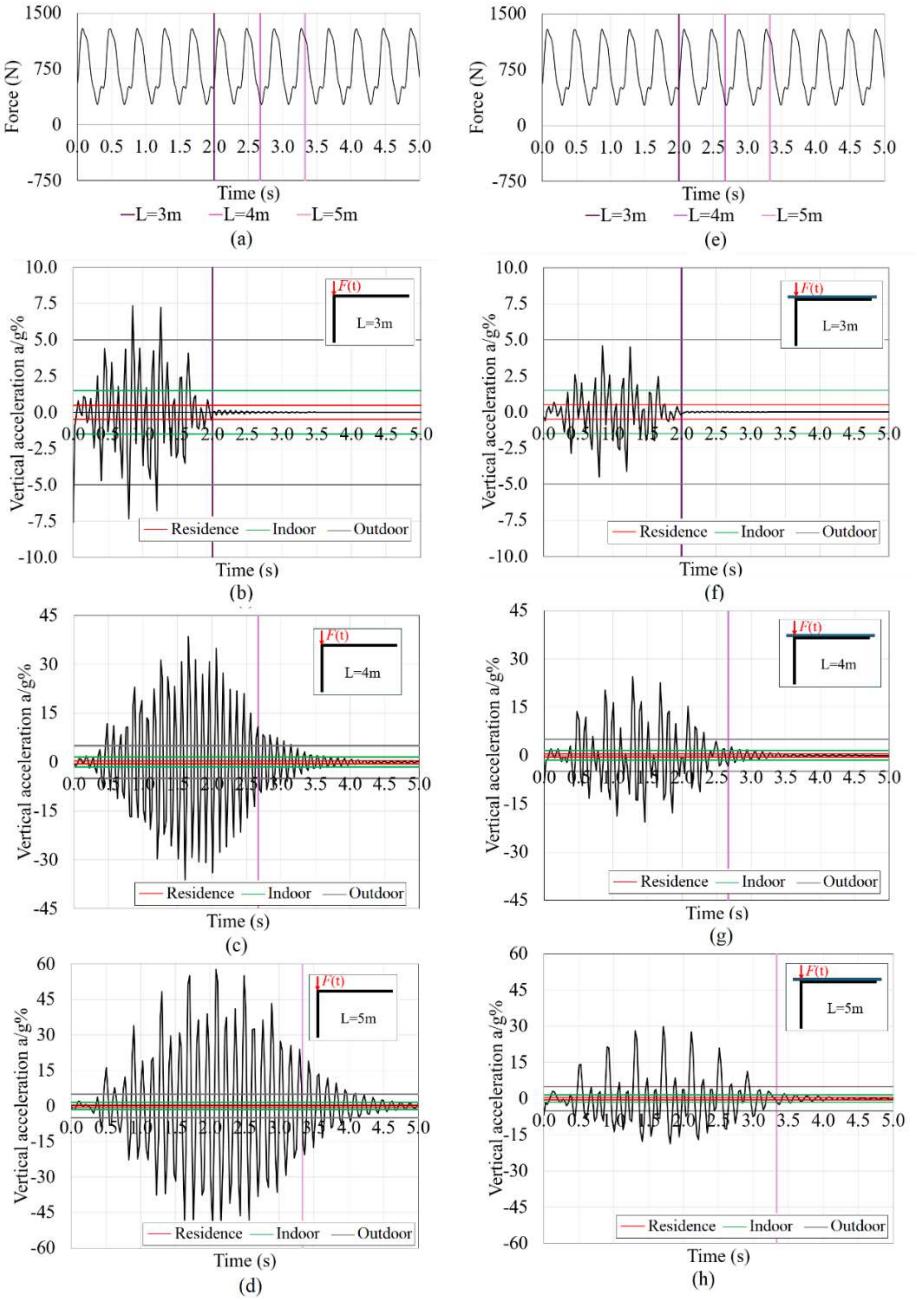

Figure N.1 (a) Vertical component of force. Pin-ended member vertical acceleration ratios for (b) Span =3m (c) Span=4m, and (d) Span=5m. Gusset-ended member acceleration rations for (b) Span =3m (c) Span=4m, and (d) Span=5m. (e) Vertical component of force. (f) Span =3m (g) Span=4m, and (h) Span=5m.